

DIGITAL SIMULATION OF FAULT LOCATION ALGORITHMS FOR EHV TRANSMISSION LINES

By



Larissa Al-Dabbagh, M. Sc. Tech (Eng.), AMIEE, MIE, Aust

Thesis submitted for the Degree of Doctor of Philosophy

of

The Victoria University of Technology

Department of Electrical and Electronic Engineering

1994

COPYRIGHT

" Attention is drawn to the fact that copyright of this thesis rests with its author. This copy of the thesis has been supplied on condition that anyone who consults it is understood to recognise that its copyright rests with its author and that no quotation from the thesis and no information derived from it may be published without the prior written consent of the author "

To:

MY MOTHER,

HUSBAND, MY SONS ' SAM ' AND ' ALEX '

SUMMARY

This thesis investigates the development of accurate fault location algorithms for EHV transmission lines based on digital simulation techniques. This research covers detailed analysis of the theory of travelling waves on transmission lines, including the frequency variance of the parameters. The analysis of the two and three terminal systems is carried out in the steady-state and transient conditions.

Analysis of the transmission line is carried out in detail in order to develop accurate techniques for estimating the distance to faults under different system operating conditions. The algorithms are based on the use of fault voltage and current phasors at the terminations of the transmission lines, and the use of the transmission line constants to compute the modal propagation parameters. The phase quantities are converted into modal quantities using the eigenvalues and eigenvectors.

The developed algorithms are tested using digital computer simulation methods, for the two and three terminal systems. Results presented in this thesis show, that the analysis of the fault location algorithms were found to be very accurate.

The thesis provides detailed studies of the three phase system transient waveforms under various system fault conditions for faults applied at different locations on the EHV transmission lines. The waveforms traces were captured using the Alternative Transient Program (ATP), the PC version of the well known Electromagnetic Transient Program (EMTP).

The presented algorithms for fault location estimations are shown to be free of the effect of source impedance variations, fault impedance variations, remote infeed contributions, point on wave of fault inception, and shunt capacitance effect. These methods are equally accurate for transposed and untransposed lines of different configurations.

The behaviour of the fault location algorithms for shunt compensated two and three terminal transmission lines are investigated.

ACKNOWLEDGEMENT

The author would like to thank her supervisor Associate professor Akhtar Kalam for his guidance throughout the research work carried out at the Department of Electrical and Electronic Engineering, Victoria University of Technology.

She would like to thank the State Electricity Commission of Victoria and the Department of Electrical and Electronic Engineering, Victoria University of Technology, for providing financial assistance.

Sincere thanks to the staff of the Department for their encouragement and help in different ways.

The author would like to acknowledge the patience, help, cooperation and support of her husband and family at all times.

Finally, the author wishes to express her gratitude to all friends and colleagues for their continuous support.

LIST OF CONTENTS

	Page No
Summary	
Acknowledgement	
List of principal symbols	
List of tables	
List of figures	
CHAPTER 1: INTRODUCTION	
1.1 Fault location methods	1
1.2 Transmission line theory and wave propagation	3
1.3 Faulted EHV transmission lines	8
1.4 Fault location on EHV transmission lines	11
1.5 Thesis objectives	22
CHAPTER 2 ANALYSIS OF POLYPHASE TRANSMISSION LINES	
2.1 Introduction	27
2.2 Basic considerations	27
2.3 Line series impedance matrix	29
2.4 Shunt admittance matrix	32
2.5 Effect of aerial ground wires	34
2.6 Electrically short lines	36
2.6.1 Single circuit transmission line	40
2.6.2 Double circuit transmission line	41
2.7 Propagation parameters	46
2.8 Representation of long transmission lines	49
CHAPTER 3 STEADY-STATE ANALYSIS OF TRANSMISSION LINES	
3.1 Introduction	51
3.2 Basic relationships	
3.2.1 Single conductor	52
3.2.2 Solution for the two - conductor problem	54
3.2.3 Polyphase transmission lines	58
3.2.4 Surge impedance, propagation constants and reflection factors	60
3.3 Steady-state response	61

3.4	Two port network	62
3.5	Simulation of the faulty transmission line	64
3.6	Transmission line transposition	67
CHAPTER 4 CIRCUIT PARAMETERS		
4.1	Introduction	74
4.2	Source representation	75
4.3	Transmission line parameters	77
4.4	Reactor parameters	82
CHAPTER 5 ACCURATE FAULT LOCATION ALGORITHM FOR EHV TRANSMISSION LINES		
5.1	Introduction	85
5.2	System configuration	87
5.3	Single phase line	88
5.4	Three phase lines	89
5.5	Modal transformation	90
5.6	Fault location measurements	93
CHAPTER 6 SHUNT COMPENSATED EHV TRANSMISSION LINES		
6.1	Introduction	94
6.2	Types of shunt reactors	95
6.3	Reactor arrangements	97
6.4	The 4 legged reactor parameters	99
6.5	Mathematical analysis	101
6.6	Fault location on shunt compensated lines	105
CHAPTER 7 THREE-TERMINAL SYSTEMS		
7.1	Introduction	112
7.2	Three-terminal system	113
7.3	Faulty section identification	115
7.4	Fault location algorithm	116
7.5	Algorithm assessment	117
CHAPTER 8 VOLTAGE AND CURRENT RESPONSE OF POLYPHASE SYSTEMS		
8.1	Introduction	118
8.2	Two terminal systems	120
8.2.1	Single phase to ground faults	121
8.2.2	Double phase faults	123

8.2.3	Double phase to ground faults	123
8.2.4	Three phase faults	124
8.2.5	Multiple faults on compensated systems	124
8.3	Three terminal systems	126
8.3.1	Single line to ground faults	126
8.3.2	Double phase to ground faults	127
8.3.3	Double phase free of earth faults	127
8.3.4	Three phase faults	128
8.3.5	Faults on compensated three terminal systems	129
8.4	Faults through earth impedance	129

CHAPTER 9 ANALYSIS AND TESTING OF THE FAULT LOCATION ALGORITHMS

9.1	Introduction	131
9.2	Selection of modes	132
9.3	Two terminal systems	132
9.3.1	Three phase faults	133
9.3.2	Single phase to ground faults	135
9.3.3	Phase to phase to ground faults	136
9.3.4	Phase to phase faults	137
9.3.5	Compensated systems	138
9.3.6	Effect of fault impedance	138
9.3.7	Prefault loading of the line	139
9.3.8	Untransposed line	140
9.3.9	Remote source impedance variations	141
9.4	Three terminal systems	142
9.4.1	Phase to phase faults	143
9.5	Effect of point on wave	145

CHAPTER 10 CONCLUSIONS AND FUTURE WORK

10.1	Introduction	148
10.2	General conclusions	149
10.3	Testing and assessment	155
10.4	Future work	158

APPENDIX A1: MODAL ANALYSIS AND WAVE PROPAGATION

A1-1	Introduction	161
A1-2	Modal analysis properties	164
A1-3	Infinite transmission line analysis	166
A1-3.1	Phase quantities analysis	166
A1-3.2	Modal quantities analysis	169
A1-4	Properties of modal transformation matrix	170

A1-5 Modal analysis	173
A1-6 Physical interpretations	176
A1-7 Conclusion	177
APPENDIX A2: SOFTWARE IMPLEMENTATION	
A2-1 COMPUTATION METHODOLOGIES	179
A2-2 MODAL TRANSFORMATION	180
APPENDIX A3: PUBLISHED WORK	182
BIBLIOGRAPHY	
183	

LIST OF PRINCIPAL SYMBOLS

Z	= Series impedance matrix per unit length
Y	= Shunt admittance matrix per unit length
Z_0	= Characteristic impedance matrix
Y_0	= Characteristic admittance matrix
λ	= Eigenvalue diagonal matrix of ZY
γ	= Diagonal propagation matrix
d_{ij}	= Distance between conductors i and j
D_{ij}	= Distance between conductor i and image of j
θ_{ij}	= Angle subtended at conductor i by images of i and j
ρ	= Resistivity
μ	= Permeability
ε	= Permittivity
ℓ	= Line length
x	= Distance to the fault
ω	= Angular velocity
S	= Eigenvector matrix of YZ
Q	= Eigenvector matrix of ZY
ψ	= $Q \cdot \gamma \cdot Q^{-1}$
α	= Attenuation constant, nepers/m
β	= Phase shift, radian/m
C_1	= natural mode 1 velocity
C_2	= natural mode 2 velocity
C_3	= natural mode 3 velocity
SE	= Sending end
RE	= Receiving end

(p)	= Phase quantity
V_S, V_R	= Sending end and receiving end voltages
I_S, I_R	= Sending end and receiving end currents
$V_{a,b,c}, I_{a,b,c}$	= Voltage and current phasors
$V_{1,2,3}, I_{1,2,3}$	= Voltage and current modal quantities
$V_{1,2,0}$	= Positive, negative and zero sequence voltages
$I_{1,2,0}$	= Positive, negative and zero sequence currents
GMR	= Geometric mean radius
GMD	= Geometric mean distance
Z_s, Z_m	= Self and mutual impedances of the line
$Z_{1,2,0}$	= Positive, negative and zero sequence impedances of the line
T	= Transformation matrix of the line
t	= Transpose of a matrix
PPS, ZPS	= Positive and zero phase sequence
B_{c1}, B_{c0}	= PPS and ZPS line capacitive susceptance
X_{c1}, X_{c0}	= $1/B_{c1}, 1/B_{c0}$
B_{ch}, B_{cg}	= Phase - phase and phase - ground capacitive susceptances
X_{ch}, X_{cg}	= $1/B_{ch}, 1/B_{cg}$
X_p, X_n	= Phase and neutral reactances of 4-legged reactor
h_1, h_0	= PPS and ZPS degrees of shunt compensation
I_{RE}	= Reactor current
Q_{SR}	= Shunt reactor rating
U	= Unit matrix
0	= Null matrix
FFT	= Fast Fourier Transform
MFT	= Modified Fourier Transform
EFT	= Exponential Fourier Transform
DFT	= Discrete Fourier Transform

Z_{s1}, Z_{s2}	= Self impedance of circuit # 1 and circuit # 2 respectively
Z_{m1}, Z_{m2}	= Mutual impedance of circuit # 1 and circuit # 2 respectively
Z_{mc}	= inter circuit mutual impedance between circuit # 1 and circuit # 2
Y_{s1}	= Self admittance of phase conductors in circuit # 1
Y_{s2}	= Self admittance of phase conductors in circuit # 2
Y_{m1}	= interphase mutual admittance of circuit # 1
Y_{m2}	= interphase mutual admittance of circuit # 2
$Z_1^1 = Z_2^1$	= Positive and negative sequence impedance of circuit # 1
$Z_1^2 = Z_2^2$	= Positive and negative sequence impedance of circuit # 2
a, b, c	= Phases a, b and c respectively
F	= Fault point
a	= Operator $1 < 120^\circ$
K	= Reflection factor
A, B, C, D	= Two port constant parameters
R	= Percentage regulation
δ	= Transmission angle
V_{ss}, V_{rs}	= Sending and receiving steady state voltages
V_{fs}, I_{fs}	= steady state voltages and currents at the at the point of fault
Z_{SS}, Z_{SR}	= Source reactance of the sending and the receiving end
Z_S', Z_R'	= Impedance of the source with reactor at the sending and receiving rends respectively
V_P, V_R, V_Q	= Voltage phasors at the sending, receiving and the Q ends of the three terminal systems
I_P, I_R, I_Q	= Current phasors at the sending, receiving and Q ends of the three terminal system
V_T	= Voltage phasor at the teen point of the three terminal system
P, R, Q	= Three ends of the three terminal system
I_{rea}	= Reactor current
Z_{rea}	= Reactor impedance

List of Tables

<u>Table</u>	<u>Page</u>
4.1 Source Parameters	77
4.2 500 kV, 384 km Horizontal Line Parameters	79
4.3 Double Circuit Line Data	80
9.1 Three - Phase - to - Ground Faults	134
9.2 Percentage Error in Fault Distance Estimation	134
9.3 Single - Phase - to - Ground Faults	135
9.4 AB - G Faults on Two Terminal System	136
9.5 Phase - to - Phase Faults (AB Faults)	137
9.6 Three - Phase Faults on Compensated System	138
9.7 Prefault Line Loading Effect	140
9.8 Faults on Untransposed Transmission Line	140
9.9 Two Phase (AB Faults)	144
9.10 AB Fault for 45 Advancement of One Source	146

List of Figures

<u>Chapter</u>	<u>Figure and Title</u>	<u>Page</u>
2	2.1 Transmission Line Section	29
	2.2 Schematic Diagram of Conductors	31
	2.3 One Section Representation	33
	2.4 Double Circuit Line	41
	2.5 Double Circuit Line Equivalent Circuit	42
	2.6 Single Circuit Transposition	42
	2.7 Double Circuit Transposition	43
	2.8 Equivalent π Representation of the Line	49
	2.9 Exact Equivalent π	50
3	3.1 Single Conductor System Representation	52
	3.2 Impedance Element	57
	3.3 Admittance Element	57
	3.4 Transmission Line Constants	62
	3.5 Simulation of Faulty Transmission Line	64
	3.6 Transposition of Phase Conductors	69
4	4.1 Two Terminal System	75
	4.2 Three Terminal System	75
	4.3 Source Representation	76
	4.4 500 kV, Twin Conductor Configuration	78
	4.5 Double Circuit 500 kV Line	78
	4.6 Shunt Reactor Model	82
5	5.1 Single Line Representation	88
	5.2 Single Line Diagram of a Three Phase Line	90
6	6.1 Possible Shunt Reactor Arrangements	98
	6.2 4 Legged Reactor Compensated Transmission Line	101
	6.3 Shunt Compensated Transmission Line	106
	6.4 Three Phase Faults on 500 kV Transposed Line	110
7	7.1 Three Terminal System - Steady condition	114
	7.2 Three Terminal System - Transient Condition	114

8	8.1 Two Terminal System	121
	8.2 A - Phase to Ground Fault, Sending End Three Phase Voltages	
	8.3 A - Phase to Ground Fault, Receiving End Voltages	
	8.4 A - Phase to Ground Fault, Fault Location at $x = 0$ km, Fault Currents	
	8.5 A - Phase to Ground Fault at $x = 0$ km, Two Terminal System, Sending End Currents	
	8.6 A-Phase to Ground Fault at $x = 0$ km, Two Terminal System. Receiving End Currents	
	8.7 A - Phase To Ground Fault at $x = 0$, Two Terminal System, Fault Cleared after 40 ms	
	8.8 A - Phase to Ground Fault at $x = 192$ km, Sending End Currents	
	8.9 A - Phase to Ground Fault at $l = 192$ km, Receiving End Currents	
	8.10 A - Phase to Ground Fault at $l = 192$ km, Sending End Currents	
	8.11 A - Phase to Ground Fault at $l = 192$ km, Sound Phase Currents	
	8.12 A - Phase to Ground fault at $l = 192$ km, Fault Persistent, Three Phase Sending End Currents	
	8.13 A - Phase to Ground Fault, Fault Cleared after 50 ms, Receiving End Sound Phase Currents	
	8.14 A - Phase to Ground Fault at $l = 192$, Fault Cleared After 50 ms, Sound Phases, Sending End Currents	
	8.15 As 8.14, Receiving End Currents	
	8.16 As in 8.15, Sending End and Receiving End, Phase A Currents	
	8.17 As in 8.16, Longer Observation Time, Fault Cleared After 50 ms	
	8.18 As in 8.14, A - Phase Voltages at the Sending, Receiving and the Fault Locations	
	8.19 AB - Fault at $l = 0$ km, Sending End Voltages	
	8.20 AB - Fault at $l = 0$ km, Receiving End Voltages	
	8.21 As in 8.20, Three Phase Sending End Currents	

- 8.22 As in 8.20, Three Phase Receiving End Currents
- 8.23 As in 8.20, Three Phase Sending End Voltages
- 8.24 As in 8.20, Three Phase Receiving End Voltages
- 8.25 As in 8.20, Three Phase Sending End Currents
- 8.26 As in 8.20, Three Phase Receiving End Currents
- 8.27 As in 8.20, Fault Currents Through the Fault Path
- 8.28 Three Phase Fault at $l = 0$ km, Three Phase Sending End Voltages
- 8.29 As in 8.28, Three Phase Receiving End Voltages
- 8.30 As in 8.28, Three Phase Sending End Currents
- 8.31 As in 8.28, Three Phase Receiving End Currents
- 8.32 A - Phase to Ground Fault at $l = 0$ km, and B - Phase at $l = 96$ km, Three Phase Sending End Voltages, Compensated System
- 8.33 As in 8.32, Three Phase Receiving End Voltages
- 8.34 As in 8.32, Zoomed Sending End Voltages
- 8.35 As in 8.32, Zoomed Receiving End Voltages
- 8.36 As in 8.32, Three Phase Sending End Currents
- 8.37 As in 8.32, Phase A - Current at the Receiving End
- 8.38 As in 8.32, Phase B - Receiving End Current
- 8.39 As in 8.32, Phase C - Receiving End Current
- 8.40 As in 8.32, Currents Through the Fault Path
- 8.41 A - Phase to Ground at $l = 0$ km, B - Phase at $l = 96$ km, Three Phase sending End Voltages
- 8.42 As in 8.32, Receiving End Voltages
- 8.43 As in 8.32, Zoomed Sending End Voltages
- 8.44 As in 8.42, Zoomed Receiving End Voltages
- 8.45 As in 8.32, A - Phase Sending End Fault Current
- 8.46 As in 8.32, B - Phase Sending End Fault Current
- 8.47 As in 8.32, The Sound C - Phase Sending End Current
- 8.48 As in 8.32, A - Phase Receiving End Current
- 8.49 As in 8.32, B - Phase Receiving End Current
- 8.50 As in 8.32, C - Phase (Sound) Receiving End Current
- 8.51 As in 8.32, Currents in the Faulty Paths
- 8.52 Sending End Three Phase Voltages, Three Terminal System (A - Ground Fault at $l = 0$ km)
- 8.53 A - Ground Fault at $l = 0$ km at End P of the Three Terminal Feeder, Three Phase Sending End Currents

- 8.54 As in 8.53, Three Phase Receiving End Currents
- 8.55 Three Phase Currents at the Q End of the Three Terminal Feeder (Fault as in 8.52)
- 8.56 As in 8.52, Sending End Currents (End P)
- 8.57 As in 8.52, Three Phase Sending End Voltages (End P)
- 8.58 As in 8.52, Three Phase Receiving End Voltages (End R)
- 8.59 As in 8.52, Three Phase End Q Voltages
- 8.60 As in 8.52, Three Phase Sending End Voltages, Fault at the Tee Point of the Three Terminal System
- 8.61 A - Ground Fault at $l = 192$ km, Three Phase Receiving End Voltages (R End)
- 8.62 As in 8.61, Q End Three Phase Voltages
- 8.63 As in 8.61, Three Phase Sending End Currents
- 8.64 As in 8.61, Three Phase Receiving End Currents (R End)
- 8.65 As in 8.61, Currents Through the Faulty Path
- 8.66 As in 8.61, Fault Cleared After 40 ms
- 8.67 AB - G Fault at $l = 0$ km, Three Phase Sending End Voltages, Fault Applied at $t = 10$ ms, and Cleared at $t = 50$ ms
- 8.68 As in 8.67, Three Phase Receiving End Voltages
- 8.69 As in 8.67, Q End Three Phase Voltages
- 8.70 As in 8.67, Three Phase Currents at the Sending End
- 8.71 As in 8.67, Three Phase Receiving End Currents
- 8.72 As in 8.67, Three Phase Currents at the Q End
- 8.73 As in 8.67, Three Phase Currents Through the Fault
- 8.74 As in 8.67, Three Phase sending End Voltages
- 8.75 As in 8.67, Three Phase receiving End Voltages
- 8.76 As in 8.67, Q End Three Phase Voltages
- 8.77 As in 8.67, Three Phase Receiving End Currents
- 8.78 As in 8.67, Three Phase Currents at the Q End
- 8.79 Three Phase to Ground Fault at $l = 192$ km, Sending End Three Phase Voltages
- 8.80 As in 8.79, Three Phase Receiving End Voltages
- 8.81 As in 8.79, Three Phase Voltages at the Q End
- 8.82 As in 8.79, Three Phase Currents at the Q End
- 8.83 As in 8.79, Three Phase Currents at the Receiving End
- 8.84 As in 8.79, Three Phase Sending End Currents
- 8.85 As in 8.79, Three Phase Currents Through the

Faulty Path

- 8.86 A - G Fault at $l = 0$ km, Three Phase Voltages at the Sending End of the Three Terminal Feeder
- 8.87 As in 8.86, Three Phase receiving End Voltages
- 8.88 As in 8.86, Q End Three Phase Voltages
- 8.89 As in 8.86, A - Phase Sending End Current
- 8.90 As in 8.86, B - Phase Sending End Current
- 8.91 As in 8.86, C - Phase Sending End Current
- 8.92 As in 8.86, Receiving End Three Phase Currents
- 8.93 As in 8.86, Q End Three Phase Currents
- 8.94 As in 8.86, The A - Phase Current in the Faulty Path
- 8.95 Compensated Three Terminal Feeder, A - Ground Fault at End P, Through 10 Ohms Resistance, Three Phase Sending End Voltages
- 8.96 As in 8.95, The Phase Receiving End Voltages
- 8.97 As in 8.95, Three Phase Q End Voltages
- 8.98 As in 8.95, Current Through the Faulty Path (A - Phase)
- 8.99 As in 8.95, Phase B and C Sending End Currents
- 8.100 As in 8.95, Phase B and C Receiving End Currents
- 8.101 As in 8.95, Three Phase Currents at the Q End
- 8.102 As in 8.95, Fault Current Through the Faulty Path

9

- 9.1 Three Phase - to - Ground Fault on 500 kV Transmission Line 134
- 9.2 Single Phase - to - Ground Fault on 500 kV Transmission Line 135
- 9.3 Phase - to - Phase - to - Ground Faults 136
- 9.4 Phase - to - Phase (AB - Faults) on 500 kV Transmission Line 137
- 9.5 Effect of Fault Resistance Variations on Accuracy 139
- 9.6 Untransposed Transmission Line 141
- 9.7 Effect of Source Capacity Variations 142
- 9.8 Phasor Diagram of the Three Phase Voltages 143
- 9.9 Two Phase (AB) Fault at 0 and 45 Degrees 146
- 9.10 Phase Shift of 45° Between S and R Ends 147

Chapter 1

INTRODUCTION

1.1 FAULT LOCATION METHODS

The use of High and Extra High voltage (EHV) transmission lines, to provide bulk power to energy centres, demands high speed protection systems and accurate fault location methods, in order to be able to restore the normal operation of the power system as quickly as possible. This chapter reviews the development in the area of Fault location and methods used for estimating the exact distance to faults on EHV transmission lines based on *Digital Simulation Techniques*. Numerous research and development has been carried out in this area. In this chapter a thorough literature survey analysing the work of other researchers with due acknowledgment for the work they have conducted on fault location techniques for EHV transmission lines.

Accurate fault location methods become particularly important in modern energy systems because of the need to optimise the use of existing assets in the wake of limited resources. Such optimum usage of such important assets is the centre focus in the current restructuring of the power industry in Australia and overseas. In the deregulated power industry, emphasis will be placed on issues related to total quality management and total quality control of generation, transmission, distribution and utilisation of electrical energy. Under these circumstances, the industry will strive to get the best possible technology, to maintain the reliability of power supply , which will be the main criteria for survival.

Reliability of power supply can be affected by the way faults are detected, the speed and accuracy of detection, and more importantly, the speed of system restoration, which will have a direct effect on the credibility of the power industry. Therefore, the accurate estimation of fault location is a crucial step for minimising the time required for restoring the energy to consumers. It is this area, in which the research presented in the thesis is carried out to investigate in depth, in order to provide accurate fault location methods for EHV transmission lines under different conditions based on digital simulation techniques.

This chapter will be devoted to the analysis of the literature survey, and to briefly indicate the complete work described in each chapter of this thesis. The analysis of the literature survey is presented in the following sequence:

1. Transmission line theory: in this part, the transmission line theory based on the frequency domain method has been considered, because of its relevance to this work. This includes the surge phenomena and travelling wave solution.
2. Faulted transients in EHV transmission lines: analysis of the power system is required to determine conditions of the power system under fault to determine fault locations on the transmission lines accurately.
3. Fault locators and fault location techniques: in this part, from the published literature, attempts have been made by many authors to analyse, develop and design different schemes and principles for fault location measurement on EHV transmission lines. Such methods are studied and analysed carefully to reveal the difficulties and sources of errors encountered in the developed algorithms and the equipment based on them. This analysis was required in order to be in a position to develop accurate scheme for fault location estimation, which can

be applied for EHV transmission lines of different configurations. It will be shown later, that the developed methods for fault location estimation are based on accurate measurements and processing of system current and voltage signals at the terminations of the transmission system.

1.2 TRANSMISSION LINE THEORY AND WAVE PROPAGATION

A complete solution of the actual problem related to wave propagation in high voltage transmission lines is impossible due to the inequalities in the earth's surface and its lack of conductive homogeneity, Carson^(1, 2) has provided a solution for this problem where the actual earth is replaced by a plane homogeneous semi-infinite solid medium.

The interest in travelling waves and surge phenomena in power systems has grown considerably because of the relevance to power line carrier communication and protection⁽³⁻⁹⁾, fault location, switching of unloaded lines and recovery voltages on circuit breakers under short line fault condition.

Wedepohl⁽¹⁰⁾ has developed a general solution of the travelling-wave phenomena in polyphase systems using matrix methods. In the past, it has been customary to assume that the earth wires in a transmission system have zero potential along their entire length. An attention was drawn⁽¹¹⁾ to the fact that this assumption is valid only if the electrical length of the spacing between towers is less than one quarter wavelength.

The calculation of electrical parameters for short and long polyphase transmission lines using a representative program is given by Galloway⁽¹²⁾ for both electrically short and long lines. A typical example of the application of the program is given which compares numerical and test results. The authors

have demonstrated that there is a close agreement between measured values and those obtained by the method described in their paper.

In analysing the electrical characteristics of polyphase transmission lines⁽¹³⁾, particular emphasis was given to the proof justifying the relatively complex approach used in reference 1. This was achieved by considering the modal parameters at infinite frequency as limiting case of the general solution, and indicating that this is different from the value obtained by earlier theories using simplifying assumptions.

The theoretical formulation of a method for multi conductor transient analysis has been developed by Wedepohl and Mohammed⁽¹⁴⁾. The method combines the use of the modified Fourier transform and the steady-state theory of natural modes. The virtues of this particular formulation are that the frequency dependence of parameters can be taken into account irrespective of the complexity of the expressions defining their steady-state values. Transient analysis with special reference to non linear problems using the modified Fourier-transform and modal analysis⁽¹⁵⁾ show the generality of these methods in handling a wide range of switching problems.

Non homogeneous multi conductor transmission systems occur in a number of instances in practice, such as cross-bonded cable system. Recursive methods of analysis fail⁽¹⁶⁾ because of the amount of computation involved. In this paper the theoretical equations for the multi conductor chain matrix were developed. It was proved that the eigenvalues of the chain matrix occur in reciprocal pairs, and that the eigenvectors of the reciprocals are simply related to those of the eigenvalues.

In analysing the surge phenomena in power systems many authors have investigated the travelling wave techniques in order to evaluate the transient response numerically and in which the effect of frequency dependent parameters are taken into account(17, 18).

In these studies the transmission line behaviour is considered in terms of forward and backward response functions. Myer and Dommel(17) in particular described the numerical modelling of frequency-dependent transmission line parameters in an electromagnetic transient program (EMTP). The non zero earth resistivity leads to line parameters which vary continuously with frequency(18). Some effects of this variation on the transient waveforms on the transmission lines are examined. In this paper, the interaction of the source impedance with the frequency-dependent line impedance is shown to have an effect on the length of the line at which the resonant frequency approaches that of the supply. A possible single-phase representation of a three-phase system is explored.

A new technique for computer simulation of transients on transmission lines with frequency dependent parameters is presented by Carroll and Nozari(19). The main disadvantage of this technique, as stated by the authors, is the possible increase in programming effort necessary to handle certain types of boundary condition.

Bickford(20) has investigated the calculation of switching transients with particular reference to line energisation. He presented two methods for such calculations, ie. lumped-parameter and a second method based on lattice diagram solution of the transmission line wave equations. The author concluded that travelling-wave methods provide an accuracy suited to the system data, and a single-phase representation may be used to determine the

relative severity of over-voltages, whereas more severe conditions must be carried out using 3-phase representation, to include the mutual effects and non-simultaneous energisation of the 3-phases to be represented.

The simulation of secondary arcing is extremely important in relation to the design and planning of single-pole-switched EHV systems⁽²¹⁾. It was found that it is commonly necessary to employ arc suppression arrangements, to reduce the secondary-arc current to levels commensurate with satisfactory extinction times. The new methods developed are employed in the simulation of a 500 kV. The paper concludes by summarising the results of studies of conventionally compensated untransposed applications.

An alternative method for computing switching over-voltages in power system based on the modified Fourier transform (M. F. T.) was given by Battisson et al.⁽²²⁾.

Calculations by the (M. F. T.) of over-voltages were compared with analogue computer solutions and found in agreement. The (M. F. T.) and its numerical inverse is described and a solution for typical power system is demonstrated including source representation.

The solution of electrical transients on lumped and distributed constant circuits was presented by Ametani⁽²³⁾. The author described a newly developed travelling-wave technique, the 'refraction-coefficient method', to solve electrical transients on complicated lumped constant circuits connected to distributed lines. A paper describing a travelling-wave technique, the refraction-coefficient method⁽²⁴⁾, to solve electrical transients on complicated lumped constant circuits connected to distributed line, is considered a step forward.

The fast Fourier transform (F. F. T.) is a computational tool which facilitates signal analysis such as power spectrum analysis and filter simulation by means of digital computers, was first presented by Cochran, Cooley et. al.(25). The (F. F. T.) is a method for efficiently computing the discrete Fourier transform (D. F. T.) of a time series (discrete data samples). The efficiency of this method is such that solutions to many problems can now be obtained substantially more economically than in the past. This is the reason for the very great interest in this technique. Subsequent to this work which was carried out mainly at the Bell Telephone Laboratories, a series of papers by Sylvia J. Day, N. Mullineux and Reed(26 - 28) were published in Great Britain.

These authors were concerned with the transient response of power networks, and due to the availability of large digital computers, it was considered possible to use Fourier Transforms methods, which take into account the frequency dependence of the parameters.

Part I(26) deals with problems which arise because of the necessity of truncating the infinite range of integration. For example if the infinite integral is not reasonably convergent, Gibbs oscillations can arise in a way comparable to their occurrence in approximating infinite Fourier series by finite trigonometric series. Part II(27) deals with the problems arising from the fact that poles of the integrand of the inverse integral may lie close to the path of integration. It is shown that the modified Fourier transform can be used to move the path of integration away from the poles and hence smooth the integrand and so enable the use of a greater step length. Part III(28) describes developments in obtaining transient response using Fourier Transforms as a "Global Response". The survey of the theory developed for obtaining the transient response using Fourier Transform is given in reference 29.

If any point of particular interest appears in the global response then that particular time interval can be investigated in finer detail.

The development of the Exponential Fourier Transform (E. F. T.) and its application to electrical transients was published by Ametani⁽³⁰⁾. The author showed that E. F. T. method gives quite a high accuracy and a very long observation time with a small number of samples in comparison with a conventional numerical Fourier transform, ie. with equally spaced sampling. The E. F. T. is particularly useful when dealing with electrical transients with a very wide range of frequency to time.

1.3 FAULTED EHV TRANSMISSION LINES

Modern, large and complex power systems increasingly demand ultra low overall fault clearing times in order to quickly restore normal system operation in a stable manner. This in turn requires very high speed protection systems which for transmission lines can be achieved using modern static distance relay comparators, of which those based upon the block average technique are an example^(31 - 36) hence a minimum operating time of typically three quarters of a cycle under idealised conditions. Johns⁽³⁷⁻³⁹⁾ has indicated that due to the presence of high frequency components in the relaying signals results in a slower operation where the measurement effectively commences after a delay.

It was shown that the basic directional criteria for directional comparison protection can be violated due to travelling wave phenomena or fault occurrence approaching a voltage zero⁽³⁴⁾. A relay design is developed using digital signal processing techniques to overcome these problems. A single-pole- autoreclosure application demands reliable selection. The need to

minimise the likelihood of single-phase faults spreading to other phases requires a phase selection be accomplished in a time compatible with ultra-high-speed fault clearance⁽³⁵⁾. It is concluded with a consideration of the performance of the new phase-selector in a typical 500 kV transmission applications .

In order to develop high-speed protection systems, comprehensive studies of the nature of faulted transients were conducted using analogue and digital simulation methods. A simulation of fault waveforms based upon linearised parameters using bench models⁽³⁶⁾ often yield an adequate indication of performance in faulted power systems. However, such methods are inaccurate when considering very high speed measurements because waveforms from which measurements must be made can pass very significant travelling wave components in both faulted and healthy phase-conductors ⁽³⁷⁾.

Dynamic simulation of power systems including detailed modelling of the primary system, current transformers, capacitor voltage transformers, protection-transducer interfacing circuits and protection system based on the clock-average distance scheme is given in reference 40.

This model provides detailed dynamic response under different primary system faults on the transmission line all the way through to the final protection trip characteristic. It does not, however take into consideration the frequency variance of the line parameters, which has significant effect on digital calculation of faulted EHV transmission lines. Kothari et. al.⁽⁴¹⁾ considered the distributed nature of transmission line parameters which can be regarded as improvement as compared to the work reported in reference 40. Humpage et. al. ⁽⁴²⁾, summarised a review of methods for analysing the electromagnetic

of transmission line equations for lossy conductors and imperfect earth was given by Clayton⁽⁵²⁾.

The development of techniques for simulating faulted transients in EHV transmission lines using travelling wave methods based on frequency variance of line parameters has opened the way to implement new protection principals which was impossible before. New generation of protection and fault detection methods based on signal processing of the power system under fault conditions become realistic only because of the ability to better simulate the faulted transients. The extensive processing of transient signals and their effect on new design principles have contributed to accurate methods for fault detection and measurements of fault location which is described in the following section.

1.4 FAULT LOCATION ON EHV TRANSMISSION LINES

Early work on research and design of fault locators and fault location methods on EHV transmission lines was based on assuming lumped parameters, perfect transposition of the line and neglecting the mutual effect and the effect of adjacent lines. These assumptions have led to different designs using different principles which had one thing in common, ie. they all suffered from inaccurate measurement.

A general and unified theory on the concept of fault location as well as directional and phase selection functions, which leads to a description of protection and fault location equipment and future solutions using computers was given in a CIGRE conference⁽⁵³⁾. An overall design of line terminal equipment comprising main and back-up protection associated with the link are also described. The effect of transient errors in the equipment used those days was presented, and a new frequency modulation equipment is described.

Richards et. al.(54) have presented a fault location method by dynamic system parameters estimation for a double-end fed transmission line using a 1/4 to 1 cycle window of data at one local end only. The system differential equations are based on a lumped parameter line model, Thevenin equivalent for transients at both ends of the line and on unknown fault resistance. Simplification of the equations is obtained by using instantaneous symmetrical components.

The estimation algorithm does not require filtering of d.c. offset and high frequency components from the recorded signals and its accuracy is illustrated in digital simulation studies. The method was used for single line to earth faults, however, the authors claimed that it can be used for double and triple phase faults by appropriately altering the sequence network's interconnection.

The development of a fault locator using the one terminal voltage and current data was presented by Takagi et. al.(55). It calculates the reactance of a faulty line, with a microprocessor, using the one terminal voltage and current data of the transmission line. Errors caused by various factors such as load flow, fault resistance and the unsymmetrical arrangement of the transmission line, are automatically corrected.

A scheme for on line digital fault locator for overhead transmission line is given by Sant et. al.(56). The authors describe a digitalised on line fault locator which takes input signals from c.t.'s. and p.t.'s. and works on a reactance ratio measurement principle. It operates in less than two cycles from the instant that the relay delivers a trip output. They claimed that the locator is capable of locating transients as well as permanent short circuit faults. The authors indicated that the accuracy of the device reduces with higher than $Z_S/Z_L = 20$,

and a special compensation is required in order to increase the resistive coverage for faults on double-end feed lines.

Saha et. al.(57,58) describes a microprocessor based fault locator with remote end infeed compensation. The device uses compensation techniques for improving accuracy. Pre-fault and fault data extracted from the a.c. currents and potentials are used to compute the distance to fault. The distance is displayed in percent of the transmission line length. Remote indication and local print out of the fault information are provided. Repair and restoration of the transmission line following a fault is thus facilitated.

The parallel line effect upon accuracy is shown to be the greatest for far-end faults, because these produce the maximum parallel-line current.

A fault location scheme by Ando et. al.(59) based on evaluation of single-end fault location for two terminal HVDC transmission lines. The scheme is designed for locating faults which uses information from only one end of the line. It uses successive reflections generated by faults. Using a differentiator and smoother the slopes of the transients are computed. The best estimated peaks of the slopes for the first two consecutive transients are obtained. The time interval between these two peaks is proportional to the fault location. This method is referred to as simple passive reflectometer (SPR).

Cook(60) describes problems involved in the precise location of faults on high voltage transmission lines. The influence of the pre-fault load on the distance to fault measurement problem is analysed and a method for accounting for load effects is presented. Two of the methods given have no simplifying assumptions and their accuracy is limited by the digital impedance relay accuracy at both end of the protected circuit.

A third method is presented which requires a digital impedance relay at one end only of the transmission line.

Ibe and Cory⁽⁶¹⁾ describe the use of improved mathematical models of transmission lines to develop a fault location algorithm for multi phase power lines which copes with high frequency transients. The telegraph equations used for a line model are solved by the method of characteristics using voltage and current samples as boundary conditions taken at one end of the line within the first few milliseconds of a fault inception. Criteria for fault location are based on a formulation involving voltage and current estimates. For fault location on multi phase systems the concept of modal analysis is used in the fault locating capability of this algorithm.

Reference 61 describes a scheme, based on travelling waves, for the protection of major transmission lines. Analytical treatment, based on an ideal single-phase line, is included to indicate how the initial travelling wave propagated from a fault and a later wave resulting from a reflection at the fault position may be identified. The time interval, between the arrivals of these two waves at the transducers which would energise the protective scheme, is proportional to the distance to the fault. The work reported in reference 61) is based on the research conducted by Crossley and McLaren ⁽⁶²⁾, which did not require communication link, although such schemes did not ensure correct discrimination for all fault conditions.

Sachdev et. al.⁽⁶³⁾ describe a non-iterative technique that estimates the location of a line fault from fundamental frequency voltages and currents measured at the line terminals. Results from computer simulation of single and multi-phase faults on a 500 kV line are presented. The results shown were

found satisfactory even if fault resistances are numerically comparable to the line impedance.

Srinivasan et. al.⁽⁶⁴⁾ found that conventional fault location schemes do not take loads and their variable impedance behaviour into account. This leads to unacceptable error in the case of radial transmission lines with loads commonly found at the 120 kV and lower levels. The authors propose a method where fault distance is obtained by solving an implicit equation. The methods as applied to different faults is illustrated by simulation methods.

Kondow et. al.⁽⁶⁵⁾ describe a microprocessor based fault locator which measures the distance to a fault point by using the one terminal voltage and current data, which was originally reported in reference 55. However, the effects from asymmetrical system parameters by phase and from the distributed capacitance of a long distance transmission line constitute error factors. The authors proposed methods for compensation for various error factors in order to improve the accuracy of the proposed fault locator.

Wiszniewski⁽⁶⁶⁾ describes several random factors which affect accuracy of fault location, introducing substantial errors in measurements of the reactance between the line terminal and the fault. It is reported that the fault resistance particularly for high loads presents a significant error in the measurement of distance. The paper assumes that the reactance is determined as an imaginary part of the quotient of voltage and current fundamental harmonics, and therefore the error in transformation of the currents is relevant only as far, as it affects reproduction of the fundamental harmonic.

Johns and Jamali⁽⁶⁷⁾ describe the development of an accurate transmission line fault location equipment which has been considered to overcome problems

caused by loss of accuracy due to non linearity of fault impedance, remote infeeds, non-transposition of conductors, and change in power system source configuration. The paper reports results of simulation studies to determine the basic accuracy of the proposed method and a brief account of the fault location equipment is also given.

Jeyasurya and Rahman⁽⁶⁸⁾ presented an algorithm which is based on using the fundamental frequency current and voltage information at both line ends and by solving the sequence network of the equivalent power system, the location of the fault can be estimated. The algorithm was evaluated using a 345 kV, 160 mile transmission line.

For parallel transmission multi terminal circuits, Nagasawa et. al.⁽⁶⁹⁾ have proposed a new fault location algorithm. The method uses the magnitude of the differential currents at each terminal. It also uses an algorithm based on a 3-terminal fault location algorithm and an equivalent conversion from an n-terminal to a 3-terminal system. The authors stated the limitation of this method to be found reasonably accurate for multi-fault occurring at the same location and same time on both lines as well as for a single-fault condition. The authors have shown some results from the EMTP program. The method is particularly recommended for sub transmission systems.

Ranjbar et. al.⁽⁷⁰⁾ suggested an alternative approach towards fault location on high voltage transmission lines. The method is based upon the distributed model of transmission lines to overcome the problems encountered in traditional approaches. The new approach considers the effect of capacitance explicitly and therefore enables the detection of faults in transmission lines more precisely.

A more practical approach for fault location on teed feeders was proposed by Aggarwal et. al.⁽⁷¹⁾. The method suggested in the paper utilises fault voltages and currents at all three ends. It is stated that the method is virtually independent of fault resistance, and largely insensitive to variations in source impedance. The paper presents the basic theory of the technique which is then tested using simulation methods. From the results presented in the paper, it is clear that a good accuracy was attained. The method is based on CAD techniques, where the simulated waveforms are subjected to the same transducer/hardware errors as those encountered in practice.

For air-insulated substations, Yoshida et. al.⁽⁷¹⁾ presented a fault locating system using optical current detector. It is stated that the proposed method shortens the time required for restoration of service after the occurrence of a bus bar fault in an air-insulated distribution substation. The authors explained, that with the recent optical and electronic technologies, accurate and compact fault locating systems become available. Such fault locating system consists of optical current detectors using Faraday effect and a fault locating processor employing digital data processing technique. The fault location is made by discriminating the direction of zero-sequence currents. Through various tests and field operation of such technology, the paper states that the performance of such system has been found with "sufficient performance for practical application", and the utilisation of digital data processing enabled the fault locating processor to be compact. After a field trial of such system for 20 months, it was confirmed that the system had sufficient performance for practical application.

A technique for locating faults on transmission lines using voltage and current measurement from one end of the faulty line was presented by Youssef⁽⁷²⁾. The main feature of this technique is that it considers the influence of the

remote-end infeed of the transmission line, the effect of the transmission line capacitance, fault resistance, prefault loading conditions, and the effect of mutual coupling between different phases of the line. It is stated that the method computes with a microprocessor the distance to fault point without any approximation. It uses recorded phase voltages and currents at the near end, then the fundamental components of the measured signals are extracted using the microprocessor filters. The modal values of the extracted signals are computed then processed to indicate the precise location of the fault. Using simulation methods, the method was found accurate for all types of shunt faults.

A travelling wave based scheme for fault detection on overhead power distribution feeders was presented by El-Hami et. al.⁽⁷³⁾. The scheme is based upon detecting fault induced high frequency components on distribution lines. The method should enable the detection of discharges from the low-level breakdown of insulators, which can not be detected by conventional methods. The location of the fault is determined by appropriate signal processing of the fault generated signals on the line. Simulation results are used to illustrate the performance of the scheme on a simple radial 11 kV feeder system. The author stated that this method is independent of pre-fault loading on the system. The authors hope to conduct further work on the effect of arcs, and the application of this technique to interconnected distribution feeders, tapped transformer arrangements, and finally to design the prototype fault locator.

Gale et. al.⁽⁷⁴⁾ have proposed a fault location algorithm based on travelling waves. Several techniques for estimating the distance to fault are discussed in the paper. Field tests revealed that the so called type A method was found viable but requires computer aided analysis of the data when applied to complex networks. It was found from the tests that the travelling wave

transients can be acquired through the existing current transformers and secondary wiring thereby avoiding the high cost of specialised coupling equipment. It was stated that a hybrid scheme referred to as type AD, which is under trial, provides 'the best' situation, since it will furnish information by real faults and how they are modified as they travel along overhead lines. No assessment of the developed schemes was given, and no obvious recommendation was stated for the best application for the proposed scheme.

A CIGRE paper by Takahashi et. al.⁽⁷⁵⁾ presented the development of a substation fault location system using optical current transducers. The method identifies the section where the fault has occurred. This is achieved by detecting the fault current within air insulated substation using optical current transducers. It is further stated that the data measured by these transducers provides reliable and fast determination of fault location for the purpose of prompt and effective recovery from power failures. The system was initially introduced in 1990 and presently according to the authors, is being applied in 78 distribution substations with satisfactory results. As far as applying the same technique to transmission substations, the authors state that a fault location system for such systems has been developed and a prototype completed for field evaluation. The necessity for introducing of such a system into transmission substations is being considered on a case by case basis for each substation.

An alternative approach for protecting transmission systems with fault generated noise by Lai et. al.⁽⁷⁶⁾ employs an arrangement involving the use of conventional connected power line communication signal traps and capacitor voltage transformers. The line traps confine the higher frequency noise-generated signals to within the protected zone and the latter are captured by specially designed stack tuners via the high voltage transformer. The paper

reports the comparison of responses for results at different fault inception angles. Results on 400 kV vertically constructed transmission lines using the EMTP program, and some experimental laboratory work with some arcing faults were presented. These tests indicated that the scheme is promising.

A novel signal processing technique for fault detection and location in EHV sub transmission and transmission lines describes a method based on fault induced high-frequency components which contain information about fault distance⁽⁷⁷⁾. A decision-maker has been designed to correlate the extracted information with the system properties. The operating time is restricted to 20 ms. The algorithm presented covers a range of fault resistance, from dead fault to very high resistance fault of the order of thousand ohms including the case of a broken conductor representation.

A fault location method for extra high voltage transmission lines is described by Jihong et. al.⁽⁷⁸⁾. It states that the main feature of this method is that both distributing nature of the line parameters and the phase difference between the fault currents from the two line ends have been taken into account. The paper concluded that the zero sequence current polarised distance relay algorithm used is sufficient to give a proper initial value of iteration to avoid false locating results.

Analysis of the reviewed literature revealed that existing fault location schemes have not been able to give accurate measurements due to different assumptions being made in each instance.

In order to develop an accurate fault location scheme, the following principles must be considered:

1. Travelling wave techniques based on modal analysis should be used for analysing faulted transients on EHV transmission lines, which are based on frequency variance of the system parameters.
2. Digital signal processing using Fourier and Fast Fourier Transformer (F. F. T.) should be used.
3. Transmission line conductors non-transposition should be taken into consideration including the effect of shunt elements.
4. The non-linearity of the fault path and the effect of the remote end source infeed.
5. The setting of fault location equipment must take into account the variation in power system source impedance under different operating conditions.
6. The equipment must be capable to operate from conventional current transformers (c.t.'s), capacitor-voltage-transformers (c.v.t.'s) and/or potential transformers (p.t.'s).
7. The mutual effect of the adjacent parallel lines on the computation of faults should be taken.

The work described in this thesis presents digital simulation techniques for the analysis for accurate fault location estimation methods based on the principles described above as applied to two and three terminal transmission systems^(79,81). These methods are further been developed to provide accurate fault location for shunt compensated EHV transmission lines.

1.5 THESIS OBJECTIVES

The research work carried out in this thesis centres on the development and analysis of efficient techniques for accurate fault location estimation on EHV transmission lines using digital simulation techniques. The research objective was to investigate the advantages, disadvantages and limitations of such methods, in order to pave the way for the development of highly accurate fault location algorithms for EHV transmission lines.

To conduct research on sensible and highly accurate algorithms for estimating the distance to fault accurately, a thorough analysis and studies of the theory of transmission lines, with particular interest in solutions in the frequency domain, was carried out. Apart from the need of a deep knowledge of sophisticated mathematical and computational skills, power system phenomena under steady-state and transient operating conditions was studied in detail.

Since the majority of modern fault locators are based on digital signal processing, a good knowledge of this area was eminent. Analysis of power system signal derivation, signal shaping, signal filtering and signal processing constitutes an essential part of modern fault locators, particularly those employing digital technology and microprocessors.

During the course of this research, a large amount of computation requiring the development of efficient computer programs for the calculation of transmission line parameters, modal analysis, steady-state and transient analysis, calculation of fault location for a single phase system, calculation of fault location on EHV transmission lines for three phase configurations on two and three terminal EHV transmission systems. In addition, numerous auxiliary^(82 - 86) computations for different mathematical manipulations⁽⁸⁷⁾ such as matrix

algebra, eigenvalue and eigenvectors calculations was developed and used. In order to test the developed algorithm, the knowledge of using the well known Electromagnetic Transient Program, the PC version of it (ATP)⁽⁸⁸⁾, was required. Generation of the steady-state faulted transmission system currents and voltages, for providing the necessary signal phasors required in the fault location algorithm, was achieved by simulating the power system models for use in the ATP computer program.

As it is described in this chapter, the extensive literature survey was carried out first, in order to give due acknowledgment and consideration to the previous work in the area of fault location techniques and methods. The survey was carried out with a focus centred on the disadvantages and advantages of existing techniques and designs, in order to be able to contribute to the improvement and development of efficient and accurate fault location algorithms. The methodologies followed in the research work described in this thesis, provide a solid foundation for the practical design of an accurate fault locator for EHV transmission lines, based on digital technology and modern signal processing using microprocessors.

Since the fault location techniques are developed for EHV transmission lines, chapter 2 provides analysis of polyphase transmission lines in details. The analysis is shown for calculating transmission line parameters⁽¹²⁾. The calculation of such parameters accurately is very important for conducting power system calculations such as short circuit analysis, load flow studies, stability studies, protection settings, harmonic analysis, and switching and lightning effects in power systems. The computation of the basic per unit length series impedance and shunt admittance matrices, the positive, negative and zero sequence impedances of a single and double circuits, propagation parameters, natural modes of propagation was used extensively in this research

as part of the computation procedure for estimating the accurate distance to fault.

The analysis of the steady-state phenomena of EHV transmission lines is given in chapter 3. In this chapter, the analysis are developed for a simple single and double wire transmission circuits, which is then extended to include multi phase transmission lines. Steady-state parameters of the line are required for the frequency under consideration as part of the total solution of the primary system. The calculation of transmission line voltages and currents, and the propagation parameters are given. The theory of two port network is described for calculating the sending end and receiving end voltages and currents. The simulation of the faulty transmission line in the form of two port network is given.

Chapter 4 describes the calculation of the system parameters. This includes the representation of the source impedances in terms of their associated fault GVA. Different source strengths between 5-35 GVA are considered. As far as the transmission line representation is concerned, the main configuration used in various studies in this work is the 500 kV, horizontal structure, 384 km length line. The other structure used is the double circuit 500 kV line with two earth wires, vertical configuration with even distribution. The calculated parameters for both these line are given. Finally, chapter 4 presents the calculation of shunt reactors used for shunt compensation^(89, 90) of the reactive power generated by the transmission line. The amount of compensation for the positive and zero sequence components is shown.

The development of the fault location algorithm for two terminal transmission lines is given in chapter 5. Analysis of the algorithm and its implementation for accurate fault location measurement is described under different conditions.

The analysis is first developed for a single phase line, which then extended for multi phase transmission circuits. The analysis is based on modal parameters derived from system phase quantities, using the eigenvalues and eigenvectors theory⁽¹⁰⁾.

Chapter 6 describes the development of the fault location algorithm for shunt compensated EHV transmission lines. The author has not come across any work published, for assessing the fault locators for compensated transmission lines. The effect caused by the shunt compensating reactors on the developed fault location algorithm is carried out in details in chapter six, with different studies on such arrangements given later in chapter 9.

The reactors used for compensation are connected to both ends of the transmission line, for a typical compensation of 75% for the positive phase sequence. The reactor used in the development is a typical 4-legged reactor scheme⁽⁸⁹⁾. Under normal loading conditions, shunt reactors are usually disconnected. When the line is lightly loaded, the transmission line becomes a generator of a large amount of reactive power. Under these conditions, the connection of shunt reactor is very effective, and in fact will improve the flexibility of the power flow in the transmission circuit. It is shown in the studies conducted, that the fault location algorithm functions correctly when the shunt reactors are connected.

Chapter 7 provides full analysis of the fault location algorithm for three terminal EHV teed feeders^(80, 91). The effect of the variation of source impedances, tee line length, fault location, and different types of balanced and unbalanced faults are presented. The analysis are carried out in order to examine the accuracy of the developed algorithm for the three terminal system.

In chapter 8, the voltage and current response in multi phase systems is given. The studies include different source GVA, transmission line configurations, pre-fault line loading, point on wave of fault inception, type of fault and fault location along the transmission line. System simulation as described in chapter 4, has been modelled on the electromagnetic transient program. Studies for deriving wave forms under different system operating conditions are carried out in order to show the behaviour of the primary system under steady-state and transient conditions.

In Chapter 9 the analysis and testing of the developed fault location algorithms are given. It is shown that the accuracy of the fault locator varies depending on the location of the fault. The most accurate results are obtained for faults approaching the middle of the line, and the highest errors are reflected in the studies for faults at the termination of the transmission line. The estimated errors in the measurements of fault location are given graphically as a function of the line length, and discussed in chapter 10.

Chapter 10 of this thesis provides the general conclusions which are derived from the investigations carried out in this research. The chapter provides suggestions for future work on fault location methods.

Chapter 2

ANALYSIS OF POLYPHASE TRANSMISSION LINES

2.1 INTRODUCTION

For any configuration of a transmission line, before any type of calculation is carried out, it is required to calculate accurately the parameters of the line. In this chapter, the calculation of circuit parameters is derived for a single or double circuits transmission lines. The effect of the earth and earth wires is included in the derived algorithms. The method followed is based on an early work as described in reference 12.

2.2 BASIC CONSIDERATIONS

In power systems, the calculation of line parameters are necessary for many studies; some are listed below:

a) Short circuit calculations; load flow analysis; steady-state and transient stability studies; protection settings; harmonic analysis and quality of power supply. Such studies require the calculation of line parameters at the power frequency and some other harmonics.

b) Radio-TV interference; power line carrier signal transmission; switching and lightning effects; behaviour of protection systems and relays under transient conditions, which require the evaluation of the parameters at frequencies ranging from few hertz to a few hundred MHz

Calculating line parameters in power systems for the above purposes is very important, particularly this is essential in modern power systems; to secure reliable system design, planning and operation. The parameters which are required for the above studies in power systems are:

- i) the basic per unit length series impedance and shunt admittance matrices;
- ii) the positive, negative and zero sequence impedances of single and/or double circuit lines and associated inter phase and inter circuit mutual couplings;
- iii) the propagation parameters such as the characteristic impedance, natural modes of propagation and their attenuation and velocity etc.
- iv) the exact equivalent π - network of line sections of different lengths.

With the availability of high speed digital computers, there is no longer a need to compromise accuracy of calculations for easy and approximate formulae. The use of the commonly applied technique based on GMD/GMR⁽⁸⁶⁾, which neglect some important factors for the sake of achieving simplicity in calculation, is not necessary any more. This is mainly due to the fact that such technique makes some other parameters meaningless and therefore impossible to derive.

In deriving the algorithms for accurately calculating the line parameters, the following basic and practical considerations will be taken into account:

- i) conductor stranding and the skin effects in them;

- ii) variable current penetration return path with finite conductivity and its contribution parameters as given by Carson's infinite series which is found to contribute as much as 40% of the values under ideal conditions even at power frequency (1);
- iii) proximity of aerial earth wires;
- iv) mutual couplings of a second circuit on the same tower or nearby circuits;
- v) unsymmetrical conductor placing at different height on the same tower with or without transposition.

2.3 LINE SERIES IMPEDANCE MATRIX

In the derivation, it will be assumed that the lines lengths are very much greater than the spacings between the conductors and the ground surface. The series impedance are defined in terms of quantities per unit length (ohm/km).

Considering a 3 conductor line shown in Fig. 2.1, the voltage drops V_1 , V_2 and V_3 along 1 m length of the line.

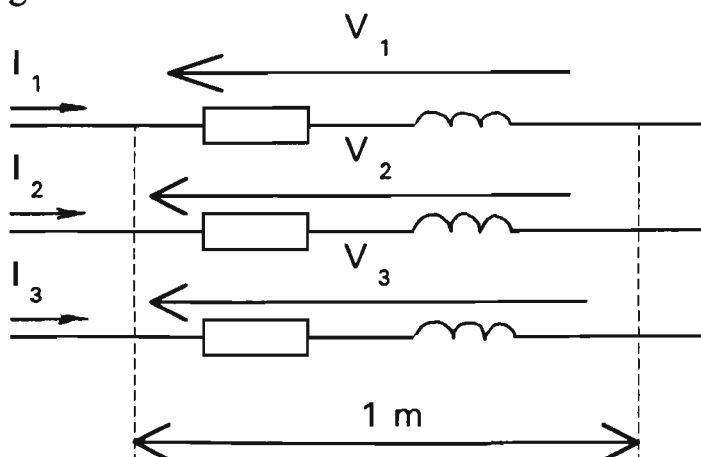


Fig. 2.1: Transmission line section

are related to the currents I_1 , I_2 and I_3 that the flow in the series circuit of the line by:

$$\begin{bmatrix} V_1 \\ V_2 \\ V_3 \end{bmatrix} = \begin{bmatrix} Z_{11} & Z_{12} & Z_{13} \\ Z_{21} & Z_{22} & Z_{23} \\ Z_{31} & Z_{32} & Z_{33} \end{bmatrix} \cdot \begin{bmatrix} I_1 \\ I_2 \\ I_3 \end{bmatrix} \quad (2.1)$$

In condensed matrix form:

$$[V] = [Z] \cdot [I] \quad (2.2)$$

Where, $[Z]$ is defined as the series impedance matrix of the line per unit length, $[V]$ is the vector of series voltage drops, and $[I]$ is the vector of series conductor currents. Equations (2.1) and (2.2) are valid irrespective of whether the voltages V_1, V_2, V_3 and the currents I_1, I_2, I_3 are balanced or unbalanced. For an n number of conductor line $[Z]$ is a symmetric ($n \times n$) matrix.

In equation (2.2), the $[Z]$ matrix can be resolved into three components, ie., $[Z_g]$, $[Z_e]$ and $[Z_c]$, so that:

$$[Z] = [Z_g] + [Z_e] + [Z_c] \quad (2.3)$$

$[Z_g]$ is purely reactive matrix and is due to the flux external to the conductors, assuming a ground of infinite conductivity.

The (i,j) th element of $[Z_g]$ (Fig. 2.2), is given by:

$$Z_g(i, j) = (j\omega\mu_0 / 2 \cdot \pi) \cdot \ln(D_{ij} / d_{ij}) \Omega / m$$

where d_{ij} = distance between the i^{th} conductor and the j^{th} conductor for $i \neq j$
 d_{ii} = external radius of the i^{th} conductor for $i = j$, and in the case of
the bundled conductors, the geometric mean radius (GMR)
of the bundle.

D_{ij} = distance between the i^{th} conductor and the image of the j^{th}
conductor on the ground surface. In the above arrangement, it is
assumed that conductor coordinates with respect to ground
surface as x - axis, and centre line of the tower as y - axis.

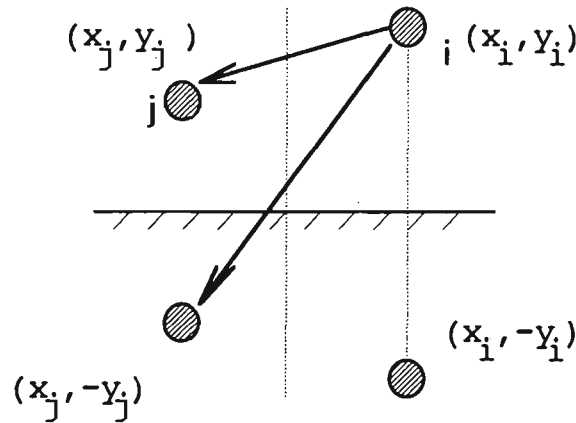


Fig. 2.2: Schematic diagram of conductors.

The $[Z_e]$ component is a full matrix with resistive and reactive elements. This is due to finite conductivity of the ground, and is known as the impedance of the earth return path. The (i,j) element of the $[Z_e]$ matrix is given by the infinite integral equation (1):

$$Z_e(i, j) = (j\omega\mu_0 / \pi) \int_{\beta=0}^{\infty} \frac{\cos((x_i - x_j)\beta) \cdot \exp(-\beta(y_i - y_j))}{(\beta + \sqrt{\beta^2 + j\omega\mu\nabla})} d\beta \quad (2.4)$$

where (x_i, y_i) and (x_j, y_j) are the coordinates of conductor i and conductor j ; $\nabla =$ conductivity of soil in $\Omega\text{-m}$; $\beta =$ integration parameter varying from zero to infinity. Analytical solution of this integral gives Bessel function (10).

The last component in equation (2.3), ie. $[Z_c]$ is a diagonal matrix with both resistive and reactive components, and is due to the impedance of the conductor itself.

It is common to use the manufacturers' values at power frequency⁽⁹¹⁾. The resistance r_c of a conductor is usually given in ohm/km; but the internal reactance of the conductors is given indirectly by means of the geometric mean radius (GMR) of the conductors⁽⁸⁶⁾.

The conductor internal impedance is calculated from the formula:

$$X_c = \frac{\ln(r / GMR)}{j\omega 2 \pi \mu_0} \quad \Omega / m \quad (2.5)$$

where r = external radius of the conductor

GMR = geometric mean radius of the conductor

For bundled conductors, the conductor internal resistance and reactance are derived by the number of conductors in a bundle⁽⁸⁶⁾.

2.4 SHUNT ADMITTANCE MATRIX

Capacitance of EHV transmission lines is the result of the potential difference between conductors; it causes them to be charged in the same manner as the plates of a capacitor when there is a potential difference between them. The

capacitance between conductors is the charge per unit of potential difference. Capacitance between parallel conductors is a constant depending on the size and spacing of the conductors.

In case of three conductor transmission line shown in Fig. 2.3, when the conductors 1, 2 and 3 are at potentials V_1 , V_2 and V_3 with respect to the ground, there are shunt currents i_1 , i_2 and i_3 . These currents are different from the series load currents which were considered in the pervious section. These currents and voltages are related by the matrix equation:

$$\begin{bmatrix} i_1 \\ i_2 \\ i_3 \end{bmatrix} = \begin{bmatrix} Y_{11} & Y_{12} & Y_{13} \\ Y_{21} & Y_{22} & Y_{23} \\ Y_{31} & Y_{32} & Y_{33} \end{bmatrix} \begin{bmatrix} V_1 \\ V_2 \\ V_3 \end{bmatrix} \quad (2.6)$$

or in condensed form: $[i] = [Y].[V]$ (2.7)

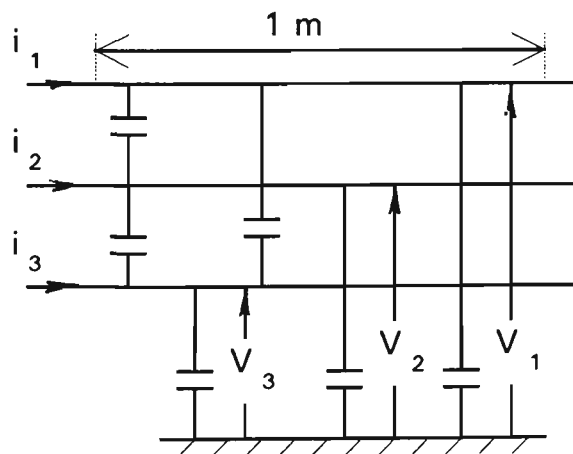


Fig. 2.3: One section representation

In equation (2.6), $[Y]$ is a symmetric matrix and is defined as the shunt admittance matrix of the line per unit length. This equation is valid for both

balanced and unbalanced conditions. The [Y] matrix can be expressed as follows:

$$[Y] = j \cdot \omega \cdot 2 \cdot \pi \cdot \epsilon_0 \cdot [B]^{-1} \quad (2.8)$$

The (i,j) element of [B] is given by:

$$B(i, j) = \ln(D_{ij} / d_{ij}) \quad (2.9)$$

The error due to finite conductivity of soil is so small that the [Y] matrix is not usually corrected for the effect of non-ideal ground.

2.5 EFFECT OF AERIAL GROUND WIRES

In case of the presence of aerial ground wires, they are first considered as additional phase conductors and the entire Z and Y matrices are formed. Consider the configuration of a three phase transmission line, the matrix equation relating voltages of the five conductors to their corresponding voltage drops are as follows:

$$\begin{bmatrix} V_1 \\ V_2 \\ V_3 \\ V_4 \\ V_5 \end{bmatrix} = \begin{bmatrix} Z_{11} & Z_{12} & Z_{13} & Z_{14} & Z_{15} \\ Z_{21} & Z_{22} & Z_{23} & Z_{24} & Z_{25} \\ Z_{31} & Z_{32} & Z_{33} & Z_{34} & Z_{35} \\ Z_{41} & Z_{42} & Z_{43} & Z_{44} & Z_{45} \\ Z_{51} & Z_{52} & Z_{53} & Z_{54} & Z_{55} \end{bmatrix} \begin{bmatrix} I_1 \\ I_2 \\ I_3 \\ I_4 \\ I_5 \end{bmatrix} \quad (2.10)$$

or in condensed form:

$$\begin{bmatrix} V_c \\ V_e \end{bmatrix} = \begin{bmatrix} Z_{cc} & Z_{ce} \\ Z_{ec} & Z_{ee} \end{bmatrix} \begin{bmatrix} I_c \\ I_e \end{bmatrix} \quad (2.11)$$

Because of the fact that conductors 4 and 5 are earthed, $V_4 = 0$ and $V_5 = 0$, which means that $[V_e] = 0$. Solving in equation (2.11) for V_c , when substituting for $V_e = 0$, the following is derived:

$$[0] = [Z_{ec}] \cdot [I_c] + [Z_{ee}] \cdot [I_e] \quad (2.12)$$

$$[I_e] = -[Z_{ee}]^{-1} \cdot [Z_{ec}] \cdot [I_c] \quad (2.13)$$

In the same way, $[V_c]$ can be described as follows:

$[V_c] = [Z_{cc}] \cdot [I_c] + [Z_{ce}] \cdot [I_e]$; and considering equation (2.13) will result in:

$$[V_c] = ([Z_{cc}] - [Z_{ce}][Z_{ee}]^{-1} \cdot [Z_{ec}]) \cdot [I_c] \quad (2.14)$$

Equation (2.14) indicates that earth wire effects are taken into consideration by modifying the full $[Z]$ matrix to give a new equivalent impedance of a 3x3 dimension as follows:

$$[Z_{eq}] = [Z_{cc}] - [Z_{ce}] \cdot [Z_{ee}]^{-1} \cdot [Z_{ec}] \quad (2.15)$$

Similar analysis for shunt currents will reveal the following:

$$\begin{bmatrix} i_1 \\ i_2 \\ i_3 \\ i_4 \\ i_5 \end{bmatrix} = \begin{bmatrix} Y_{11} & Y_{12} & Y_{13} & Y_{14} & Y_{15} \\ Y_{21} & Y_{22} & Y_{23} & Y_{24} & Y_{25} \\ Y_{31} & Y_{32} & Y_{33} & Y_{34} & Y_{35} \\ Y_{41} & Y_{42} & Y_{43} & Y_{44} & Y_{45} \\ Y_{51} & Y_{52} & Y_{53} & Y_{54} & Y_{55} \end{bmatrix} \cdot \begin{bmatrix} V_1 \\ V_2 \\ V_3 \\ V_4 \\ V_5 \end{bmatrix} \quad (2.16)$$

or in condensed form:

$$\begin{bmatrix} i_c \\ i_e \end{bmatrix} = \begin{bmatrix} Y_{cc} & Y_{ce} \\ Y_{ec} & Y_{ee} \end{bmatrix} \cdot \begin{bmatrix} V_c \\ V_e \end{bmatrix} \quad (2.17)$$

The potential of the earth is zero, ie., $[V_e] = 0$, hence:

$$[i_c] = [Y_{cc}][V_c], \text{ where in this case } [Y_{eq}] = [Y_{cc}]$$

which means that the effect of aerial wires is accounted for by forming the full Y matrix as explained in section 2.4 of this chapter. By eliminating the rows and columns corresponding to the earth wires, ie. 4 and 5, the above example gives a 3 x 3 equivalent shunt admittance. In spite of the fact that a line with three phase wires and two earth wires is considered in the above described case, the same procedure can be applied to any line with any number of phase conductors and earth wires to formulate the equivalent impedance and admittance matrices.

2.6 ELECTRICALLY SHORT LINES

In this section a method for calculating the derived parameters for electrically short lines is given. The method is based on symmetrical components,

assuming conductor symmetry. To simplify analysis for some problems, the phase voltages V_a , V_b , V_c , and the currents I_a , I_b , I_c are transformed into another set of quantities known as symmetrical components, using linear transformation. The new quantities $[V_{012}]$ are obtained by transforming the phase quantities $[V_{abc}]$, ie.;

$$[V_{012}] = [T]^{-1} \cdot [V_{abc}] \quad (2.18)$$

and for the currents:

$$[I_{012}] = [T]^{-1} \cdot [I_{abc}] \quad (2.19)$$

and using the transformation matrix we can write:

$$[V_{abc}] = [T] \cdot [V_{012}] \quad (2.20)$$

and:

$$[I_{abc}] = [T] \cdot [I_{012}] \quad (2.21)$$

The transformation matrix $[T]$ is defined as:

$$[T] = \begin{bmatrix} 1 & 1 & 1 \\ 1 & a^2 & a \\ 1 & a & a^2 \end{bmatrix} \quad (2.22)$$

and

$$[T]^{-1} = \frac{1}{3} \begin{bmatrix} 1 & 1 & 1 \\ 1 & a & a^2 \\ 1 & a^2 & a \end{bmatrix} \quad (2.23)$$

in the above equations the vector $a = 1 \angle 120^\circ$.

It is now clear that equations 2.1 and 2.8 above, can be transformed from phase quantities into symmetrical components using similar technique, ie. :

$$[V_{abc}] = [Z_{abc}] \cdot [I_{abc}] \quad (2.24)$$

and:

$$[i_{abc}] = [Y_{abc}] \cdot [V_{abc}] \quad (2.25)$$

These are transformed into symmetrical component quantities as follows:

$$[V_{012}] = [Z_{012}] \cdot [I_{012}] \quad (2.26)$$

and

$$[i_{012}] = [Y_{012}] \cdot [V_{012}] \quad (2.27)$$

where:

$$[Z_{012}] = [T]^{-1} \cdot [Z_{abc}] \cdot [T] \quad (2.28)$$

$$\text{and } [Y_{012}] = [T]^{-1} \cdot [Y_{abc}] \cdot [T] \quad (2.29)$$

It is important to note that when the sequence impedance and admittance matrices $[Z_{012}]$ and $[Y_{012}]$ are diagonal matrices, the symmetrical components become mutually independent, and therefore resolve mutually dependent phase voltages and currents into mutually independent symmetrical component voltages and currents. Furthermore, $[Z_{012}]$ and $[Y_{012}]$ become diagonal only and only when $[Z_{abc}]$ and $[Y_{abc}]$ are balanced.

For three-phase transmission lines, $[Z_{abc}]$ is said to be balanced if it takes the form

$$[Z_{abc}] = \begin{bmatrix} Z_s & Z_m & Z_m \\ Z_m & Z_s & Z_m \\ Z_m & Z_m & Z_s \end{bmatrix} \quad (2.30)$$

for which:

$$[Z_{012}] = \begin{bmatrix} Z_s + 2Z_m & 0 & 0 \\ 0 & Z_s - Z_m & 0 \\ 0 & 0 & Z_s - Z_m \end{bmatrix} \quad (2.31)$$

or:

$$[Z_{012}] = \begin{bmatrix} Z_0 & 0 & 0 \\ 0 & Z_1 & 0 \\ 0 & 0 & Z_2 \end{bmatrix} \quad (2.32)$$

From equation 2.31, we can write: $Z_0 = Z_s + 2Z_m$, $Z_1 = Z_s - Z_m$, and $Z_2 = Z_s - Z_m$, which are defined as the zero, positive and negative sequence impedances respectively. Similar definitions can be derived for zero, positive and negative sequence admittances.

In spite of the fact that symmetrical component method is widely used, it is important to note that such method becomes powerful only when the three phase network is balanced but the terminal conditions may or may not be balanced. There is no advantage in symmetrical component method if the network itself is unbalanced, in which case direct solution in term of phase quantities becomes simpler. Therefore, it is necessary to stress that whenever a sequence quantity of a line or a component of a network is referred to, *it is implicitly assumed that the line or the component is balanced*. This applies even if the lines are regularly transposed, when their sequence impedances and admittances are referred to, they are assumed to be regularly transposed.

2.6.1 Single Circuit Transmission Line

In case of fully transposed lines, the $[Z_{abc}]$ matrix becomes balanced. Considering equations (2.1) and (2.29), it is evident that:

$$Z_s = (Z_{11} + Z_{22} + Z_{33}) / 3 \quad (2.33)$$

$$Z_m = (Z_{12} + Z_{13} + Z_{23}) / 3 \quad (2.34)$$

where zero sequence impedance:

$$Z_0 = Z_s + 2Z_m \quad (2.35)$$

and the positive sequence impedance is:

$$Z_1 = Z_s - Z_m \quad (2.36)$$

and negative sequence impedance is:

$$Z_2 = Z_s - Z_m \quad (2.37)$$

Following the same procedure as above, similar equations for the sequence admittances can be derived.

2.6.2 Double circuit Transmission Line

A typical configuration for a double circuit transmission line and its equivalent circuit is given in Figs. 2.4 and 2.5.

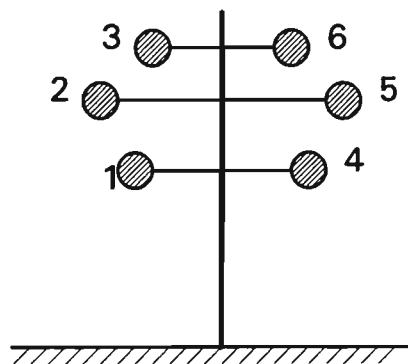


Fig. 2.4: Double circuit line

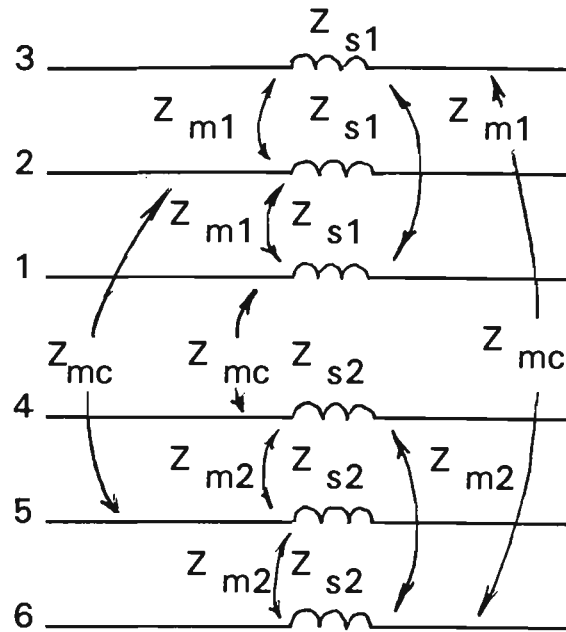


Fig. 2.5: Double circuit line equivalent circuit.

The basic impedance matrix of a double circuit transmission line is of a 6 x 6 dimension. Assuming a complete transposition both within individual circuits and between both circuits, a perfectly balanced circuit results as shown in Fig. 2.6 for a single circuit and 2.8 for a the double circuit respectively.

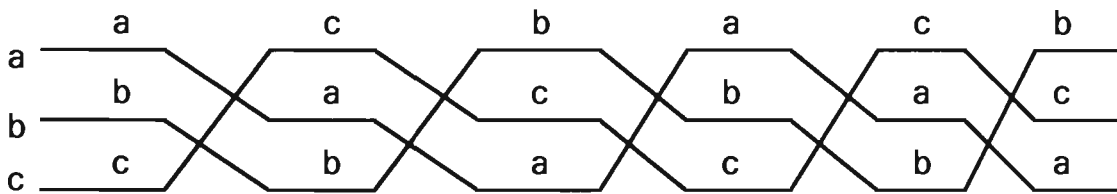


Fig. 2.6: Single circuit transposition

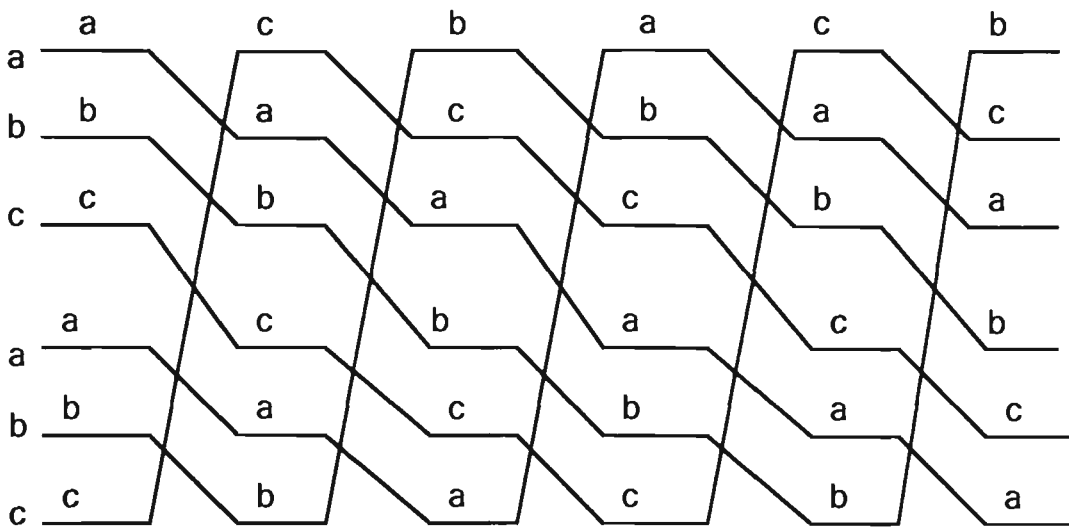


Fig. 2.7: Double circuit transposition.

For double circuit transmission line, the basic equivalent impedance is a 6 x 6 matrix. Assuming a complete transposition both within individual circuit and between both circuits; perfectly balanced circuit will result as shown in Fig. 2.7. In this case, the corresponding $[Z]$ and $[Y]$ matrices will take the following forms:

$$[Z] = \begin{bmatrix} Z_{s1} & Z_{m1} & Z_{m1} & Z_{mc} & Z_{mc} & Z_{mc} \\ Z_{m1} & Z_{s1} & Z_{m1} & Z_{mc} & Z_{mc} & Z_{mc} \\ Z_{m1} & Z_{m1} & Z_{s1} & Z_{mc} & Z_{mc} & Z_{mc} \\ Z_{mc} & Z_{mc} & Z_{mc} & Z_{s2} & Z_{m2} & Z_{m2} \\ Z_{mc} & Z_{mc} & Z_{mc} & Z_{m2} & Z_{s2} & Z_{m2} \\ Z_{mc} & Z_{mc} & Z_{mc} & Z_{m2} & Z_{m2} & Z_{s2} \end{bmatrix} \quad (2.38)$$

and

$$[Y] = \begin{bmatrix} Y_{s1} & Y_{m1} & Y_{m1} & Y_{mc} & Y_{mc} & Y_{mc} \\ Y_{m1} & Y_{s1} & Y_{m1} & Y_{mc} & Y_{mc} & Y_{mc} \\ Y_{m1} & Y_{m1} & Y_{s1} & Y_{mc} & Y_{mc} & Y_{mc} \\ Y_{mc} & Y_{mc} & Y_{mc} & Y_{s2} & Y_{m2} & Y_{m2} \\ Y_{mc} & Y_{mc} & Y_{mc} & Y_{m2} & Y_{s2} & Y_{m2} \\ Y_{mc} & Y_{mc} & Y_{mc} & Y_{m2} & Y_{m2} & Y_{s2} \end{bmatrix} \quad (2.39)$$

where Z_{s1} = self impedance of phase conductors in circuit # 1

Z_{s2} = self impedance of phase conductors in circuit # 2

Z_{m1} = interphase mutual impedance of circuit # 1

Z_{m2} = interphase mutual impedance of circuit # 2

Z_{mc} = inter circuit mutual impedance between circuits # 1 and # 2

and Y_{s1} = self admittance of phase conductors in circuit # 1

Y_{s2} = self admittance of phase conductors in circuit # 2

Y_{m1} = interphase mutual admittance of circuit # 1

Y_{m2} = interphase mutual admittance of circuit # 2

Y_{mc} = inter circuit mutual admittance between circuits # 1 and # 2

When applying the symmetrical component transformation given in equations 2.27 and 2.28, it can be established that the positive and negative sequence parameters of circuit # 1 are not affected by the proximity of circuit # 2 and vice versa. However, the zero sequence parameters are affected by the inter circuit mutual coupling.

$$Z_1^1 = Z_2^1 = Z_{s1} - Z_{m1} = \text{positive and negative sequence impedance of circuit \# 1.}$$

$$Z_1^2 = Z_2^2 = Z_{s2} - Z_{m2} = \text{positive and negative sequence impedance of circuit \# 2.}$$

$$Z_0^1 = Z_{s1} - 2Z_{m1} = \text{zero sequence impedance of circuit \# 1.}$$

$$Z_0^2 = Z_{s2} - 2Z_{m2} = \text{zero sequence impedance of circuit \# 2.}$$

Z_{01} and Z_{02} are defined by ignoring the proximity of the other circuit. Let V_{11}, V_{12}, V_{10} and I_{11}, I_{12}, I_{10} be the positive, negative and zero sequence voltages and currents respectively of circuit # 1 and let V_{21}, V_{22}, V_{20} and I_{21}, I_{22}, I_{20} be the positive, negative and zero sequence voltages and currents respectively of circuit # 2. It is possible to write the following relationships.

$$V_1^1 = Z_1^1 \cdot I_1^1 \quad (2.40)$$

and

$$V_2^1 = Z_2^1 \cdot I_2^1 \quad (2.41)$$

In equations (2.39) and (2.40), it is clear that the positive and negative sequence voltages of circuit # 1 are not affected by currents in circuit # 2. However, the zero-sequence voltages induced in circuit #1 and # 2 are affected by the inter circuit coupling as given in the following relationships:

$$V_0^1 = Z_0^1 + 3Z_{mc} I_0^2 \quad (2.42)$$

and

$$V_0^2 = Z_0^2 I_0^2 + 3Z_{mc} I_0^1 \quad (2.43)$$

In case when both circuit are *operating in parallel* and transposition of conductors across the two sides of the tower is also assumed, *the effective* positive, negative and zero-sequence impedance *per circuit* are given by:

$$Z_1 = Z_2(Z_1^1 + Z_1^2)/2 \quad \Omega/m/\text{circuit} \quad (2.44)$$

$$Z_0 = (Z_0^1 + Z_0^2)/2 + 3Z_{mc} \quad \Omega/m/\text{circuit} \quad (2.45)$$

2.7 PROPAGATION PARAMETERS

For long transmission lines, the representation of the line can be defined in a different way. As it was explained in chapter 2, let $[P] = [Z].[Y]$ and let $\lambda_1, \lambda_2, \dots, \lambda_n$ be the n eigenvalues of the $n \times n$ matrix P . Let Q_1, Q_2, \dots, Q_n be the n number of linearly independent $n \times 1$ eigenvectors of the matrix P corresponding to the eigenvalues.

The eigenvalues λ_i are assembled diagonally to form an $(n \times n)$ diagonal matrix $[\lambda]$. The n eigenvectors are also assembled in the same order as the corresponding eigenvalues to form an $(n \times n)$ matrix $[Q]$. This means, for 3 conductor transmission line:

$$[\lambda] = \begin{bmatrix} \lambda_1 & 0 & 0 \\ 0 & \lambda_2 & 0 \\ 0 & 0 & \lambda_3 \end{bmatrix} \quad (2.46)$$

and

$$[Q] = \begin{bmatrix} Q_{11} & Q_{12} & Q_{13} \\ Q_{21} & Q_{22} & Q_{23} \\ Q_{31} & Q_{32} & Q_{33} \end{bmatrix} \quad (2.47)$$

It can be shown⁽¹⁰⁾ that:

$$[Q].[P].[Q]^{-1} = [\lambda] \quad (2.48)$$

The columns of $[Q]$ (ie. the eigenvectors) are called the natural modes distributions of voltages on the line conductors and the corresponding eigenvalues give the *natural mode propagation constants* $\gamma_1, \gamma_2, \gamma_3$ by the relationships:

$$\gamma_1 = \sqrt{\lambda_1}, \gamma_2 = \sqrt{\lambda_2}, \gamma_3 = \sqrt{\lambda_3} \quad (2.49)$$

In general, the propagation constants are complex quantities which can be expressed as follows:

$$\gamma_1 = \alpha_1 + j\beta_1, \gamma_2 = \alpha_2 + j\beta_2, \gamma_3 = \alpha_3 + j\beta_3 \quad (2.50)$$

where: $\alpha_1, \alpha_2,$ and α_3 are called the attenuation constants (nepers/m) and β_1, β_2 and β_3 are called the phase shift constants (radian/m) of the natural modes 1, 2 and 3 respectively. The natural mode velocities are, of course, given by:

$$C_1 = w / \beta_1; C_2 = w / \beta_2 \text{ and } C_3 = w / \beta_3 \quad (2.51)$$

For currents, similar natural distribution matrix S exists such that:

$$S = Q_t^{-1} \quad (2.52)$$

The propagation constants of current modes are the same as those of voltage modes. The characteristic impedance of transmission lines is defined as:

$$[Z_o] = [Q].[Q]^{-1} \cdot [Z].[Q_t]^{-1} \quad (2.53)$$

The natural mode characteristic impedance matrix $[Z_o]$ is a diagonal matrix given by:

$$[Z_o] = [\gamma]^{-1} \cdot [Q]^{-1} \cdot [Z].[Q_t]^{-1} \quad (2.54)$$

It is useful to note that a function of a matrix $[P]$, $f([P])$ can be evaluated readily by using the relationship:

$$f([P]) = [Q^{-1}] \cdot f([\lambda]) \cdot [Q] \quad (2.55)$$

A function of a diagonal matrix is simply obtained by:

$$f([\lambda]) = \begin{bmatrix} f(\lambda_1) & 0 & 0 \\ 0 & f(\lambda_2) & 0 \\ 0 & 0 & f(\lambda_3) \end{bmatrix} \quad (2.56)$$

As an example, the exponential function of matrix $[P]$ is:

$$\exp[P] = [Q]^{-1} \begin{bmatrix} e^{\lambda_1} & 0 & 0 \\ 0 & e^{\lambda_2} & 0 \\ 0 & 0 & e^{\lambda_3} \end{bmatrix} \cdot [Q] \quad (2.57)$$

The above relationship together with the eigenvalues and eigenvectors obtained can be readily used to compute all the derived parameters of transmission lines.

2.8 REPRESENTATION OF LONG TRANSMISSION LINES

In the previous sections, the parameters $[Z]$ and $[Y]$ are distributed and expressed in per unit length. For lines of length ℓ , the line can be represented by a π -network as shown in Fig. 2.8.

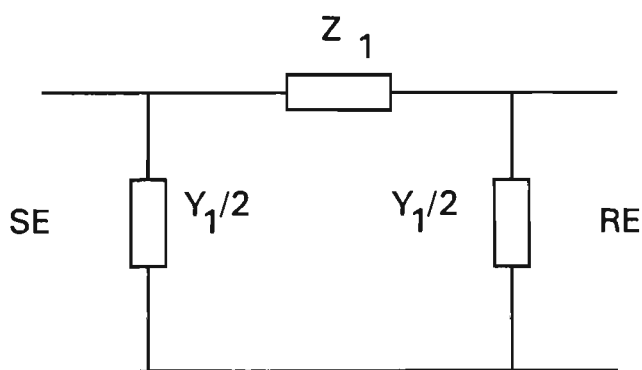


Fig. 2.8 : Equivalent π representation of the line

The above representation gives accurate results for 50 Hz lines of up to about 100 km. In case of longer lines, the lumping of parameters leads to errors. However, an equivalent π network can be derived between the sending end (SE) and the receiving end (RE) as shown in Fig. 2.9.

For the circuit shown in Fig. 2.10, the following definitions are applied:

$$Z_{SR} = Z_0 \cdot \sinh(\gamma \cdot \ell) \quad (2.58)$$

and

$$Y_{SS} = Y_0 \cdot \tanh(\gamma \cdot \ell / 2) \quad (2.59)$$

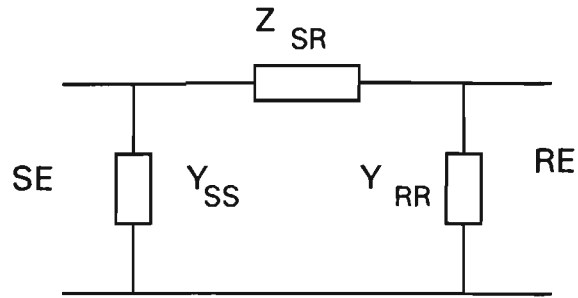


Fig. 2.9: Exact equivalent π

The same equivalent circuit can be derived for positive, negative and zero-sequence components independently.

In case of unbalanced transmission line analysis (phase co-ordinates), equations 2.58 and 2.59 are valid, but Z_{SR} , Z_{SS} , Z_0 , Y_0 and $\gamma \cdot l$ are all matrices involving evaluation of matrix functions which, of course, can be readily accomplished by using equation 2.55.

Chapter 3

STEADY-STATE ANALYSIS OF TRANSMISSION LINES

3.1 INTRODUCTION

Transmission lines are a means of conveying power or signals from one point to another. From such a broad definition, any system of wires can be considered as forming one or more transmission lines. However, if the properties of these lines must be taken into account, the transmission lines might as well be arranged in some simple, constant pattern. This will make the properties much easier to calculate, and it will also make them constant for any type of transmission line. Thus, all practical transmission lines are arranged in a uniform pattern, which simplifies calculation, reduces costs and increases convenience.

In this chapter the properties and performance of transmission lines under steady-state operating conditions are given. The analysis is developed for a simple configuration which is extended to multi phase transmission lines. The computation of steady state values is required for the digital computation of fault currents and voltages. The accurate measurement of fault location will depend on the accuracy of computing the sending and receiving end currents and voltages for the frequency under consideration.

The steady-state analysis is usually carried out to provide initial conditions for the digital simulation program, which calculates the sending and receiving end voltages and currents for a given fault on the power line. These values are

required for accurate measurement of fault location on transmission lines, which is described in detail in chapter 4 of this thesis.

3.2 BASIC RELATIONSHIPS

In order to develop the necessary algorithm for steady-state solution of poly-phase transmission lines, the fundamental relationships are presented using the theory of wave propagation in simple systems^(10 - 12).

3.2.1 Single conductor

Consider a single conductor in presence of an infinite earth plane which is shown schematically in Fig. 3.1.

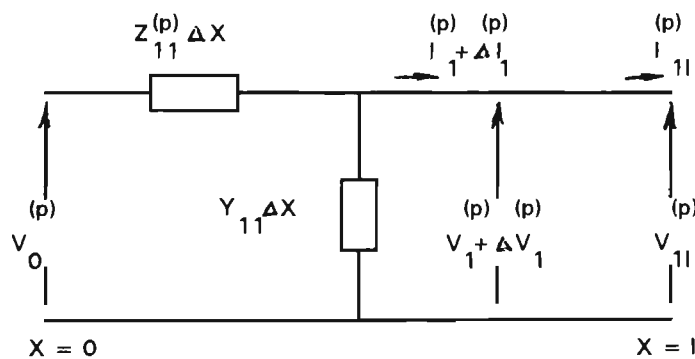


Fig. 3.1: Single conductor system representation.

The diagram of Fig. 3.1 shows one element of the system considered. It is possible to write the following fundamental equations relating to the element as follows:

$$\frac{dV_1^{(p)}}{dx} = -Z_{11}^{(p)} \cdot I_1^{(p)} \quad (3.1)$$

$$\frac{dI_1^{(p)}}{dx} = -Y_{11}^{(p)} \cdot V_1^{(p)} \quad (3.2)$$

By taking the first derivatives of equations 3.1 and 3.2, ie.

$$\frac{d^2V_1^{(p)}}{dx^2} = -Z_{11}^{(p)} \cdot \frac{dI_1^{(p)}}{dx} \quad (3.3)$$

$$\frac{d^2I_1^{(p)}}{dx^2} = Y_{11}^{(p)} \cdot \frac{dV_1^{(p)}}{dx} \quad (3.4)$$

and combining 3.1 and 3.2 with 3.4 and 3.3 we get :

$$\frac{d^2V_1^{(p)}}{dx^2} = Z_{11}^{(p)} \cdot Y_{11}^{(p)} \cdot V_1^{(p)} \quad (3.5)$$

$$\frac{d^2I_1^{(p)}}{dx^2} = Y_{11}^{(p)} \cdot Z_{11}^{(p)} \cdot I_1^{(p)} \quad (3.6)$$

The solution for $V_1^{(p)}$ is :

$$V_1^{(p)} = A \exp(-\gamma \cdot x) + B \exp(-\gamma \cdot x) \quad (3.7)$$

where A and B are arbitrary constants and :

$$\gamma_1 = \sqrt{Z_{11}^{(p)} \cdot Y_{11}^{(p)}} \quad (3.8)$$

$V_1^{(p)}$ will have two components, one travelling in the forward direction and the other in the reverse direction. Equation 3.7 is rewritten as:

$$V_1^{(p)} = S_{11} [V_1^{(c+)} \exp(-\gamma_1 \cdot x) + V_1^{(c-)} \exp(\gamma_1 \cdot x)] \quad (3.9)$$

where S_{11} is an arbitrary constant.

The current is derived from V_1 using equation 3.9:

$$\begin{aligned} I_1^{(p)} &= -[Z_{11}^{(p)}]^{-1} \frac{dV_1^{(p)}}{dx} \\ &= [Z_{11}^{(p)}]^{-1} \gamma_1 S_{11} [V_1^{(c+)} \exp(-\gamma_1 \cdot x) - V_1^{(c-)} \exp(\gamma_1 \cdot x)] \\ &= [Z_{11}^{(0)}]^{-1} S_{11} V_1^{(c)} \end{aligned} \quad (3.10)$$

$$\text{where } Z_{11}^{(0)} = \frac{Z_{11}^{(p)}}{\gamma_1} = \sqrt{\frac{Z_{11}^{(p)}}{Y_{11}^{(p)}}} \quad (3.11)$$

and

$$V_1^{(c)} = V_1^{(c+)} \exp(-\gamma_1 x) - V_1^{(c-)} \exp(\gamma_1 \cdot x) \quad (3.12)$$

3.2.2 Solution for the 2-conductor problem

As was stated in reference 10, the main difficulty in solving the 2-phase and in general multi phase problem is due to the fact that second order rates of change of voltage and current in each phase are a function of the voltages or currents in all phases. Considering Fig. 3.2, it is possible to write these equations in condensed forms:

$$\frac{dV^{(p)}}{dx} = Z^{(p)} I^{(p)} \quad (3.13)$$

and

$$\frac{dI^{(p)}}{dx} = -Y^{(p)} V^{(p)} \quad (3.14)$$

$$\frac{d^2 V^{(p)}}{dx^2} = Z^{(p)} Y^{(p)} V^{(p)} = P V^{(p)} \quad (3.15)$$

Since

$$Z_{(t)}^{(p)} = Z^{(p)} \text{ and } Y_{(t)}^{(p)} = Y^{(p)}$$

$$\begin{aligned} \frac{d^2 I^{(p)}}{dx^2} &= Y^{(p)} Z^{(p)} I^{(p)} = Y_t^{(p)} Z_t^{(p)} I^{(p)} = \\ &= [Z^{(p)} Y^{(p)}]_t \cdot I^{(p)} = P_t \cdot I^{(p)} \end{aligned} \quad (3.16)$$

where P is a square matrix defined as:

$$P = \begin{bmatrix} P_{11} & P_{12} \\ P_{21} & P_{22} \end{bmatrix} = \begin{bmatrix} (Z_{11}^{(p)} Y_{11}^{(p)} - Z_{12}^{(p)} Y_{12}^{(p)}) & -(Z_{11}^{(p)} Y_{12}^{(p)} - Z_{12}^{(p)} Y_{22}^{(p)}) \\ (Z_{12}^{(p)} Y_{11}^{(p)} - Z_{22}^{(p)} Y_{12}^{(p)}) & -(Z_{12}^{(p)} Y_{12}^{(p)} - Z_{22}^{(p)} Y_{22}^{(p)}) \end{bmatrix} \quad (3.17)$$

The matrix solution is based on a linear transformation of voltage and subsequent manipulation, so that second order differential relationships involve diagonal matrices only.

Mutual effects are thus eliminated, making a direct solution for component voltages and currents possible. The detailed analysis is given in Appendix A1 of reference 10. However, it is possible to relate symmetrical component and phase quantities of voltages as:

$$V^{(p)} = SV^{(c)} \quad (3.18)$$

substituting into equation 3.15 and rearranging yields:

$$\frac{d^2V^{(c)}}{dx^2} = S^{-1}PSV^{(c)} = \gamma^2V^{(c)} \quad (3.19)$$

where

$$\gamma^2 = S^{-1}PS \quad (3.20)$$

Matrix S is chosen in such a way that γ is a diagonal matrix of the form:

$$\gamma^2 = \begin{bmatrix} \gamma_1^2 & 0 \\ 0 & \gamma_2^2 \end{bmatrix} \quad (3.21)$$

It is possible to write the following two second order differential equations for the two conductors considered:

$$\frac{d^2V_1^{(c)}}{dx^2} = \gamma_1^2V_1^{(c)} \quad (3.22)$$

$$\frac{d^2V_2^{(c)}}{dx^2} = \gamma_2^2V_2^{(c)} \quad (3.23)$$

For which the solution can be expressed as in the following:

$$V_1^{(c)} = V_1^{(c+)} \exp(-\gamma_1 \cdot x) + V_1^{(c-)} \exp(\gamma_1 \cdot x) \quad (3.24)$$

$$V_2^{(c)} = V_2^{(c+)} \exp(-\gamma \cdot x) + V_2^{(c-)} \exp(\gamma_2 \cdot x) \quad (3.25)$$

The equivalent circuit for the 2-conductor transmission line is given in Fig. 3.2 for the impedance element and in Fig. 3.3 for the admittance element.

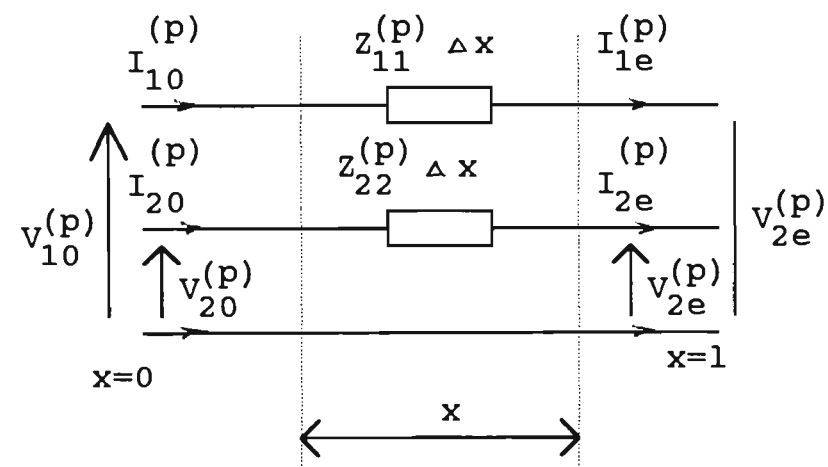


Fig. 3.2: Impedance element

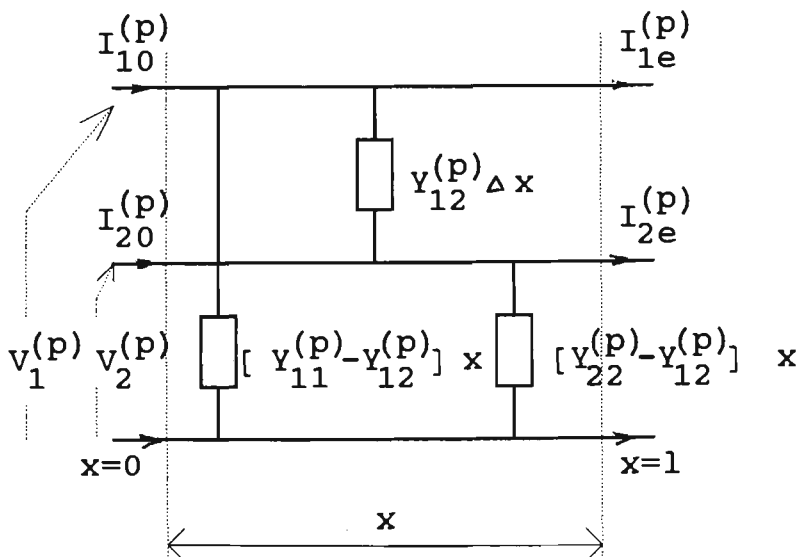


Fig. 3.3: Admittance element

3.2.3 Polyphase Transmission Lines

Considering a similar approach as that for the single conductor and two conductor lines, for polyphase transmission line, the second order matrix differential equations for voltages and currents are:

$$\frac{d^2 V^{(p)}}{dx^2} = P V^{(p)} \quad (3.28)$$

and
$$\frac{d^2 I^{(p)}}{dx^2} = P I^{(p)} \quad (3.29)$$

where the phase and symmetrical component quantities are related by the following linear transformation:

$$V^{(p)} = S V^{(c)} \quad (3.30)$$

$$I^{(p)} = Q I^{(c)} \quad (3.31)$$

It is well known from the theory of symmetrical components that phase voltages V_1, V_2, V_3 and phase currents I_1, I_2, I_3 are related to symmetrical components voltages V_+, V_-, V_0 and currents I_+, I_-, I_0 through the connection matrices:

$$S = Q = \begin{bmatrix} 1 & 1 & 1 \\ a^2 & a & 1 \\ a & a^2 & 1 \end{bmatrix} \quad (3.32)$$

where $a = 1 \angle 120^\circ$

Rewriting equations 3.28 and 3.29 by considering equations 3.30 and 3.31, the following equations are found :

$$\frac{d^2 V^{(c)}}{dx^2} = S^{-1} P S V^{(c)} = \gamma^2 V^{(c)} \quad (3.33)$$

$$\frac{d^2 I^{(c)}}{dx^2} = Q^{-1} P Q I^{(c)} = \gamma^2 I^{(c)} \quad (3.34)$$

A suitable choice of matrices S and Q will result in diagonal matrices:

$$\gamma^2 = S^{-1} P S \quad (3.35)$$

and
$$\gamma^2 = Q^{-1} P Q \quad (3.36)$$

By solving equations 3.33 and 3.34 a series of simple wave equations, ie. :

$$\frac{d^2 V_1^{(c)}}{dx^2} = S^{-1} P S V_1^{(c)} = \gamma_1^2 V_1^{(c)} \quad (3.37)$$

$$\frac{d^2 I_1^{(c)}}{dx^2} = Q^{-1} P Q I_1^{(c)} = \gamma_1^2 I_1^{(c)} \quad (3.38)$$

or in general form:

$$\frac{d^2 V_i^{(c)}}{dx^2} = S^{-1} P S V_i^{(c)} = \gamma_i^2 V_i^{(c)} \quad (3.39)$$

and
$$\frac{d^2 I_i^{(c)}}{dx^2} = Q^{-1} P Q I_i^{(c)} = \gamma_i^2 I_i^{(c)} \quad (3.40)$$

from which the solutions are expressed in the following general form:

$$V_i^{(c)} = \exp(-\gamma_i \cdot x) V_i^{(c)} + \exp(\gamma_i \cdot x) V_i^{(c)} \quad (3.41)$$

$$I_i^{(c)} = \exp(-\gamma' \cdot x)I_i^{(c)} + \exp(\gamma' \cdot x)I_i^{(c)} \quad (3.42)$$

It may be seen⁽¹⁰⁾ that $\gamma^2 = \gamma^2$. Once having determined the n values of γ^2 , the Q and S matrices are solved one column at a time by solving the system of homogenous dependent simultaneous equations:

$$(P - \gamma_i^2)S_i = 0 \quad (3.43)$$

$$(P_i - \gamma_i^2)Q_i = 0 \quad (3.44)$$

where i indicates that the elements of column i of the respective matrices that are to be considered. Since these systems of equations are dependent (owing to the vanishing of the determinant of the coefficients), one value in each column is specified arbitrarily and the remaining elements are evaluated accordingly. The n values of γ_j are known as eigenvalues values and the corresponding S_j and Q_j as eigenvectors.

3.2.4 Surge impedance, propagation constants and reflection factors

The surge impedance for a single conductor case is defined as the ratio between voltage and current in an infinite line, or a terminal impedance which gives a reflection factor of zero, ie. ;

$$K = \frac{Z_{11r} - Z_{11}^{(0)}}{Z_{11r} + Z_{11}^{(0)}} = 0 \quad (3.45)$$

$$\text{or } Z_{11r} = Z_{11}^{(0)} \quad (3.46)$$

The polyphase surge impedance is defined as:

$$Z^{(0)} = S\gamma^{-1}S^{-1}Z^{(p)} \quad (3.47)$$

The polyphase surge admittance is:

$$Y^{(0)} = [Z^{(0)}]^{-1} \quad (3.48)$$

and polyphase reflection factor can be defined as:

$$K = [Z_r + Z^{(0)}]^{-1} [Z_r - Z^{(0)}] \quad (3.49)$$

Finally the propagation coefficients for polyphase systems can be expressed as:

$$V^{(p)} = S \cosh(\gamma_r) S^{-1} V_0^{(p)} - Z_0 Q \sinh(\gamma_r) Q^{-1} I_0^{(p)} \quad (3.50)$$

$$I^{(p)} = -Q \sinh(\gamma_r) Q^{-1} [Z^{(0)}]^{-1} V_0^{(p)} + Q \cosh(\gamma_r) Q^{-1} I_0^{(p)} \gamma \quad (3.51)$$

3.3 STEADY-STATE RESPONSE

When Fourier Transform is used, the final product becomes one of solving the steady-wave equation at a range of frequencies. Due to the multiplicity of conductors in a power-transmission system, the solution of the resultant simultaneous differential equations, which are independent, becomes very complex. The steady-state propagation properties of transmission lines are obtained using the method of modal analysis⁽¹⁴⁾. Consider the system voltage steady-state equation as :

$$\frac{d^2V}{dx^2} = PV \quad (3.52)$$

$$\text{where } P = ZY \quad (3.53)$$

Z and Y are the system series impedance and shunt admittance matrices. The transform of equation 3.52 into a system of independent differential equations gives the following solution .

$$V = \exp(-\psi x)V_i + \exp(\psi x)V_r \quad (3.54)$$

where:

$$\psi = Q \cdot \gamma \cdot Q^{-1} \quad (3.55)$$

By using the properties of matrix functions equation 3.54 can be written as:

$$V = Q \exp(-\gamma \cdot x) Q^{-1} V_i + Q \exp(\gamma \cdot x) Q^{-1} V_r \quad (3.56)$$

3.4 TWO PORT NETWORK

Considering the wave equation 3.52 and the analysis described in reference 37, the constant ABCD parameters of the transmission line can be evaluated (Fig. 3.4).

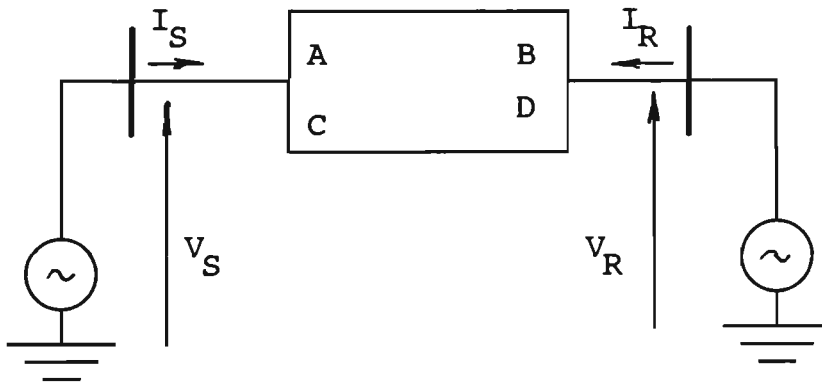


Fig. 3.4: Transmission line constants.

The sending end and receiving end voltages and currents are related as⁽³⁷⁾:

$$\begin{bmatrix} V_s \\ I_s \end{bmatrix} = \begin{bmatrix} A & B \\ C & D \end{bmatrix} \begin{bmatrix} V_r \\ I_r \end{bmatrix} \quad (3.57)$$

Where:

$$A = \cosh(\psi x)$$

$$B = \sinh(\psi x) Z_0$$

$$C = Y_0 \sinh(\psi x)$$

$$D = Y_0 \cosh(\psi x) Z_0$$

Equation 3.57 indicates that a multi conductor transmission line interconnecting two systems as in Fig. 3.3, can be expressed in the form of a two port network from which the steady-state voltages and currents can be computed from the solution of matrix equations. However, the accurate measurement of fault location on a multi conductor polyphase transmission line requires accurate computation of voltages and currents at both ends of the line, which in turn depends on the initial values derived from the steady-state solution of the wave equation.

The occurrence of a fault on the transmission line causes the disturbance to be propagated away from the fault, towards and ultimately into each source⁽³⁸⁾. A proportion of the disturbance is reflected from the terminating busbars and from within each source network, to constitute a series of travelling waves which are ultimately damped by the system as a whole. Such a phenomenon represents a wide frequency variation, and it is therefore necessary to evaluate the system equation over the entire frequency spectrum of the disturbance, which will constitute the complete transient response. The solution of the wave equation at the power frequency will provide all system parameters in the steady-state condition. In order to simulate the faulty polyphase transmission

line digitally the line can be represented in a series of cascaded sections before and after the fault as explained in the following section.

3.5 SIMULATION OF THE FAULTY TRANSMISSION LINE

A polyphase multi-conductor transmission line under fault condition can be represented as a series of cascaded network sections as shown in Fig. 3.5

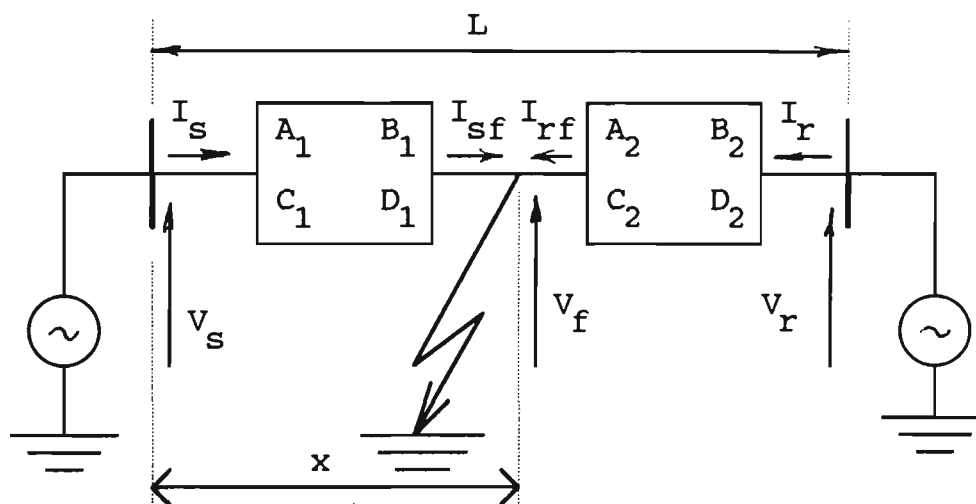


Fig. 3.5: Simulation of Faulty Transmission line.

The digital simulation is based on expressing the relationships between the two sides of the first two port networks to the fault through the transfer matrix of the section constants. The output of the first section is related to the receiving end parameters through the transfer matrix of constants representing the second section shown in Fig. 3.5.

The first section of the polyphase transmission line can be expressed as follows:

$$\begin{bmatrix} V_s \\ I_s \end{bmatrix} = \begin{bmatrix} A_1 & B_1 \\ C_1 & D_1 \end{bmatrix} \begin{bmatrix} V_f \\ I_f \end{bmatrix} \quad (3.58)$$

where

$$A_1 = \cosh(\psi \cdot x)$$

$$B_1 = Y_0 \sinh(\psi \cdot x) Z_0$$

$$C_1 = Y_0 \sinh(\psi \cdot x)$$

$$D_1 = Y_0 \cosh(\psi \cdot x) Z_0$$

and for the second section :

$$\begin{bmatrix} V_f \\ I_f \end{bmatrix} = \begin{bmatrix} A_2 & B_2 \\ C_2 & D_2 \end{bmatrix} \begin{bmatrix} V_r \\ I_r \end{bmatrix} \quad (3.59)$$

where:

$$A_2 = \cosh(\psi(L - x))$$

$$B_2 = \sinh(\psi(L - x)) Z_0$$

$$C_2 = Y_0 \sinh(\psi(L - x))$$

$$D_2 = Y_0 \cosh(\psi(L - x)) Z_0$$

In the above equation the distance to fault is designated as x and the total line length as L , ie., the sending end busbar is considered as a reference.

From the above matrix equations 3.58 and 3.59, it is possible to calculate the steady-state voltage at any selected location x and the knowledge of the pre-fault steady state voltages at the two terminating busbars.

It is also possible to relate the sending and receiving ends voltages and currents through the transfer matrix constants as follows :

$$\begin{bmatrix} V_s \\ I_s \end{bmatrix} = \begin{bmatrix} A_2 & B_2 \\ C_2 & D_2 \end{bmatrix} \begin{bmatrix} A_2 & B_2 \\ C_2 & D_2 \end{bmatrix} \begin{bmatrix} V_r \\ I_r \end{bmatrix} \quad (3.60)$$

or :

$$\begin{bmatrix} V_s \\ I_s \end{bmatrix} = \begin{bmatrix} A & B \\ C & D \end{bmatrix} \begin{bmatrix} V_r \\ I_r \end{bmatrix} \quad (3.61)$$

where:

$$A = A_1 A_2 + B_1 C_2$$

$$B = A_1 B_2 + B_1 D_2$$

$$C = C_1 A_2 + D_1 C_2$$

$$D = C_1 B_2 + D_1 D_2$$

It is possible to derive matrix equations for the steady-state voltage at the fault location⁽³⁷⁾, and the steady-state currents at the two terminating busbars from the solution of equations 3.58 - 3.61.

$$V_{fs} = (A_2 - B_2 B^{-1} A) V_{rs} + B_2 B^{-1} V_{ss} \quad (3.62)$$

$$I_{ss} = (C - DB^{-1} A) V_{rs} + DB^{-1} V_{ss} \quad (3.63)$$

$$I_{rs} = B^{-1} (V_{ss} - AV_{rs}) \quad (3.64)$$

It is obvious that all the above three matrix equations are expressed in terms of known steady-state voltages at the two terminating busbars. For example V_{ss} is the vector of the nominal sending end voltages and V_{rs} is the vector of the

receiving end voltages calculated from prefault loading of the transmission line.

For simplicity of load representation and to avoid a full load flow analysis for the given simple system, the load can be represented by using the concept of reactive and active power flows in the line as follows:

1. Per-unit or percentage regulation, since the flow of reactive power will cause the voltage drop in the line when the resistance of the line is neglected, ie.:

$$V_{rs} = R.V_{ss} \quad (3.65)$$

where R is the percentage regulation

2. Transmission angle δ - models the real power flow in the line, since the flow of active power depends mainly on the phase shift between the sending and receiving end voltages if the resistance is neglected, and assuming the sending end voltage as the reference vector, ie.:

$$V_{ss} = V_{ss} \angle 0^\circ$$

$$V_{rs} = V_{ss} \angle \delta^\circ$$

3.6 TRANSMISSION LINE TRANSPOSITION

In case of unsymmetrical spacing of transmission line conductors, flux linkages and therefore inductances of each phase will be different. This will result in

unbalanced receiving end voltages even when sending end voltages and line currents are balanced.

A different inductance in each phase also results in an unbalanced circuit which will induce voltages in the adjacent communication line even when line currents are balanced. This problem can be rectified by exchanging the positions of conductors at regular intervals along the line such that, each conductor occupies the original position of every other conductor over an equal distance. The effect of transposition is to balance the mutual capacitive and inductive coupling between phases. Line transposition reduces the electrostatic and electromagnetic interface, or coupling, between the power line and communication circuits. This is due to the fact that the electrostatically induced voltages balance out over a complete set of transpositions. Line transposition also results in reduced electromagnetically induced emfs in adjacent conductors.

For long transmission lines, discrete transposition of conductors is often performed at the termination of each section or at intermediate points there in. These discrete transpositions must be modelled because they represent points of abrupt electrical discontinuity. Because of conductors' swapping, transmission lines are joined to a section with a different characteristic impedance. As a result, partial reflections of the incident travelling wave components can occur at these points. A typical, commonly used transposition arrangement is given in Fig. 3.6, on which the fault is shown in the middle of the transposition cycle.

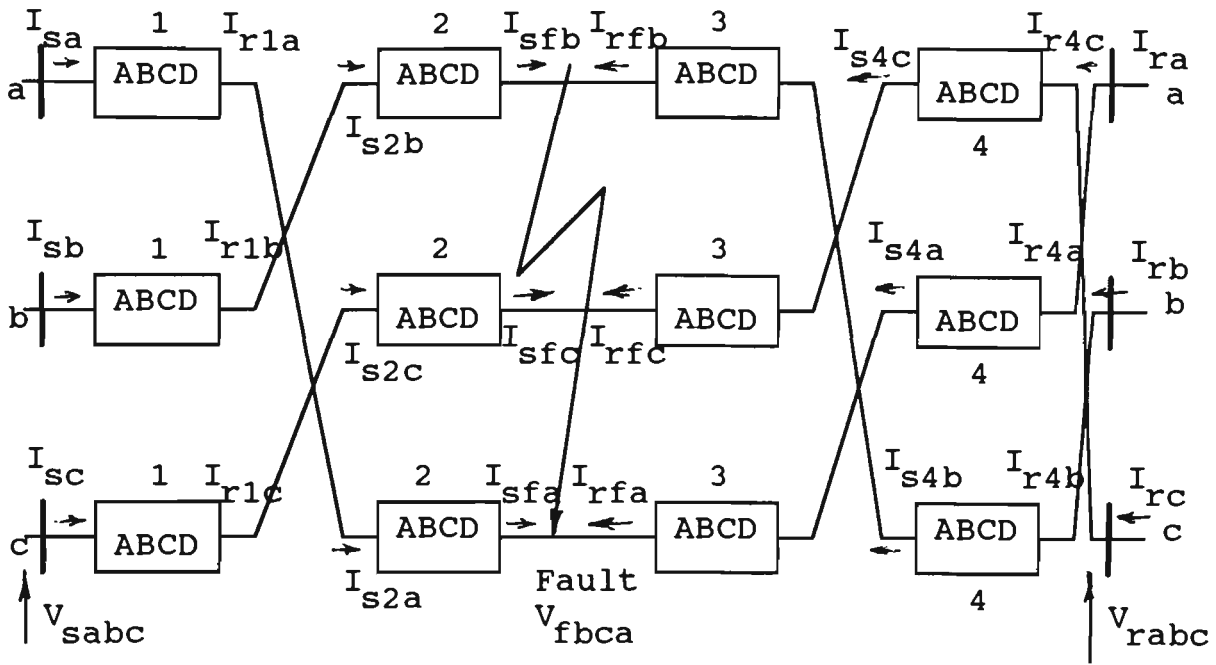


Fig. 3.6: Transposition of phase conductors.

Considering Fig. 3.6 it is evident that the discrete transposition and fault location effectively divide the homogeneous line length into four sections. Initially the two-port transfer matrices describing each of this homogeneous section are calculated. They are uniquely ordered in accordance with the conductor positions (a, b, c). Therefore, the transfer equations for each homogeneous section can be expressed as:

$$\begin{bmatrix} V_{sabc} \\ I_{sabc} \end{bmatrix} = \begin{bmatrix} A_1 & B_1 \\ C_1 & D_1 \end{bmatrix} \begin{bmatrix} V_{r1abc} \\ I_{r1abc} \end{bmatrix} \quad (3.66)$$

$$\begin{bmatrix} V_{s2bca} \\ I_{s2bca} \end{bmatrix} = \begin{bmatrix} A_2 & B_2 \\ C_2 & D_2 \end{bmatrix} \begin{bmatrix} V_{sfbca} \\ I_{sfbca} \end{bmatrix} \quad (3.67)$$

$$\begin{bmatrix} V_{fbca} \\ I_{rfbca} \end{bmatrix} = \begin{bmatrix} A_3 & B_3 \\ C_3 & D_3 \end{bmatrix} \begin{bmatrix} V_{r2bca} \\ I_{r2bca} \end{bmatrix} \quad (3.68)$$

$$\begin{bmatrix} V_{s3cab} \\ I_{s3cab} \end{bmatrix} = \begin{bmatrix} A_4 & B_4 \\ C_4 & D_4 \end{bmatrix} \begin{bmatrix} V_{r3cab} \\ I_{r3cab} \end{bmatrix} \quad (3.69)$$

where

$$A_1 = A_4 = \cosh(\psi \cdot L / 3)$$

$$B_2 = B_4 = \sinh(\psi \cdot L / 3)$$

$$C_1 = C_4 = Y_0 \sinh(\psi \cdot L / 3)$$

$$D_1 = D_4 = Y_0 \cosh(\psi \cdot L / 3)$$

The other submatrices defining the transfer matrix representing the second and third line sections can be calculated by substituting $(x - L/3)$ and $(2L/3 - x)$ respectively into the hyperbolic functions, ie.:

$$A_2 = \cosh(\psi \cdot (x - L / 3))$$

$$B_2 = \sinh(\psi \cdot (x - L / 3))$$

$$C_2 = Y_0 \sinh(\psi \cdot (x - L / 3))$$

$$D_2 = Y_0 \cosh(\psi \cdot (x - L / 3)) Z_0$$

and

$$A_3 = \cosh(\psi \cdot (2 \frac{L}{3} - x))$$

$$B_3 = \sinh(\psi \cdot (2 \frac{L}{3} - x)) Z_0$$

$$C_3 = Y_0 \sinh(\psi \cdot (2 \frac{L}{3} - x))$$

$$D_3 = Y_0 \cosh(\psi \cdot (2 \frac{L}{3} - x)) Z_0$$

In a similar way, the transfer matrices can be found for a fault location in either of the other two line sections.

Analysis of the transmission line steady-state relies on representing the line as two-port networks, ie. the equivalent line section before and after the fault location. In case of untransposed lines, the matrix equation involves simple matrix multiplication as shown below.

$$\begin{bmatrix} V_s \\ I_s \end{bmatrix} = \begin{bmatrix} A_1 & B_1 \\ C_1 & D_1 \end{bmatrix} \cdot \begin{bmatrix} A_2 & B_2 \\ C_2 & D_2 \end{bmatrix} \cdot \begin{bmatrix} V_f \\ I_{sf} \end{bmatrix} = \begin{bmatrix} A_s & B_s \\ C_s & D_s \end{bmatrix} \begin{bmatrix} V_f \\ I_{sf} \end{bmatrix} \quad (3.70)$$

and

$$\begin{bmatrix} V_f \\ I_{sf} \end{bmatrix} = \begin{bmatrix} A_3 & B_3 \\ C_3 & D_3 \end{bmatrix} \cdot \begin{bmatrix} A_4 & B_4 \\ C_4 & D_4 \end{bmatrix} \cdot \begin{bmatrix} V_r \\ I_r \end{bmatrix} = \begin{bmatrix} A_r & B_r \\ C_r & D_r \end{bmatrix} \cdot \begin{bmatrix} V_r \\ I_r \end{bmatrix} \quad (3.71)$$

In case of transposed lines, it is important to consider the reorientation of conductors. This can be achieved by introducing a transposition matrix [T] which relates the voltage and current vectors on adjacent sides of the transposition, ie.

$$\begin{aligned} & [V_{r1}, I_{r1}]' \text{ to } [V_{s2}, I_{s2}]' \\ & [V_{r2}, I_{r2}]' \text{ to } [V_{s3}, I_{s3}]' \text{ and} \\ & [V_{r3}, I_{r3}]' \text{ to } [V_r, I_r]' \end{aligned}$$

where

$$\begin{bmatrix} V_{r1} \\ I_{r1} \end{bmatrix} = [V_{r1a} V_{r1b} V_{r1c} I_{r1a} I_{r1b} I_{r1c}]^t \quad (3.72)$$

$$\begin{bmatrix} V_{s2} \\ I_{s2} \end{bmatrix} = [V_{s2b} V_{s2c} V_{s2a} I_{s2b} I_{s2c} I_{s2a}]^t \quad (3.73)$$

and

$$\begin{bmatrix} V_{s3} \\ I_{s3} \end{bmatrix} = [V_{s3c} V_{s3a} V_{s3b} I_{s3c} I_{s3a} I_{s3b}]^t \quad (3.74)$$

In equating vectors on adjacent sides of the transposition, the following matrix equation is obtained:

$$\begin{bmatrix} V_{r1a} \\ V_{r1b} \\ V_{r1c} \\ I_{r1a} \\ I_{r1b} \\ I_{r1c} \end{bmatrix} = \begin{bmatrix} T & 0 \\ 0 & T \end{bmatrix} \cdot \begin{bmatrix} V_{s2b} \\ V_{s2c} \\ V_{s2a} \\ I_{r2b} \\ I_{r2c} \\ I_{r2a} \end{bmatrix} \quad (3.75)$$

where

$$[T] = \begin{bmatrix} 0 & 0 & 1 \\ 1 & 0 & 0 \\ 0 & 1 & 0 \end{bmatrix} \quad (3.76)$$

The above methodology for representing discrete transposition of transmission lines can be readily adapted for an untransposed line. In case of untransposed lines the connection matrix $[T]$ is simply a (3×3) unitary matrix, i.e.:

$$[T] = \begin{bmatrix} 1 & 0 & 0 \\ 0 & 1 & 0 \\ 0 & 0 & 1 \end{bmatrix} \quad (3.77)$$

Therefore, the connection matrix [T] will have a different structure for transposed and untransposed lines. Using the appropriate form of equations 3.76 or 3.77, it is possible to relate voltages and currents of each section given in Fig. 3.6.

In calculating the distance to fault, all studies required the computation of current and voltage phasors from the faulty transmission system. These signals, together with the knowledge of transmission line parameters derived from modal analysis, are used in the fault location algorithm for accurate estimation of the fault location. Such an analysis was used for both two terminal and three terminal systems as shown in chapter 4.

Chapter 4

CIRCUIT PARAMETERS

4.1 INTRODUCTION

In order to study the power system under different conditions using digital simulation methods, it is necessary to represent system parameters as accurate as possible. The results based on such simulations will depend on the way each element of the system under consideration is represented. For the purpose of assessing the accuracy of the fault location algorithms described in chapter 5, a power system comprising of two terminals and three terminals are considered. Each system consists of generators, transmission lines, and shunt reactors. The latter are included in this study in order to investigate the behaviour of the fault location algorithms for shunt compensated transmission lines, which are described in chapter 6.

The generator representation allows the incorporation of different source strength, depending on the short circuit levels under consideration. In all studies represented in this work, all three phase impedances are included as mutually coupled circuits. The transformer reactance is included with the source, which is simulated as an infinite busbar.

Transmission lines are represented for a typical 500 kV system in form of a fully transposed system, and for comparison purposes, the untransposed line simulation is also included. This was essential for investigating the fault location algorithms developed in chapters 5 and 7

Shunt reactors representation is carried out for a typical compensation of 75% of the line capacitance. The reactors, each comprising half of the total compensation required, are connected at the transmission line termination.

A single line diagram of the represented two terminal system is shown in Fig. 4.1, and for three terminal system is given in Fig. 4.2

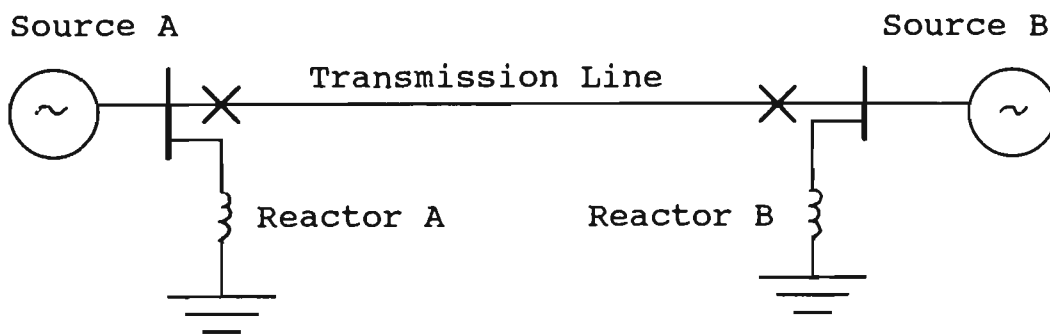


Fig. 4.1: Two Terminal System

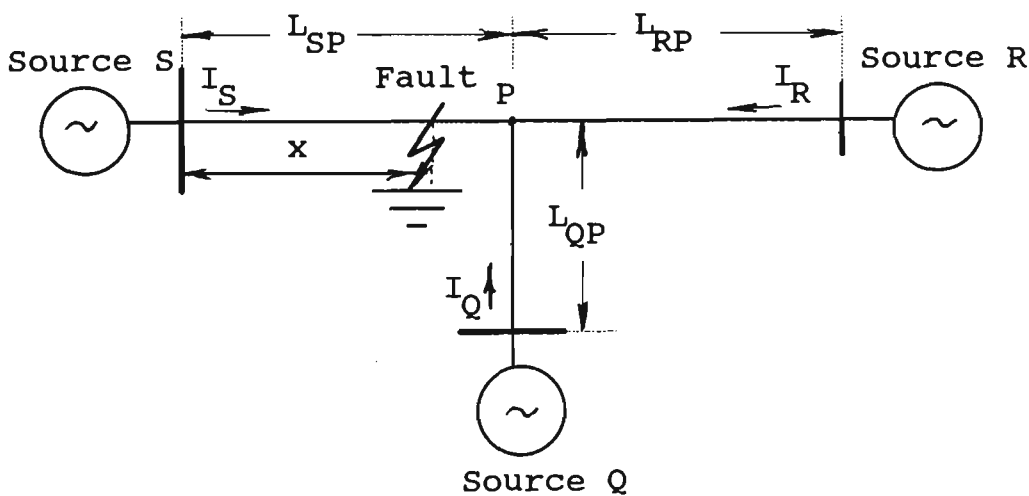


Fig. 4.2: Three Terminal System

4.2 SOURCE REPRESENTATION

In this research, because of the emphasis on the fault location measurement on EHV transmission lines, the generation representing the source in the

simulation studies, is represented in the form of an infinite busbar, behind a series impedance. A three-phase model for the source used in all simulation studies presented in this research is given in Fig. 4.3.

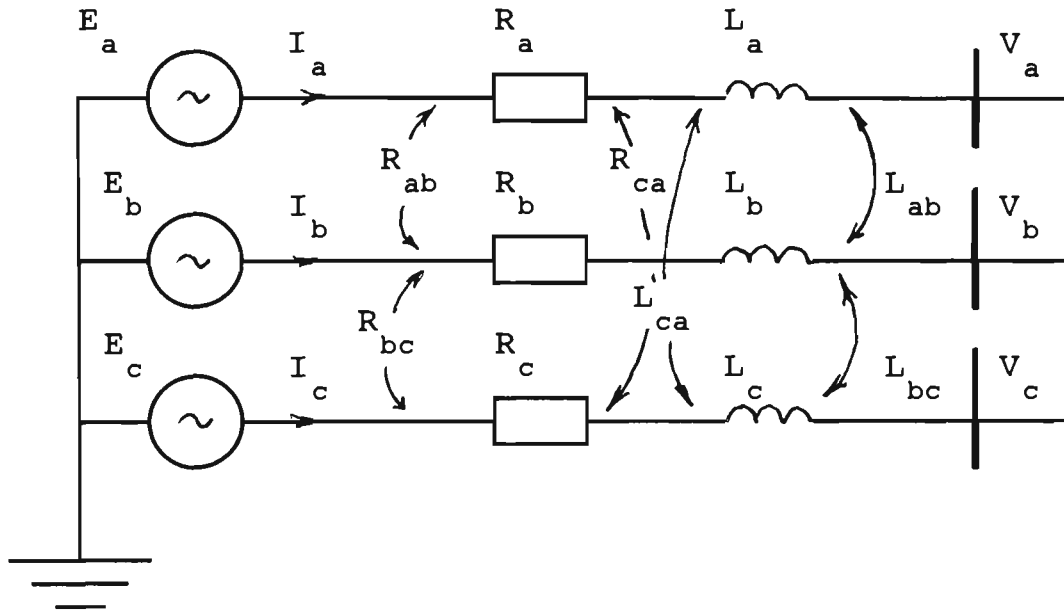


Fig. 4.3: Source Representation

The analysis and the assessment of the fault location algorithms were carried on systems with different source strength. For the two terminal systems, the source impedances first were assumed at equal strength, i.e., both sides A and B (Fig.4.3) have the same fault MVA. Other conditions were also investigated when the two sides had different fault MVA.

Since both the two terminal and the three terminal systems were assumed as infinite busbars, the source impedance was kept constant with constant terminal voltages at 500 kV.

In order to facilitate different loading conditions for the power lines, the phase angle of each source can be controlled individually. When the line was required to operate without loading, the angles at both ends were assumed the same and equal to zero. In case of three terminal network, all the three sources

were assumed to have the same angle, for simulating no load transfer between the three sides prior to fault inception.

For simulating a certain power flow in the transmission lines, the phase angle of sources can be adjusted, so that these angles are different. It is also possible to control the direction of the power flow in the line, by simply letting the angle of one source be either leading or lagging the reference source by a certain value. The greater the phase shift between the system sources, the more power will flow in the corresponding line. Such a facility was useful for testing the operation of the fault location algorithm under different conditions.

Typical values used for source representation are given in table 4.1.

Table 4.1: Source Parameters

Parameter	Value
Source Impedance	5, 10, 15, 20,35 GVA
Source Z_{s0} / Z_{s1} ratio	1.0
Source X / R	30.0

4.3 TRANSMISSION LINE PARAMETERS

In the analysis of the fault location algorithm, different types of balanced and unbalanced faults were investigated on a typical 500 kV, 384 kms, twin conductor transmission line with two earth wires. In some other studies, a double circuit arrangement, with vertical configuration was used. These two arrangements are given in Fig. 4.4 and 4.5 respectively.

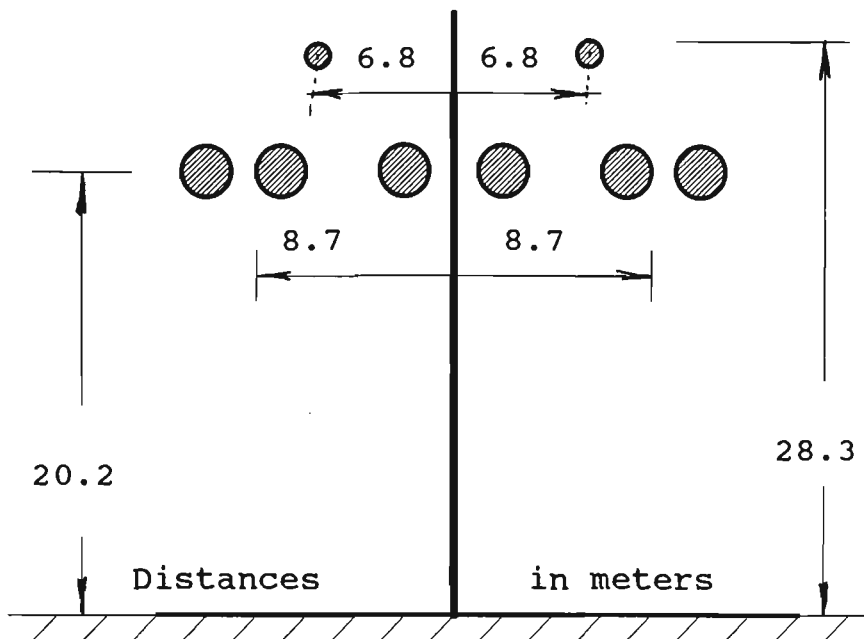


Fig. 4.4: 500 kV, twin conductor configuration

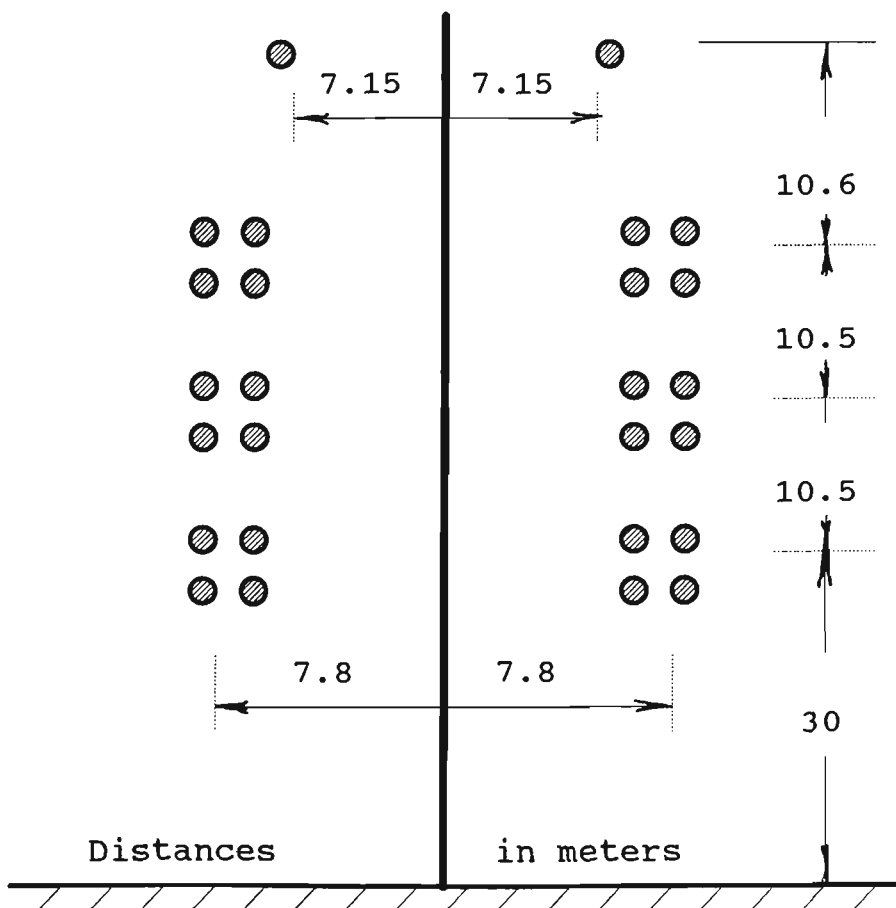


Fig. 4.5: Double circuit 500 kV line

The main parameters of the transmission line of Fig. 4.4 are given in Table 4.2

Table 4.2: 500 kV, 384 km, horizontal line parameter

Parameter	Value
Phase Conductors	2 x 84/19/0.35 cm ACSR with 0.45 bundle spacing
Earth wires	7/0.35 cm A.W.
Earth resistivity	100 Ω -m
Conductor resistance	0.03387 Ω /km (at power frequency)
Earth wire resistance	1.882 Ω /km (at power frequency)
Conductor reactance	0.7865E-02 Ω (at power frequency)
Earth wire reactance	0.388 Ω /km (at power frequency)
Conductor overall radius	9.1 cm
Earth wire overall radius	0.64 cm
Line length	384 km

Transmission line impedance matrix is calculated to be as:

$$Z = \begin{bmatrix} 0.0863 + j0.6536 & 0.0639 + j0.1335 & 0.0716 + j0.1727 \\ 0.0694 + j0.13335 & 0.0863 + j0.6536 & 0.0716 + 0.1727 \\ 0.0176 + 0.1727 & 0.0172 + 0.1727 & 0.0879 + 0.6478 \end{bmatrix} \Omega/\text{m}$$

The calculated admittance matrix is:

$$Y = \begin{bmatrix} 0.2657 & -0.0155 & -0.0426 \\ -0.0155 & 0.2657 & -0.0426 \\ -0.0426 & -0.0426 & 0.2729 \end{bmatrix} \times 10^{-5} \text{ Siemens/km}$$

For the double circuit 500 kV line, the basic data are given in Table 4.3 below.

Table 4.3: Double circuit, 500 kV line data

Parameter	Values
Phase conductors	4 x 54/7/3.0 mm
Bundle spacing	460.0 mm
Earth wires	30/7/2.5 mm
Earth resistivity	100 Ω - m
Conductor resistance	d.c. at 20 ^o C: 0.0758 Ω /km a.c. at 75 ^o C: 0.0951 Ω /km
Earth wire resistance	d.c. at 20 ^o C: 0.196 Ω /km a.c. at 75 ^o C: 0.239 Ω /km
Conductor reactance	Diameter of conductor: 25 mm Thickness of Aluminium: 8 mm
Earth wire reactance	Diameter of Earth wire: 16.95 mm Thickness of Aluminium: 4.727 mm
Transmission line length	273 km
Charging MVAR's	286.8 MVAR's
Shunt compensation Reactor	2 x 100 MVAR's
Line geometry	See Fig. 4.4

Calculated line parameters:

Series resistance matrix:

$$R = \begin{bmatrix} .61113 & .38063 & .39296 & .37288 & .37979 & .39094 \\ .38063 & .62933 & .40944 & .37979 & .39004 & .40553 \\ .39296 & .40944 & .67404 & .39094 & .40553 & .42599 \\ .37288 & .37979 & .39094 & .61113 & .38063 & .39296 \\ .37979 & .39004 & .40553 & .38063 & .62933 & .40944 \\ .39094 & .40553 & .42599 & .39296 & .40944 & .67404 \end{bmatrix} \times 10^{-1} \Omega/\text{km}$$

The reactance matrix:

$$X = \begin{bmatrix} .443416 & .185965 & .129305 & .169961 & .149493 & .115873 \\ .185965 & .424865 & .161648 & .149493 & .151617 & .125781 \\ .129305 & .161648 & .393403 & .115873 & .125781 & .121873 \\ .169961 & .149493 & .115873 & .443416 & .185965 & .129305 \\ .149493 & .151617 & .125781 & .185965 & .424865 & .161648 \\ .115873 & .125781 & .121873 & .129305 & .161648 & .393403 \end{bmatrix} \Omega/\text{km}$$

The admittance matrix:

$$Y = \begin{bmatrix} .3639 & -.0805 & -.0259 & -.0488 & -.0288 & -.0138 \\ -.0805 & .3783 & -.0806 & -.0288 & -.0394 & -.0289 \\ -.0259 & -.0806 & .3668 & -.0138 & -.0289 & -.0475 \\ -.0488 & -.0288 & -.0138 & .3639 & -.0805 & -.0259 \\ -.0288 & -.0394 & -.0289 & -.0805 & .3783 & -.0806 \\ -.0138 & -.0289 & -.0475 & -.0259 & -.0806 & .3668 \end{bmatrix} \times 10^{-5}$$

Siemens/km

4.4 REACTOR PARAMETERS

In the studies carried out in this thesis, the transmission lines were investigated without and with compensation. For the lines used, a typical compensation of 75% was used for the positive phase sequence components. The reactors used were of 4 legged reactors. The compensation was equally divided at the line terminating ends. The phase reactance and the reactance of the neutral were calculated as shown below. The basic reactor configuration is given in Fig. 4.6.

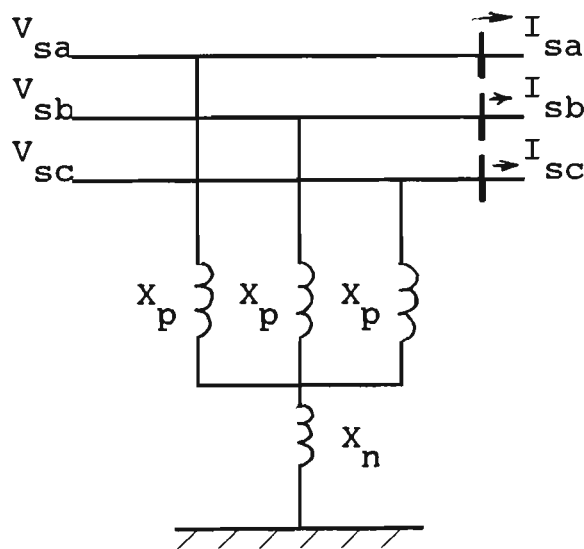


Fig. 4.6: Shunt Reactor Model

For the 500 kV, 384 km horizontal configuration transmission line given in Fig.4.3, for 75% compensation for the positive phase sequence $h_1 = 0.75$, the zero phase sequence compensation factor h_0 is calculated from the following :

The reactive power generated by the transmission line:

$$Q_{SR} = \sqrt{3}V_L \cdot I_{xc} = V_L^2 \cdot B_{cl} \quad (4.1)$$

Where: Q_{SR} = the three phase reactive power generated by the
transmission line

V_L = the line-to-line voltage

B_{c1} = the positive sequence charging susceptance

The above equation defines the MVAR rating of the required shunt reactor. Such a reactor is usually divided into two halves, each half being connected to the sending and receiving ends of the line respectively. Therefore, the rating of one reactor will be(90):

$$Q_{SR} = V_L^2 \cdot h_1 \cdot B_{c1} \cdot \ell / 2 = 500^2 \times 0.75 \times 5.13755 \times 10^{-6} \times 384 / 2 \approx 185 \text{ MVA}$$

For the above positive sequence phase compensation of 0.75, the phase reactance X_p is calculated from:

$$X_p = \frac{1}{h_1 \cdot B_{c1}} \quad (4.2)$$

and the zero phase sequence compensation h_0 can be calculated from the following(107):

$$h_0 = 1 + \frac{B_{c1}}{B_{c0}} (h_1 - 1) \quad (4.3)$$

which means that h_0 is:

$$h_0 = 1 + \frac{5.13755 \times 10^{-6}}{3.36691 \times 10^{-6}} (0.75 - 1) = 0.6185$$

and X_n is found⁽⁹⁰⁾ as:

$$X_n = \frac{h_1 B_{c1} - h_0 B_{c0}}{3h_1 B_{c1} h_0 B_{c0}} \quad (4.4)$$

which means:

$$X_n = 1915.6 \, \Omega$$

and $X_p = \frac{1}{h_1 B_{c1}} = 675.851 \, \Omega$

Both values for X_n and X_p represent the total reactances for both reactors.

Therefore for each reactor, the parameters of Fig. 5.4 will be:

$$X_n = \frac{1}{2} 1915.6 = 957.814 \, \Omega$$

$$X_p = \frac{1}{2} 675.527 = 337.93 \, \Omega$$

Chapter 5

ACCURATE FAULT LOCATION ALGORITHM FOR EHV TRANSMISSION LINES

5.1 INTRODUCTION

Power systems are considered to be one of the most complex engineering systems. This is due to the vast number of generators, transmission lines, sub transmission and distribution systems. In order to transfer the bulk power from the location it is generated to the place where it is used, hv and EHV transmission lines are used.

The reliability and high quality of power supply depends on the accuracy of protection and control systems used. In order to maintain system stability, high and ultra high speed protection systems are used. For, the restoration of power will depend on accurate methods for isolating the faulty part of the power system as soon as possible, and the ability to locate the precise distance to fault along the faulty line. The required accuracy will depend on the method used for detection, and will be directly related to the accuracy of measuring the signals used in the fault location algorithm employed. Different fault location methods have been developed^(54 - 59), for measuring the distance to fault. In modern fault location devices⁽⁵⁸⁾, although some improvement has been made, it is reported that the high accuracy of locating the fault remains a problem, in spite of the efforts to improve their performance.

The major drawback of most of the fault location devices, is due to the assumptions made and which are incorporated in the fault location algorithm.

Assumptions like perfect balanced transmission lines could have significant effect in case of untransposed lines. The fact that shunt capacitance is not considered can have additional contribution to the error experienced in the measurement of fault location. Mutual coupling between phases of one line, and between different circuits of transmission lines adds other factors to the inaccuracy in locating the faults (64 - 66).

In order to improve the accuracy of fault location techniques for EHV and UHV transmission lines, the fault location algorithm described in this chapter is based on the use of the current and voltage phasors and the transmission line parameters⁽⁶⁷⁾. The derivation of the main current and voltage signals is made from an accurate measurement of fault signals in the frequency domain, which considers the affect of travelling waves and the solution of the wave equation for the faulty transmission circuit.

A basic power system consisting of an EHV transmission circuit interconnecting two power sources of different strengths is considered first. The sending end and receiving end of the line are separated by the fault location, which is assumed along the line. Both sources have contribution to the fault, and the accuracy of measuring the sending end and receiving end voltages and currents, will affect the accuracy of measuring the distance to the fault location.

The accurate measurement of system voltages and currents under fault conditions is particularly important when unmanned substations are subjected to faults. Such faults result in the dispatch of maintenance personnel to the site. Power is usually restored after determining the location of the fault and evaluating the situation. Such a situation arises particularly when there is limitation on the remote monitoring information about the fault. Recent work

by Takahashi et al⁽⁷⁵⁾ indicates the development of a substation fault location system using optical current transducers (OCT's). The data measured by the OCT's provides reliable and fast determination of fault location for the purpose of prompt and effective recovery from power failures. The effectiveness of this method is demonstrated in defining on which feeder the fault is, rather than the exact fault location on a particular feeder. It determines on what section of a busbar the fault is located, under busbar fault conditions.

The fault location algorithm for measuring the location of the fault along the EHV transmission lines accurately is given in detail in this chapter. The basis of the approach followed in this work addresses the foregoing problems and takes into account the practical limitations, hence extending the capabilities for variety of practically encountered system and fault conditions. The method is based on utilising voltage and current signals at both ends of the EHV transmission line. By using modal analysis (Appendix A1), and based on the superposition technique, superimposed modal quantities used instead of the total phase values. This reduces the error which may be caused by line loading or source impedances.

5.2 SYSTEM CONFIGURATION

The single line diagram for the system considered is given in Fig. 5.1. The fault can be applied at any location of the transmission line. The source impedance can be changed to reflect the short circuit level at each end. The system is represented by equivalent networks for each source, the line section to the fault location, and the line section after the fault location. The distance to fault x and the total line length are also shown.

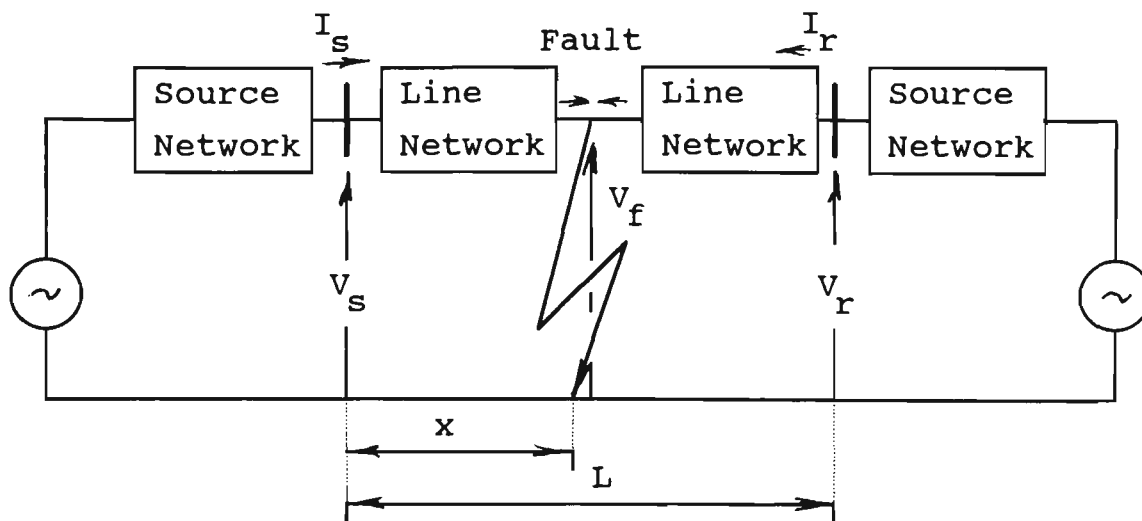


Fig. 5.1: Single line representation

In the following section, it will be shown, that there is no need to define precisely the fault impedance and the characteristics of the fault path, since the algorithm used will eliminate these factors from the computation of the fault location.

5.3 SINGLE PHASE LINE

For a single phase line shown in Fig. 5.1, the following relationships are applicable for steady-state voltage V_f across the fault at a distance x from the sending end, expressed in terms of measured voltages at the sending and receiving ends:

$$V_f = \cosh(\gamma \cdot x)V_s - Z_0 \sinh(\gamma \cdot (L - x))I_s \quad (5.1)$$

$$V_f = \cosh(\gamma \cdot (L - x))V_r - Z_0 \sinh(\gamma \cdot (L - x))I_r \quad (5.2)$$

In the above equations, both the propagation constant γ and the surge impedance Z_0 are defined as:

$$\gamma = \sqrt{ZY} \quad (5.3)$$

$$Z_0 = \sqrt{\frac{Z}{Y}} \quad (5.4)$$

respectively, where Z is the line series impedance and Y is the line shunt admittance per unit length. In order to avoid any difficulty in defining the precise value and characteristics of the fault path, equations (5.1) and (5.2) are equated to eliminate the V_f , and by some rearrangement, an accurate evaluation of the distance to fault as measured from the sending end is derived as:

$$X = [\tanh^{-1}(B/A)]/\gamma \quad (5.5)$$

where:

$$A = Z_0 \cosh(\gamma.L)I_r - \sinh(\gamma.L)V_r + Z_0 I_s \quad (5.6)$$

$$B = \cosh(\gamma.L)V_r - Z_0 \sinh(\gamma.L)I_r - V_s \quad (5.7)$$

In defining all the parameters in equation 5.5-5.7, the distance to fault can be computed accurately. In calculating x , there will be a small imaginary part which is neglected, and only the real part is considered. The parameters of the line (Z and Y) are known usually, and from the measured phasors of voltages and currents at both ends, the precise distance to fault can be computed.

5.4 THREE PHASE LINES

The computation of distance to fault described above can not be implemented directly for poly-phase transmission lines, since a number of phases are involved. Basically, the method can be extended to cater for multi phase circuits. In order to derive the expression for three phase transmission lines, a single line diagram representation which is shown in Fig. 5.2 is used.

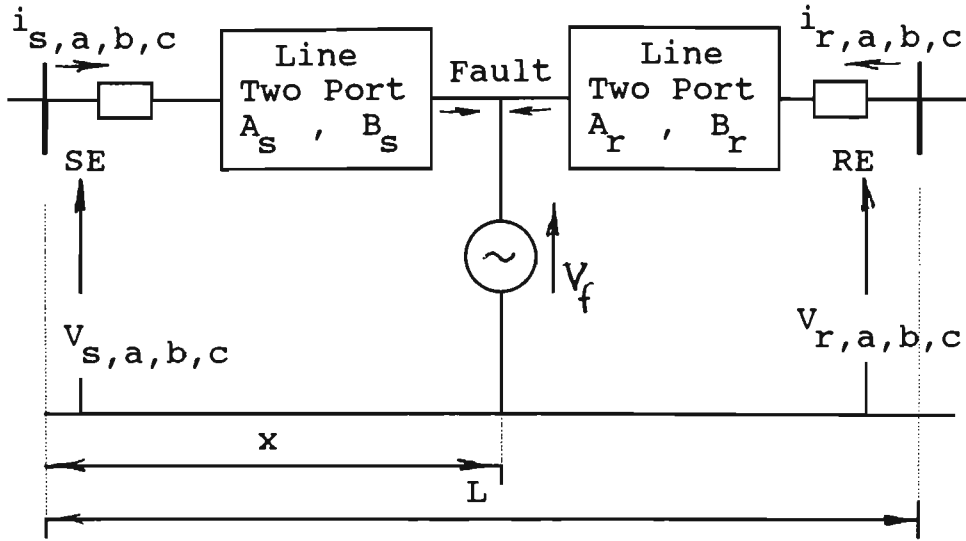


Fig. 5.2: Single line diagram of a three phase line

In case of three phase voltages and currents vectors and arrays are used for describing different parameters, eg., the sending end and receiving end currents and voltages are described as: $[I_{s,a,b,c}]$, $[I_{r,a,b,c}]$, $[V_{s,a,b,c}]$, and $[V_{r,a,b,c}]$, and based on the two port network representation, the two port matrices $[A_s]$, $[B_s]$, $[A_r]$, $[B_r]$ are all 3 x 3 matrices. These are usually defined from line parameters, ie line series impedance and shunt admittance matrices (Z and Y). Considering Fig. 5.2, the multi phase equivalent of equations 5.1 and 5.2 can be expressed as follows:

$$[V_{fa,b,c}] = [A_s] \cdot [V_{sa,b,c}] - [B_s] \cdot [I_{sa,b,c}] \quad (5.8)$$

$$[V_{fa,b,c}] = [A_r] \cdot [V_{rab,c}] - [B_r] \cdot [I_{rab,c}] \quad (5.9)$$

In most cases the line sections are treated as homogeneous. If it is necessary, these sections can be formed to include any discrete line transposition.

5.5 MODAL TRANSFORMATION

The important aspect in applying the fault location algorithm developed for single phase circuit into multi phase circuits lies in de-coupling equations 5.8 and 5.9 into uncoupled or independent equations which in effect describe

equivalent single-phase networks similar to that given in Fig. 5.1. In order to do this, the theory of natural modes is used. The method is well described in reference 10 and presented in detail in Appendix A1. The method of modal analysis is widely used in numerous power system analysis papers⁽³⁷⁾, for analysing the power system under fault conditions.

In brief, the method of modal analysis basically involves finding the matrix of eigenvectors of the $[Z].[Y]$ product ($[Q]$), and the $[Y].[Z]$ product ($[S]$). Using this technique, the voltages and currents derived from each phase a, b, c at each end would be transformed to corresponding modal voltage and current quantities 1, 2, 3 by means of the corresponding $[Q]$ and $[S]$ eigenvectors matrices:

$$[V_{sn}] = \begin{bmatrix} V_{s1} \\ V_{s2} \\ V_{s3} \end{bmatrix} = [V_{s1} \quad V_{s2} \quad V_{s3}]^T = [Q]^{-1} \cdot [V_{sa} \quad V_{sb} \quad V_{sc}]^T \quad (5.10)$$

$$[I_{sn}] = \begin{bmatrix} I_{s1} \\ I_{s2} \\ I_{s3} \end{bmatrix} = [I_{s1} \quad I_{s2} \quad I_{s3}]^T = [S]^{-1} [I_{sa} \quad I_{sb} \quad I_{sc}]^T \quad (5.11)$$

In using the theory of natural modes, even the multi conductor transmission line can be represented in a form similar to the one given in Fig. 5.1, ie, the multi phase transmission line can be represented as single phase uncoupled models. Therefore, for each single circuit, there are three pairs of such equations corresponding to the modes 1, 2, 3. For mode 2 for example, the equations would be:

$$V_{f2} = A_{s2}V_{s2} - B_{s2}I_{s2} \quad (5.12)$$

$$V_{r2} = A_{r2}V_{r2} - B_{r2}I_{r2} \quad (5.13)$$

In case of double circuit transmission lines, there will be six modes, which in turn result in six pairs of equations similar to the form of equations 5.12 and 5.13. For each mode these equations can be equated to define the relevant distance x , eg for mode one:

$$X = [\tanh^{-1}(\frac{-B_1}{A_1})] / \gamma_1 \quad (5.14)$$

where:

$$A_1 = Z_{01} \cosh(\gamma_1 \cdot L) I_{r1} - \sinh(\gamma_1 \cdot L) V_{r1} + Z_0 I_s \quad (5.15)$$

$$B_1 = \cosh(\gamma_1 \cdot L) V_{r1} - Z_{01} \sinh(\gamma_1 \cdot L) I_{r1} - V_{s1} \quad (5.16)$$

In order to calculate each modal surge impedance, the matrix product is calculated:

$$[Z_{0n}] = [\gamma]^{-1} [Q]^{-1} [Z][S] \quad (5.17)$$

in which $[\gamma]$ is a diagonal matrix of modal propagation constants comprising the square root of eigenvectors of the matrix product $[Z][Y]$. Therefore,

$$[Z_{0n}] = [Z_{01} \quad Z_{02} \quad Z_{03}] \quad (5.18)$$

the individual values being modal surge impedances. If perfect line transposition is assumed, the calculation of modal surge impedances and propagation constants is simplified since it is readily shown, for example the mode 2 surge impedance for a single circuit line can be expressed directly in terms of the positive phase sequence line impedance Z_1 and shunt admittance Y_1 per unit length of line as $Z_{02} = \sqrt{Z_1 / Y_1}$, similarly $G_2 = \sqrt{Z_1 Y_1}$. The assumption of perfect transposition leads to eigenvectors matrices which are equal, ie,

$$[S] = [Q]$$

and which are independent of the line geometry. In this case there is no need to calculate the voltage and current eigenvectors, and they will take the following form:

$$[S] = [Q] = \begin{bmatrix} 1 & 1 & 1 \\ 1 & 0 & -2 \\ 1 & -1 & 1 \end{bmatrix} \quad (5.19)$$

The algorithm has been found accurate even when perfect line transposition is assumed as it is explained in chapter 9.

5.6 FAULT LOCATION MEASUREMENTS

In order to test the accuracy of the algorithm, faults were applied on a transmission line in a digital simulation, and from the voltage and current phasors at both ends of the line, the modal transformation was carried out, so that the values were entered into the algorithm to compute the distance to fault x . For a single phase representation, the algorithm was found extremely accurate, ie, for any location of the fault, along the line, the assumed and measured location had been found to be very close.

For testing the algorithm further, a three phase model has been developed for computing fault location from the voltage and current phasors. Modal analysis is used to calculate the earth and aerial modes, from which a separate distance to fault is computed for each mode, which in turn define the fault location. Full details of test results in testing the developed algorithm are given in chapter 9.

Chapter 6

SHUNT COMPENSATED EHV TRANSMISSION LINES

6.1 INTRODUCTION

The control of power flow through EHV transmission lines mainly depends on the parameters of the line and the relative voltage magnitudes and angles at the terminating ends of the line. For the purpose of reactive power compensation in EHV long transmission lines, one or two banks of Y-connected shunt reactors with solidly earthed neutral are commonly employed⁽⁹⁰⁾. The rating of reactors is expressed in terms of their MVAR at rated voltage, per-phase reactance, or degree of shunt compensation⁽⁹³⁾.

Shunt reactors are also used for the purpose of suppressing of secondary arc in case of a single-circuit transmission lines, since neutralisation of shunt capacitive coupling between phases makes single-pole switching feasible on longer lines⁽⁹³⁾. By proper connection of EHV reactors used to wholly or partially compensate the normal line charging current, they can be used for ground fault suppression at a moderate additional cost^(94, 95).

In EHV transmission lines, capacitive charging current of lines and cables is approximately proportional to the square of system voltage and directly proportional to line length. Hence, capacitive current of EHV systems is mainly compensated for a number of reasons^(96, 97) :

- 1) To improve stability of transmission

- 2) To reduce power frequency and transient system overvoltages
- 3) To prevent self excitation of generators when connecting open circuited lines.

6.2 TYPES OF SHUNT REACTORS

For compensating the capacitance of EHV systems, various shunt reactor arrangements exist which may be classified as follows:

- 1- Linear reactors⁽⁹⁷⁾;
- 2- Externally controlled reactors⁽⁹⁸⁾;
- 3- Self- saturated reactors⁽⁹⁹⁾.

Reactors in EHV transmission lines are connected to the system either directly or via the secondary or the tertiary windings of intermediate transformers. At 500 kV level and above, only single-phase units have been used. In case of very long lines, shunt reactors may be used in conjunction with series capacitance. Under such circumstances, total reactive and capacitive power compensation has to be avoided for stability consideration⁽⁹⁹⁾. A 60% inductance and capacitance compensation may be the best compromise, although under light load conditions 100% shunt compensation is required⁽⁹⁰⁾.

There are two types of externally controlled reactors, ie.

- a) d.c. controlled reactors (transductors), and
- b) thyristor-controlled shunt reactors.

The main advantage of transducers is due to their static nature, they cannot loose synchronism with the system even under fault conditions. They can maintain a good average level of voltage but not suitable to deal with fast fluctuating load, due to their relatively slow response. The other disadvantage of transducers become evident when a saturable reactor generates harmonics other than the power frequency.

Thyristor-controlled reactors can achieve a continuous, relatively fast (0.01 s)⁽¹⁰⁰⁾ control of reactive power generation on a large scale. Such schemes are particularly applicable for suppression of voltage fluctuation caused by severe loads⁽¹⁰¹⁾.

Self-saturated reactors were developed first⁽¹⁰²⁾ for suppressing voltage fluctuations due to disturbing loads (arc furnaces in particular) and for reactive power control on EHV transmission systems. In these reactors, lower order harmonic currents are internally eliminated so that only harmonics of the $4n+1$ order can appear under steady-state conditions (n = number of limbs). Ideal reactive power control is achieved by using the reactor together with a series slope⁽¹⁰¹⁾ connecting capacitance and a parallel capacitor (to provide the leading VAR range). Static VAR compensators may use one of the following saturable reactors:

- a) the Quin reactors⁽¹⁰²⁾;
- b) the Twin-Tripler reactor⁽¹⁰²⁾;
- c) the Treble -Tripler reactor⁽¹⁰³⁾.

A detailed study of the twin and treble-tripler arrangements is presented in reference 100.

6.3 REACTOR ARRANGEMENT

The majority of faults in power systems are of single-phase to ground faults (mainly due to lightning), and of transitory nature, single-pole autoreclosure is found to greatly improve power system stability⁽⁹⁵⁾, provided that such faults could be successfully cleared. However, opening the circuit breakers on the ends of the faulted line conductor does not assure fault clearance. The isolated conductor is still capacitively and inductively coupled to the magnitude of and the rate of rise of steady-state recovery voltage.

In case of long transmission lines, because of the high system voltage and the high capacitive coupling (which is considered to be the most important)⁽⁹⁵⁾, both secondary arc current and recovery voltage are that much higher so that some means of neutralising the capacitive coupling has to be employed.

Kimbark⁽⁹⁵⁾ has developed a method to help secondary arc extinction by using a 4 legged reactor scheme. Economically the scheme is highly justified since EHV reactors have to be used for reactive power control and the cost of the additional neutral reactor required for secondary arc suppression is a small fraction of the cost of the main reactor.

Peterson et. al.⁽¹⁰⁴⁾ have suggested the neutralisation of capacitive coupling by the addition of a capacitor connected across the terminals of each breaker pole, proportional to the particular line being switched. Field tests and hybrid computer programs using lumped parameters, 500 kV transmission line model, have been performed to simulate single-pole switching and to evaluate the dead time required for arc extinction⁽¹⁰⁵⁾.

Kimbark⁽¹⁰⁶⁾ has produced very useful sets of families of curves that can be suited to any line construction, by relating both the residual arc current and the steady-state recovery voltage to the positive and zero degrees of shunt compensation (h_1, h_0). Residual arc current, steady-state recovery voltage and natural frequency of transient recovery voltage have been considered and the loci of each of them has been plotted in a rectangular coordinates h_0 versus h_1 . The charts help to know the correct degree of shunt compensation (h_0) that corresponds to the desired degree of compensation (h_1) for corresponding values of secondary arc current and steady-state recovery voltage. Kimbark has extended his work⁽¹⁰⁶⁾ by developing the reactor arrangement necessary to neutralise capacitive coupling in a double circuit line. He has considered the elimination of the effect of inductive coupling which was neglected in his previous analysis⁽¹⁰⁷⁾. Typical reactor schemes used for reactive power compensation are given in Fig. 6.1

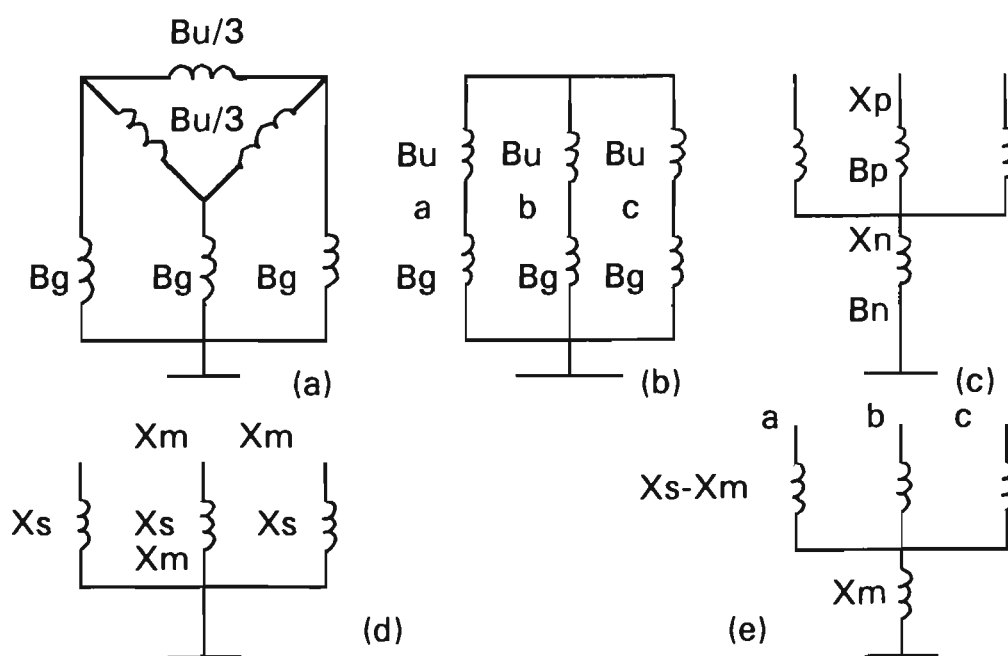


Fig 6.1: Possible shunt reactor arrangement for reactive power compensation: (a) & (b) - 6 reactor Scheme, (c) & (e) - 4 reactor Scheme.

For the schemes of Figs. 6 a, b and d, the total MVAR rating of the group of shunt reactors is the same, equals that required for shunt compensation under normal conditions. For 4 - reactor scheme, the phase reactors have the same total rating as that of Figs. 6.1 a, b & d.

The neutral reactor carries no current under steady-state conditions, it is energised under unsymmetrical fault conditions. Therefore its rating is a small fraction of the three main reactor ratings⁽⁷³⁾. According to Kimbark⁽⁷³⁾, from the economical and technical viewpoints, schemes of Figs. 6.1c, d and e are the most economical. Hence the scheme of Fig. 6.1 c is the one which is considered in this work.

6.4 THE 4 LEGGED REACTOR PARAMETERS⁽⁹⁰⁾

Considering Fig. 6.1 c, the positive phase sequence and zero phase sequence (PPS and ZPS respectively) are calculated by applying a set of PPS and ZPS voltages respectively to the 3-phase. Therefore it follow that:

$$X_1 = X_p \quad (6.1)$$

$$X_o = X_p + 3X_n \quad (6.2)$$

Similarly for Fig. 6.1 a:

$$X_1 = X_{lg} \cdot X_{lh} / (X_{lh} + X_{lg}) \quad (6.3)$$

$$X_o = X_{lg} \quad (6.4)$$

For the two circuits of Figs 6.1a and c to be equal, the corresponding quantities of equations 6.1 to 6.4 should be equal, ie.

$$X_1 + 3X_n = X_{lg} \quad (6.5)$$

$$X_1 = (X_{lg} \cdot X_{lh}) / (X_{lh} + 3X_{lg}) \quad (6.6)$$

For reactive power compensation

$$B_{L1} = h_1 B_{c1} \quad (6.7)$$

and for total elimination of interphase capacitive coupling:

$$B_{Lo} = h_o B_{c1} \quad (6.8)$$

It is shown in reference (107) that the phase and neutral reactances of the 4 reactor scheme are given by:

$$X_n = \frac{h_1 B_{c1} - h_o B_{co}}{3h_1 B_{c1} \cdot h_o B_{co}} \quad (6.9)$$

$$X_p = \frac{1}{h_1 B_{c1}} \quad (6.10)$$

where h_1 and h_o are the PPS and ZPS degrees of shunt compensation.

The MVAR rating of each reactor is :

$$Q_{SR} = \frac{V^2}{X_1} \quad (6.11)$$

or

$$Q_{SR} = V^2 \cdot h_1 B_{c1} \cdot \frac{l}{2} \quad (6.12)$$

SR1 = The two port matrix representing the near sending end shunt reactor . It is evaluated as follows :

$$\begin{bmatrix} V_{Sa} \\ V_{Sb} \\ V_{Sc} \end{bmatrix} = \begin{bmatrix} V_{sa1} \\ V_{sb1} \\ V_{sc1} \end{bmatrix} \begin{bmatrix} Z_1 + Z_n & Z_n & Z_n \\ Z_n & Z_1 + Z_n & Z_n \\ Z_n & Z_n & Z_1 + Z_n \end{bmatrix} \begin{bmatrix} I_{a1} \\ I_{b1} \\ I_{c1} \end{bmatrix} \quad (6.15)$$

$$\text{or : } V_s = V_{s1} = Z_{SR} \cdot I_1 \quad (6.16)$$

where

$$Z_1 = R_1 + jX_1$$

$$Z_n = R_n + jX_n$$

A quality factor of 250 has been used⁽⁹⁰⁾ to get both Z_1 and Z_n . From equation 6.16 the currents through the phase reactors are :

$$[I_1] = [Z_{SR1}]^{-1} \cdot [V_s] = [Z_{SR1}]^{-1} \cdot [V_{s1}] \quad (6.17)$$

$$\text{assuming } [Y_{SR}] = [Z_{SR}]^{-1}$$

but :

$$[I_1] = [Y_{SR1}] \cdot [V_s] = [Y_{SR1}] \cdot [V_{s1}] \quad (6.18)$$

$$\text{but: } [I_s] = [I_1] + [I_{s1}] \quad (6.19)$$

$$\text{or: } [I_s] = [Y_{SR1}] \cdot [V_s] + [I_{s1}] \quad (6.20)$$

which means that voltage and current transforms input to the sending end reactor are related to the corresponding output quantities by :

$$\begin{bmatrix} V_S \\ I_S \end{bmatrix} = \begin{bmatrix} U & O \\ Y_{SR1} & U \end{bmatrix} \begin{bmatrix} V_{S1} \\ I_{S1} \end{bmatrix} \quad (6.21)$$

where $[Y_{SR1}] =$ sending end reactor admittance matrix, which is found from $[Z_{SR1}]^{-1}$.

From Fig. 6.2, the following relationship can be written:

$$\begin{bmatrix} V_{S1} \\ I_{S1} \end{bmatrix} = \begin{bmatrix} A & B \\ C & D \end{bmatrix} \begin{bmatrix} V_{R1} \\ I_{R1} \end{bmatrix} \quad (6.22)$$

where A , B , C and D are transmission line constants.

$[Y_{SR1}]$ - receiving end shunt reactor admittance matrix = $[Z_{SR2}]$

Since each reactor compensates for half of line charging current:

$$[Z_{SR1}] = [Z_{SR2}] \quad (6.23)$$

$$[Y_{SR1}] = [Y_{SR2}] \quad (6.24)$$

From equation (6.21) it follows that :

$$\begin{bmatrix} V_S \\ I_S \end{bmatrix} = \begin{bmatrix} U & O \\ Y_{SR1} & U \end{bmatrix} \begin{bmatrix} A & B \\ C & D \end{bmatrix} \begin{bmatrix} U & O \\ Y_{SR2} & U \end{bmatrix} \begin{bmatrix} V_R \\ I_R \end{bmatrix} \quad (6.25)$$

or

$$\begin{bmatrix} V_S \\ I_S \end{bmatrix} = \begin{bmatrix} A_T & B_T \\ C_T & D_T \end{bmatrix} \begin{bmatrix} V_R \\ I_R \end{bmatrix} \quad (6.26)$$

where

$$\begin{bmatrix} A_T & B_T \\ C_T & D_T \end{bmatrix} = \begin{bmatrix} U & O \\ Y_{SR1} & U \end{bmatrix} \begin{bmatrix} A & B \\ C & D \end{bmatrix} \begin{bmatrix} U & O \\ Y_{SR2} & U \end{bmatrix} \quad (6.27)$$

In deriving equation 6.25, it is assumed that the line is homogeneous. However, due to transposition, this is not the case but each transposed section is dealt with separately as a homogeneous section and then the multiport equations for the 3-transposition sections are combined to yield a single two-port equation for the whole line. Three quantities are required under steady-state conditions, ie. sending end current, receiving end current and the voltage at the point of the fault, before the fault occurs. These three quantities are obtained from equation 6.26. An additional letter "S" is added to the subscript of each variable to distinguish them from fault quantities .

$$V_{SS} = A_T \cdot V_{SR} + B_T \cdot I_{SR} \quad (6.28)$$

$$I_{SS} = C_T \cdot V_{SR} + D_T \cdot I_{SR} \quad (6.29)$$

It follows that :

$$I_{SR} = B_T^{-1} \cdot V_{SS} - B_T^{-1} \cdot A_T \cdot V_{SR} \quad (6.30)$$

$$I_{SS} = (C_T - D_T \cdot B_T^{-1} \cdot A_T) \cdot V_{RS} + D_T \cdot B_T^{-1} \cdot V_{SS} \quad (6.31)$$

By assuming that the fault occurs at a distance "X" from the sending end the line constant matrix given in equation 6.25 and can be split into two matrices. Then matrices correspond to line lengths "X" and ' $\ell - X$ ' respectively so that

$$\begin{bmatrix} A & B \\ C & D \end{bmatrix} = \begin{bmatrix} A_1 & B_1 \\ C_1 & D_1 \end{bmatrix} \begin{bmatrix} A_2 & B_2 \\ C_2 & D_2 \end{bmatrix} \quad (6.32)$$

Steady-state voltages and currents at the point of fault are related to voltages and currents at the receiving end as follows :

$$\begin{bmatrix} V_{fs} \\ I_{fs} \end{bmatrix} = \begin{bmatrix} A_{T2} & B_{T2} \\ C_{T2} & D_{T2} \end{bmatrix} \begin{bmatrix} V_{RS} \\ I_{RS} \end{bmatrix} \quad (6.33)$$

Using this equation with equations 6.30 and 6.31 we get

$$V_{fs} = (A_{T2} - B_{T2} \cdot B_T^{-1} \cdot A_T) \cdot V_{RS} + B_{T2} \cdot B_T^{-1} \cdot V_{SS} \quad (6.34)$$

where V_{fs} = steady-state voltage transform at the point of fault before the fault occurs

$$\begin{bmatrix} A_{T2} & B_{T2} \\ C_{T2} & D_{T2} \end{bmatrix} = \begin{bmatrix} A_2 & B_2 \\ C_2 & D_2 \end{bmatrix} \begin{bmatrix} U & O \\ Y_{SR2} & U \end{bmatrix} \quad (6.35)$$

In these above equations, the steady-state quantities I_{SS} , I_{RS} and V_{fs} may be considered in phasor form and converted directly to the time domain without the need to go through the inverse Fourier transform.

6.6 FAULT LOCATION ON SHUNT COMPENSATED LINES

In chapter 5, an accurate algorithm for fault location on EHV transmission lines is described. The algorithm is not dependent on the impedance of the source(s), and for the accurate measurement of the fault location, only voltages and currents at the sending and receiving ends of the faulty line and the parameters of the line are required.

In this section, the shunt compensated transmission line is considered, where the line terminated from both ends by shunt reactors. Fig. 6.3 shows a typical 3-phase transmission line connected to two sources and terminated by reactors from both ends of the line. The reactors affect the reactive power flow in the line, and their effect is evident particularly when the line is lightly loaded or open circuited at the receiving end. In the case of long radial lines without the reactors, the line becomes a generator of reactive power, hence the voltage at the receiving end may be greater than the voltage at the sending end. This phenomena is referred to as the Ferranti Effect⁽⁸⁶⁾. When reactors are switched on, they absorb the reactive power generated by the line and therefore, the voltage at the end of the line can be kept within reasonable limits

Under normal full load conditions, the reactors are disconnected in order to be able to improve the flow of power through the line. In some cases, for long transmission lines which are heavily loaded, means for injecting reactive power may be required to improve the flow of power and hence increase the stability limit of the transmission circuit. In order to analyse the transmission line when terminated by shunt reactors at both ends, we consider the transmission system given in Fig. 6.3. The reactors are shown on the source side at each termination.

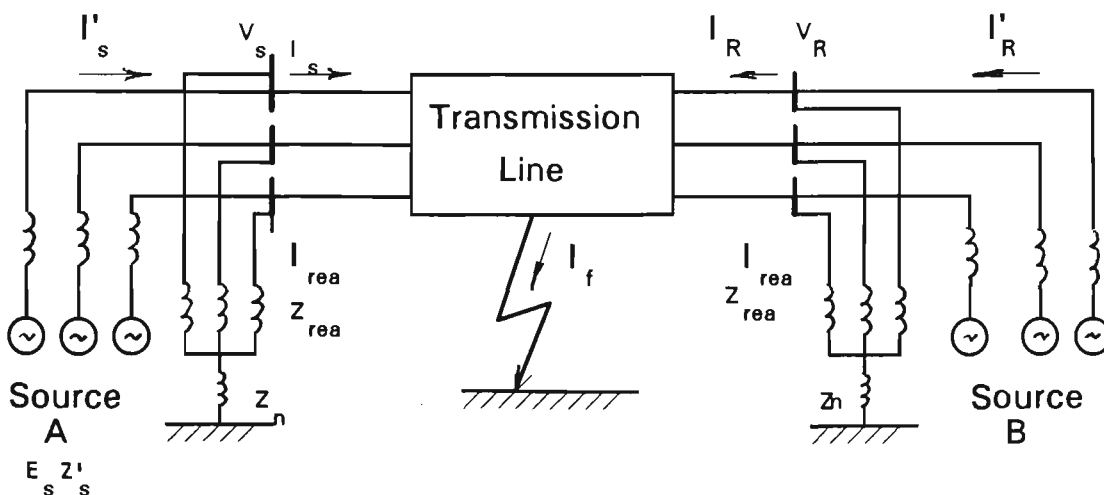


Fig. 6.3: Shunt compensated transmission line

From Fig. 6.3, the sending end vector of the three-phase voltages is:

$$\begin{bmatrix} V_{sa} \\ V_{sb} \\ V_{sc} \end{bmatrix} = \begin{bmatrix} E_{sa} \\ E_{sb} \\ E_{sc} \end{bmatrix} - \begin{bmatrix} Z_{sa} & O & O \\ O & Z_{sb} & O \\ O & O & Z_{sc} \end{bmatrix} \cdot \begin{bmatrix} I_{sa} \\ I_{sb} \\ I_{sc} \end{bmatrix} \quad (6.36)$$

or in a condensed form:

$$[V_s] = [E_s] - [Z_s] \cdot [I_s] \quad (6.37)$$

In a similar way, we can express the three-phase sending end source voltages in terms of the reactor impedances and reactor currents as follows:

$$\begin{bmatrix} V_{sa} \\ V_{sb} \\ V_{sc} \end{bmatrix} = \begin{bmatrix} Z_{Ra} + Z_n & Z_{Rb} & Z_{Rc} \\ Z_{Ra} & Z_{Rb} + Z_n & Z_{Rc} \\ Z_{Ra} & Z_{Rb} & Z_{Rc} + Z_n \end{bmatrix} \cdot \begin{bmatrix} I_{Ra} \\ I_{Rb} \\ I_{Rc} \end{bmatrix} \quad (6.38)$$

or in a condensed form:

$$[V_s] = [Z_{RE}] \cdot [I_{rea}] \quad (6.39)$$

where Z_R and I_R are reactor impedance and reactor currents respectively.

At the sending end busbar, we can write the following:

$$[I'_s] - [I_s] = [I_{rea}] \quad (6.40)$$

Combining equations 6.32 and 6.34 and considering equation 6.35 gives:

$$[E_s] - [I_s]' \cdot [Z_s] = [I_{rea}] \cdot [Z_{rea}] \quad (6.41)$$

from equation 6.41 and considering equation 6.40:

$$[Z_s] = \frac{[E_s] - [I_{rea}] \cdot [Z_{rea}]}{[I_s] + [I_{rea}]} \quad (6.42)$$

which will be called $[Z_s]'$, and without the reactor the source impedance will be:

$$[Z_s] = \frac{[E_s] - [V_s]}{[I_s]} \quad (6.43)$$

Dividing both sides of equations 6.42 and 6.43, we get:

$$\frac{[Z_s]'}{[Z_s]} = \frac{[I_s]}{[I_s] + [I_{rea}]} \quad (6.44)$$

or $[Z_s]' = K \cdot [Z_s]$, where K is less than one, and calculated from:

$$K = \frac{[I_s]}{[I_s] + [I_{rea}]} \quad (6.45)$$

This means, that the source reactance is modified as a result of connecting the shunt reactors, namely, the new source reactance with the shunt reactor will be different from the original source reactance. The reactance of the source on the receiving end can be derived in a similar way to be as follows:

$$[Z_R]' = K' \cdot [Z_R] \quad (6.46)$$

where K' is less than one, calculated from:

$$K' = \frac{I_R}{[I_R] + [I_{rea}]} \quad (6.47)$$

From the above analysis, it is evident that the connection of shunt reactors at the termination of the transmission line will have some effect on the source impedance. The source impedance has an effect on the calculation of fault currents in the transmission line.

In chapter 5, it was shown that the calculation of the fault location on EHV transmission line can be defined as in the following equation:

$$X = \{\tanh^{-1} [-B/A]\} / \gamma \quad (6.48)$$

where:

$$A = Z_o \cosh(\gamma \cdot \ell) I_R - \sinh(\gamma \cdot \ell) V_R + Z_o I_s \quad (6.49)$$

$$\text{and } B = \cosh(\gamma \cdot \ell) V_R - Z_o \sinh(\gamma \cdot \ell) I_R - V_s \quad (6.50)$$

From equation 6.48 and the expressions for A and B, it is clear that for shunt compensated transmission lines, the algorithm for the determination of fault location on EHV uncompensated transmission lines can be used. This is due to the fact that although the source impedance at both the sending and receiving ends of the line will be modified, the accuracy of calculation of the fault location will be practically in the same order. The derived fault location algorithm depends on the accurate measurements of the sending and receiving end currents and voltages as phasor quantities, and the propagation parameters of the transmission line, ie., Z_o , γ , and the per unit length transmission line constants, ie., the series impedance and the shunt admittance respectively. The

algorithm does not depend on the variation of source impedance, which can happen in any power system due to normal and abnormal switching activities under different conditions.

The above analysis were concluded from the studies of a two terminal power system interconnected by an EHV transmission line as in Fig. 6.3. The tests were carried out for 75% compensation calculated as shown in Appendix (3). For a three-phase faults along the 384 kms, 500 kV line at 0, 96, 192, 288 and 384 kms of the line length, for uncompensated and compensated lines, the results are given in Fig. 6.4. From these results, it is evident, that while the error is slightly higher at the termination of the line, it is significantly lower as we move away from the receiving and sending ends of the line toward the middle of the line. The most accurate measurement of the fault location for both compensated and uncompensated lines is when the fault is in the middle of the line.

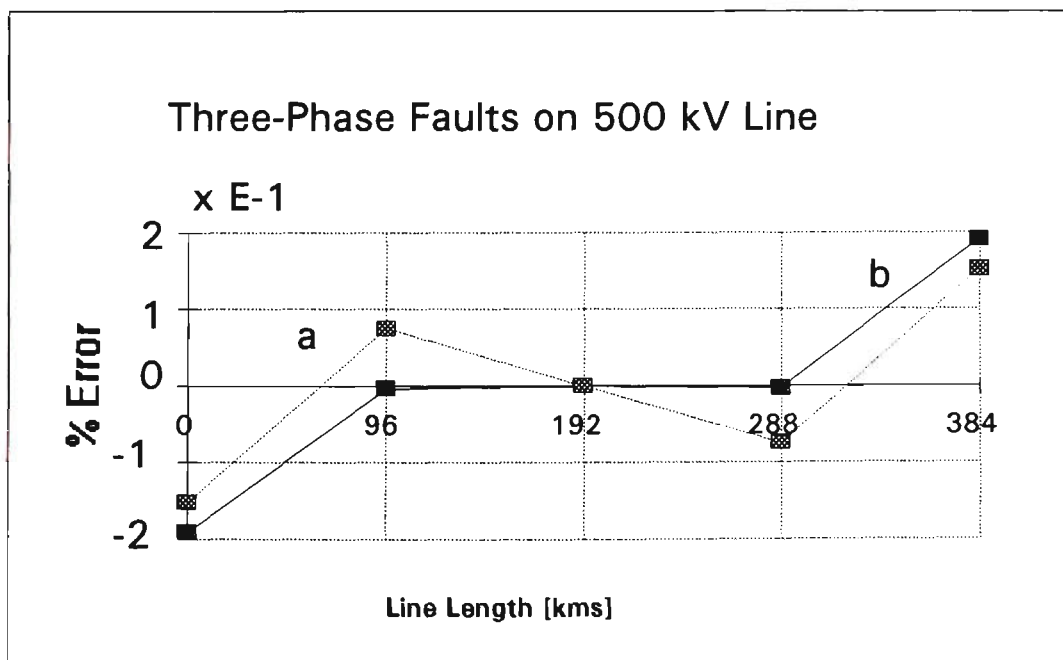


Fig. 6.4: Three phase faults on 500-kV, transposed line:
 a) Without compensation, b) With 75% compensation

In case of using shunt reactors for compensating the excessive reactive power of the line when it is lightly loaded, and for improving the extinction of the arc under autoreclose conditions, it is possible to operate the line with shunt reactors connected on or off the line. Such operational variations will have an effect on the equivalent source impedance of the terminating sources. These variation of source impedance have little effect on the accuracy of computing the location of the fault on EHV shunt compensated transmission lines.

Chapter 7

THREE-TERMINAL SYSTEMS

7.1. INTRODUCTION

This chapter presents a method for accurate fault location for three terminal transmission lines, which is based on the method which was fully developed in chapter 5 for two terminals. The effect of including three terminal EHV transmission lines on the accuracy of fault location algorithm is analysed. Different methods of feeder configuration have various consequences on the accuracy of fault location. The calculation method is based on modal analysis and the use of current and voltage phasors extracted from the three terminals ends of the considered system.

It is important to accurately measure the exact location of faults occurring on EHV transmission lines. This is due to the fact that there is little visual evident of the location of the fault, hence a delay in the repair of the line means longer undue outage of the line. Furthermore, post clearance tests performed on the line at reduced voltage can be misleading and inconclusive.

The use of conventional methods for the measurement of the fault location using simple impedance measurement is not reliable and inaccurate.

The development of fault location algorithm for two terminal networks is not directly applicable for three or multi-terminal transmission lines. This applies particularly to algorithms used for conventional fault location methods using one-terminal AC voltage and current. Nagasawa (69) et. al. describe a new

fault location algorithm for multi-terminal two parallel transmission lines. The method uses the magnitude of the differential current at each terminal and also uses an algorithm based on a three-terminal fault location algorithm and an equivalent conversion from n-terminal to a three-terminal system. The EMTP (Electromagnetic transient program) is used for simulating the results.

This chapter presents a new method for calculating the exact fault location for three terminal EHV transmission lines. The new technique is based on digital computation of the power frequency component of the three-phase current and voltage phasors at the line terminals. As for the two terminal transmission lines^(79, 80), the algorithm developed for the three-terminal transmission line is virtually independent of fault resistance and largely insensitive to variations in source impedance, line configuration including line transposition ⁽⁸⁰⁾.

7.2 THREE TERMINAL SYSTEM

A typical three-terminal transmission line is given in Fig. 7.1 for the steady state conditions. Fig. 7.2 shows the same system under fault conditions.

The algorithm for accurate fault location for two terminal transmission lines described in chapter 5 is further developed for three terminal transmission systems.

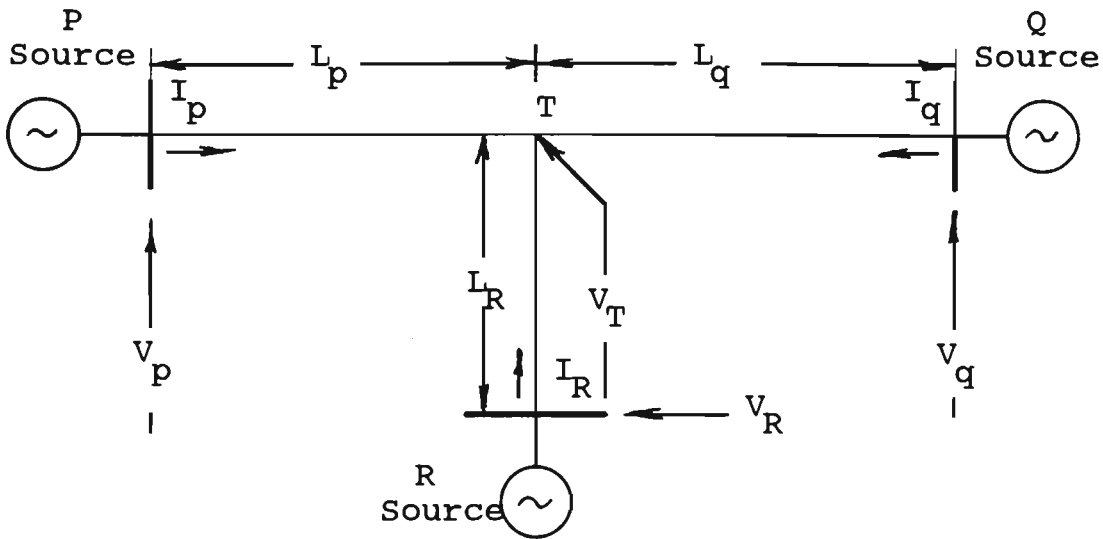


Fig. 7.1: Three terminal system-steady state condition

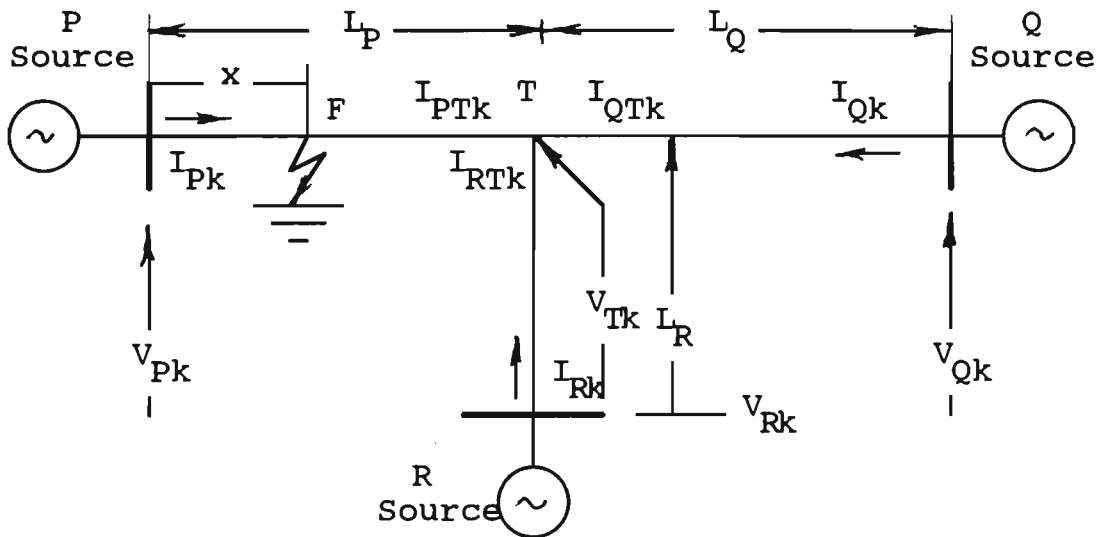


Fig. 7.2: Three terminal system-transient condition

To evaluate the fault location on any part of the three terminal transmission line, information about the voltage and current phasors at the three ends has to be obtained. To satisfy this requirement, some type of data synchronisation is required. This means that the data must have a common reference point⁽¹⁰⁸⁾. It should be stated that in practice, if one end is designated as reference, then the mismatch in recorded data at any of the other two ends rarely ever exceeds two samples when compared to the reference-end data⁽⁹¹⁾. However, in the fault location algorithm, it is emphasised that means for synchronising data

within the computation procedure to maintain a high degree of accuracy, particularly when there is any possible mismatch of data in case when the three fault recorders at the three ends were triggered at different time.

It is required to evaluate the voltage at the tee point from the knowledge of the pre-fault power frequency voltage and current phasors which are obtained using Discrete Fourier Technique (D. F. T.) (91). The voltage relationship obtained at the T point as function of voltages and currents at the three ends are given as follows:

$$V_{PT} = \cosh(\gamma L_P)V_P - Z_o \sinh(\gamma L_P)I_P \quad (7.1)$$

$$V_{QT} = \cosh(\gamma L_Q)V_Q - Z_o \sinh(\gamma L_Q)I_Q \quad (7.2)$$

$$V_{RT} = \cosh(\gamma L_R)V_R - Z_o \sinh(\gamma L_R)I_R \quad (7.3)$$

When the data is synchronised, and taking end P say as a reference, $V_{PT}=V_{QT}=V_{RT}=V_T$. Any mismatch would be seen in the phase angles of the sampled data, which can be corrected by shifting the data at the unsynchronised ends few samples until the errors due to sampling are minimised.

7.3 FAULTY SECTION IDENTIFICATION

Considering Fig. 7.1, it is possible to define the faulty leg of the three terminal transmission line using a comparison procedure for the three voltages V_P , V_Q and V_R phasor measurements. From the measured voltages, it is possible to establish the faulty section by comparing each time and evaluating the relationship between the sampled values. If a fault say near the R end occurs, the voltage at the other two ends P and Q will be very similar but the voltage for R will be different. If there is no significant difference in the voltages

obtained from the data received from all three ends, it can be assumed that the fault is at the tee point itself.

7.4 FAULT LOCATION ALGORITHM

The technique followed in locating the fault from the nearest end is similar to that of the two terminal transmission line. Consider a fault at point F of the three terminal system given in Fig. 7.2 on the PT leg. Using the two-port matrix relationship, both the fault point and the tee point phasors as a function of the phasors at the three ends are given as:

$$V_{Fk} = \cosh(\gamma_k x) V_{Pk} - Z_{ok} \sinh(\gamma_k x) I_{Pk} \quad (7.4)$$

and:

$$V_{Fk} = \cosh(\gamma_k L_{Pk} - \gamma_k x) V_{Tk} + Z_{ok} \sinh(\gamma_k L_{Pk} - \gamma_k x) I_{PTk} \quad (7.5)$$

also:

$$V_{Tk} = \cosh(\gamma_k L_{Rk}) V_{Rk} - Z_{ok} \sinh(\gamma_k L_{Rk}) I_{Rk} \quad (7.6)$$

$$I_{PTk} = Y_{ok} \sinh(\gamma_k L_{Qk}) - \cosh(\gamma_k L_{Qk}) I_{Qk} + Y_{ok} \sinh(\gamma_k L_{Rk}) V_{Rk} - \cosh(\gamma_k L_{Rk}) I_{Rk} \quad (7.7)$$

where:

$$D_k = -V_{Pk} + A_k \cosh(\gamma_k L_{Pk}) Z_{ok} \sinh(\gamma_k L_{Pk})$$

$$C_k = -Z_{ok} I_{Pk} + A_k \sinh(\gamma_k L_{Pk}) - Z_{ok} B_k \cosh(\gamma_k L_{Pk})$$

$$B_k = -\cosh(\gamma_k L_{Qk}) I_{Qk} + Y_{ok} \sinh(\gamma_k L_{Rk}) V_{Rk} - \cosh(\gamma_k L_{Rk}) I_{Rk} + Y_{ok} \sinh(\gamma_k L_{Qk}) V_{Qk}$$

$$A_k = \cosh(\gamma_k L_{Qk}) V_{Qk} - Z_{ok} \sinh(\gamma_k L_{Qk}) I_{Qk}$$

where k=1 for Earth mode, 2 and 3 for Aerial modes, x is the distance to fault.

A simple manipulation of equations 7.4-7.7 yields:

$$X = \{ \tanh^{-1}(D_k / C_k) \} / \gamma_k \quad (7.8)$$

where D_k , C_k and γ_k are defined above.

7.5 ALGORITHM ASSESSMENT

The modelling used for assessing the algorithm is based on an early work (28), which includes both the distributive nature of the line, and its frequency dependent parameters. This modelling provides a realistic instantaneous values of voltages and currents at the terminating busbars, for any type of fault and source conditions. Results are presented for 400 kV transmission line given in chapter 4 of this thesis, with the following relevant parameters:

- i) earth resistivity (assumed homogeneous) = $100 \Omega - m$
- ii) source X/R ratio = 30, $Z_{S0}/Z_{S1} = 0.5$.

The error expected is expressed as a percentage of the length of a particular leg of the tee and given as:

$$\% \text{ error} = \frac{X_{estimated} - X_{actual}}{L_{tee}} \times 100 \quad (7.9)$$

The analysis of the accuracy of the fault location algorithm for symmetrical tee configuration given in Fig. 7.1 is carried out (28). Results from studies on three terminal systems are given in chapter 9.

Chapter 8

VOLTAGE AND CURRENT RESPONSE OF POLYPHASE SYSTEMS

8.1 INTRODUCTION

Modern power systems are large in size and complexity. When such power systems are subjected to different abnormal operations such as short circuits or open conductors it is very important to isolate the faulty sections of the system using ultra high speed protection relays (37). In order to be able to design ultra high speed protection systems, it is extremely vital to be able to carry out extensive research and development on EHV transmission lines under fault conditions. Accurate digital simulation methods for analysing faulted transmission lines revealed(38), that the precise nature of current and voltage wave forms, particularly during the first half cycle, is very important. The modern theory of transmission lines is used in this chapter to predict the fault-transient behaviour of multi conductor overhead transmission lines.

High speed measurements of the faulty EHV overhead transmission lines possess a significant travelling wave components in both faulted and healthy phase conductors. Modern digital relays have to be able to measure signals during a very short period of time following fault inception. Transient wave forms under fault conditions depend on the nature of the earth return, conductor configuration, fault location and point on wave of fault initiation. An accurate representation of the transmission line including the frequency variance provides realistic results, which can be used for developing and testing different new algorithms for digital relaying and measurements purposes.

When power system conditions are changed from healthy into faulty mode, it undergoes a form of non linearity involving a change in the system matrix. Wedepohl and Mohammed⁽¹⁵⁾ have highlighted this problem when they investigated sequential pole closure problem associated with switching surge phenomena. Under fault conditions this phenomena is accentuated because the point of non linearity usually occurs at an intermediate point between the terminating busbars.

This chapter use accurate method for simulating faulted EHV transmission lines to provide the appropriate transient waveforms for subsequent use for protection and measurement purposes.

In order to provide accurate information of the transient waveforms for further processing in the fault location algorithm, the method used for computation of the necessary signals will significantly affect the accuracy of fault location on EHV transmission lines.

This chapter will analyse different abnormal operations of the system under consideration caused by different short circuits on the EHV transmission lines. When these faults occur, the protection system should be able to isolate the faulty system as soon as possible, in order to maintain system stability, and to safeguard the equipment which are subjected to heavy stresses. Subsequent to fault isolation, the location of the fault is identified in order to restore the energy in the line quickly. Since the developed algorithm for locating the fault position on the line depends on the measured steady-state filtered voltage and current signals at the terminations of the line, it is the objective of this chapter to show system behaviour before the fault inception, during the fault and after

removing the fault. Simulation studies will be shown for two and three terminal transmission systems.

For the simulation studies performed in this chapter, the ATP (the PC version of the EMTP)⁽⁸⁸⁾ program has been used. The transmission line is simulated as fully transposed system and considering the distributed nature of the line with its modal parameters.

8.2 TWO TERMINAL SYSTEMS

In order to study the behaviour of the two terminal systems, the simulation of the systems was based on the following:

1. The transmission lines are fully transposed
2. 500 kV lines of horizontal configuration as it was discussed in chapter 4, which is shown on Fig. 4.4 of the same chapter
3. The two terminating sources are of 35 GVA each
4. Shunt reactors parameters are as given in chapter 4, and shown in Fig. 4.5 of the same chapter.
5. The length of the line was assumed = 384 km

In most cases, faults were applied at $t=10$ ms, and cleared after two cycles (40 ms). The wave forms are given for solution time of up to 140 ms, in order to observe the behaviour of the system after fault clearance. Faults are assumed to be of the metallic (bolted) faults. However, faults through impedance were also considered, and discussed in this chapter in Section 8.4.

The fault was assumed to start after five milliseconds of normal system operation. After 50 milliseconds, that fault was cleared. System behaviour

under these three states of operation was recorded at different location of the EHV transmission system. The wave forms for a single phase to ground fault are given for phase A fault. These traces are shown on Figures 8.1 - 8.17.

8.2.1 Single Phase to Ground Faults

The two terminal system under investigation is given in Fig. 8.1

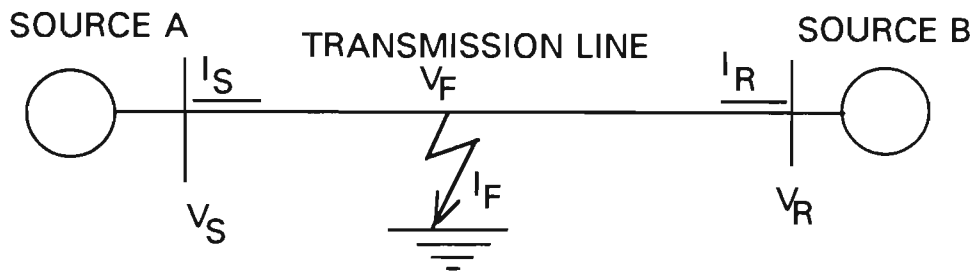


Fig. 8.1: Two terminal system

A short circuit applied at the sending end of the system given in Fig. 8.1 after 5 ms of normal steady state operation will force phase A voltage to zero. The voltage of phase A regains its value after fault clearance which is assumed to happen after fifty ms.

The three phase waveforms at the sending end are given in Fig. 8.2. The effect on these waveforms is indicated by the ripples on the healthy B and C phase voltages. Similar effect is shown in Fig. 8.3 for the voltage waveforms at the receiving end. The current waveforms for this type of fault are given in Figs. 8.4, 8.5 and 8.6 for the currents through the fault, sending end and receiving end respectively.

[kU,]

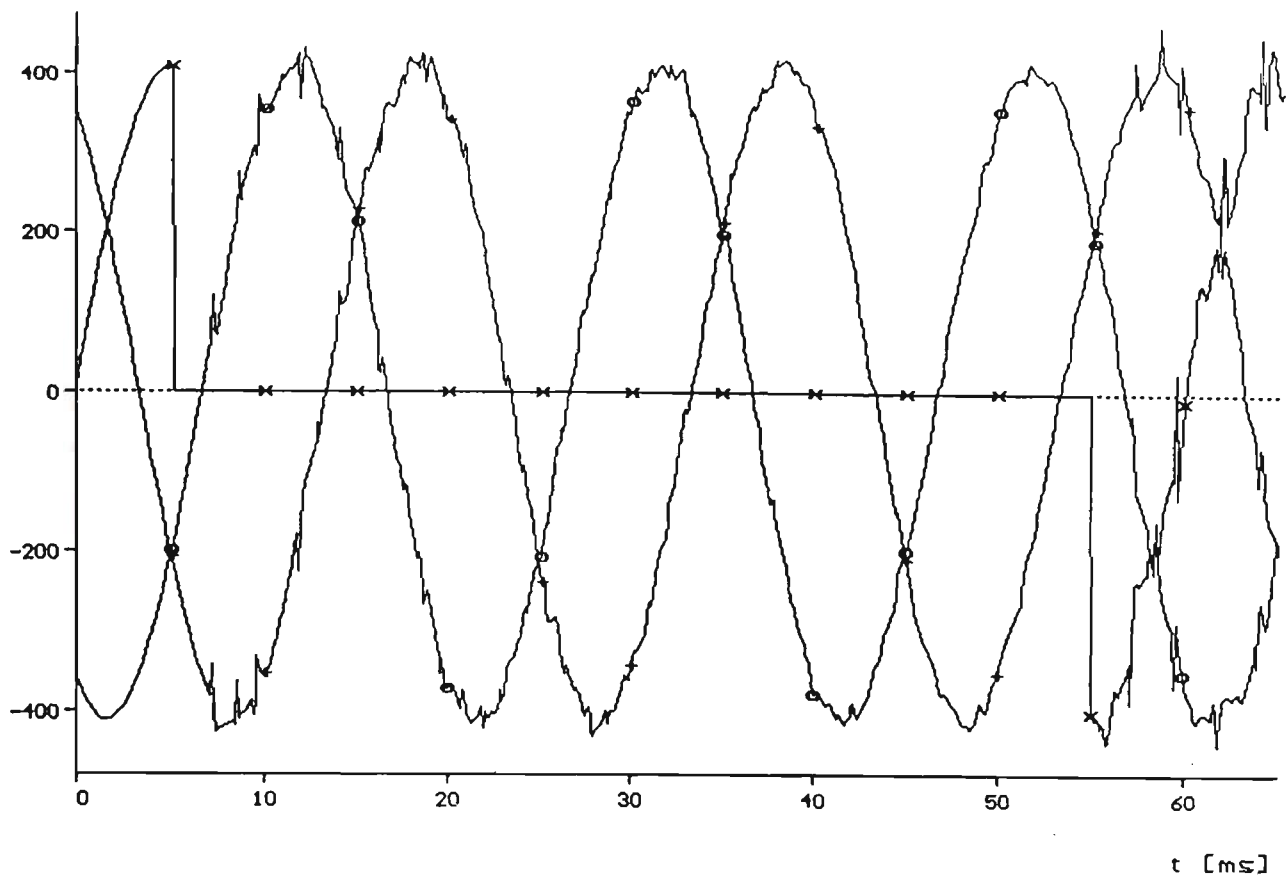


Fig. 8.2: A-Phase to ground Fault, Sending End Three Phase Voltages,

(x) : Red, (o) : Yellow, (+) Blue , Two Terminal System, Fault location at $x=0$

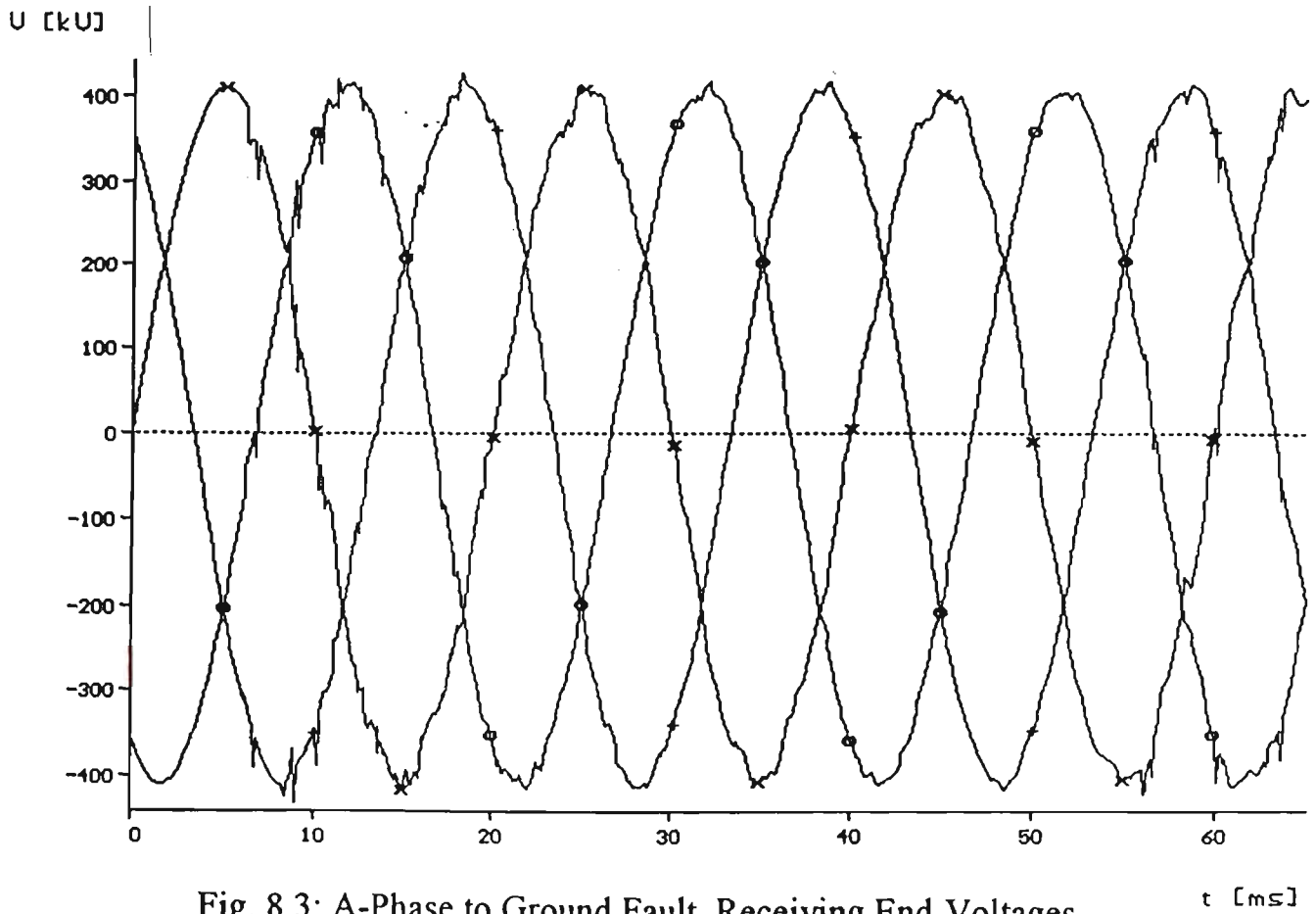


Fig. 8.3: A-Phase to Ground Fault, Receiving End Voltages

(x): Red, (o): Yellow, (+): Blue, Two Terminal System, Fault Location at $x=0$

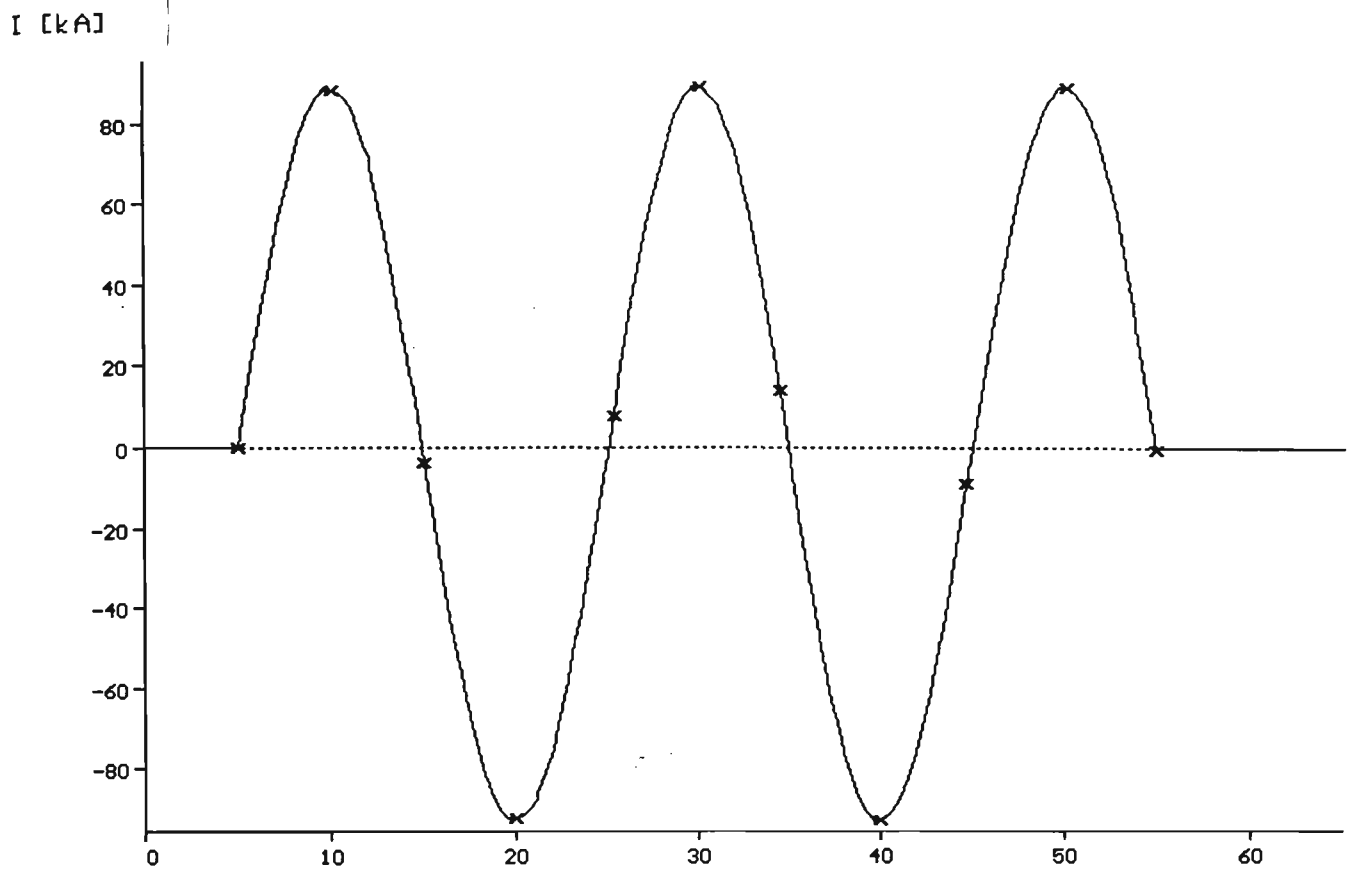


Fig. 8.4: A-Phase to Ground Fault, Fault Location at $x=0$

t [ms]

Fault Current, (x) Red, (o): Yellow, (+): Blue, Two Terminal System

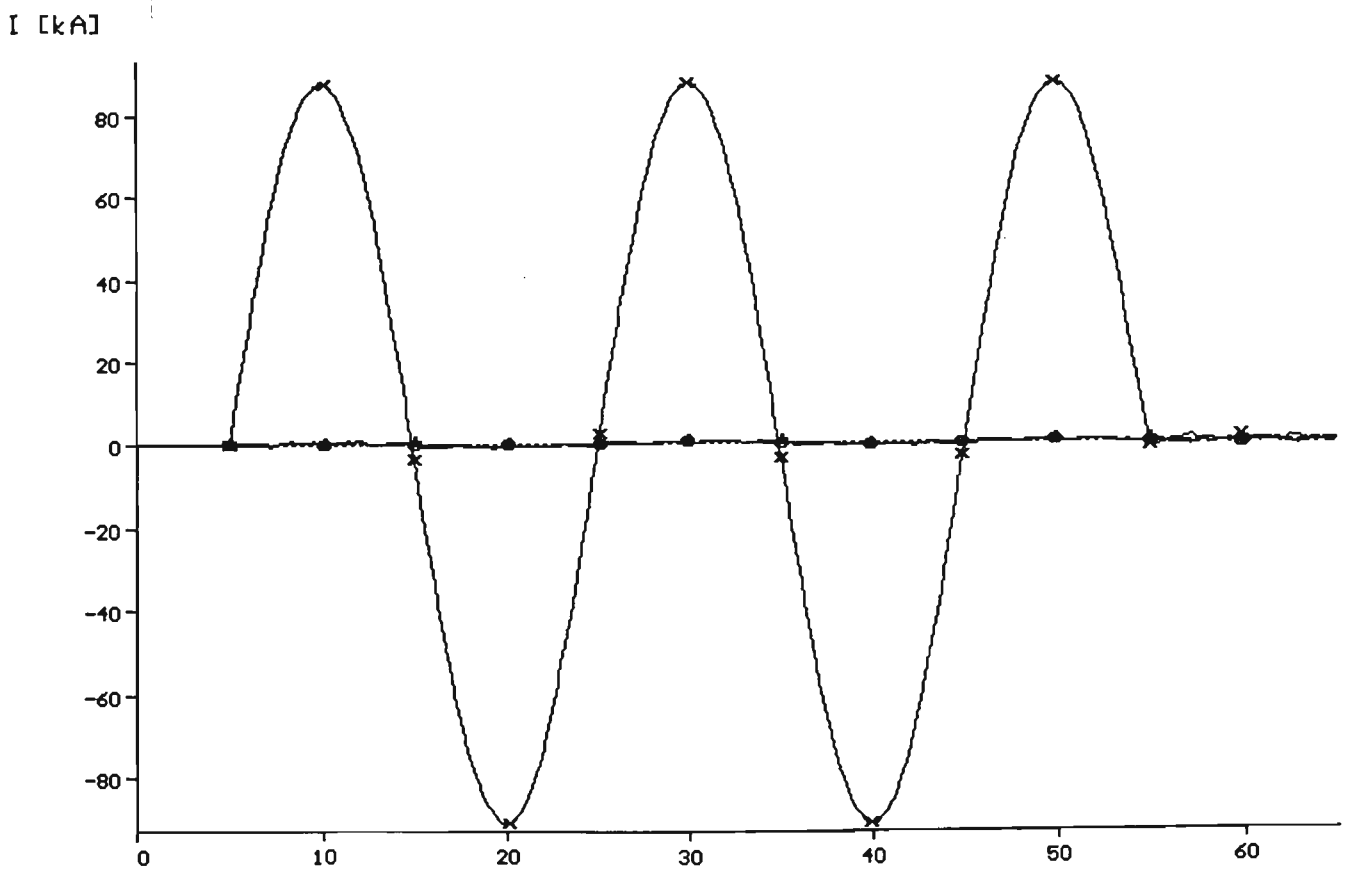


Fig. 8.5: A-Phase to Ground Fault at $x=0$, Two terminal System,

t [ms]

Sending End Currents, (x): Red, (o): Yellow, (+): Blue

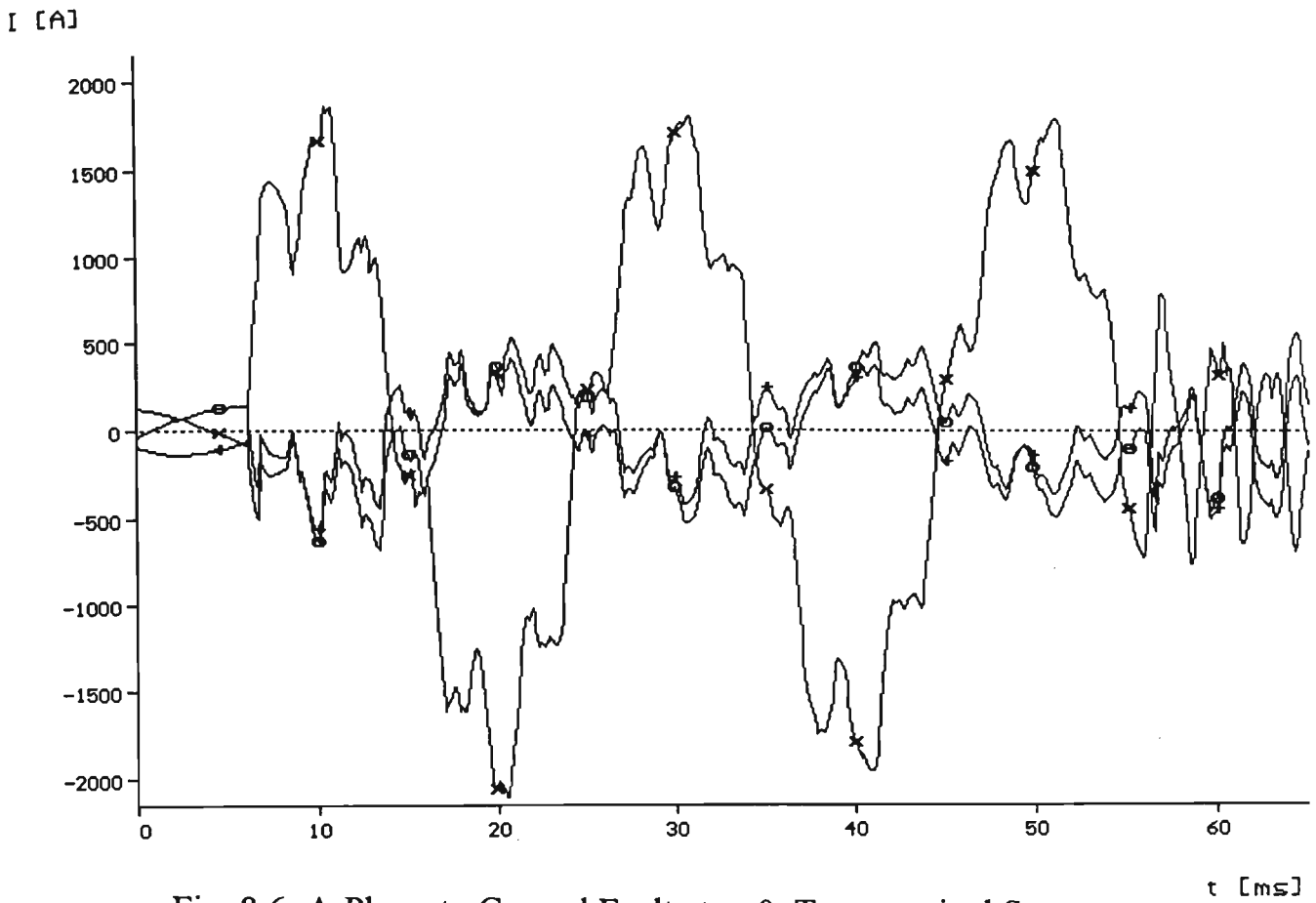


Fig. 8.6: A-Phase to Ground Fault at $x=0$, Two terminal System,
Receiving End Currents, (x): Red, (o): Yellow, (+): Blue

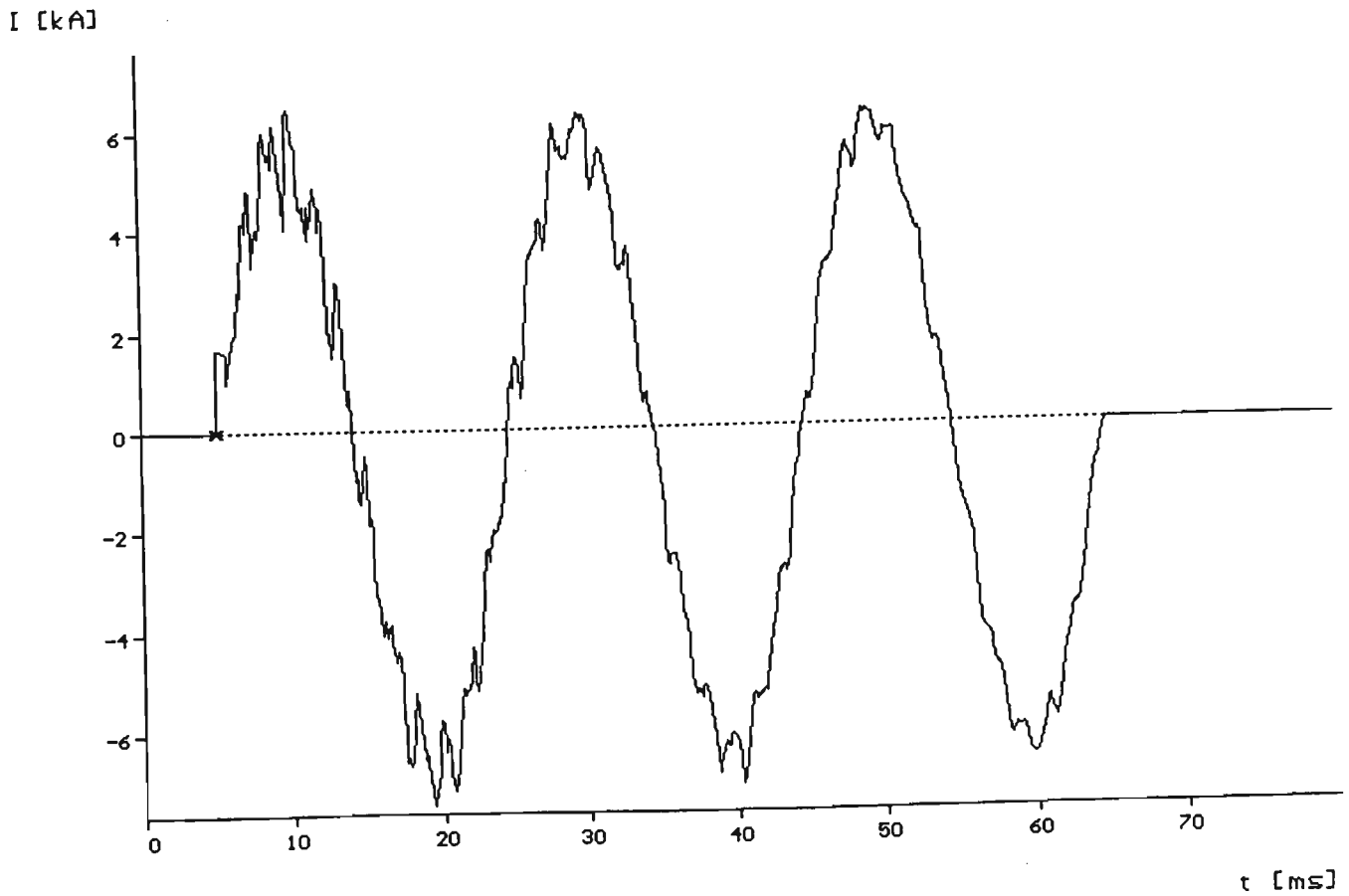


Fig. 8.7: A-Phase to Ground Fault at $x=0$, Two terminal System,
Fault cleared after 40 ms, fault current, (x): Red, (o): Yellow, (+): Blue

For a single phase to ground fault at the middle of the transmission line, detailed waveforms for voltages and current traces are given in Figs. 8.7-8.18. The fault current through the fault path is given in Fig. 8.7, whereas the sending and receiving end currents are given in Figs. 8.8 and 8.9 respectively.

The three phase currents measured at the sending end of the line for this type of fault are given in Fig. 8.10. The currents in the healthy phases at the sending end are magnified in Fig. 8.11. In Fig. 8.12, the sending end currents are given for the same location of the fault (at the middle of the line), the fault was not cleared as in the previous cases.

The waveforms of the healthy currents at the receiving end for a fault at the middle of the line on the A phase, are shown in Fig. 8.13. The healthy phases currents of the sending end are given in Fig. 8.14, and a clearer trace for this case is given in Fig. 8.15, where traces are given over 40 ms of the system real time. The sending and receiving end fault currents in phase A are given on the same figure as shown in Fig. 8.16, whereas Fig. 8.17 shows phase a fault currents at the sending, receiving end and current through the fault path on the same graph for comparison. The voltage waveforms for this type of fault for the sending end and receiving end and at the fault location for fault on phase A are given in Fig. 8.18.

The above traces of currents and voltages under single phase to ground fault (AG) are given on the line interconnecting two power systems of equal strength. These waveforms contain valuable information, particularly required when high speed protection systems are implemented, which operate from signals containing high frequency components. It is not possible to design such systems as previously was assumed in case of slow relays, based on the 50 Hz signal component only.

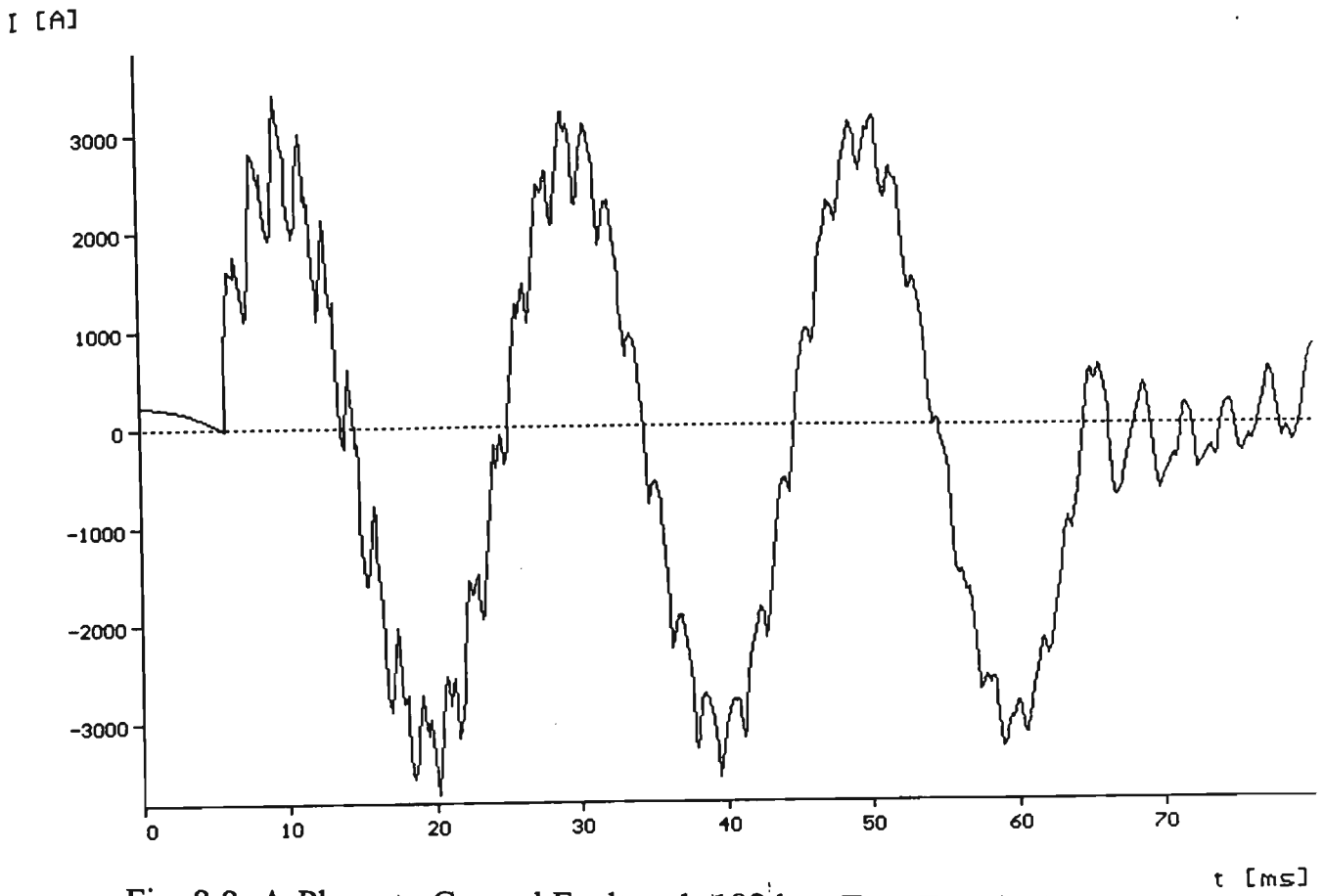


Fig. 8.8: A-Phase to Ground Fault at $l=192$ km, Two Terminal System,
Red Phase at the Sending End, fault cleared after 40 ms.

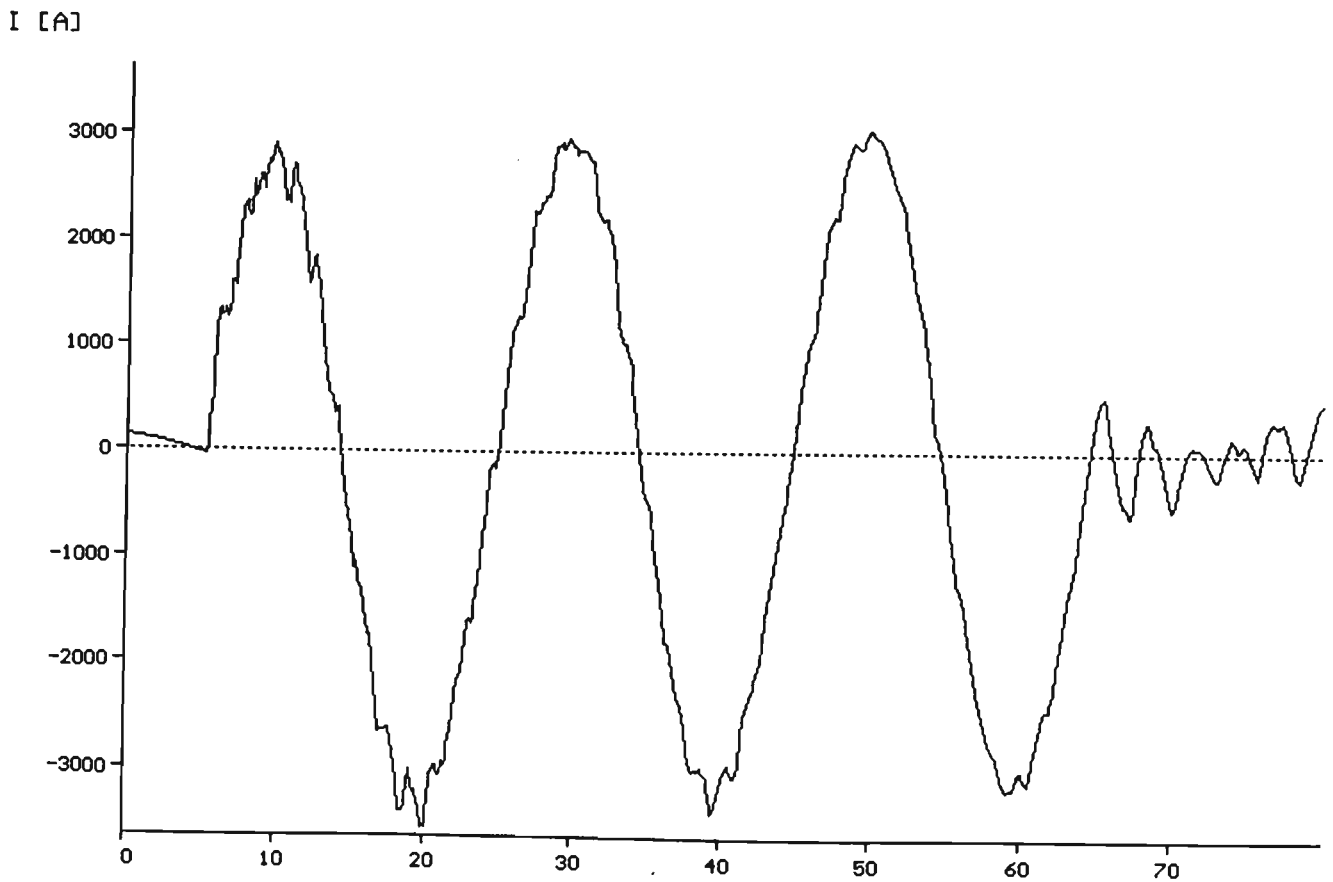


Fig. 8.9 A-Phase to Ground fault at $l=192$ km, Two terminal System
Red Phase Receiving End Current, Fault cleared after 40 ms

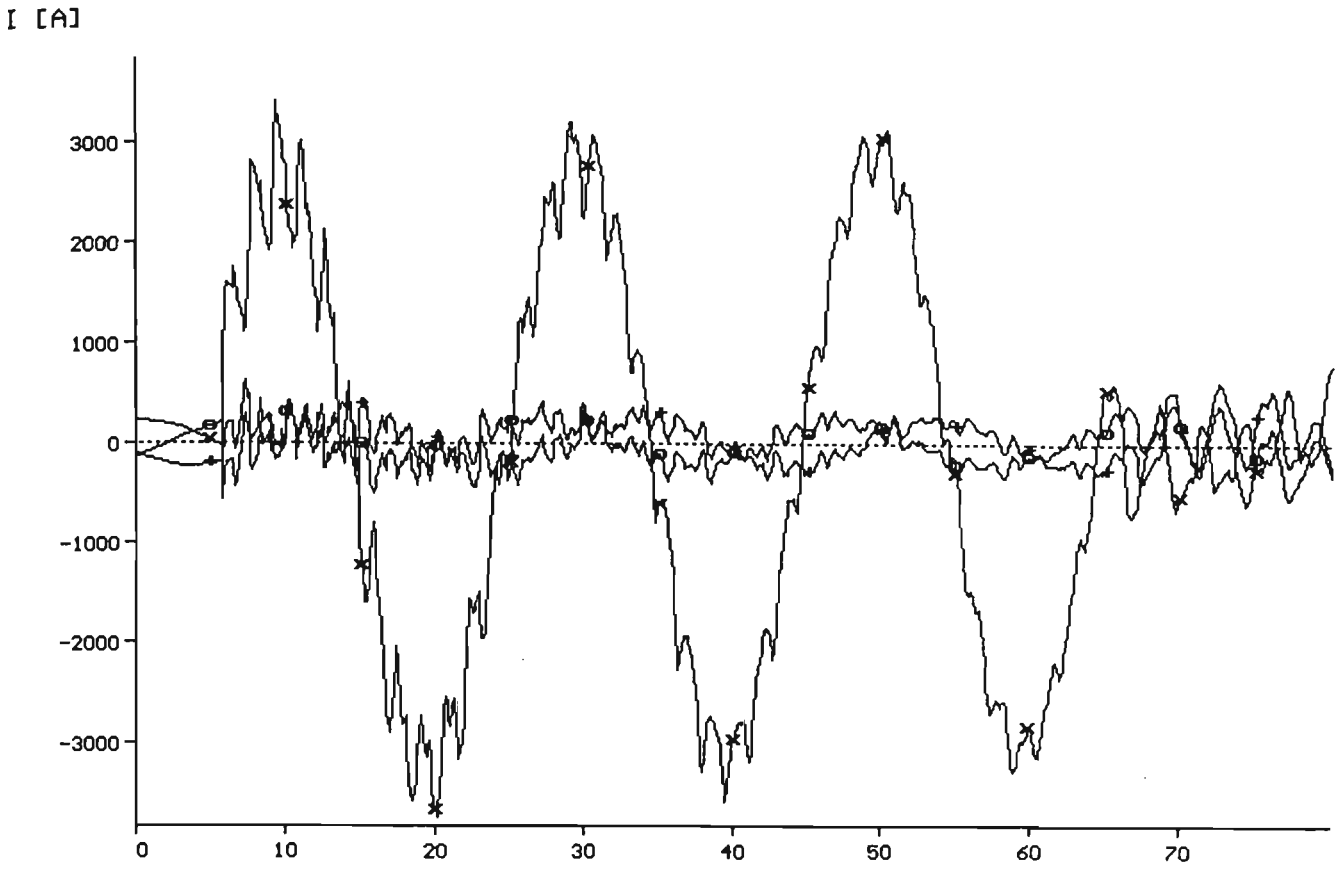


Fig. 8.10: A-Phase to Ground Fault at $l=192$ km, Two Terminal System t [ms]
 Three phase currents at the sending end, (x): Red, (o): Yellow, (+): Blue

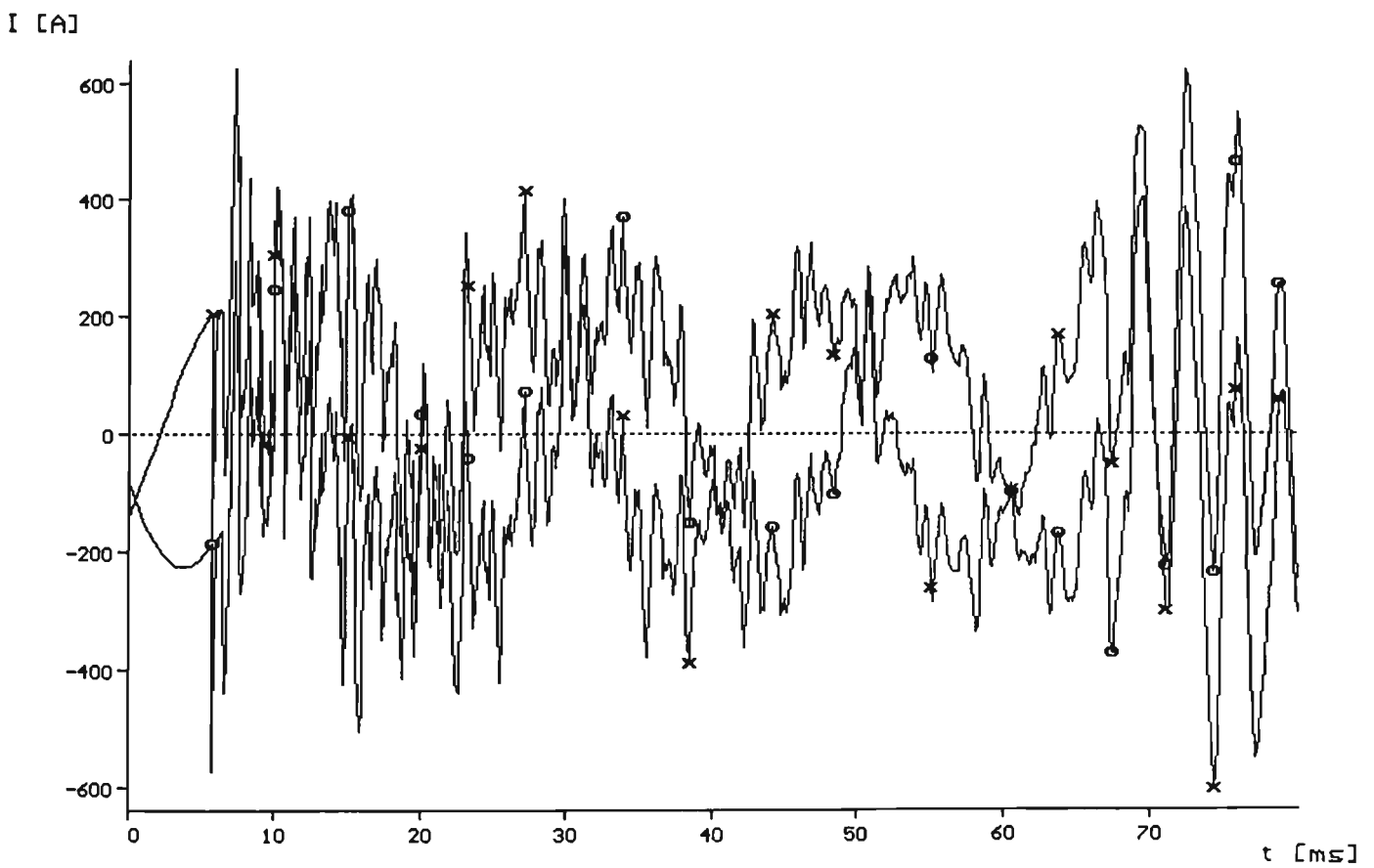


Fig. 8.11: A-Phase to Ground Fault at $l=192$ km, Two Terminal System, Sound
 phases (B and C) Currents, fault cleared after 50 ms, (x): A, (o): B, (+): C

[I, A]

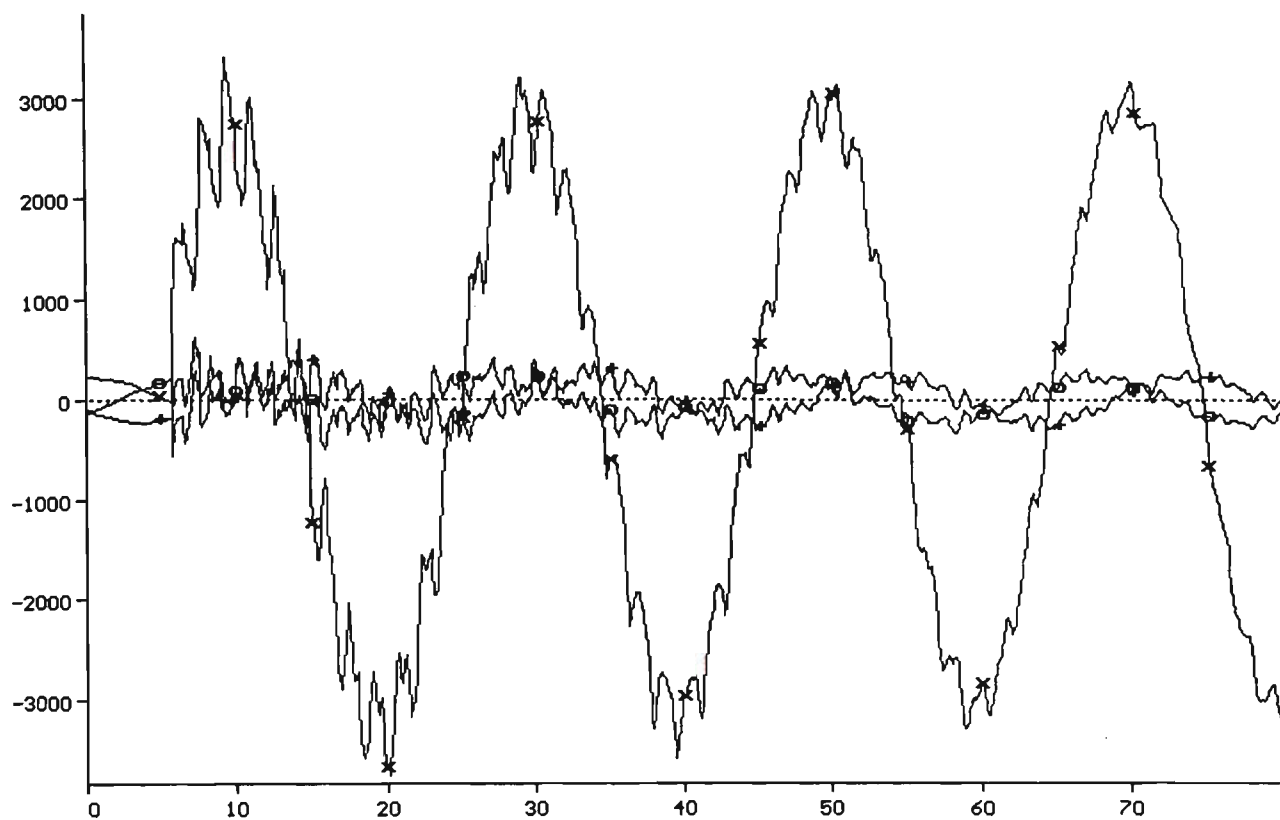
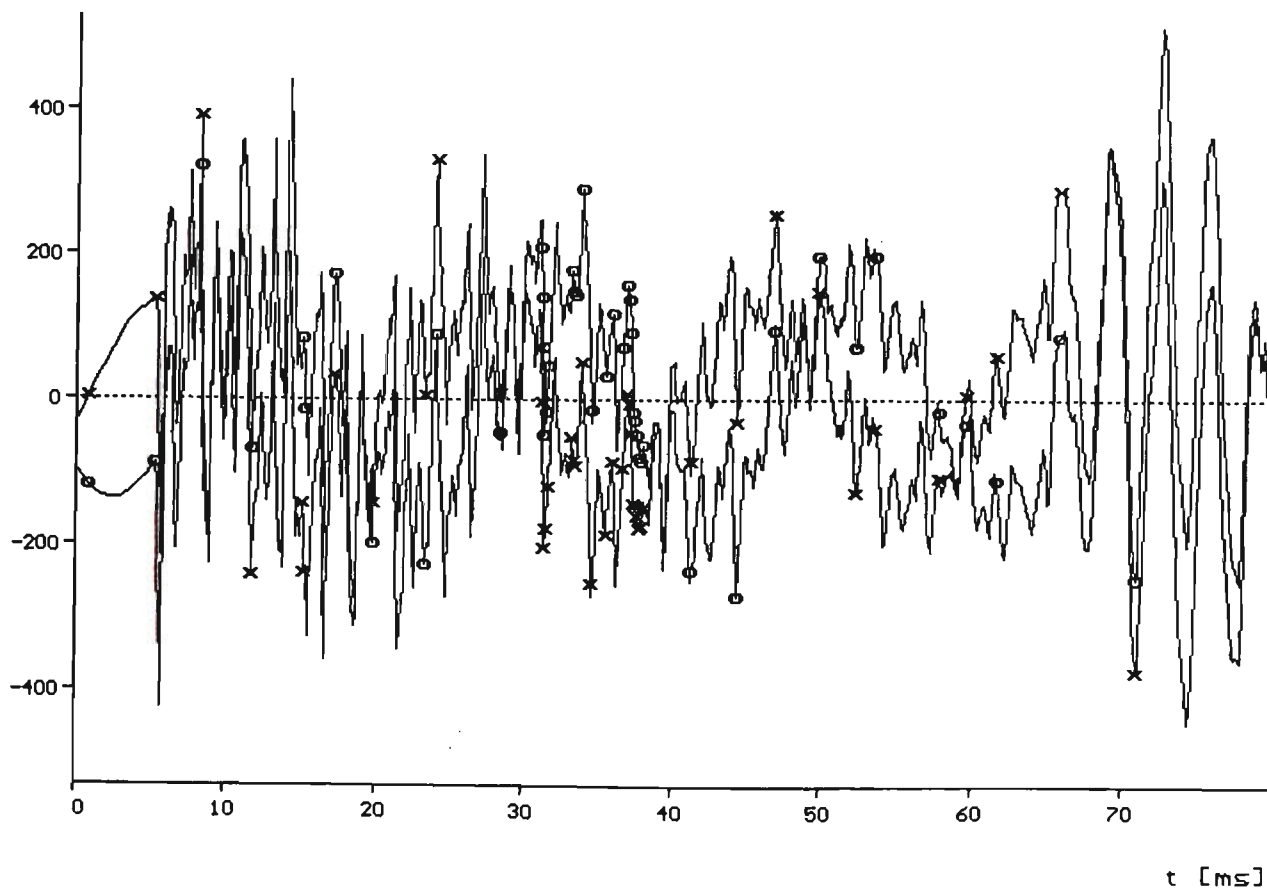


Fig. 8.12: A-Phase Fault - to - Ground at $l = 192$ km, Persistent Fault, two Terminal System, Three Phase Sending End Currents, (x): A, (o): B, (+): C

I [A]



t [ms]

Fig. 8.13: A - Phase - to - Ground Fault, Cleared after 50 ms at $l = 192$ km, Two Terminal System, B and C Receiving End Currents, (x): B, (o): C

I [A]

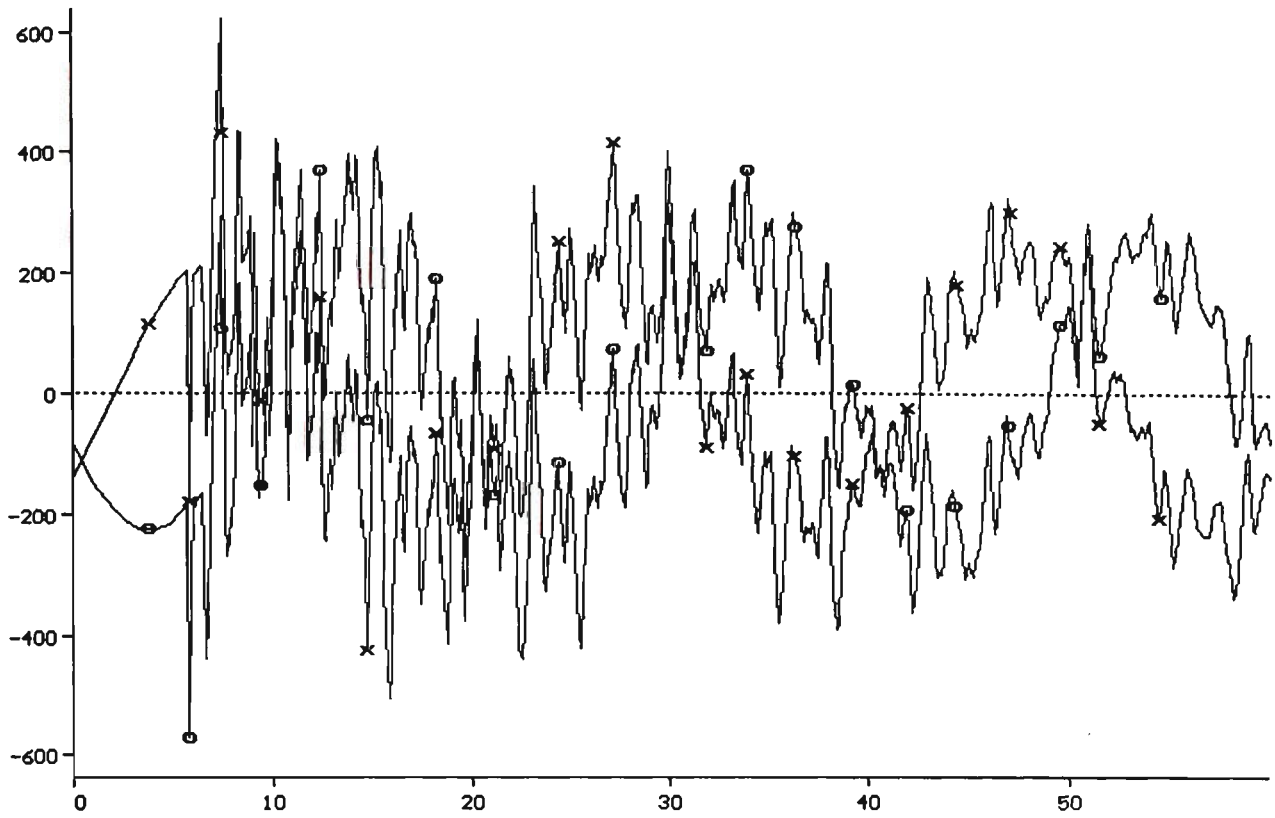


Fig. 8.14: A-Phase to Ground fault at $l=192$ km, Two Terminal System, t [ms]
Fault Cleared after 50 ms, B and C Sending End Currents, (x): B, (o): C

I [A]

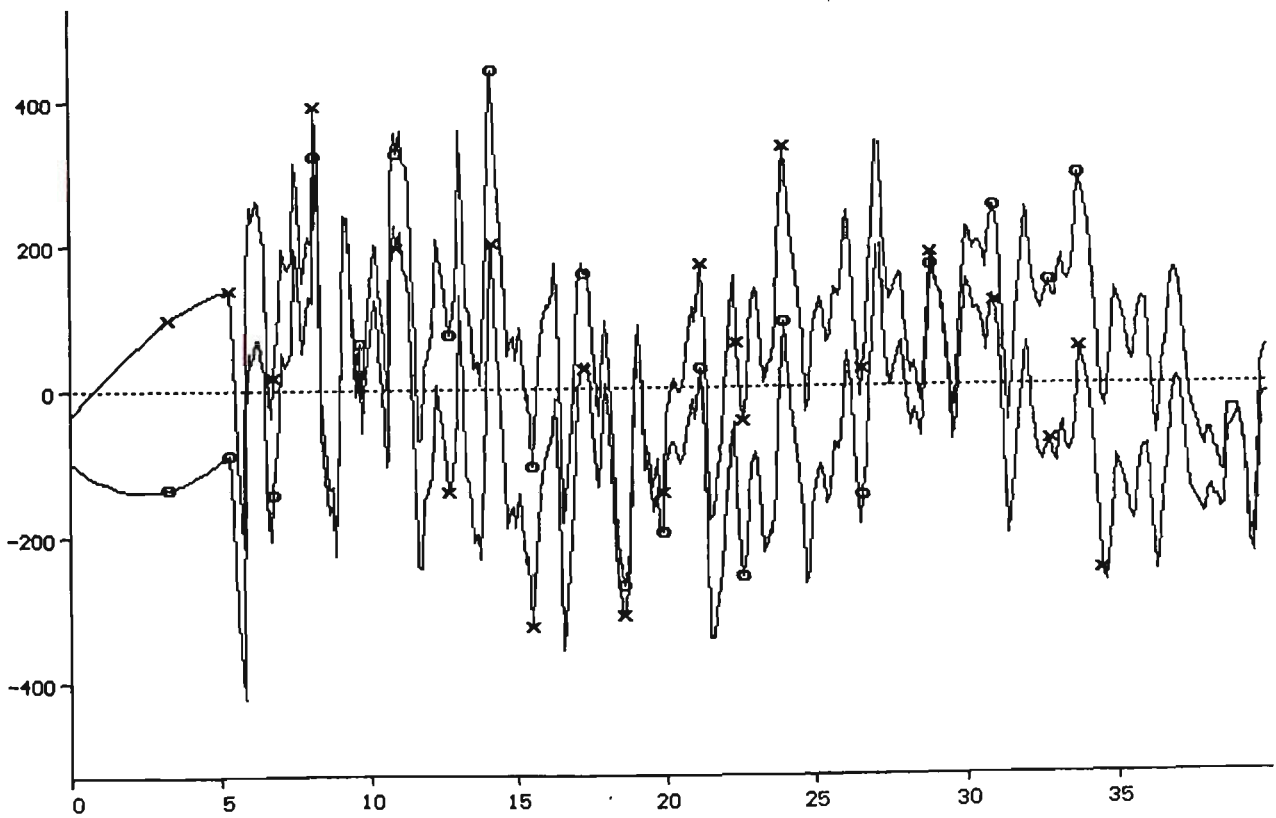


Fig. 8.15: A-Phase to Ground fault at $l=192$ km, Two terminal System, t [ms]
Fault Cleared after 50 ms, B and C Receiving End Currents Zoomed

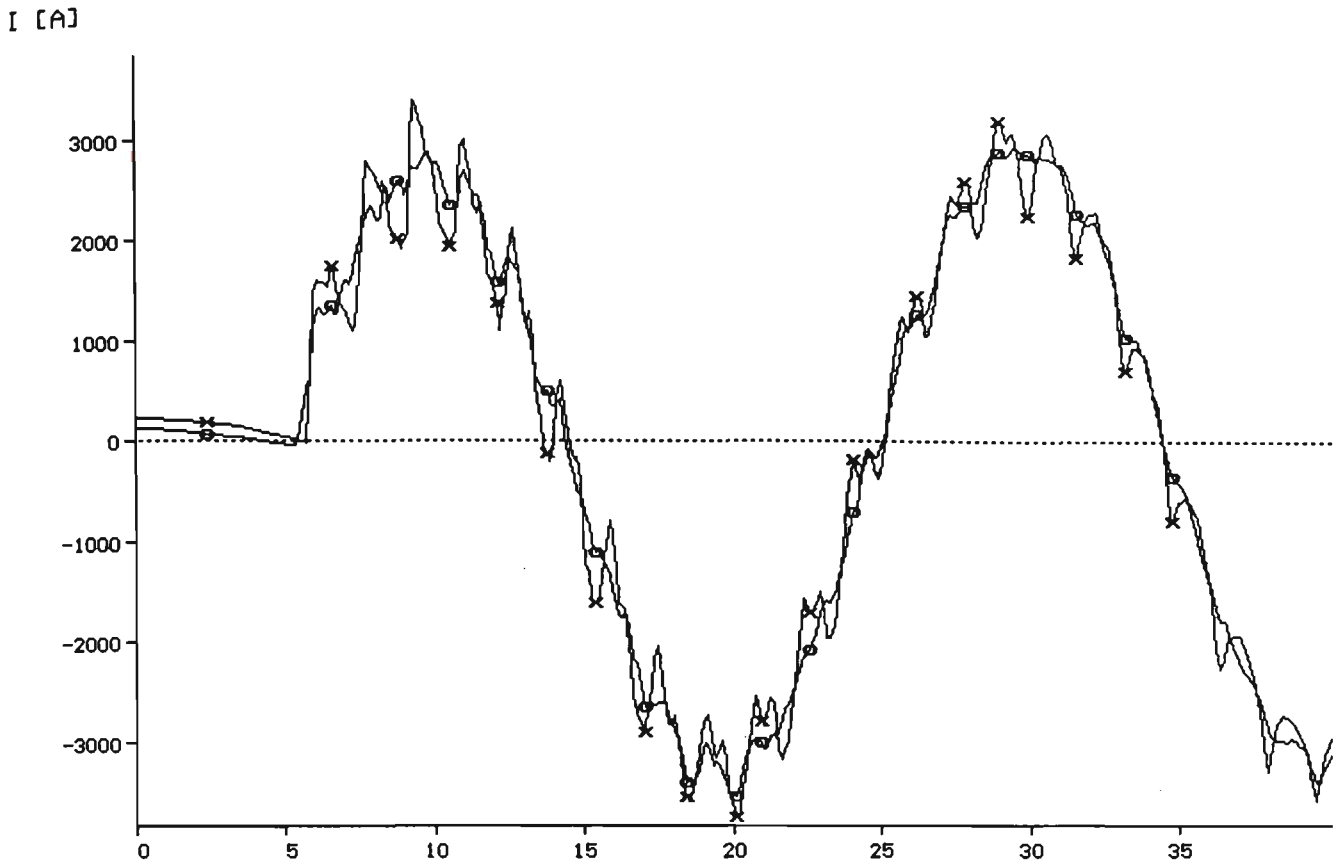


Fig. 8.16: A-Phase to Ground Fault at $l=192$ km, Two terminal System, t [ms]
 Sending End and Receiving end Phase A currents, (x): S, (o): R

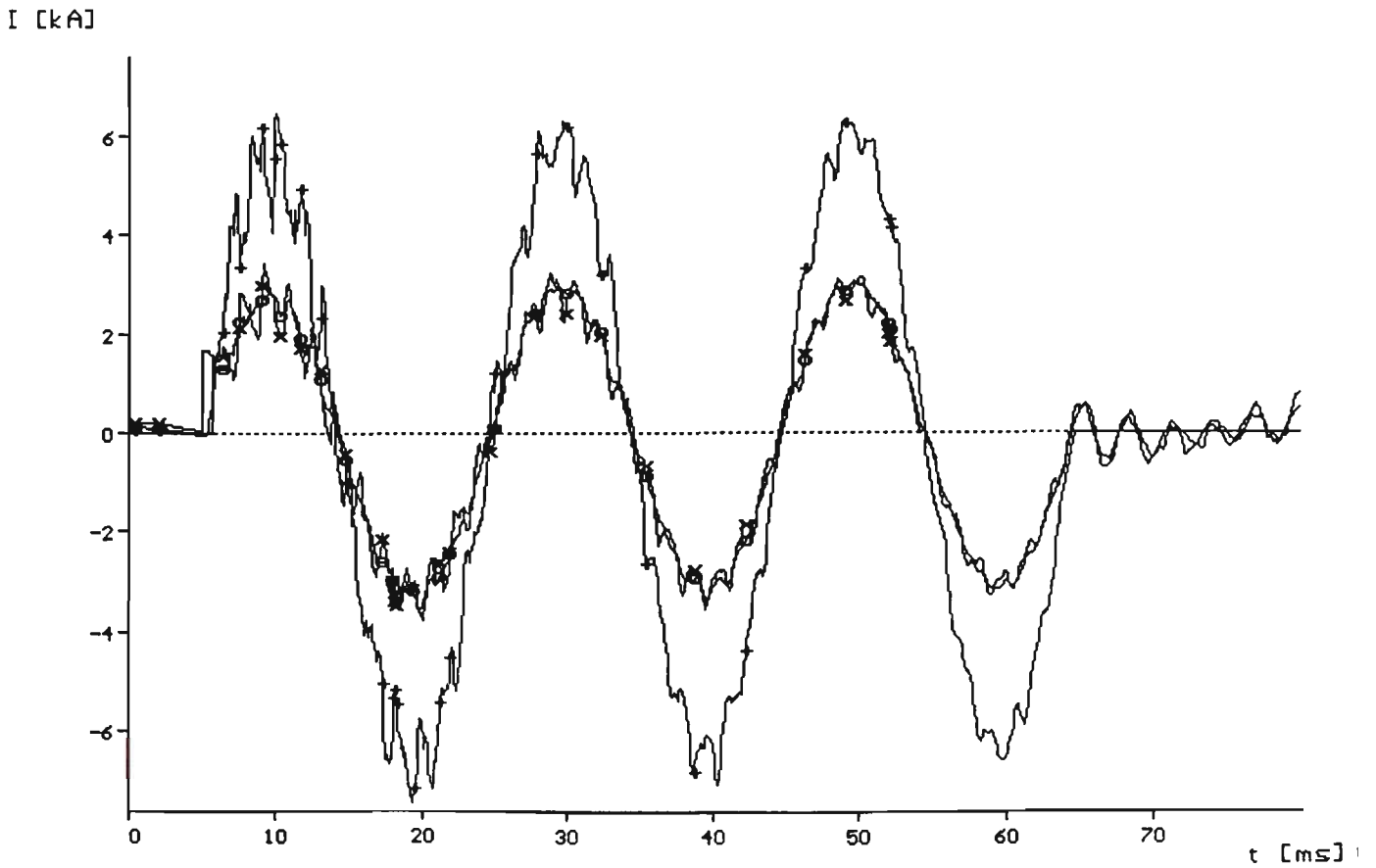


Fig. 8.17: A-Phase to Ground Fault at $l=192$ km, Two Terminal System, Fault
 Cleared after 50 ms, as in Fig. 8.16, Longer time Response

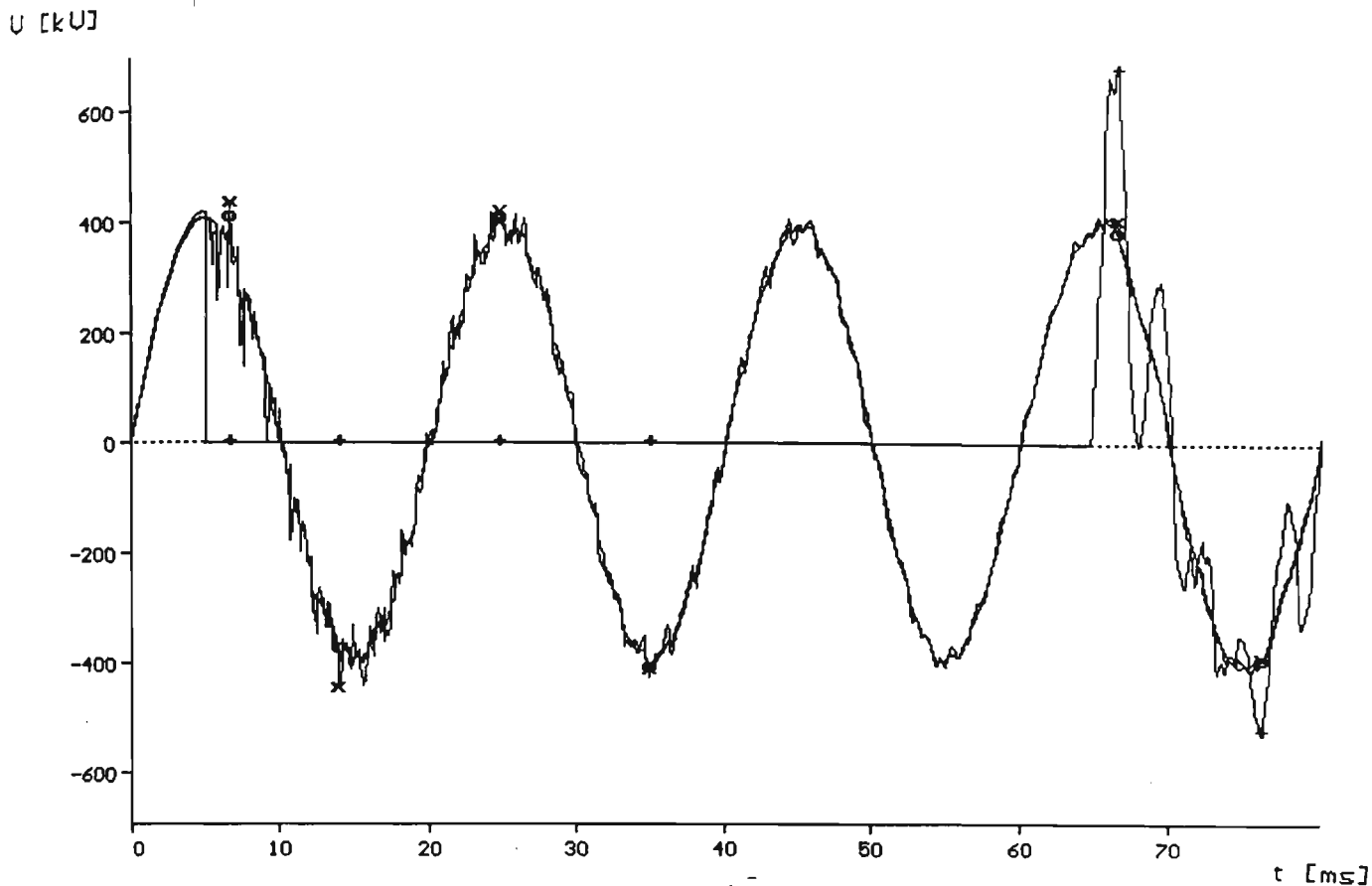


Fig. 8.18: A-Phase to Ground Fault at $l=192$ km, Two Terminal System, Fault Phase Voltages at the Sending End(x), Receiving End (o), At the Fault (+)

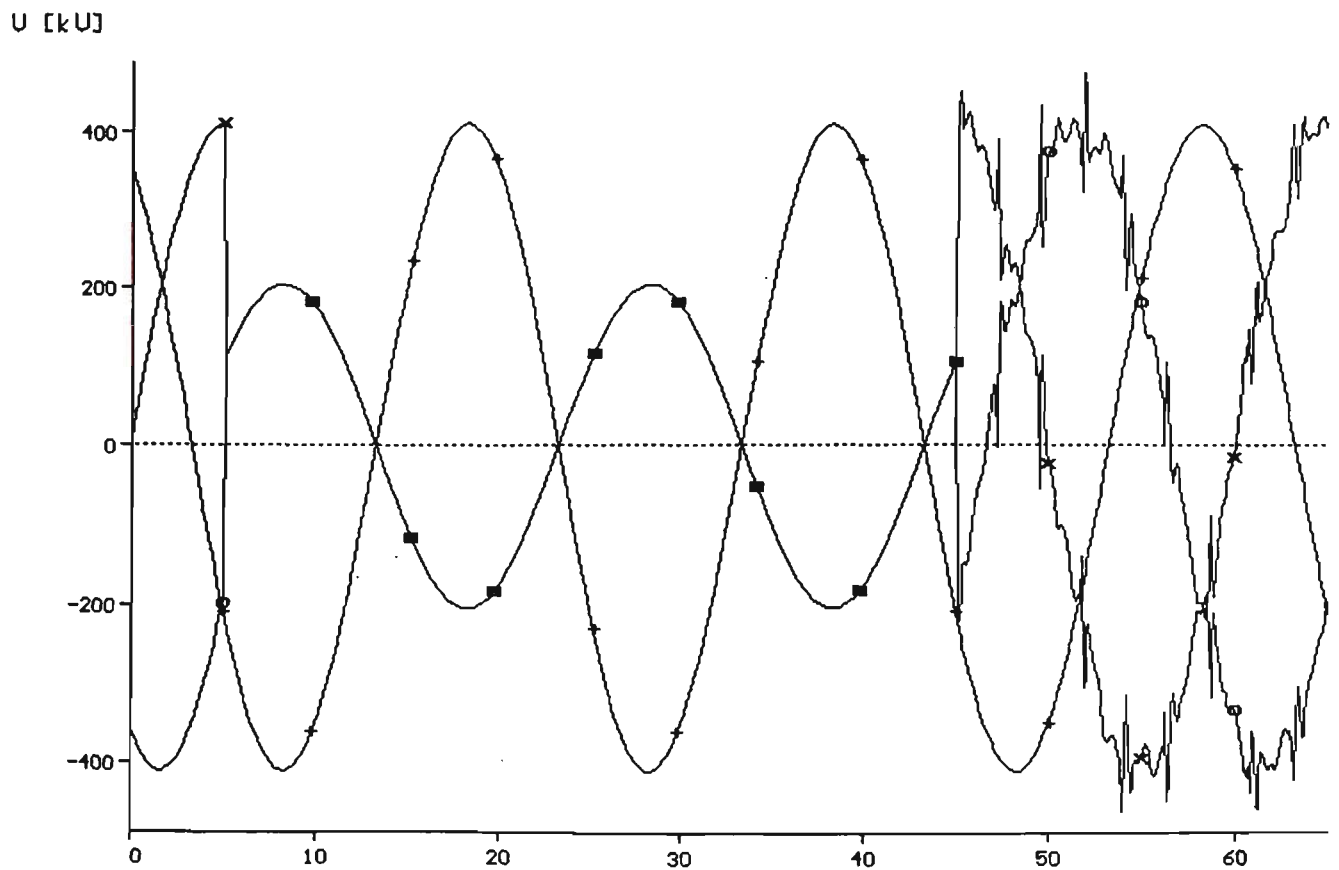


Fig. 8.19: AB-Fault at $l=0$, Two Terminal System, Sending end Three phase Voltages, (x): A, (o): B, (+): C

8.2.2 Double Phase faults

In case of double phase free of earth faults, it was assumed that the fault occurs at the sending end of the line after 5 ms, and cleared after 40 ms of the fault initiation. Fig. 8.19 show the three phase voltages at the sending end of the line. The receiving end voltages are shown in Fig. 8.20. In Fig. 8.21, the three phase sending end currents are given. The two faulty phase currents are indeed equal in magnitude and in exact opposition to each other, as it was expected.

The magnitude of the healthy phase current is so small compared to the faulty phases currents, that it was difficult to show on the same graph. The receiving end currents are very much disturbed by this fault, which is 384 km away from it. This is shown in Fig. 8.22, where the currents of the faulty phases, although disturbed, but still equal in magnitude and opposite in sign, whereas, the healthy phase current has maintained its shape to a certain extent.

8.2.3 Double Phase to Ground faults

A phase-to-phase-to-ground fault between A and B phases (AB-G) was assumed at the sending end of the line, at the time when the A-phase voltage was at its 90 degrees (at $t = 5$ ms). The fault was assumed to be cleared after 40 ms. The sending end voltages under these conditions are shown in Fig. 8.23. It is clear that voltage waveforms are far from pure sinusoidal even after 25 ms after fault clearance. This phenomena is not so bad at the receiving end of the line as it is shown in Fig. 8.24. As far as currents are concerned, the waveforms for the same fault conditions are shown at the sending end, receiving end and through the fault path in Figs. 8.25, 8.26 and 8.27 respectively.

[kU, U]

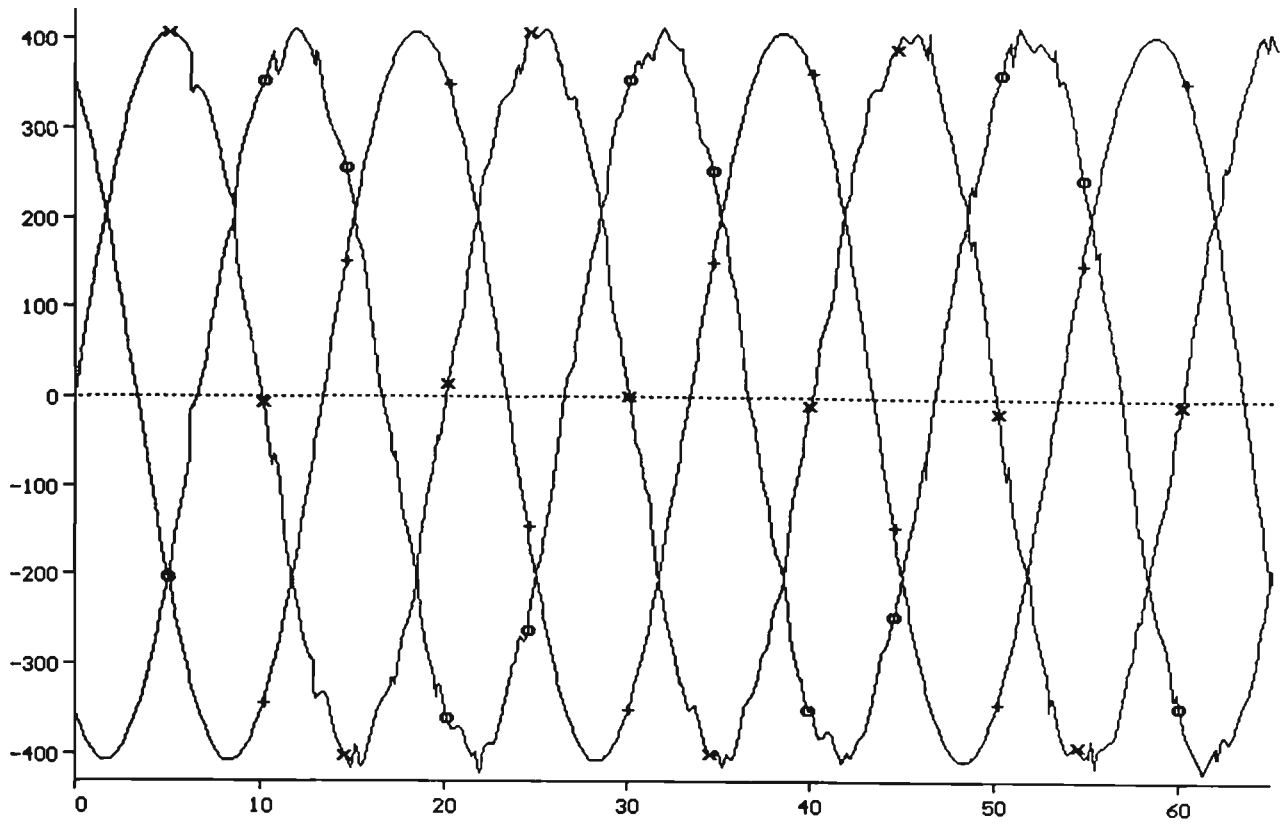


Fig. 8.20: AB-Fault at $x=0$, Two Terminal System, Three Phase Voltages t [ms]

Receiving End, (x): A, (o): B, (+): C

I [kA]

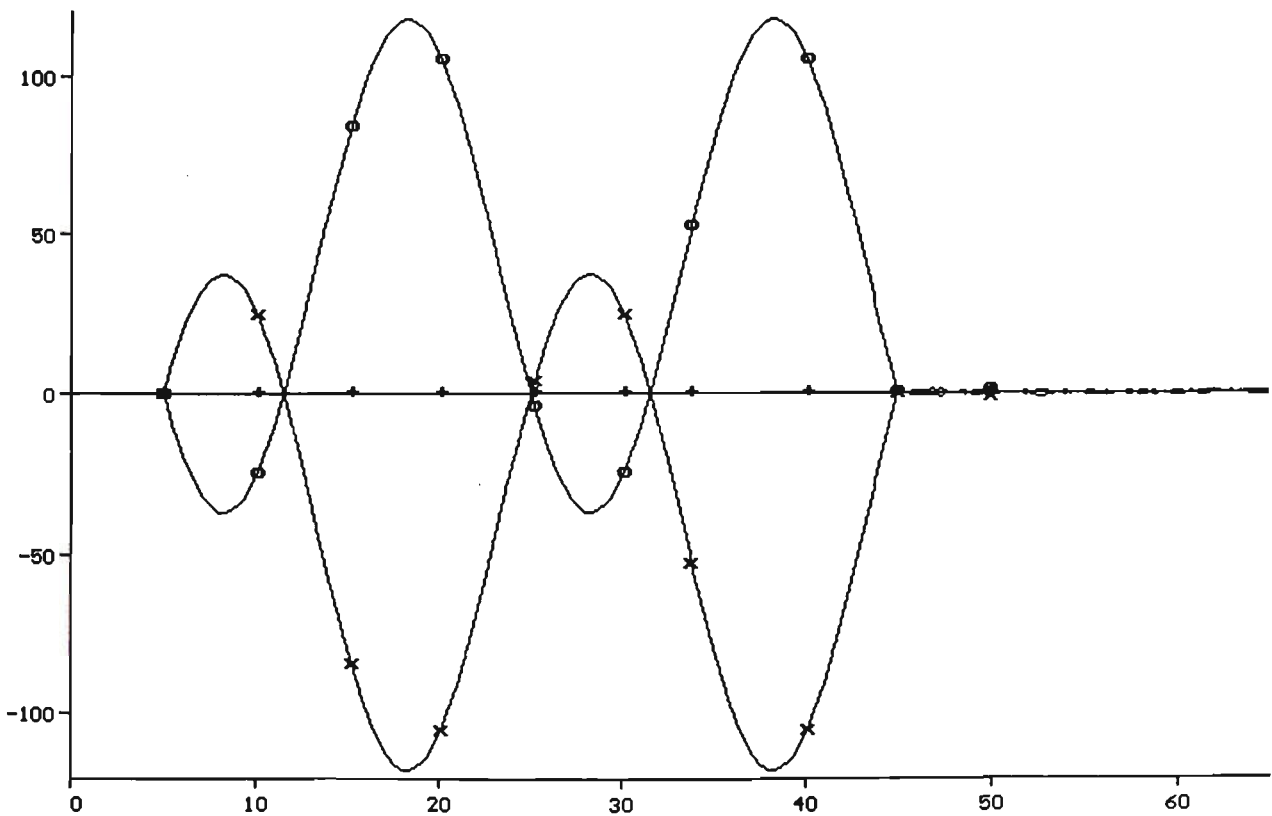


Fig. 8.21: AB-Fault at $l=0$, Two Terminal System, Three Phase Sending End t [ms]

Currents, (x): A, (o): B, (+): B, Fault Cleared after 40 ms

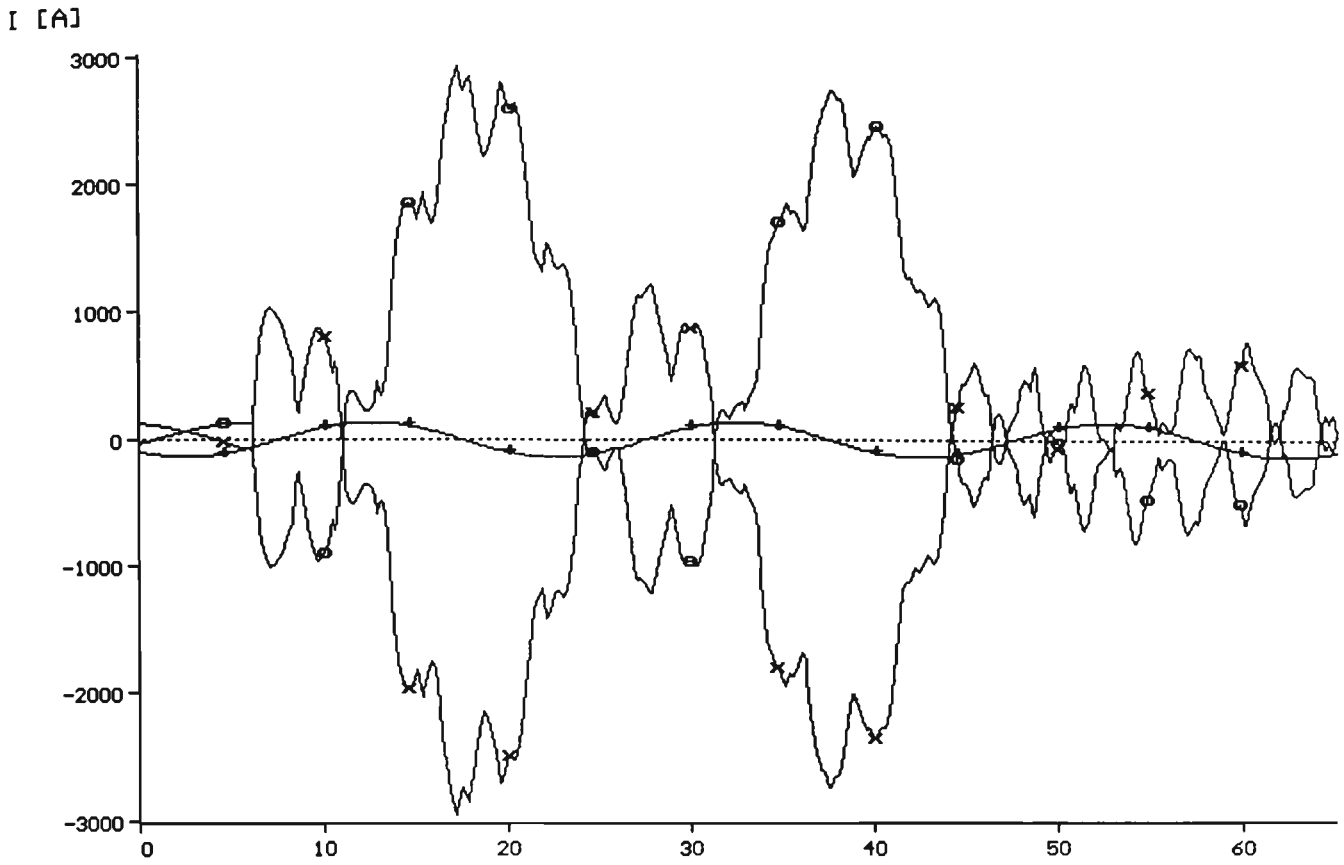


Fig. 8.22: AB-Fault at $l=0$, Two Terminal System, Three Phase Receiving End t [ms]
 Currents, (x): A, (o): B, (+): C, Fault Cleared after 40 ms

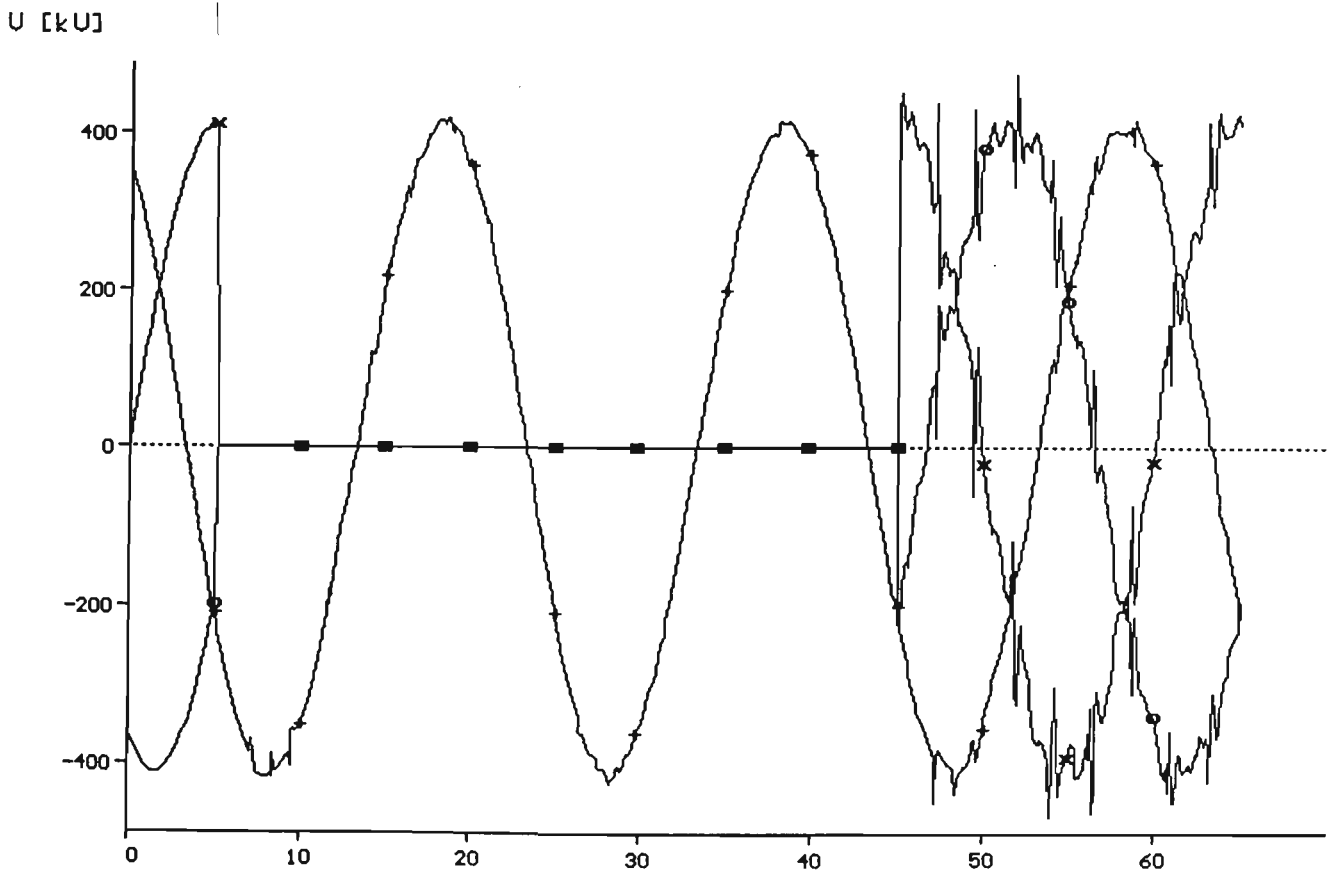


Fig. 8.23: AB-Ground Fault at $l=0$, Two Terminal System, Three Phase t [ms]
 Sending End Voltages, (x): A, (o): B, (+): C, Fault cleared after 40 ms

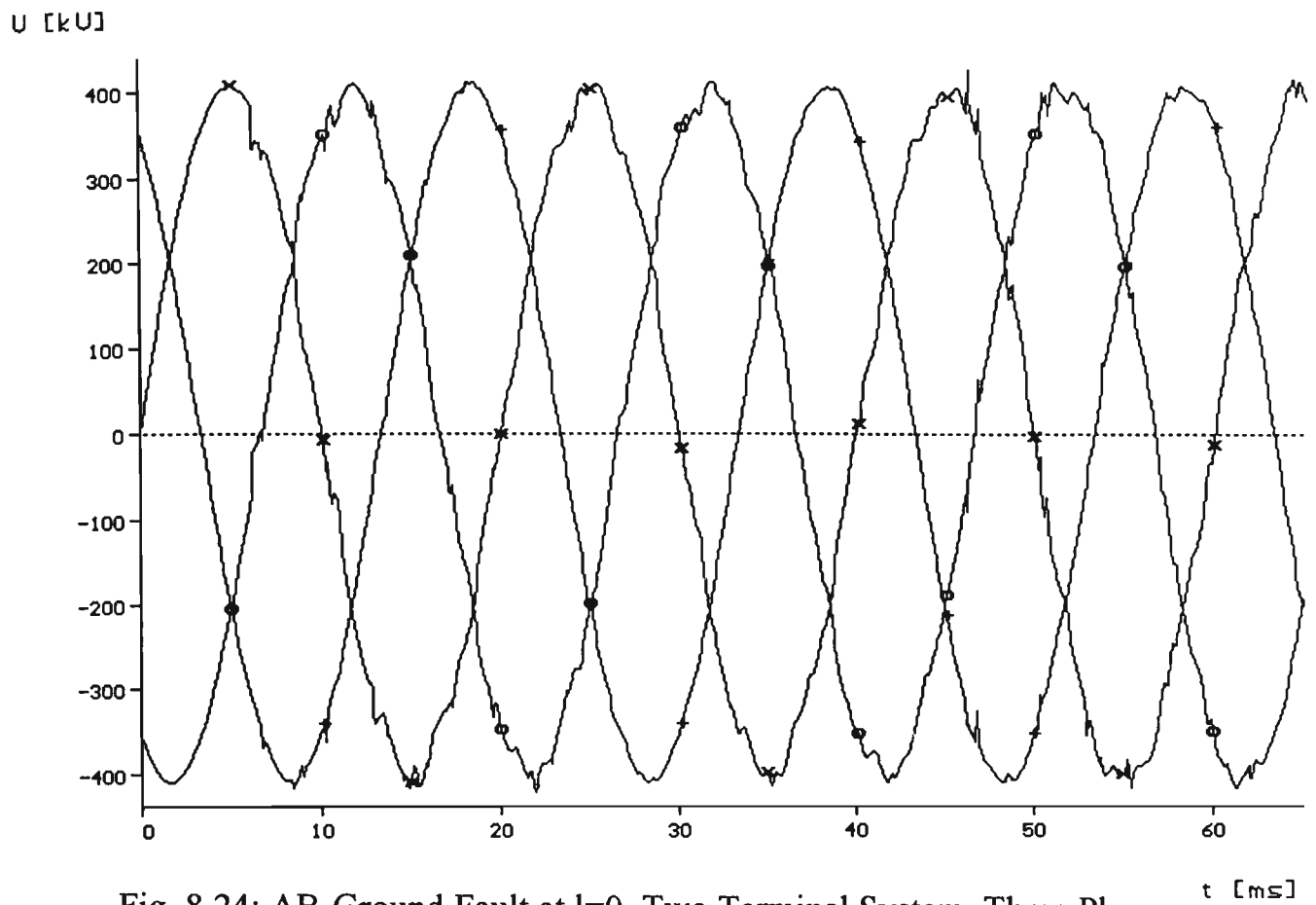


Fig. 8.24: AB-Ground Fault at $l=0$, Two Terminal System, Three Phase
 Receiving End Voltages, (x): A, (o): B, (+): C, Fault Cleared after 40 ms

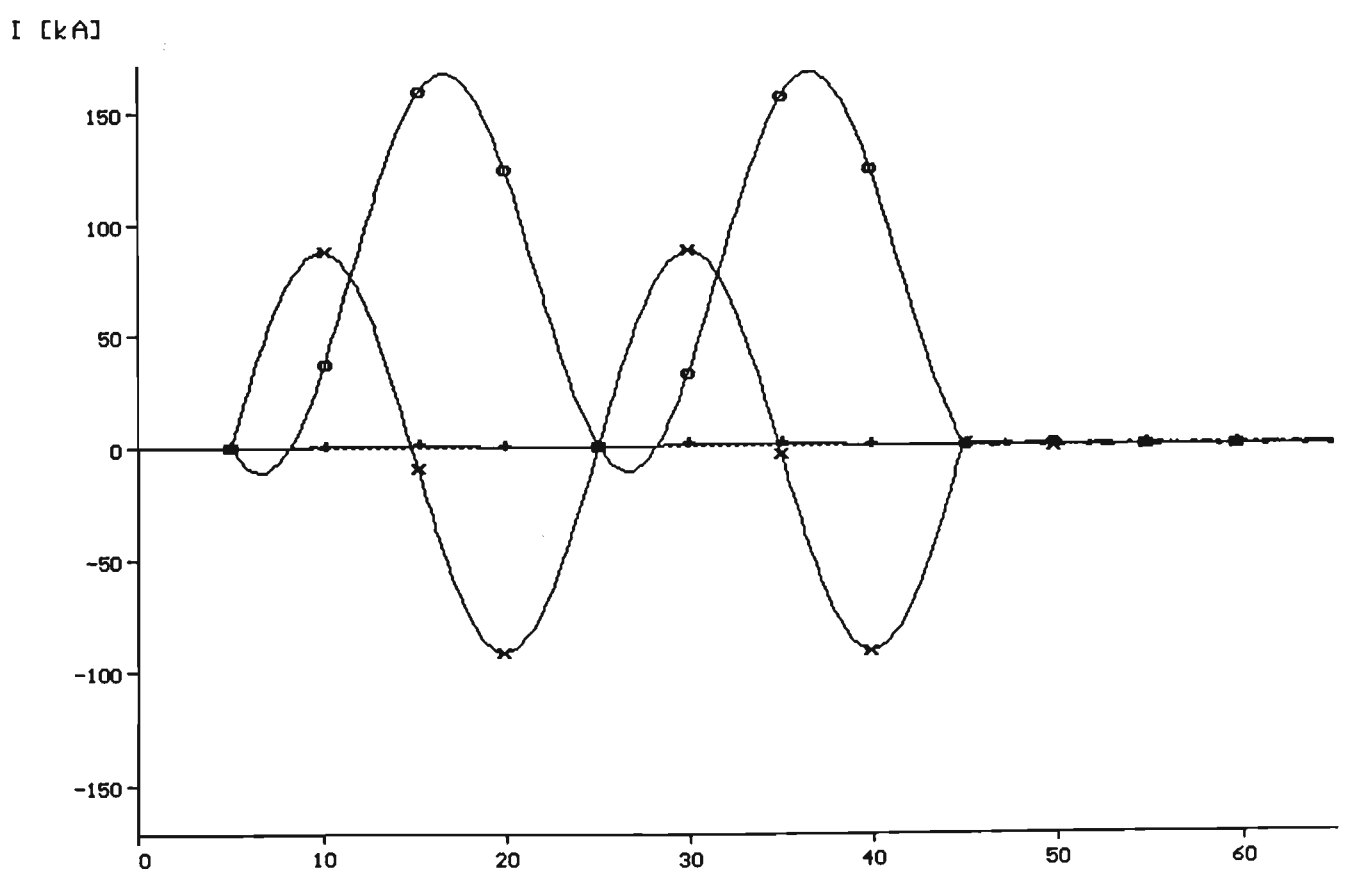


Fig. 8.25: AB-Ground Fault at $l=0$, Two Terminal System, Three Phase
 Sending End Currents, (x): A, (o): B, (+): C, Fault Cleared after 40 ms.

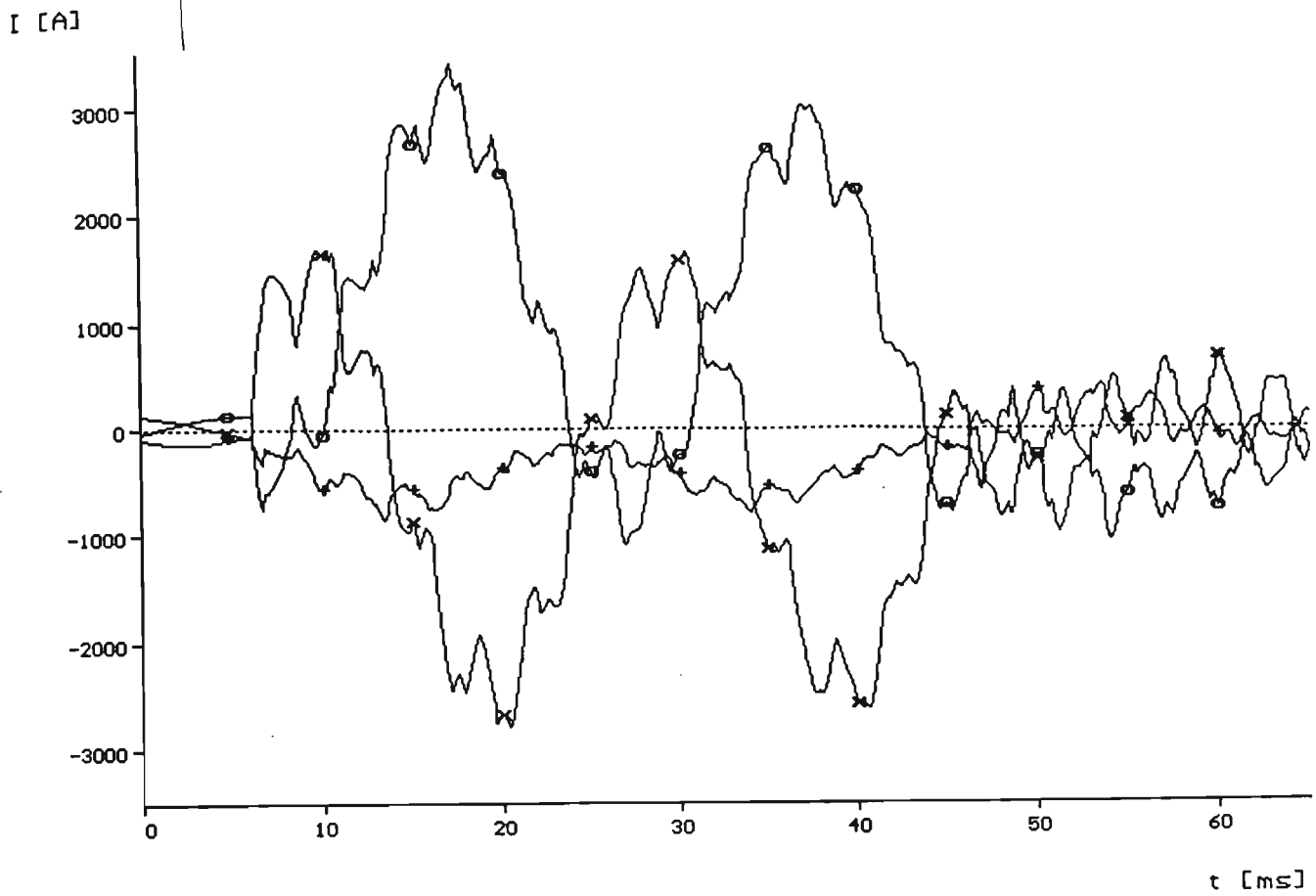


Fig. 8.26: AB-Ground Fault at $l=0$, Two Terminal System, Three Phase Receiving End Currents, (x): A, (o): B, (+): C, Fault cleared after 40 ms.

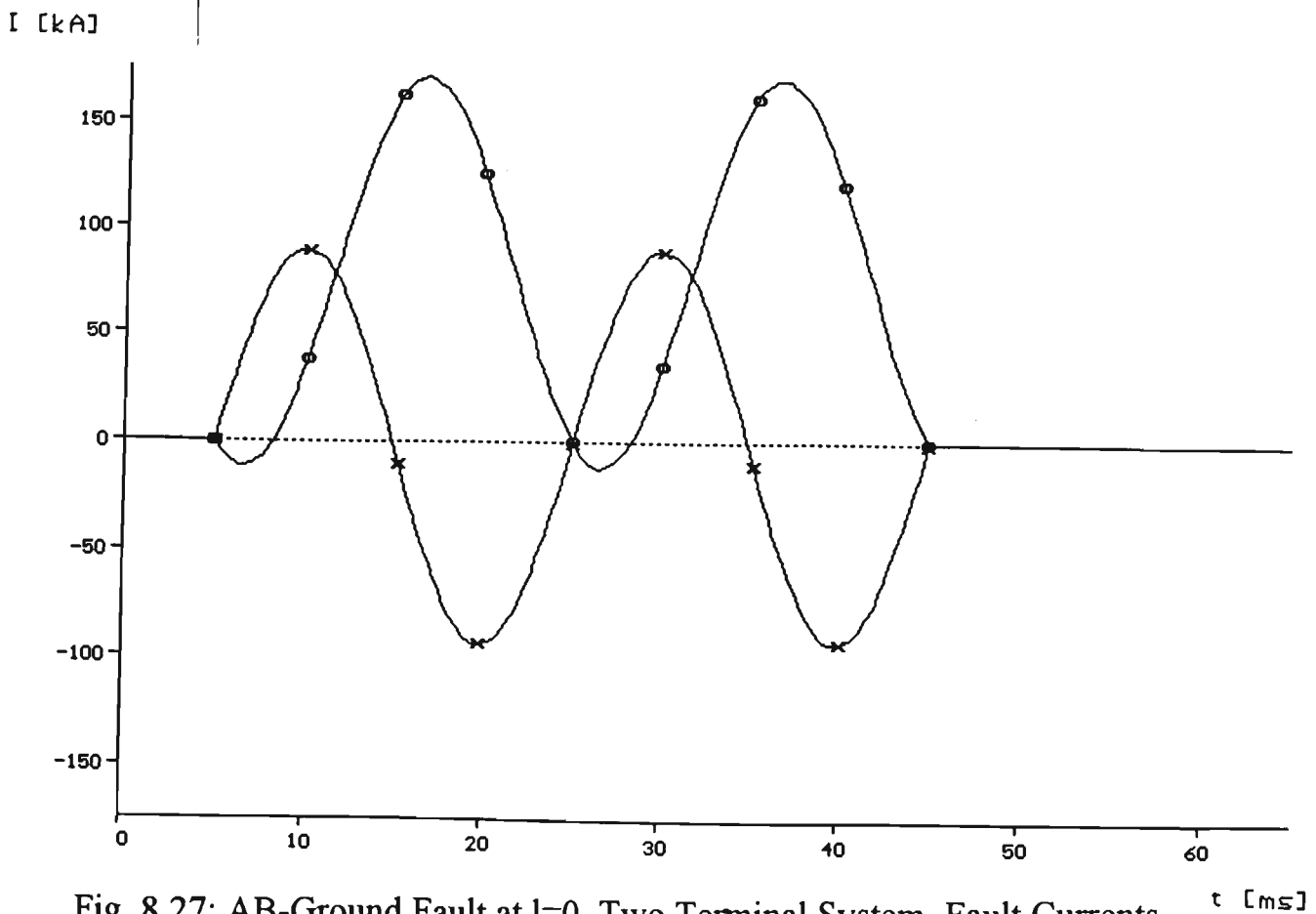


Fig. 8.27: AB-Ground Fault at $l=0$, Two Terminal System, Fault Currents Through the Faulty Path (x) A, (o): B, Fault Cleared after 40 ms.

In case of currents, the currents at the receiving end are much more disturbed than the currents at the sending end, where the fault was applied.

8.2.4 Three Phase faults

For a three phase to ground fault at the sending end of the line, the fault inception has occurred after 5 ms of system normal operation, and cleared after 40 ms. It is shown in Fig. 8.28, the complete collapse of all three phase voltages, which have a lot of noise after fault clearance as it shown in the indicated graph. However, voltages at the receiving end remained in a reasonably good shape as shown in Fig. 8.29, in spite of the complete voltage collapse at the sending end of the line. This is mainly due to the strong source behind the line at the receiving end, and the long distance to fault (384 km).

The wave forms of the three phase currents at the sending end and receiving end of the transmission line are given in Figs. 8.30 and 8.31 respectively. It is clear that current waveforms at the sending end under these conditions are much worse than those at the receiving end. The disturbance on the current waveforms has remained even 30 ms after fault clearance.

8.2.5 Multiple Faults on Compensated Systems

In order to simulate a multiple fault in the two terminal system, phase A fault is assumed to occur at the sending end of the transmission line, and a 10 ms later, it is followed by phase b to ground fault at 96 km from the sending end. Both faults were assumed to be cleared after 40 ms. The waveforms of the sending end and receiving end voltages are given in Figs. 8.32 and 8.33

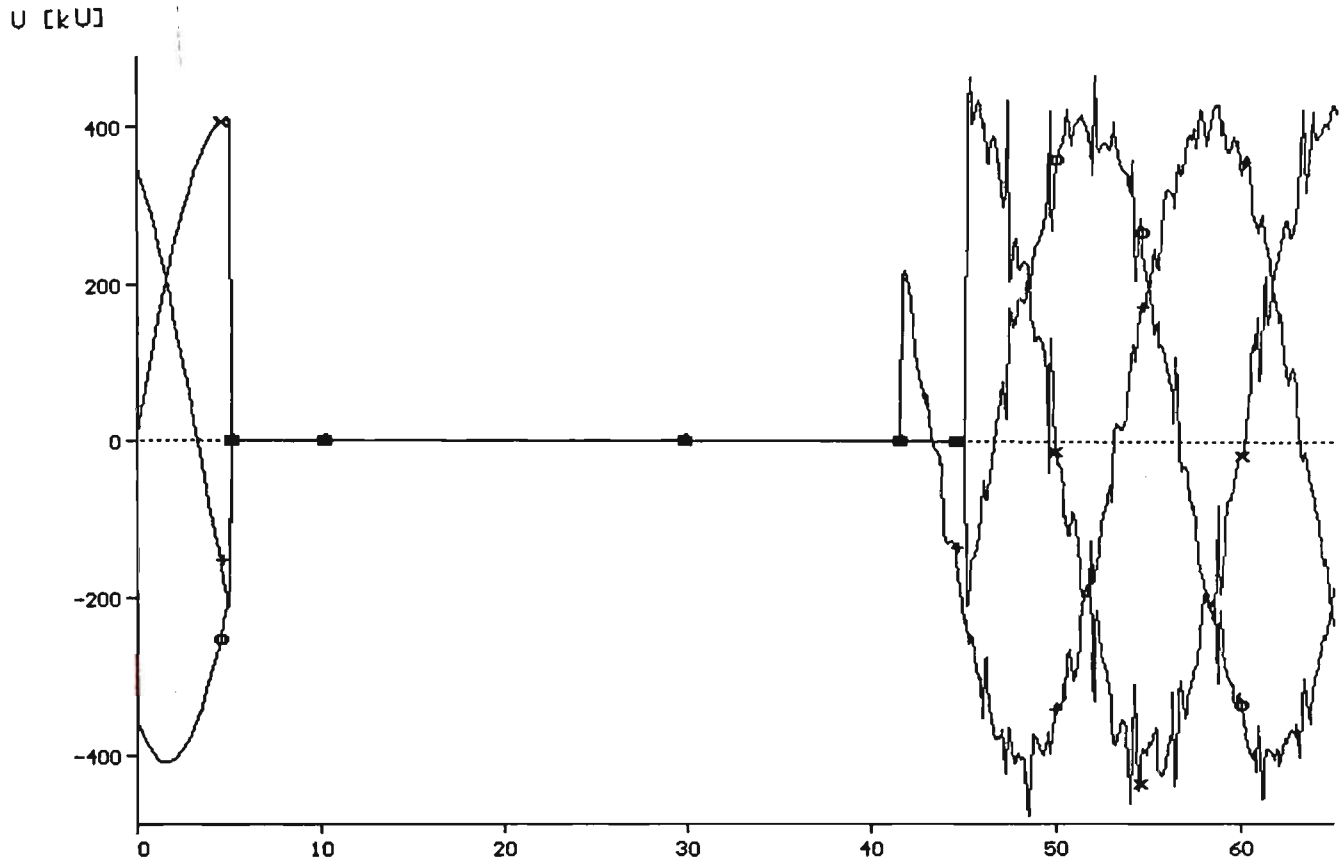


Fig. 8.28: Three Phase Fault at $l=0$, Two Terminal System, Three Phase Sending End voltages, (x): A, (o): B, (+): C, Fault Cleared after 40 ms.

U [kU]

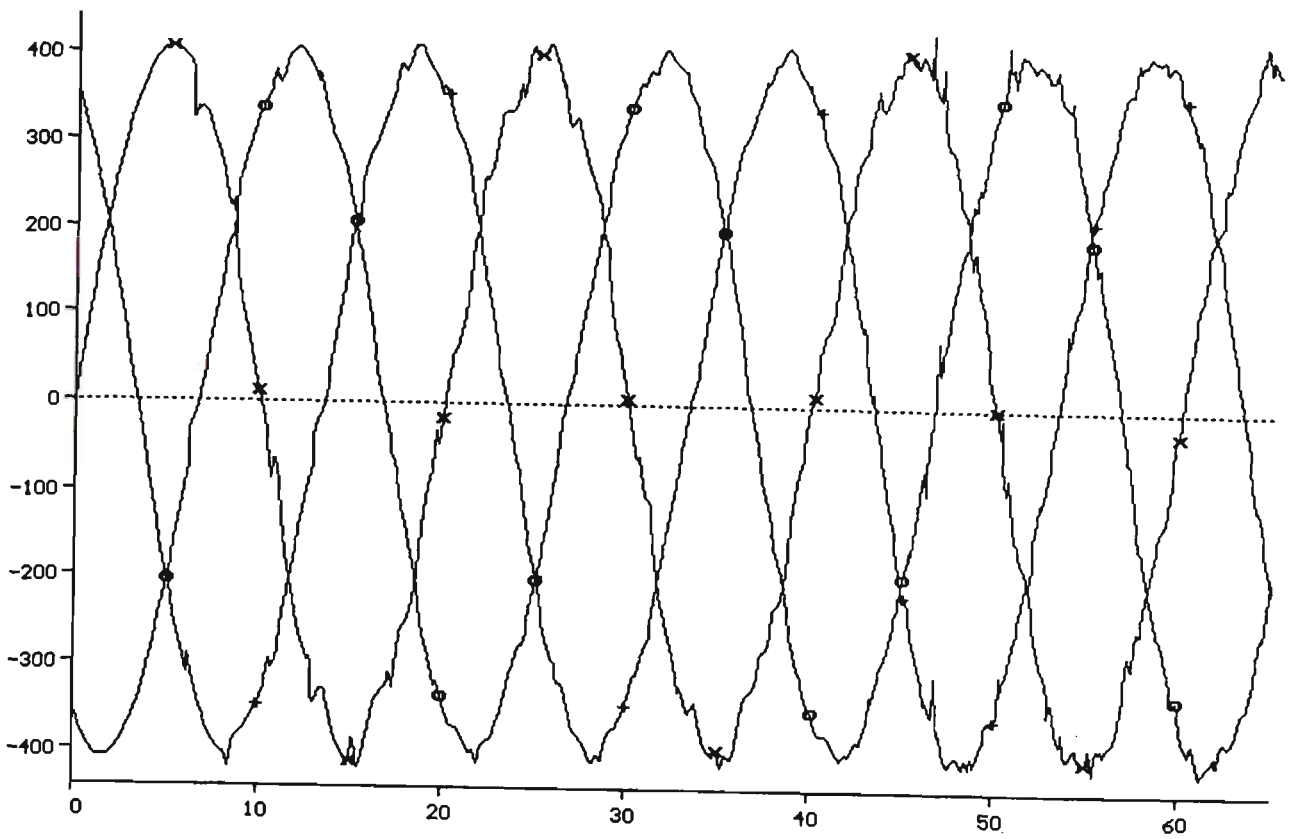


Fig. 8.29: Three Phase Receiving End Voltages, Two Terminal System, Three Phase Fault to G at $t=0$, (x): A, (o): B, (+): C

I [kA]

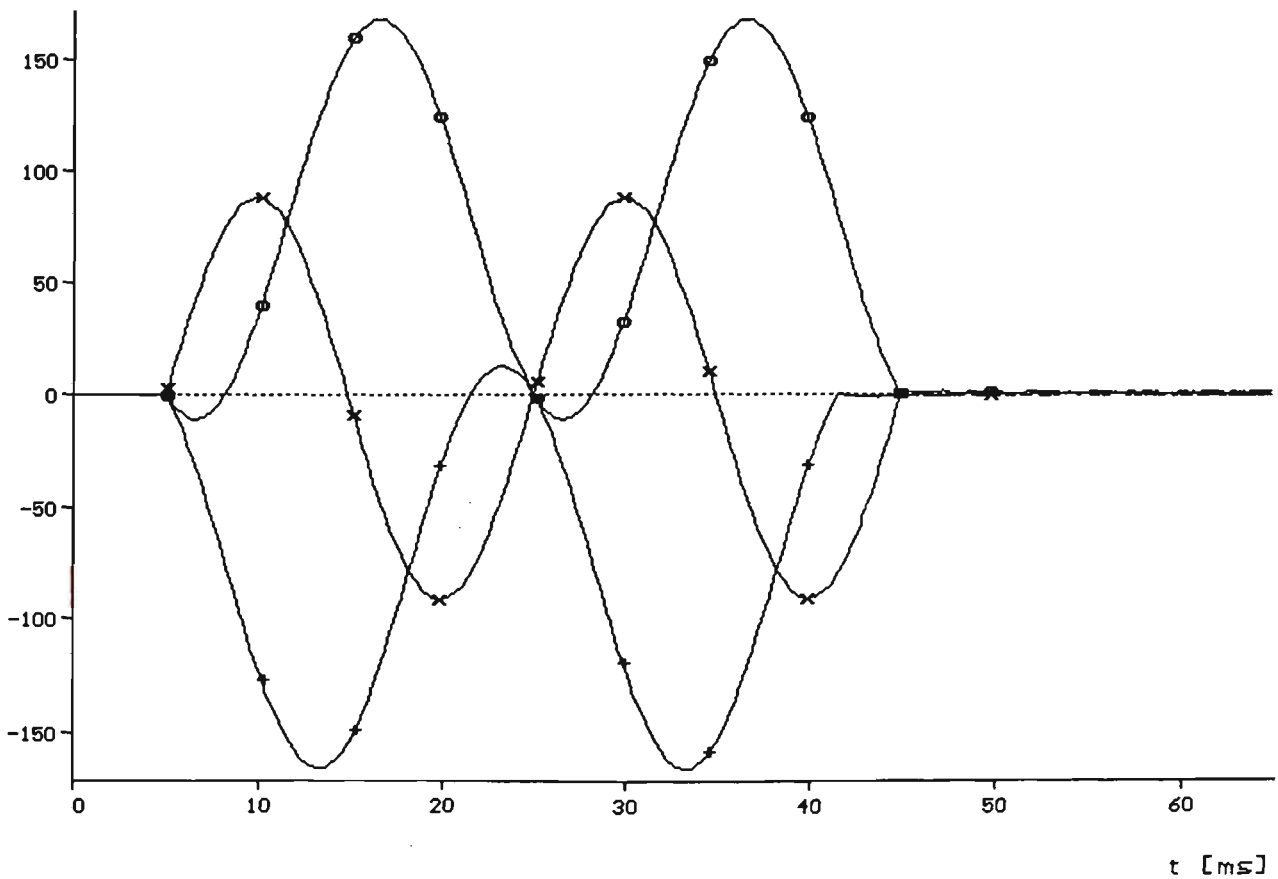


Fig 8.30: Three Phase Sending End Currents for Three Phase to G Fault at $t=0$, Fault Cleared After 40 ms, Two Terminal System, (x): A, (o): B, (+): C

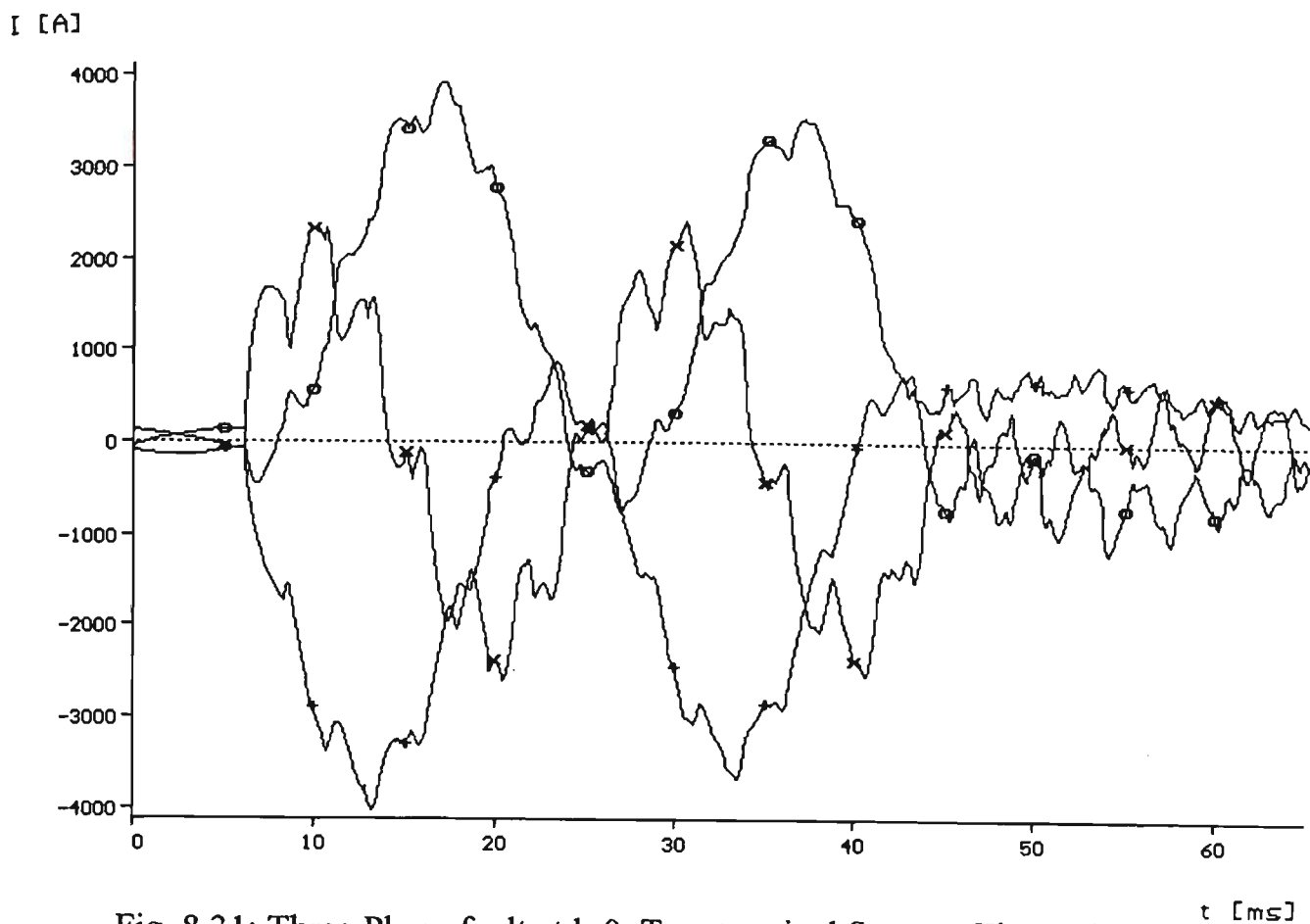


Fig. 8.31: Three Phase fault at $l=0$, Two terminal System, Three Phase Receiving End Currents, (x): A, (o): B, (+): C, fault Cleared after 40 ms

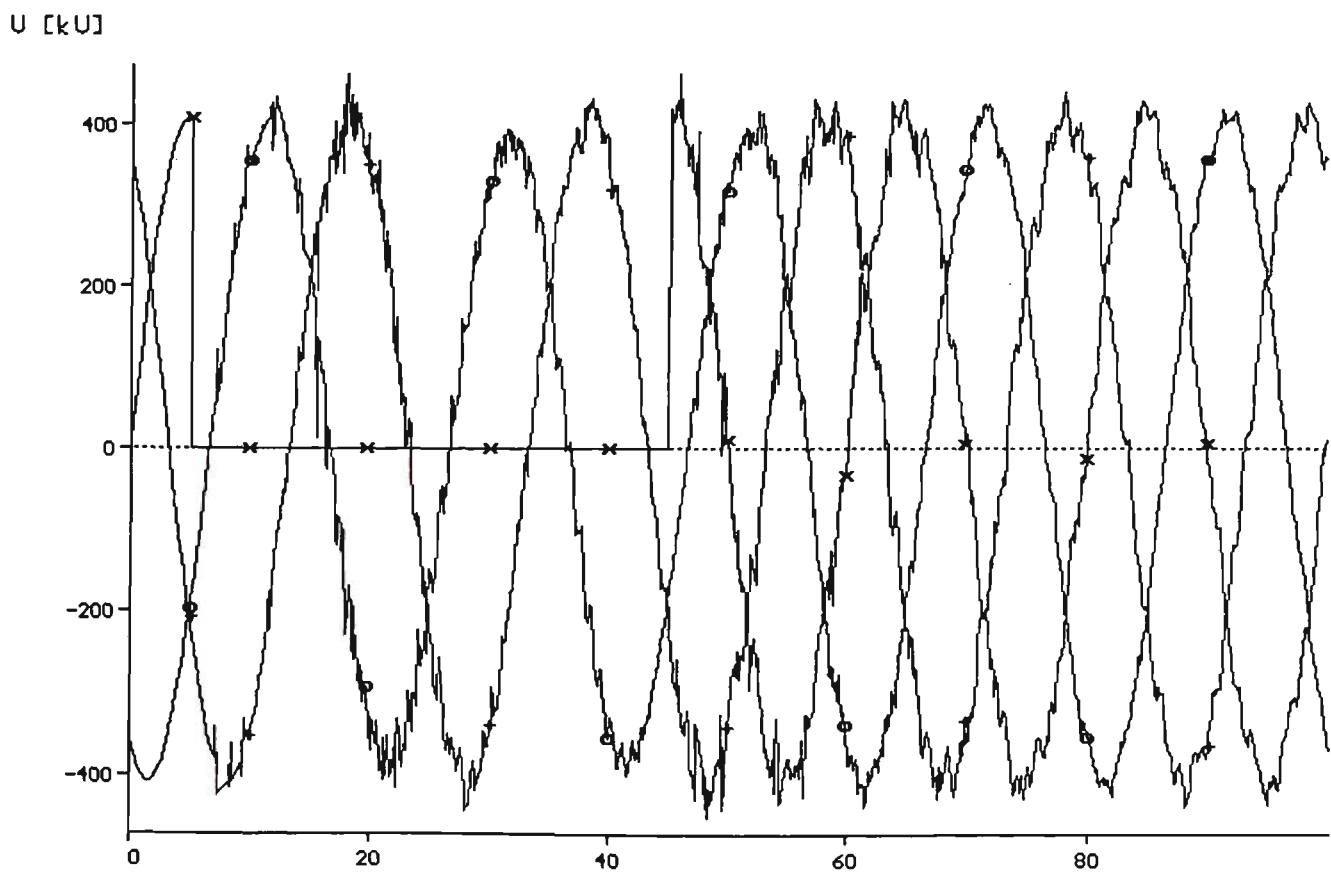


Fig. 8.32: A- Phase to Ground fault at $l=0$ km, and B-Phase at $l=96$ km, Compensated System, Three Phase Sending End Voltages

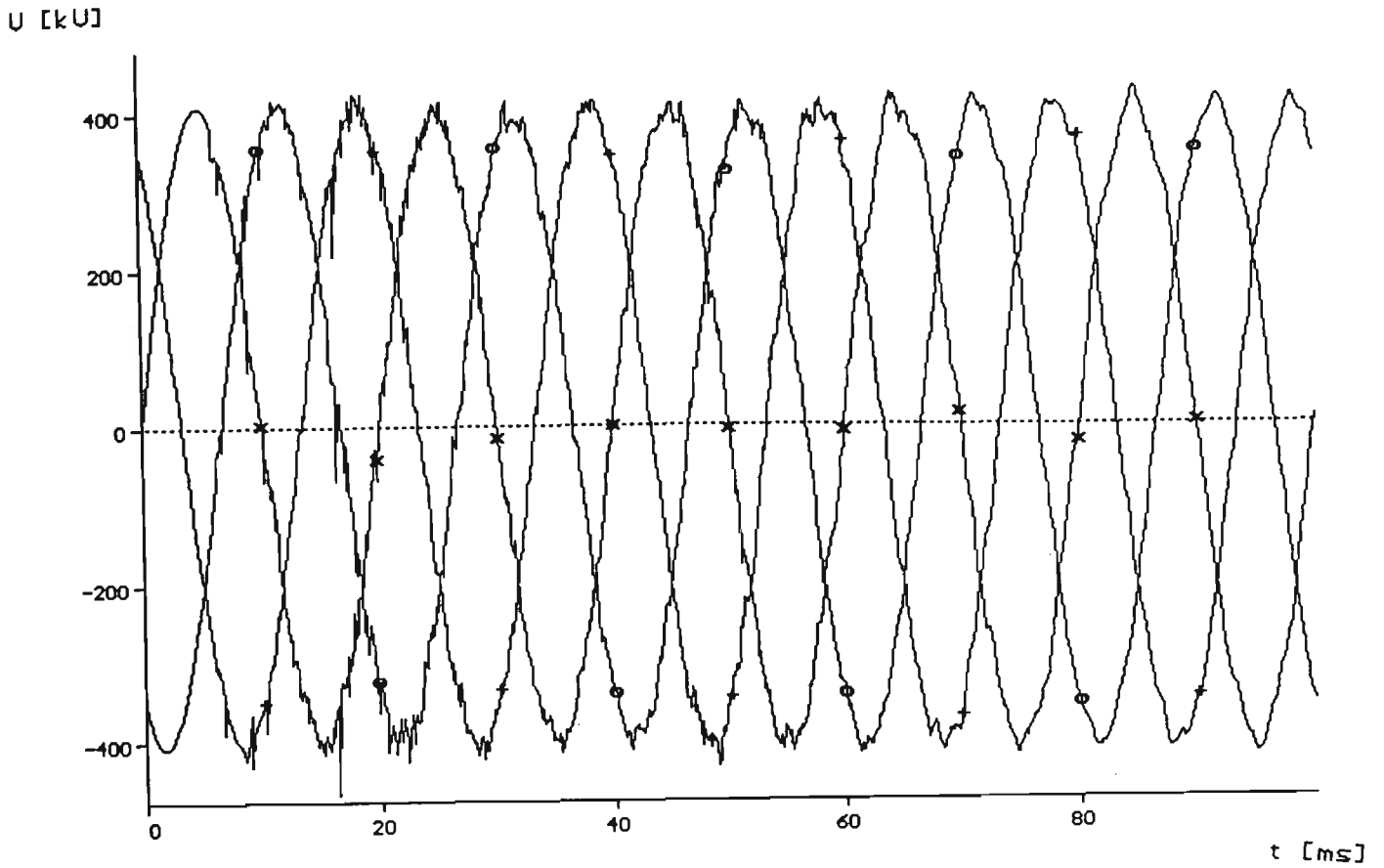


Fig. 8.33: A-Phase to G fault at $l=0$ km, and B-Phase to G at $l=96$ km, Three Phase Receiving End Voltages, (x): A, (o): B, (+): C, Fault Cleared after 40 ms.

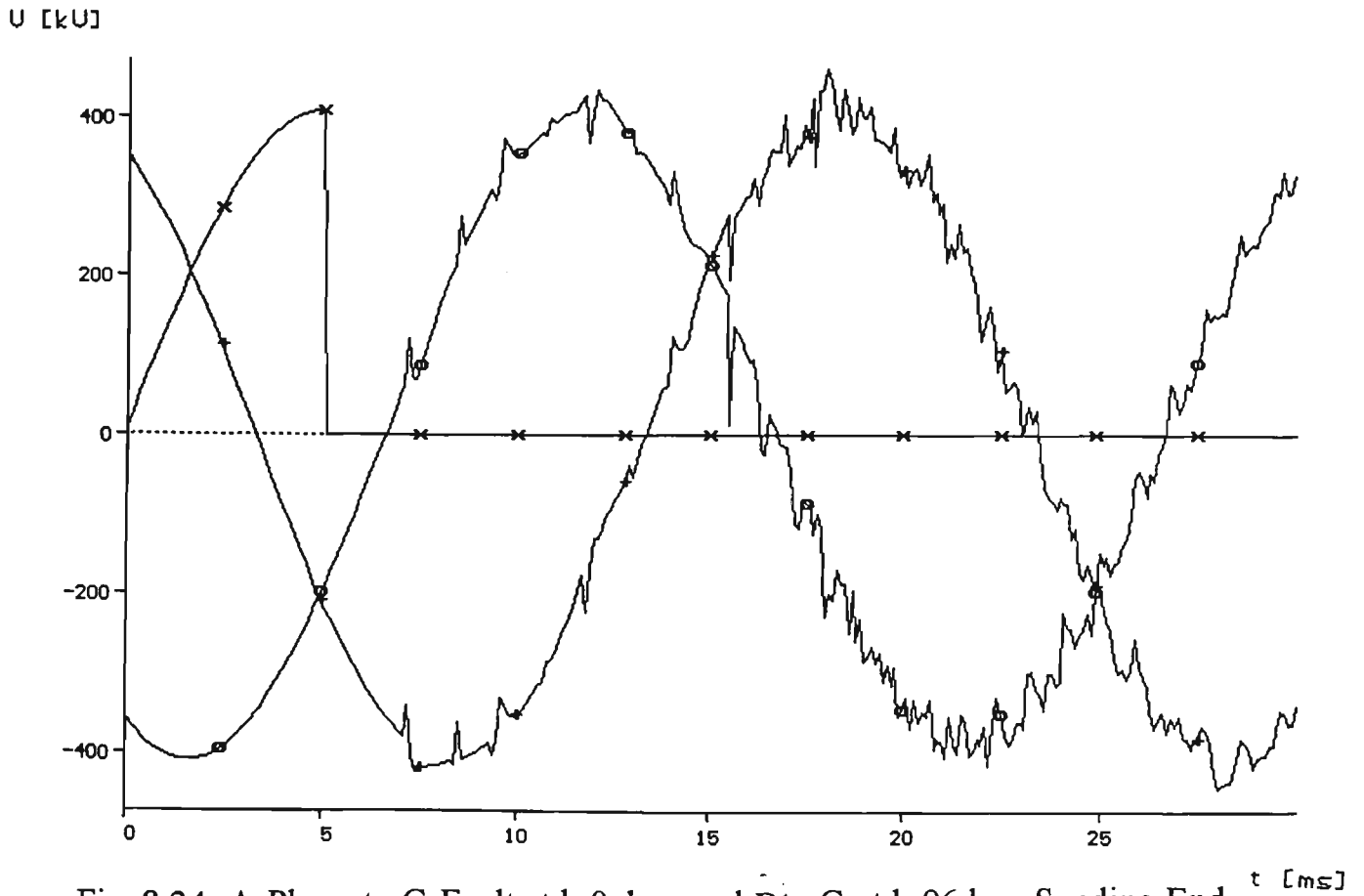


Fig. 8.34: A-Phase to G-Fault at $l=0$ km, and B to G at $l=96$ km, Sending End Voltages Zoomed, (x): A, (o): B, (+): C, fault Cleared after 40 ms.

U [kV]

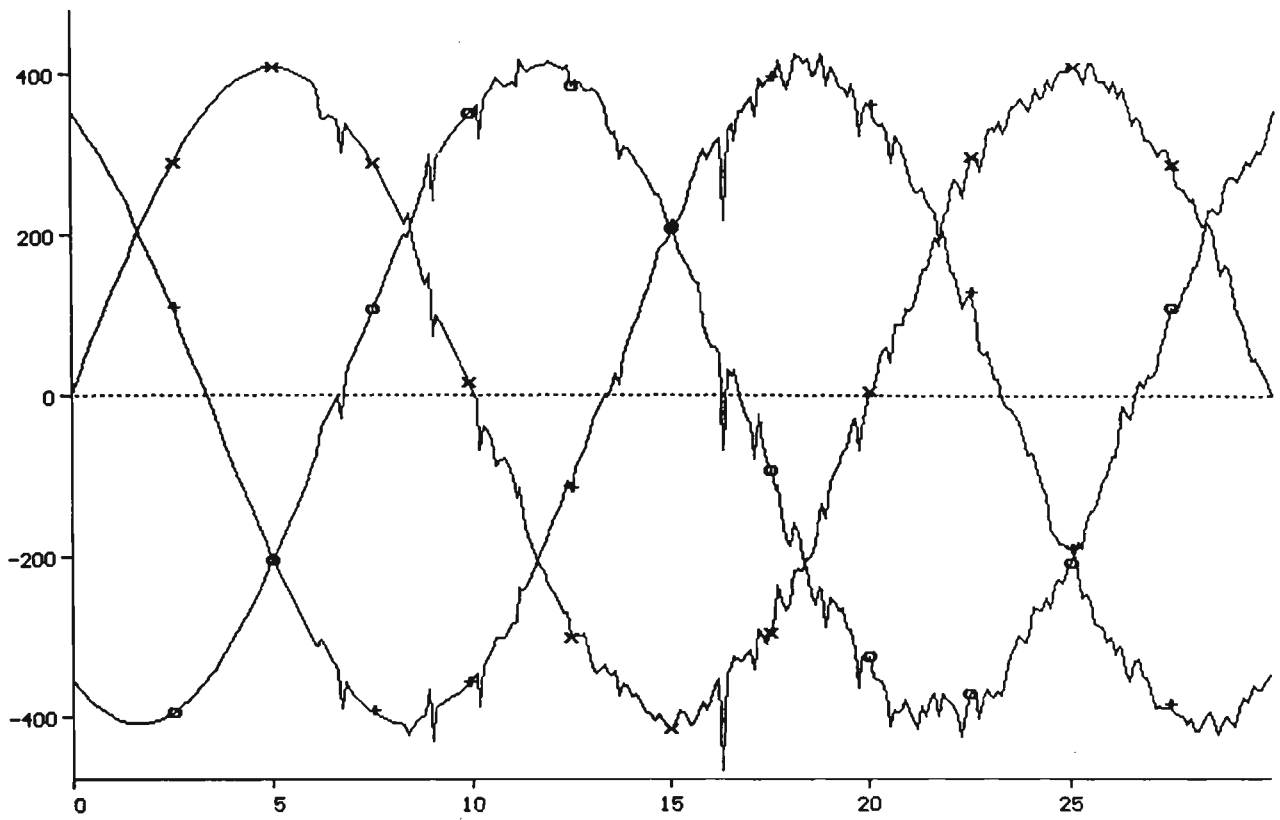
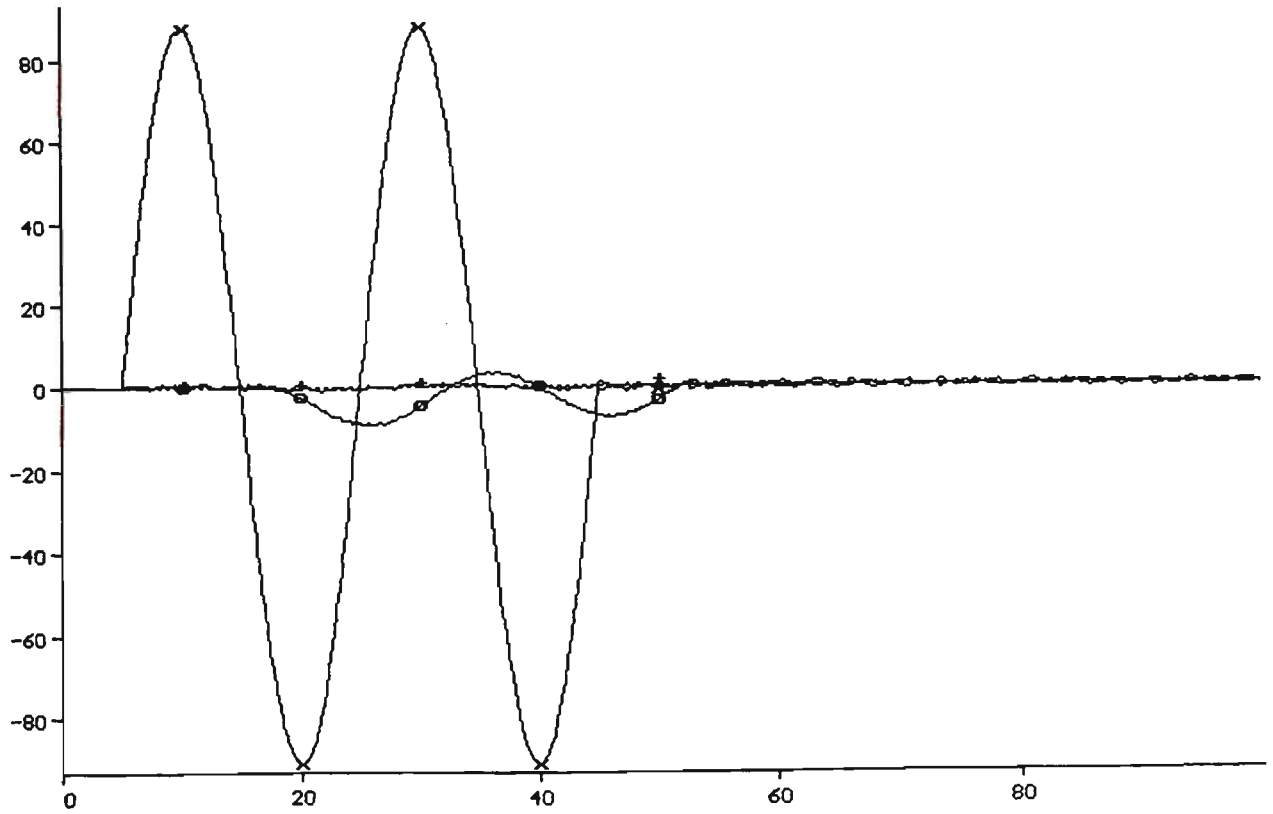


Fig. 8.35: A-Phase to G fault at $l=0$ km, B-G at $l=96$ km, Receiving End t [ms]

Three phase Voltages Zoomed, Fault cleared after 40 ms.

I [kA]



t [ms]

Fig. 8.36: A-Phase to G fault at $l=0$ km, and B-G at $l=96$ km, Three Phase Sending End Currents, (x): A, (o): B, (+): C, Fault Cleared after 40 ms.

respectively. A zoomed trace for these voltages are given in Figs. 8.34 and 8.35 respectively.

The three phase sending end current waveforms are given in Fig. 8.36, where phase A current is the predominant, since it is a close up fault. Phase B fault current is much lower since it is at 96 km away from the source. Both currents are assumed to be cleared after 40 ms.

The receiving end currents for the three phases are given separately for clarity on Figs. 8.37, 8.38 and 8.39 for A, B and C respectively. The current in the faulty path is given in Fig. 8.40, where it is clearly shown that these current are cleared in the due time when they are near to their zero values.

The sending end and receiving end three phase voltages are given in Figs. 8.41 and 8.42 respectively. Zoomed waveforms for the sending end and receiving end voltages over 30 ms are given in Figs. 8.43 and 8.44 respectively. The sending end three phase currents are given in Figs. 8.45, 8.46 and 8.47 for A, B and C phases respectively. A significant noise is noticed on the sound phase current at the receiving end as it is shown in Fig. 8.48. This is due to the effect of the faulty phases on the sound phase through the mutual coupling between the three phases.

The contribution to the above fault from the receiving end is less significant than from the sending end, because the fault on phase A is 384 km away, and on phase B is 296 km away from the fault location. The sound and faulty phases receiving end currents are given separately in Figs. 8.48, 8.49 and 8.50 for A, B and C phases respectively. The current through the fault path is given in Fig. 8.51.

I [A]

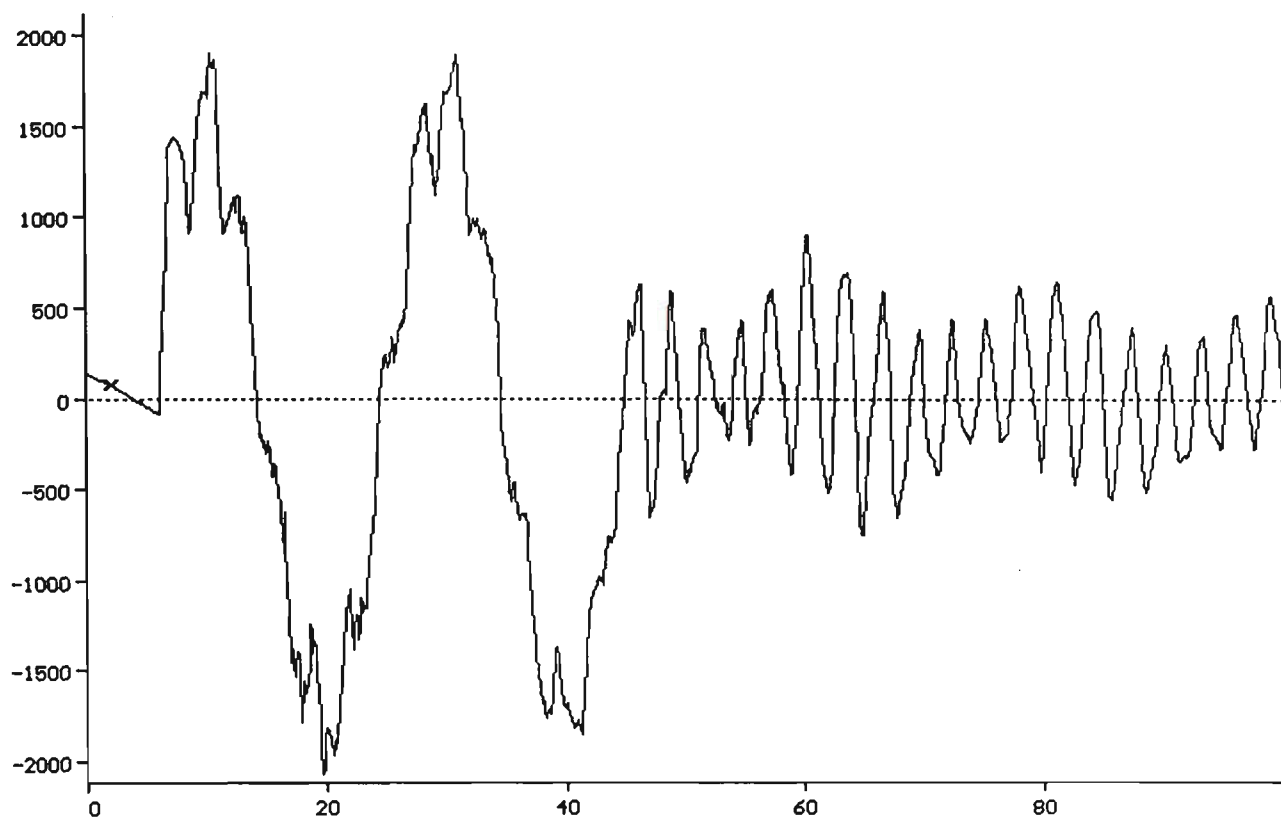


Fig. 8.37: A-Phase to G fault at $l=0$ km, and B-G at $l=96$ km, Phase A Current t [ms]

I [A]

at the Receiving End of the Line, Fault Cleared after 40 ms.

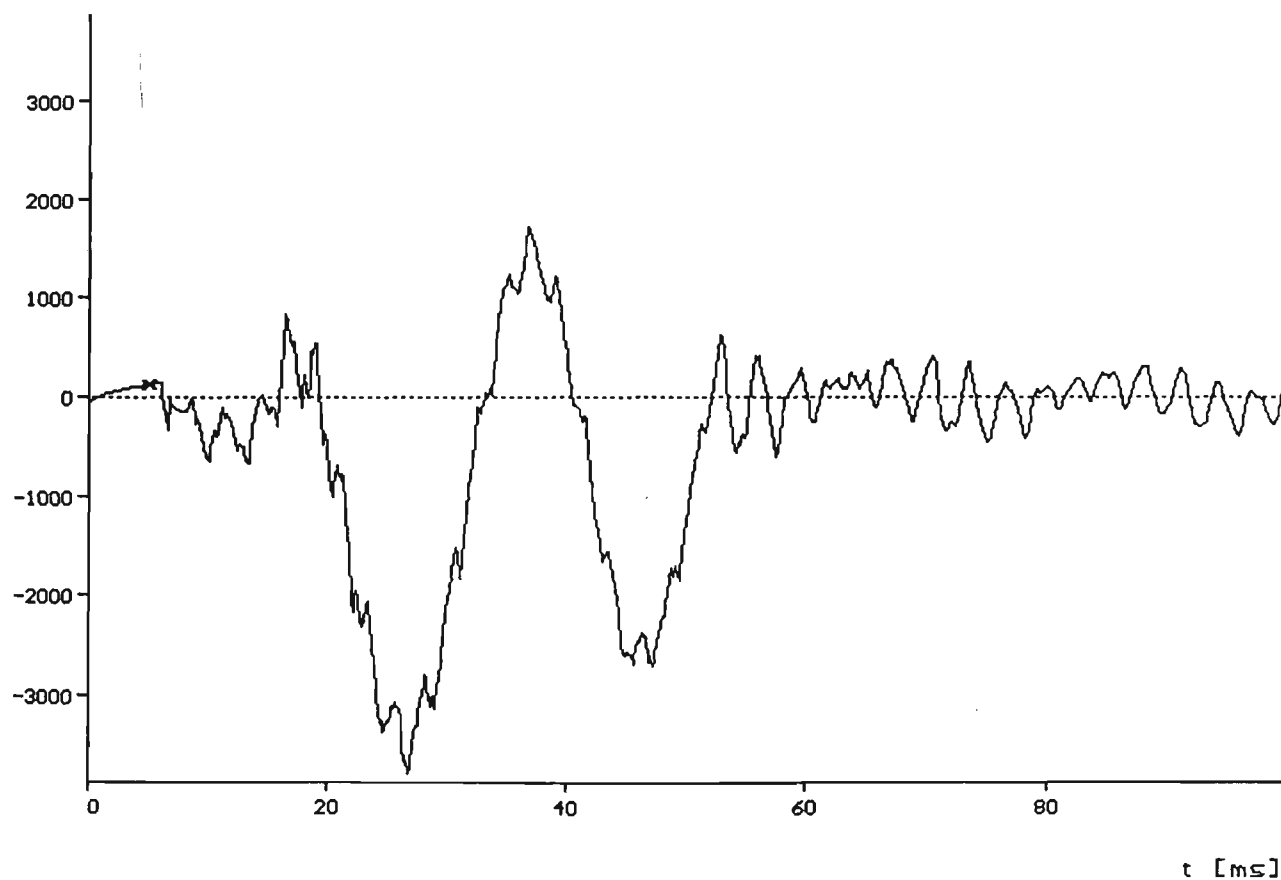


Fig. 8.38: A-Phase to Ground fault at $l=0$ km, and B-G at $l=96$ km, Phase B Receiving End Current, fault Cleared after 40 ms.

I [A]

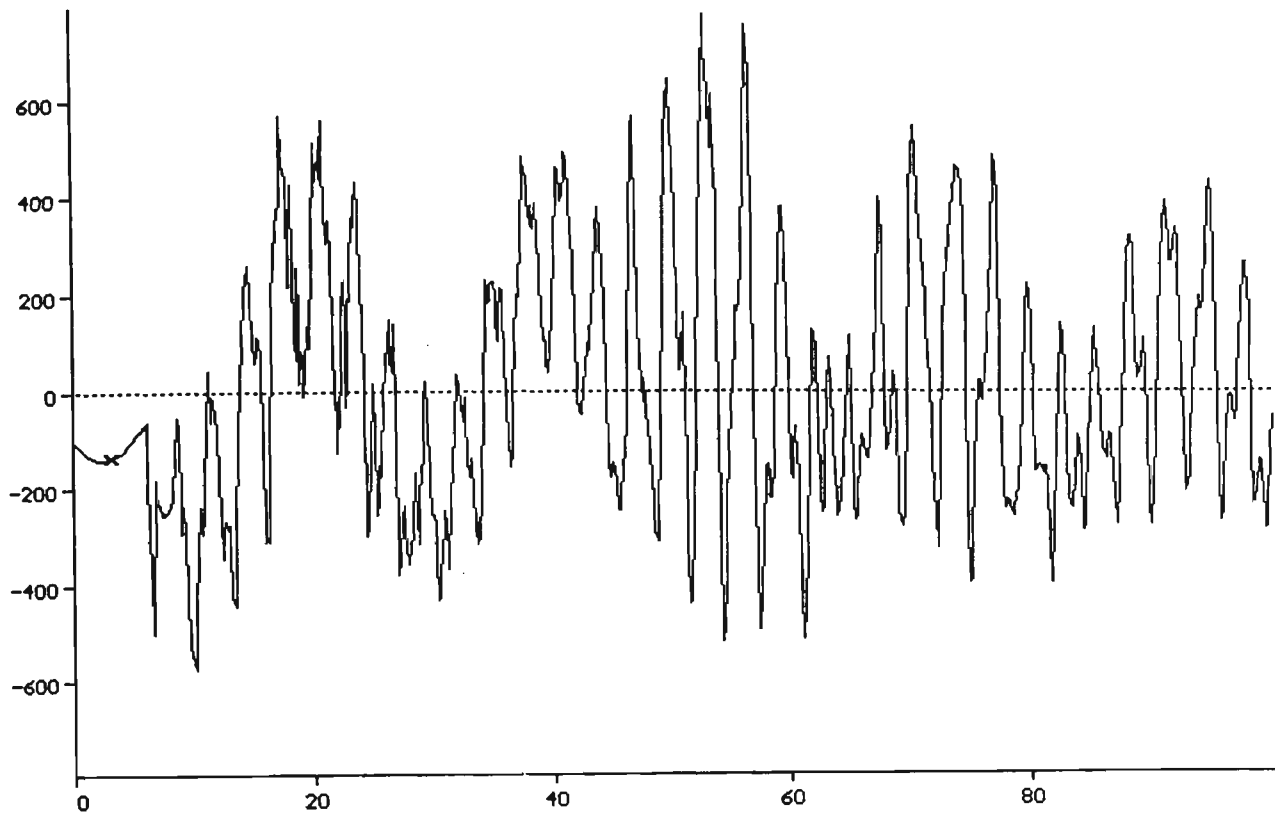
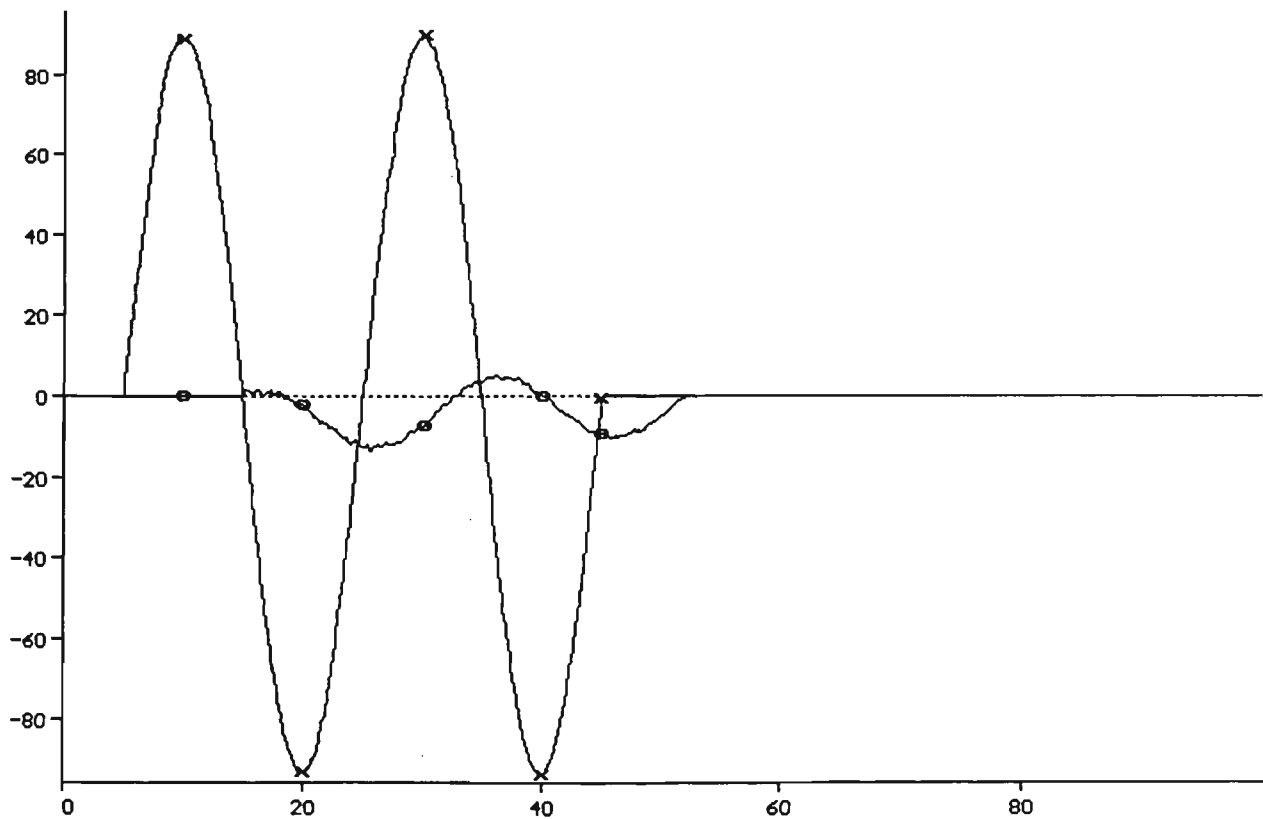


Fig. 8.39: A-Phase to G fault at $l=0$ km, and B-G at $l=96$ km, Phase C t [ms]

Receiving End Current, fault Cleared after 40 ms

I [kA]



t [ms]

Fig. 8.40: A-Phase to G Fault at $l=0$ km, and B-G at $l=96$ km, Currents through the fault path.

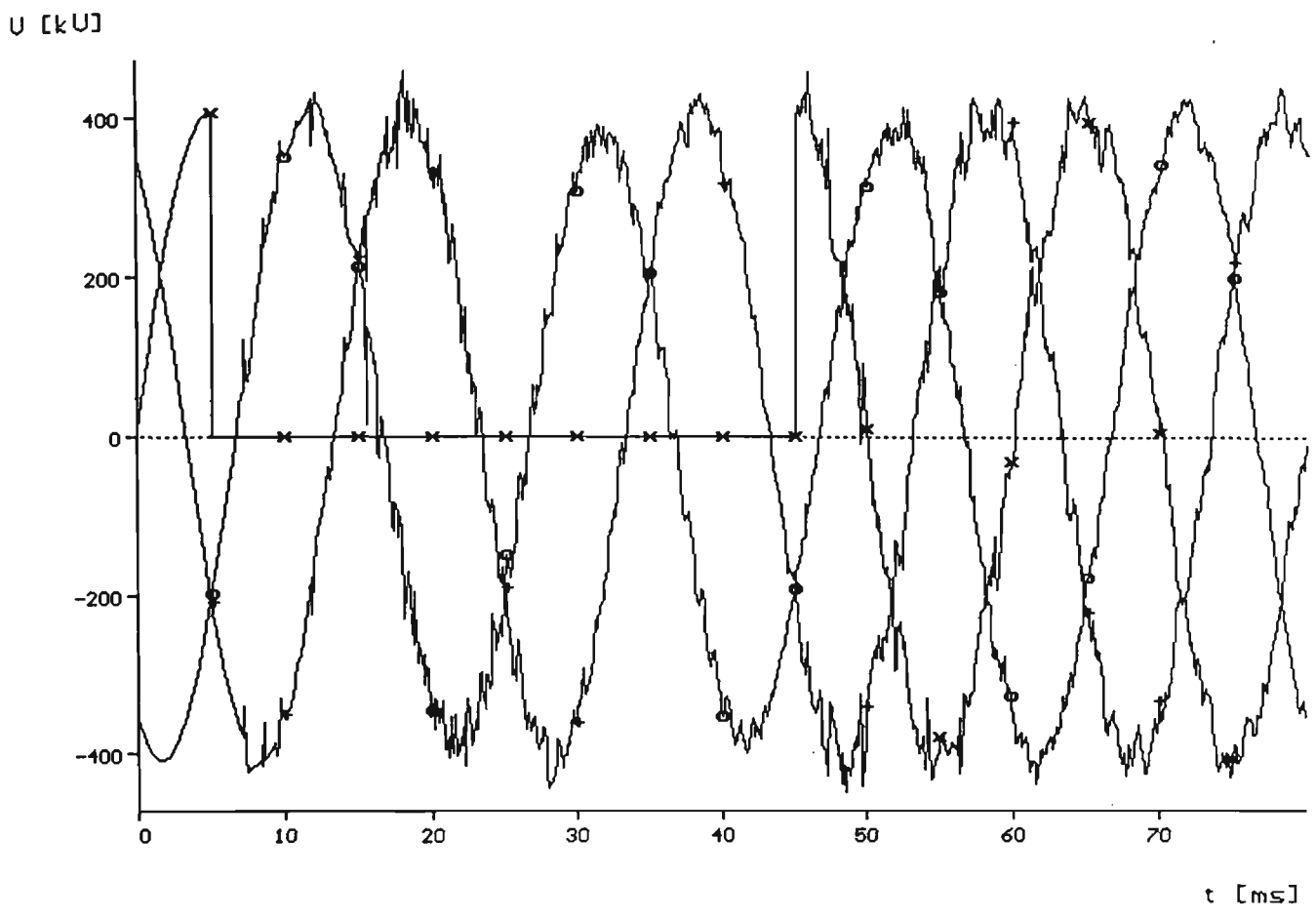


Fig. 8.41: A-Phase to G at $l=0$, B-Phase at $l=96$ km, Two Terminal System,
 Three phase Sending End Voltages, (x): A, (o): B, (+): C

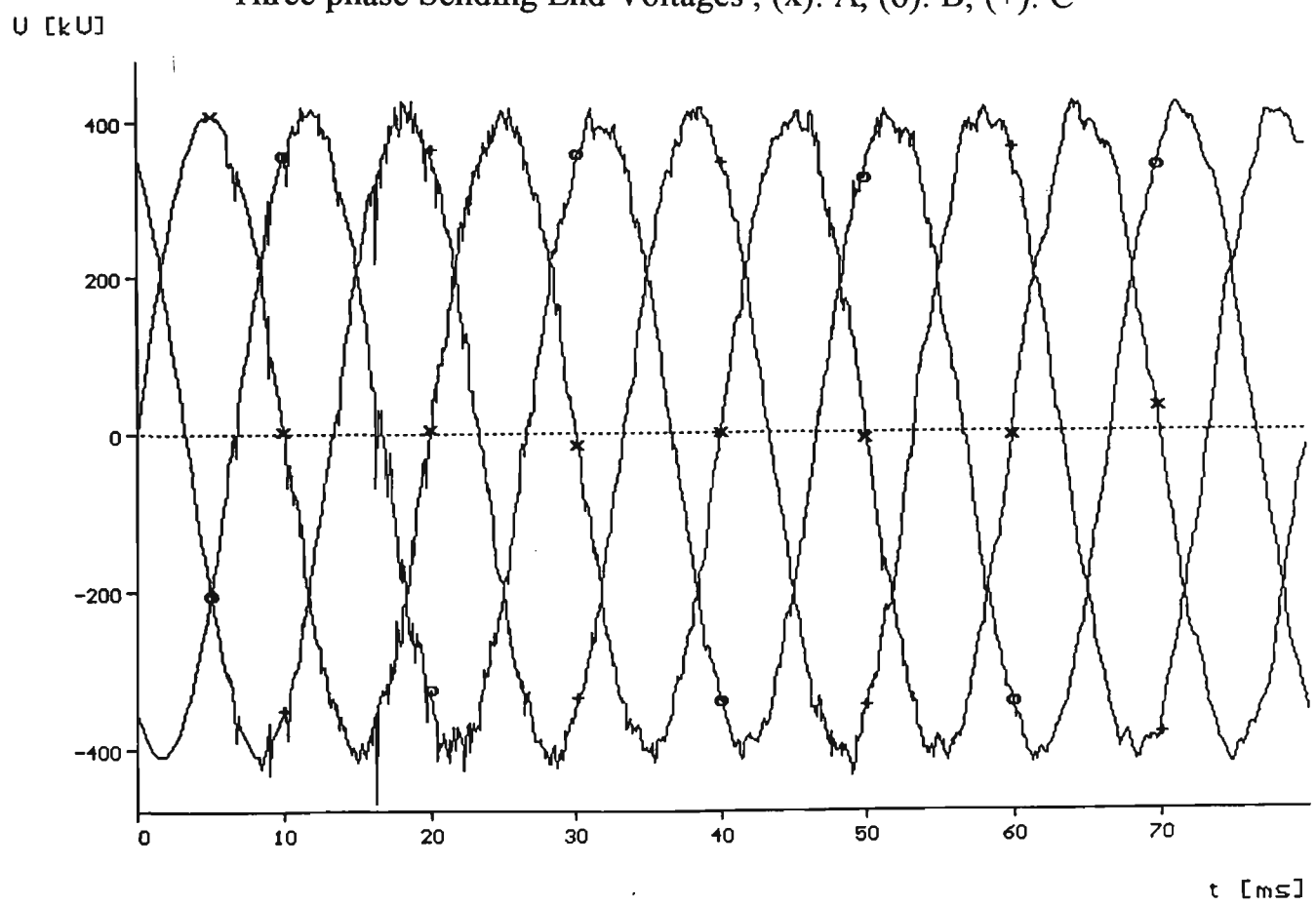


Fig. 8.42: A-Phase to G Fault at $l=0$, B to G at $l=96$, Two Terminal System,
 Three Phase Receiving End Voltages, (x): A, (o): B, (+): C

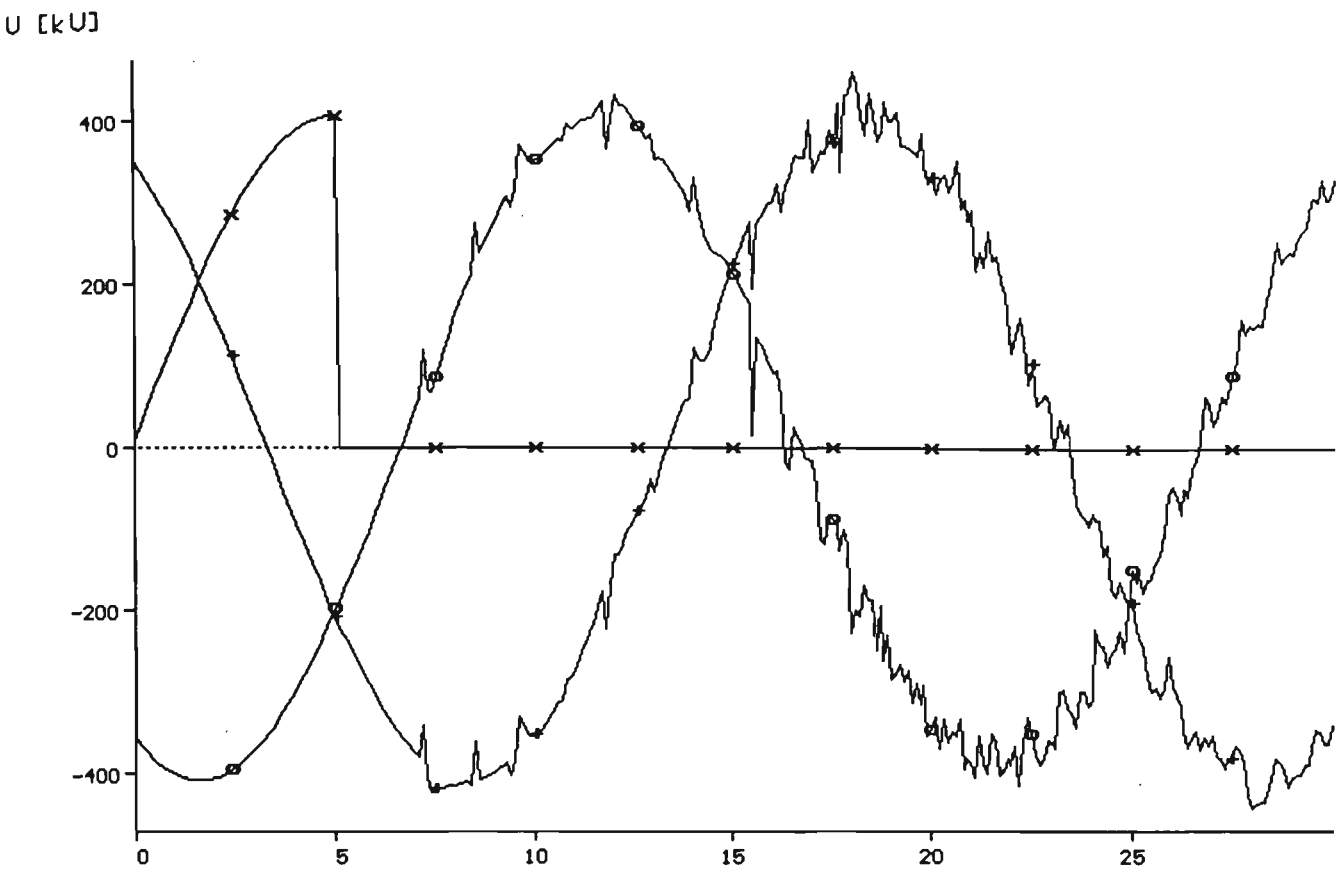


Fig. 8.43: Zoomed Sending End Voltages of Fig. 8.41 t [ms]

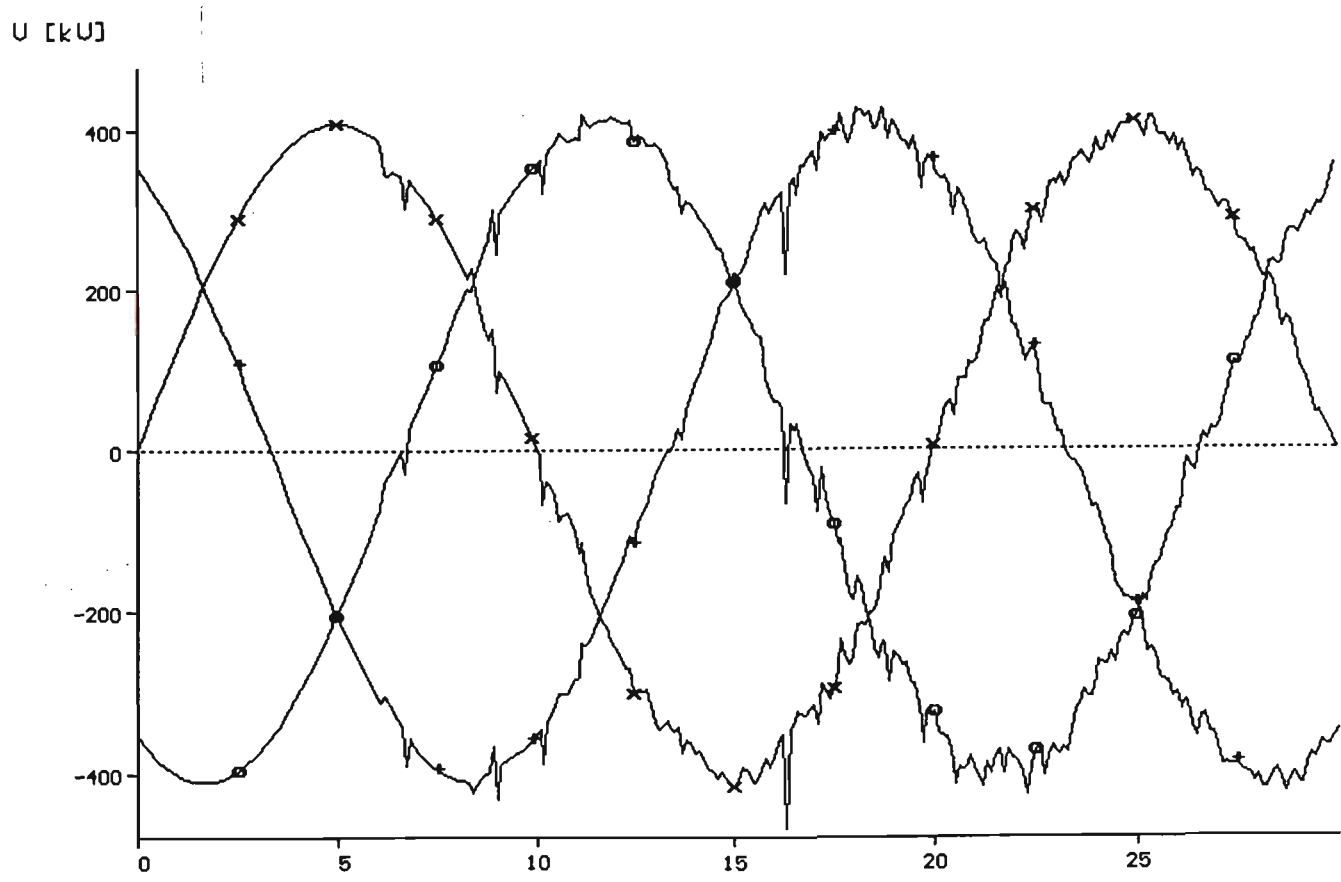


Fig. 8.44: Zoomed Receiving End Voltages of Fig. 8.42 t [ms]

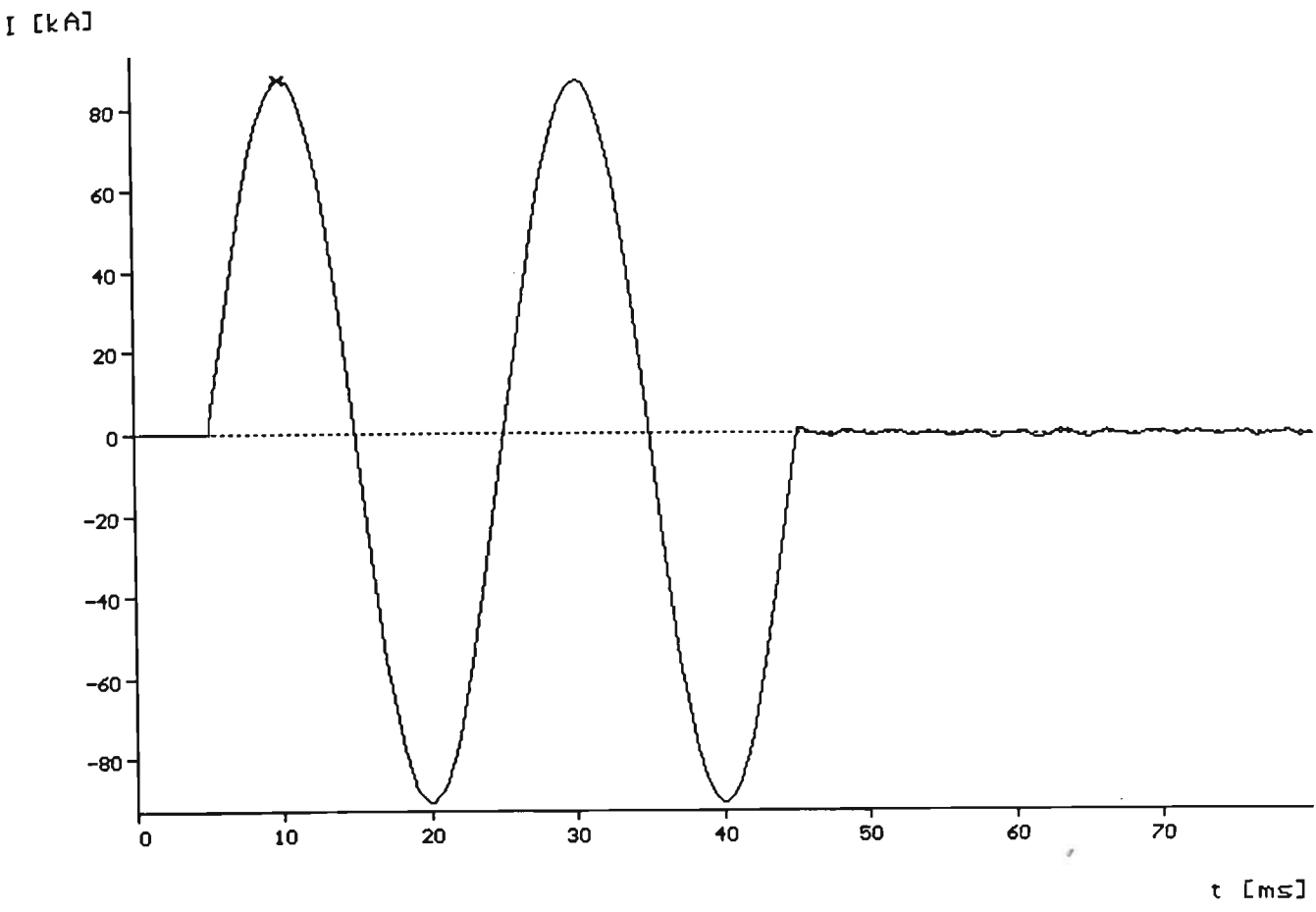


Fig. 8.45: Sending End Current of Phase A, for a Fault in A Phase at $l=0$, and B Phase at $l=96$ km, Two Terminal System

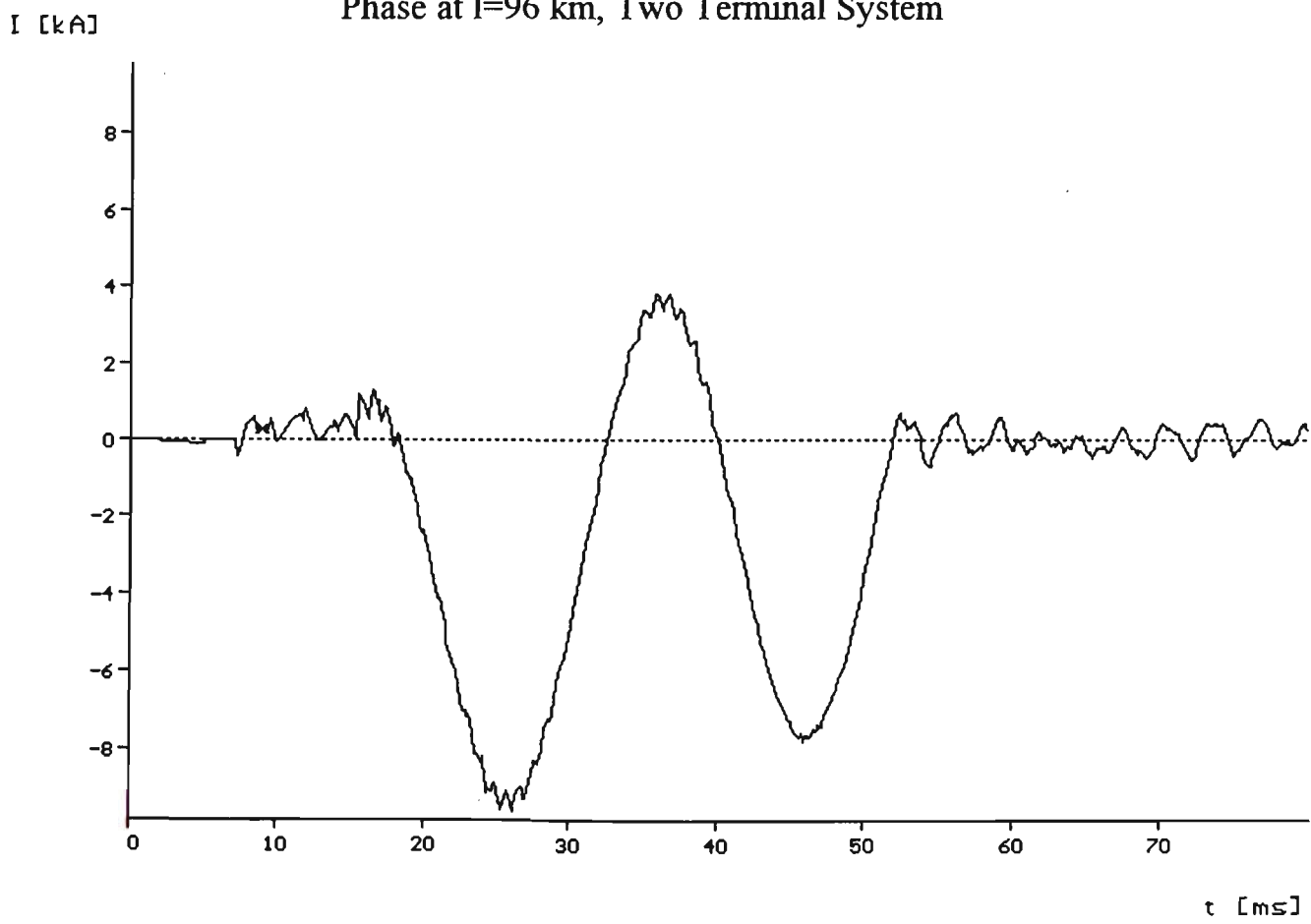


Fig. 8.46: Phase B Sending End Fault Current, for A-Phase at $l=0$, and B-Phase at $l=96$ km, Two Terminal System

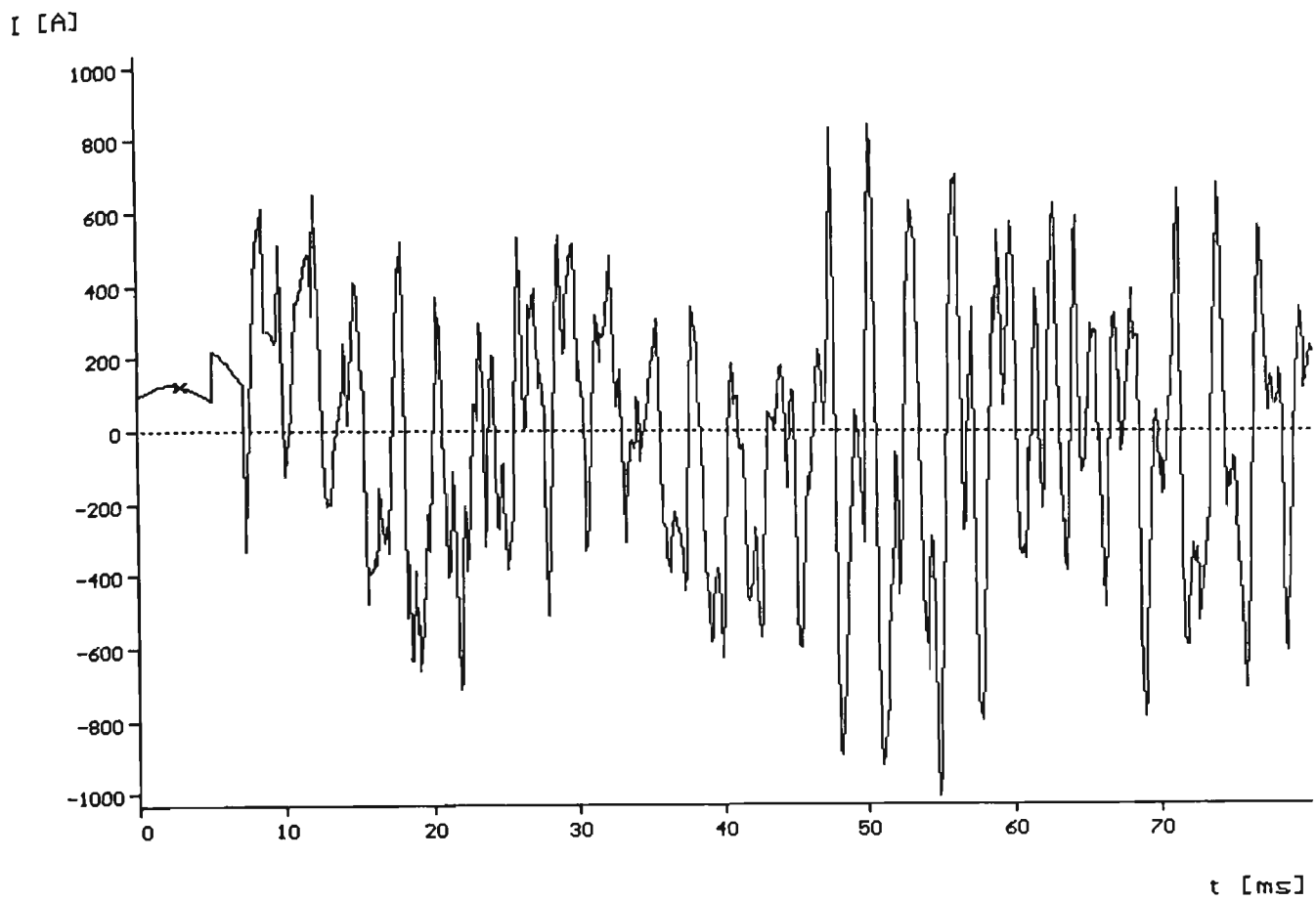


Fig. 8.47: The Healthy Phase Sending End Current for A-G at $l=0$, and B-G at $l=96$ km, Two terminal System

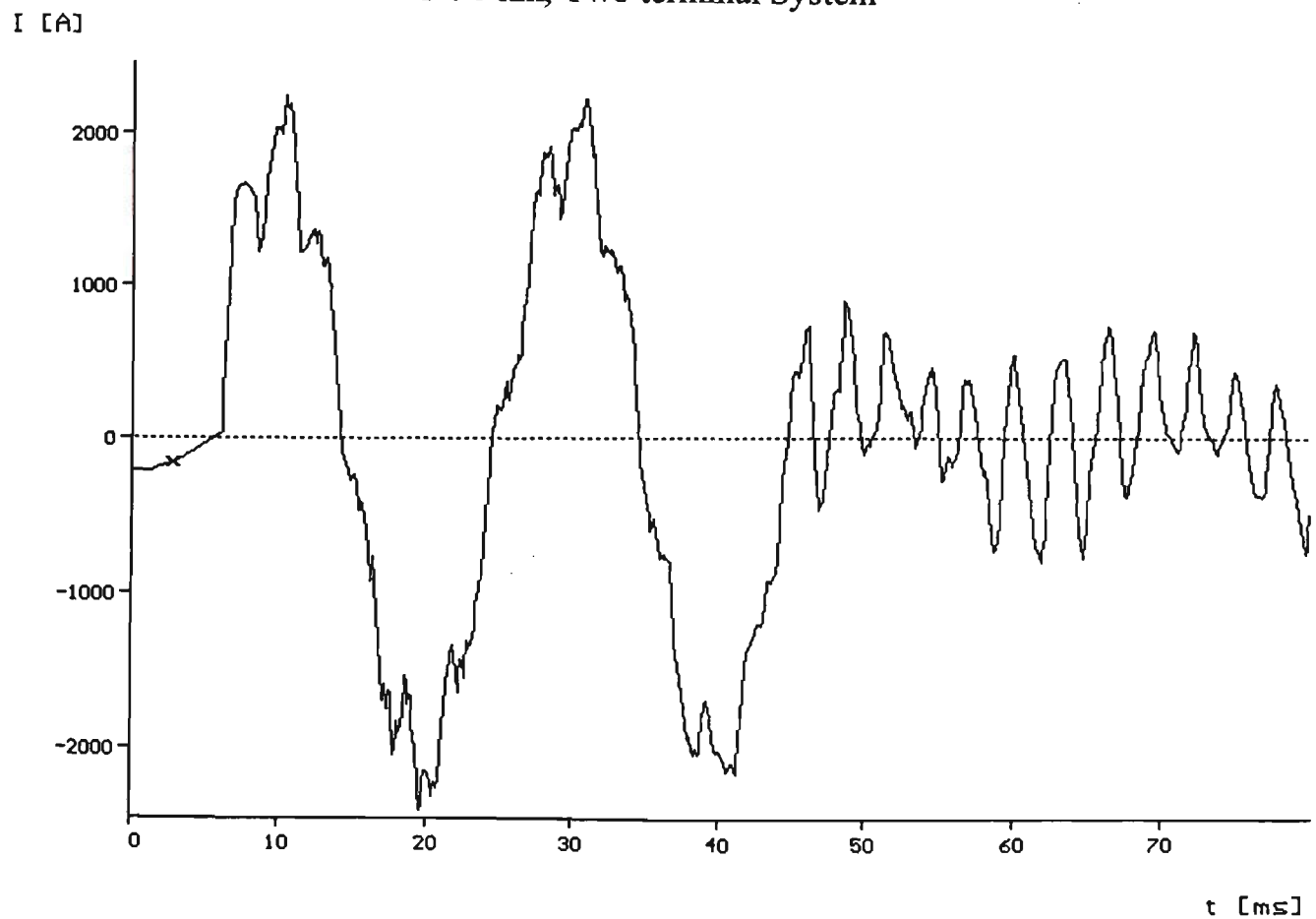


Fig. 8.48: The Receiving End A Phase Current , for Fault in A-G at $l=0$, B-G at $l=96$ km, Two terminal System

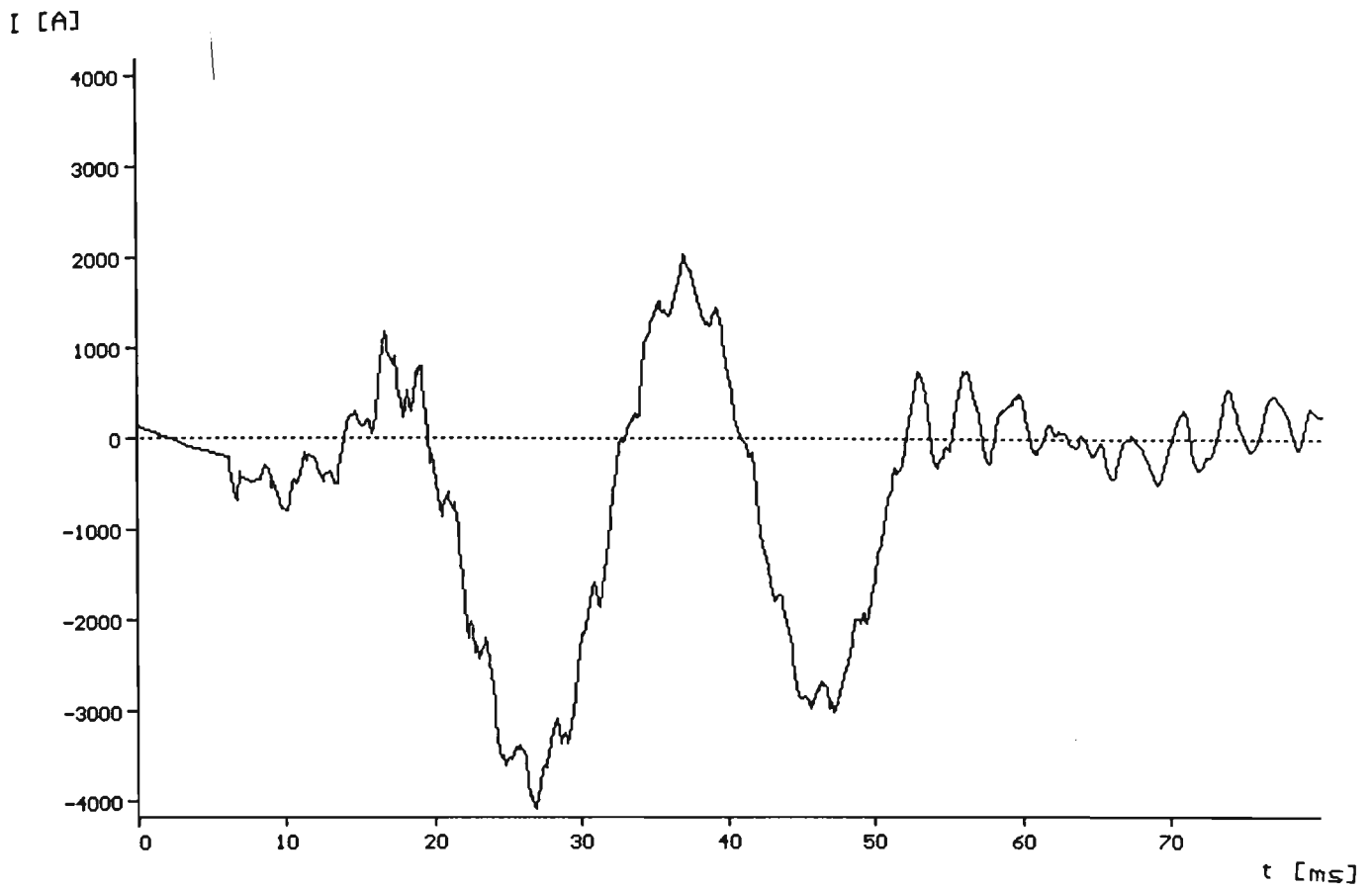


Fig. 8.49: B - Phase Receiving End Current for A - G Fault at $l=0$ km , and B-G at $l=96$ km, Two terminal System

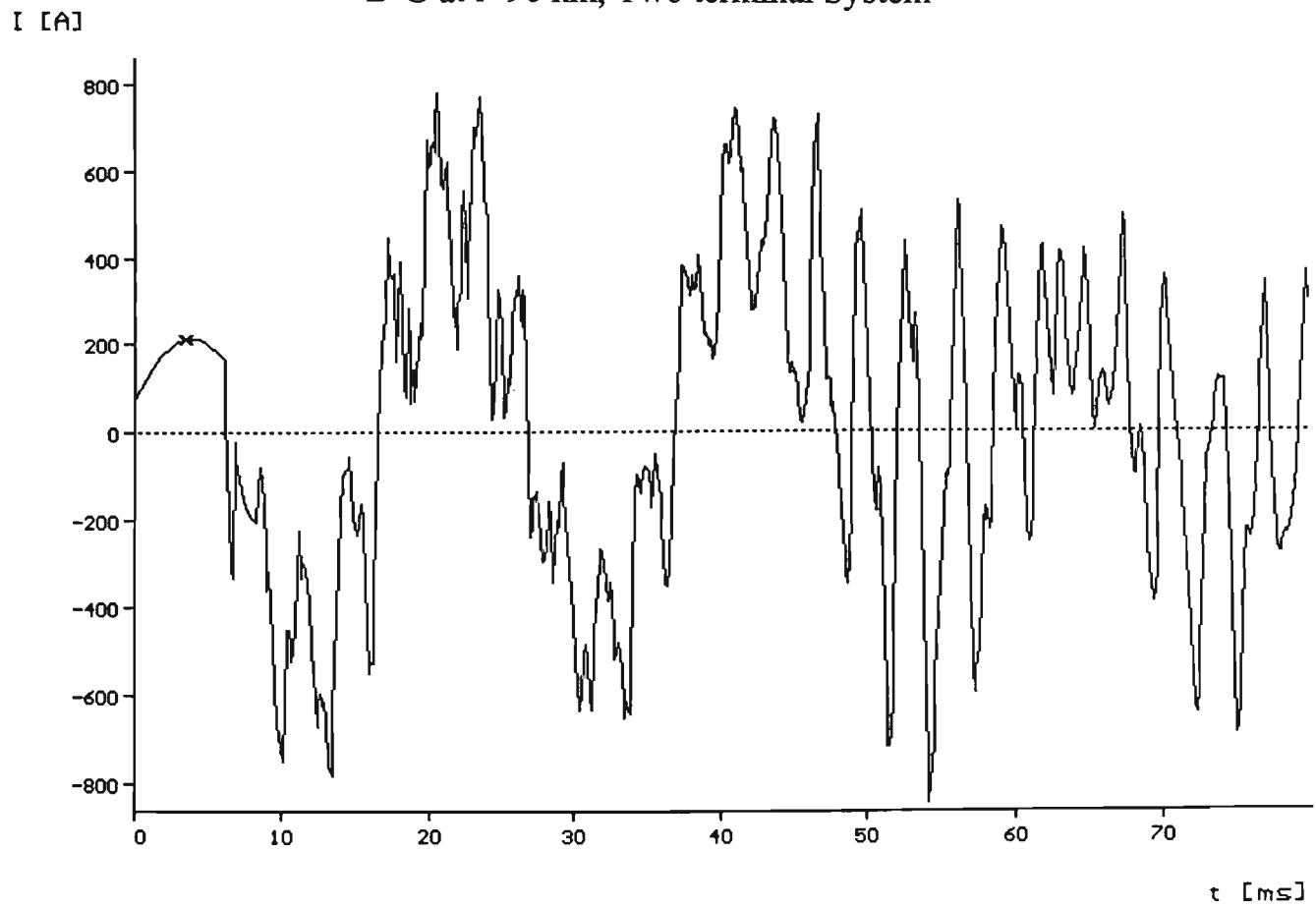


Fig. 8.50: The Receiving End Current in the Healthy Phase C, for A-G fault at $l=0$, and B-G Fault at $l=96$ km, Two terminal System

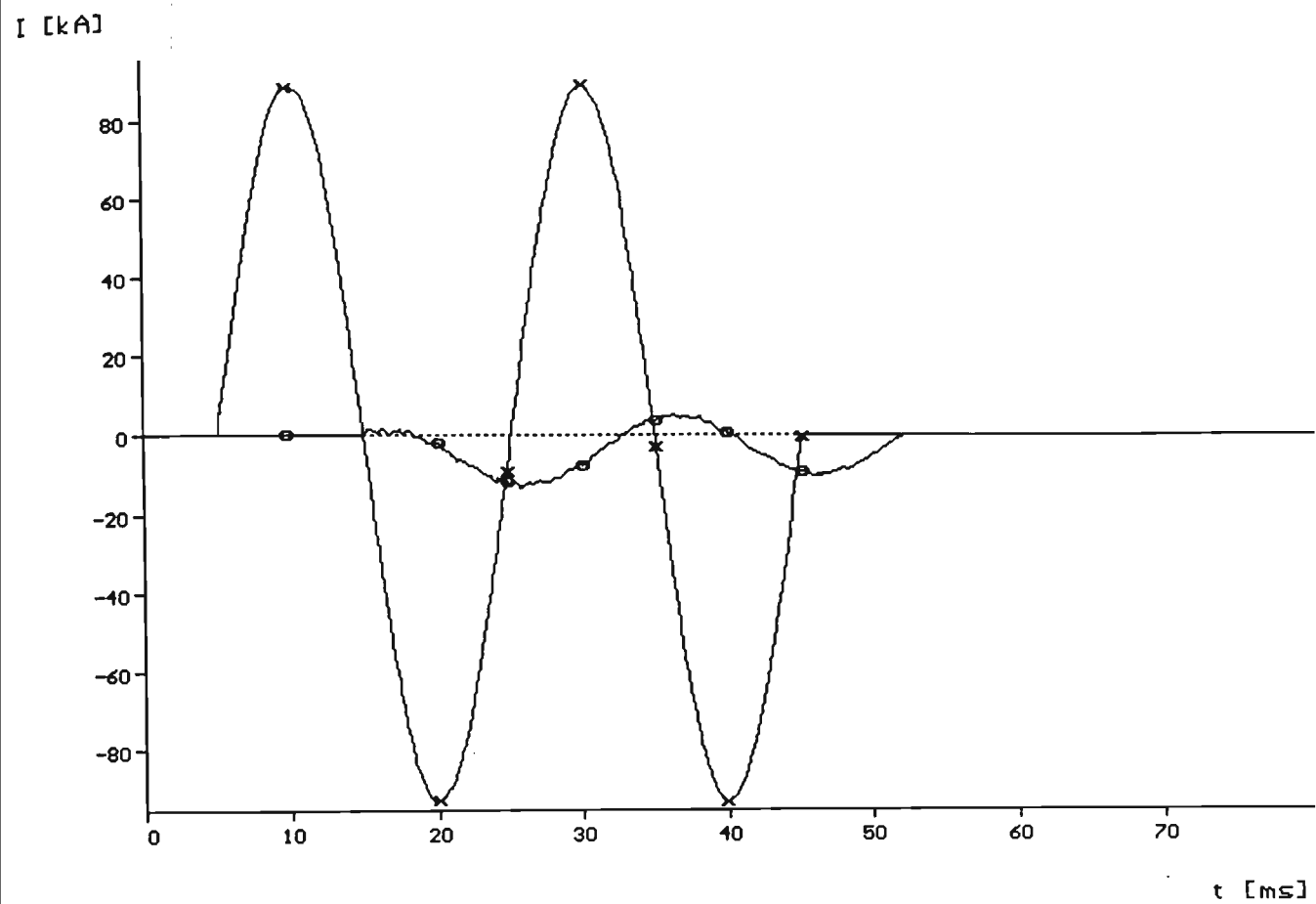


Fig. 8.51: Currents in the Faulty Path, for A-G Fault at $l=0$, and B-G Fault at $l=96$ km, Two Terminal System

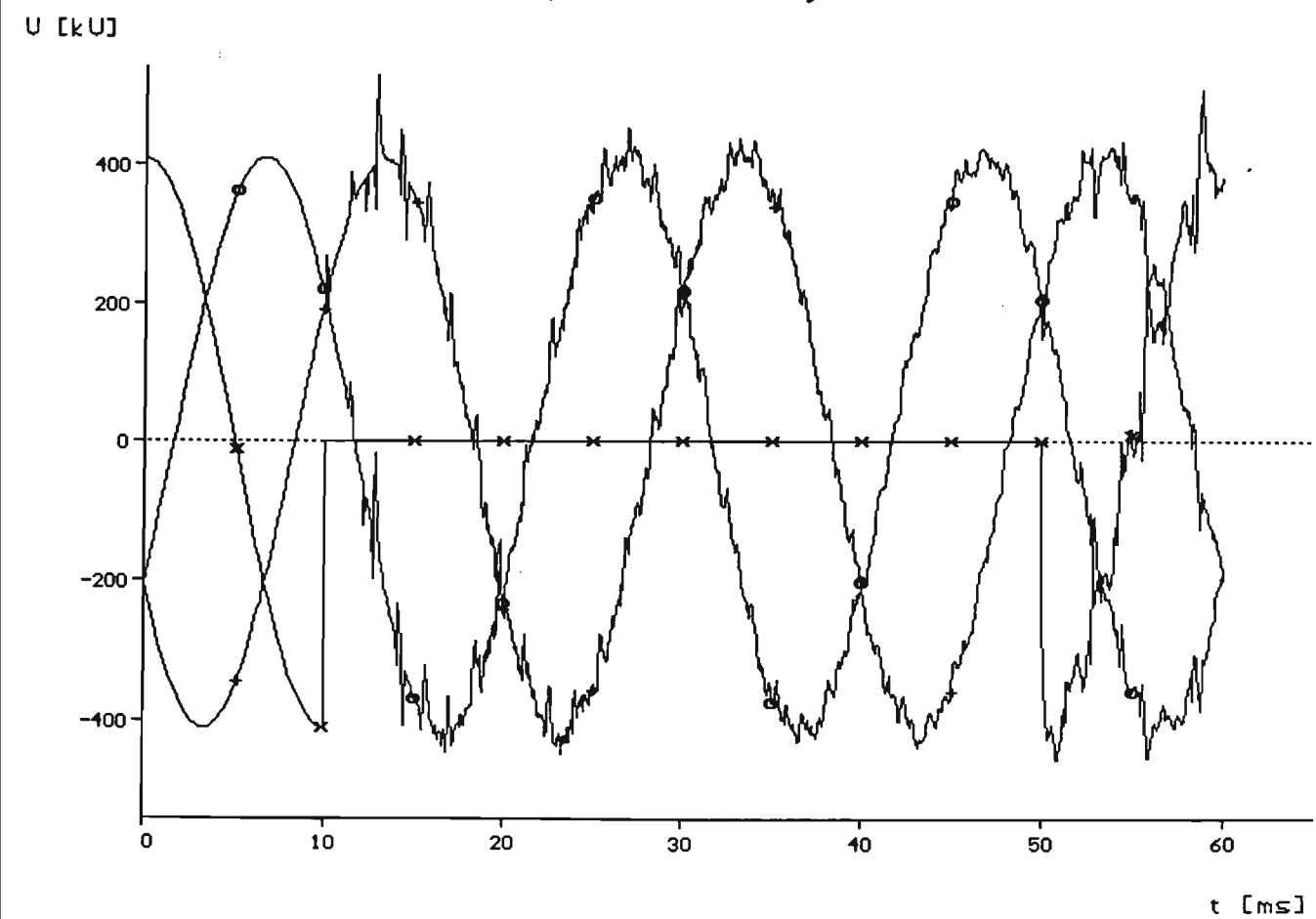


Fig. 8.52: A-G Fault at $l=0$ of the Three Terminal 500 kV System, Three Phase
Voltages at the Sending End, Fault Cleared after 40 ms

8.3 THREE TERMINAL SYSTEMS

As it was shown in Fig. 7.2 of chapter 7, the three terminal system is assumed to have the same lengths for each tee feeder equal to 196 km. A single phase to ground fault is assumed on phase A (A-G), the fault is applied at the sending end of the three terminal system (end P).

8.3.1 Single Line to Ground faults

The fault is assumed on phase A, at the sending end section of the tee feeder (at P). As it is shown in Fig. 8.52, the voltage of phase A collapsed to zero, and the healthy phase voltages also were affected by this fault. This influence is indicated by the noise superimposed on the sinusoidal waveforms. The disturbance of the healthy phases and the faulty one remains disturbed after 15 ms of fault clearance. Under these conditions, the current waveforms in all three phases at the sending end P, receiving end R, tee end Q and the fault currents through the fault path are shown in Figs. 8.53, 8.54, 8.55 and 8.56 respectively.

For a single phase to ground fault (A-G) at the middle of the PT feeder (at 96 km from the sending end P), the waveforms of the three phase voltages for the sending end P, receiving end R and the Q end of the tee feeder are shown in Figs. 8.57, 8.58 and 8.59 respectively.

For a similar fault but at the tee pint T of the tee feeder, the three phase voltages at the sending, receiving and Q ends of the three terminal system are shown in Figs. 8.60, 8.61 and 8.62 respectively. The waveforms of the three phase currents at the sending end P, receiving end R and the Q end of the tee feeder are shown in Figs. 8.63, 8.64 and 8.65 respectively. The behaviour of

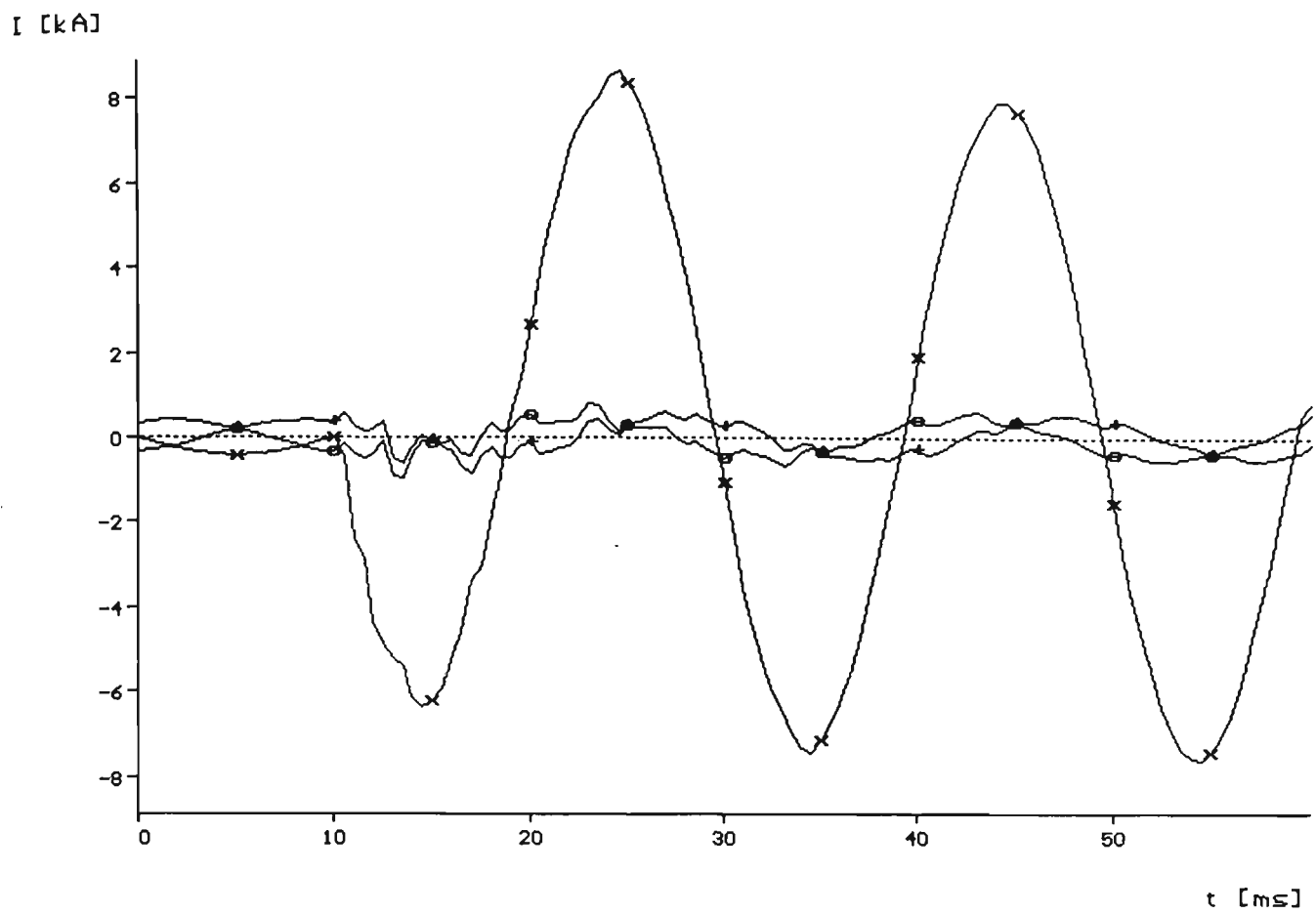


Fig. 8.53: A-G fault at $l=0$ at End P of the Three Terminal Feeder, Three Phase

Sending End Currents, Fault Cleared after 40 ms

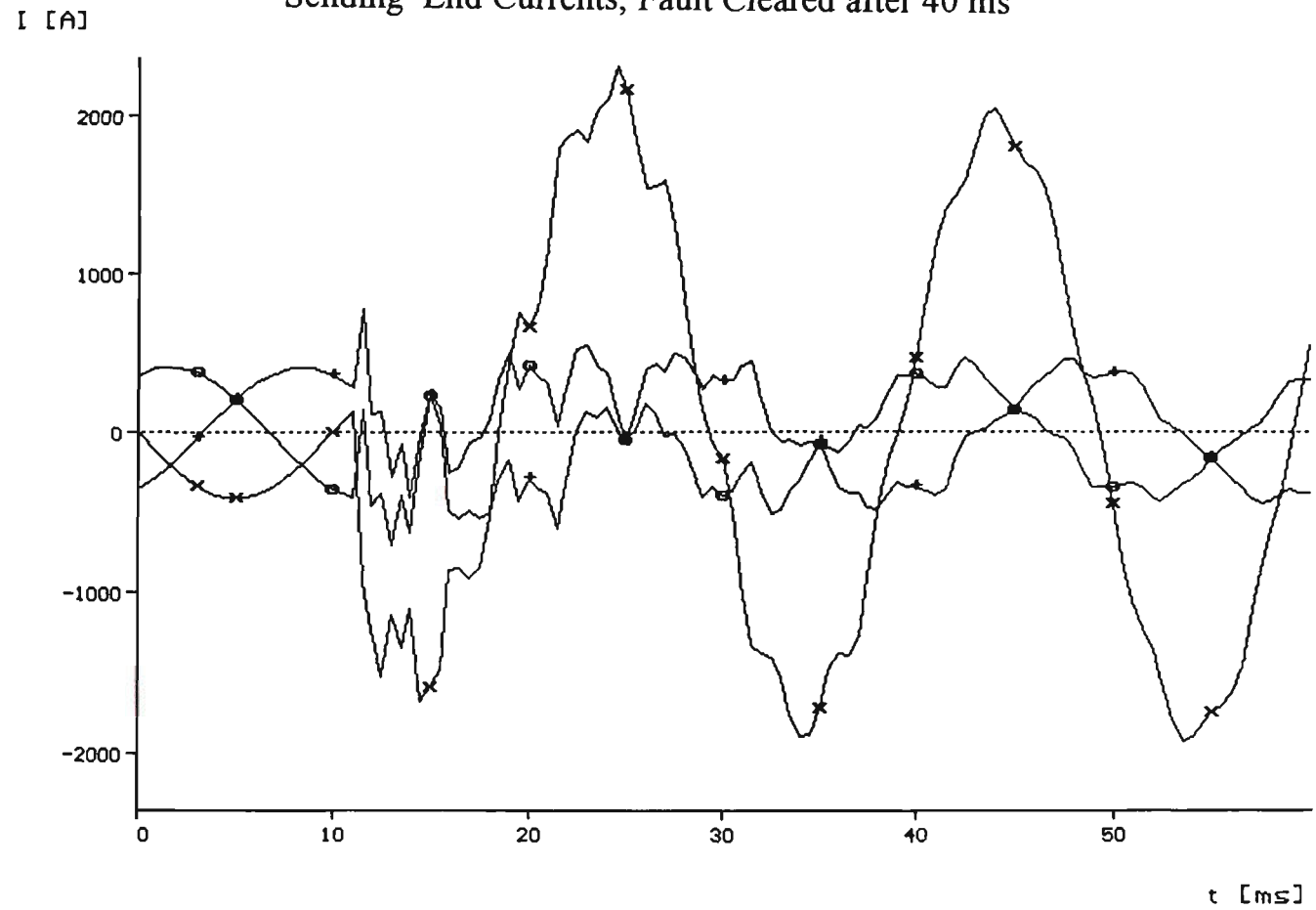


Fig. 8.54: Three Terminal Feeder, A-G Fault at $l=0$ of the P End, Three Phase

Receiving End Currents, (x): A, (o): B, (+): C

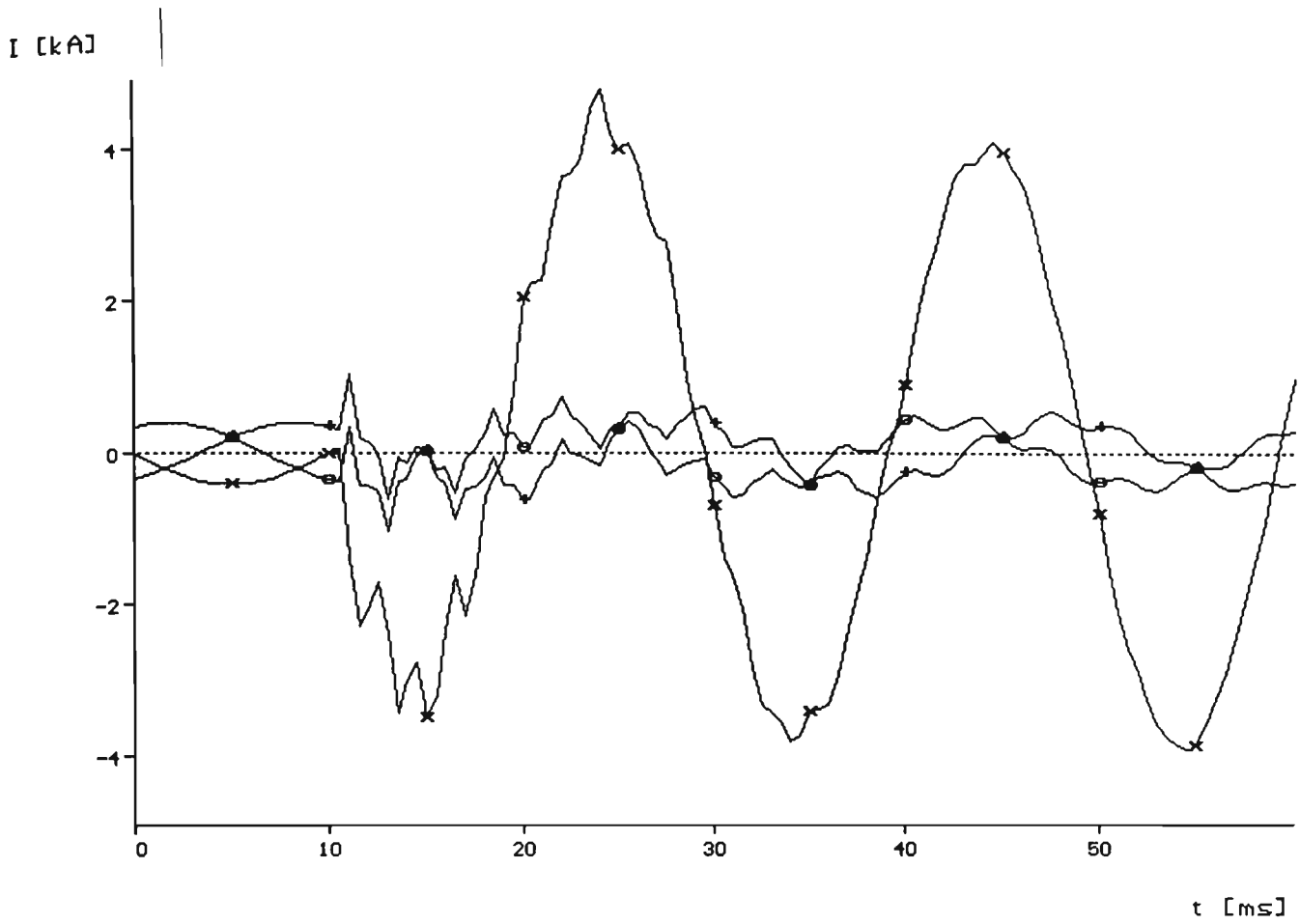


Fig. 8.55: The Three Phase Currents at the Q End of The Three Terminal

Feeder, Fault Cleared after 40 ms.

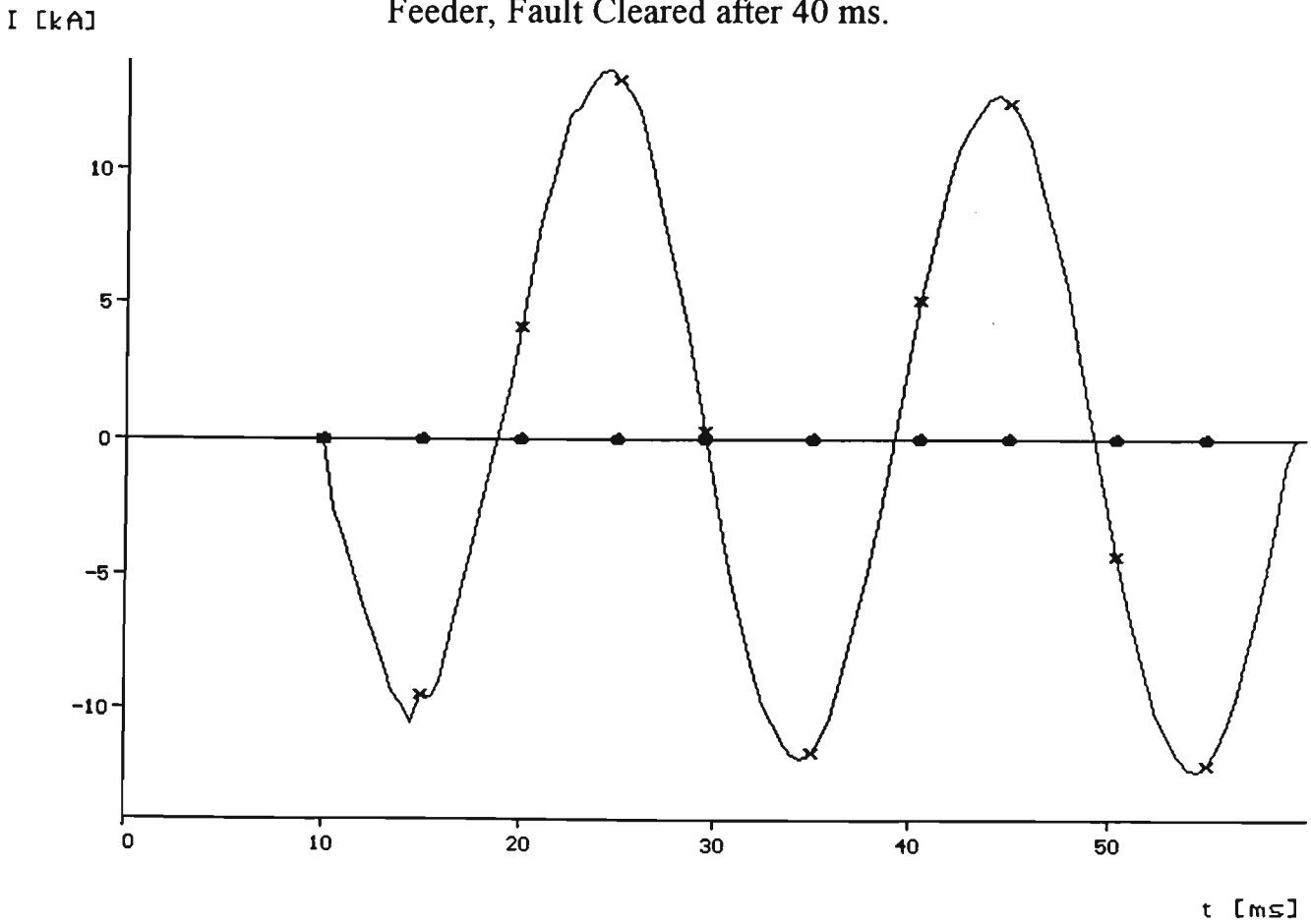


Fig. 8.56: Current in the Faulty Path for A-G Fault at $l=0$ of the Sending End

Feeder P, (x): A, (o): B, (+): C

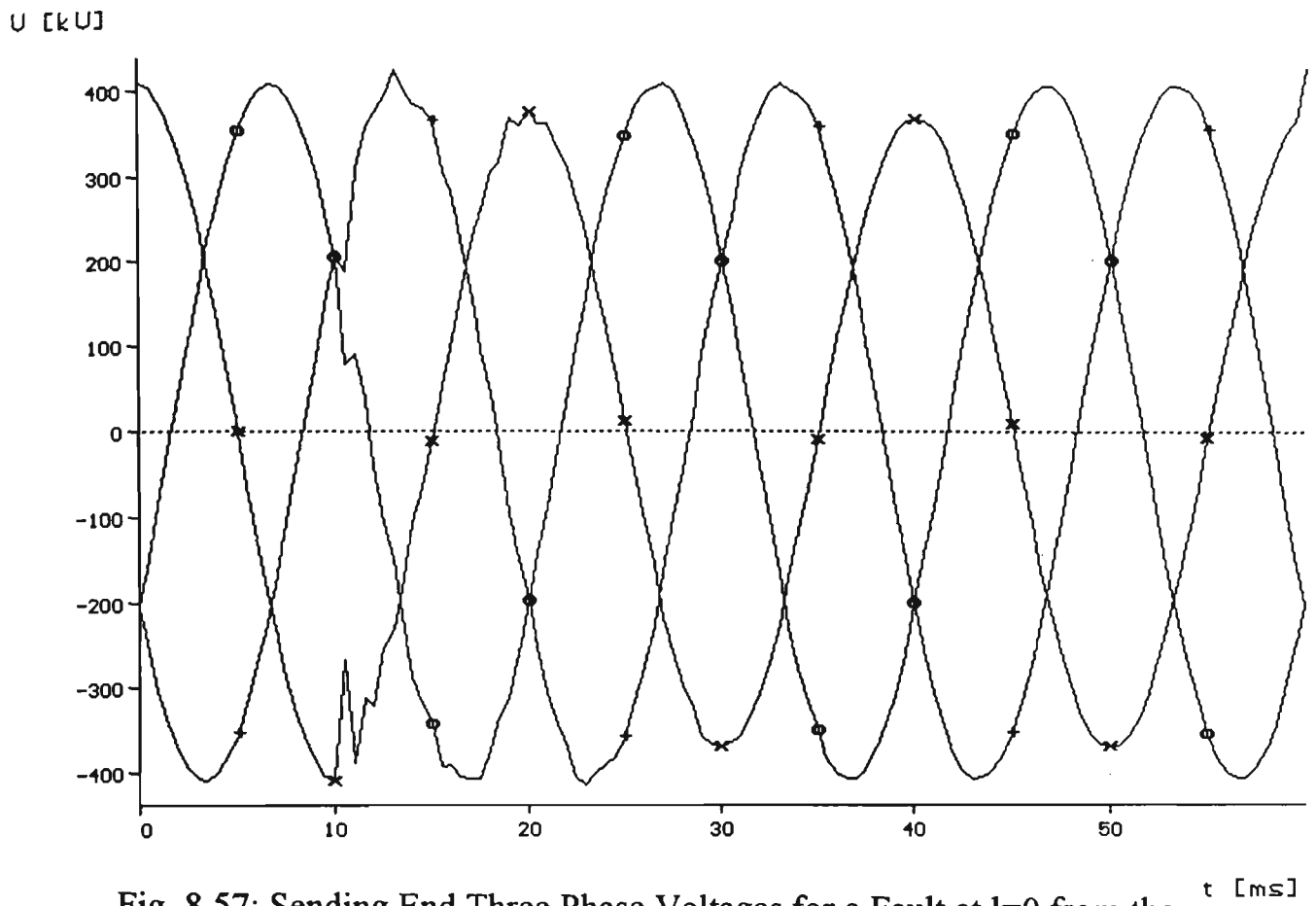


Fig. 8.57: Sending End Three Phase Voltages for a Fault at $l=0$ from the

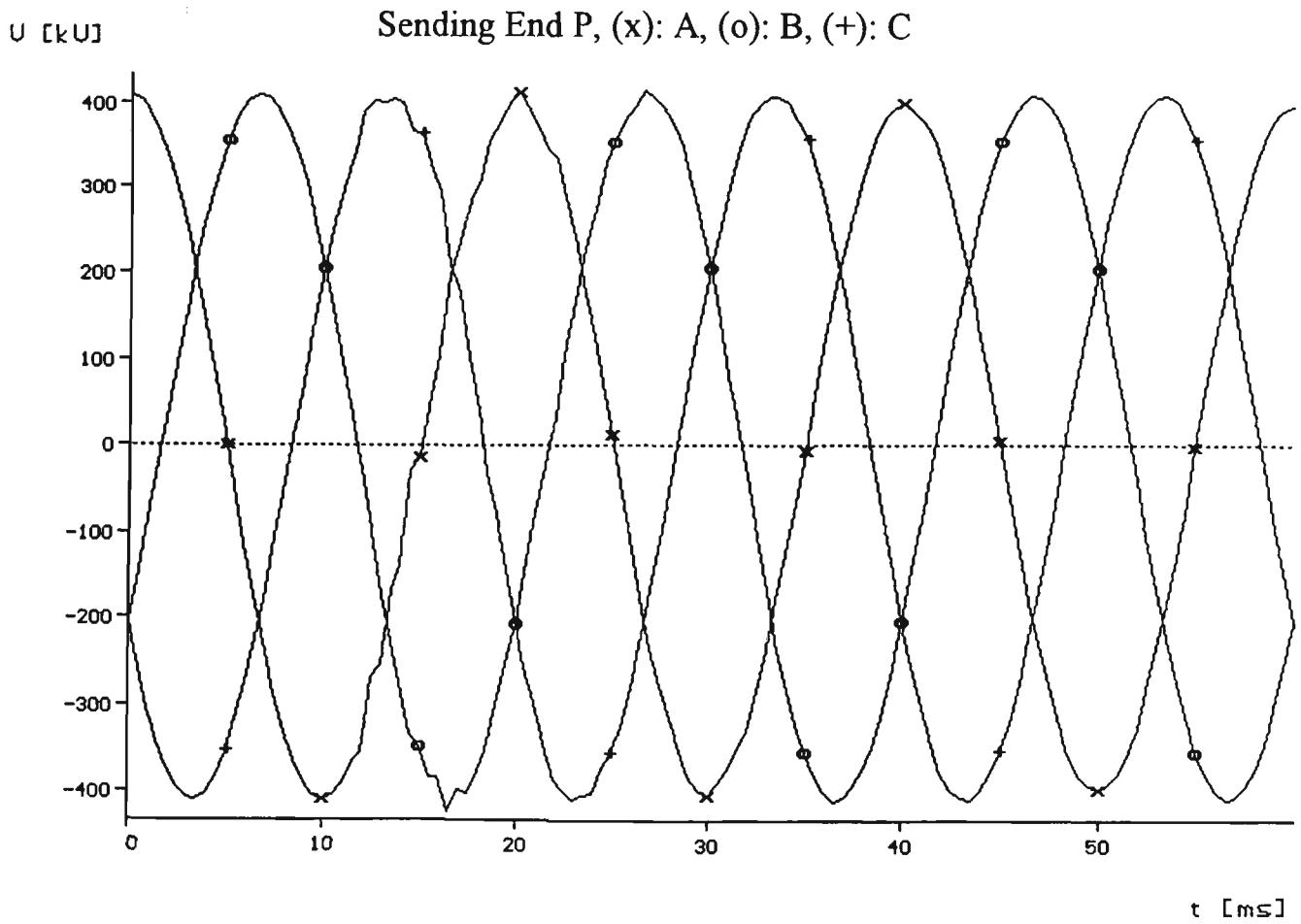


Fig. 8.58: Three Phase Receiving End Voltages, for A G Fault at $l=0$ from the
Sending End P, (x): A, (o): B, (+): C

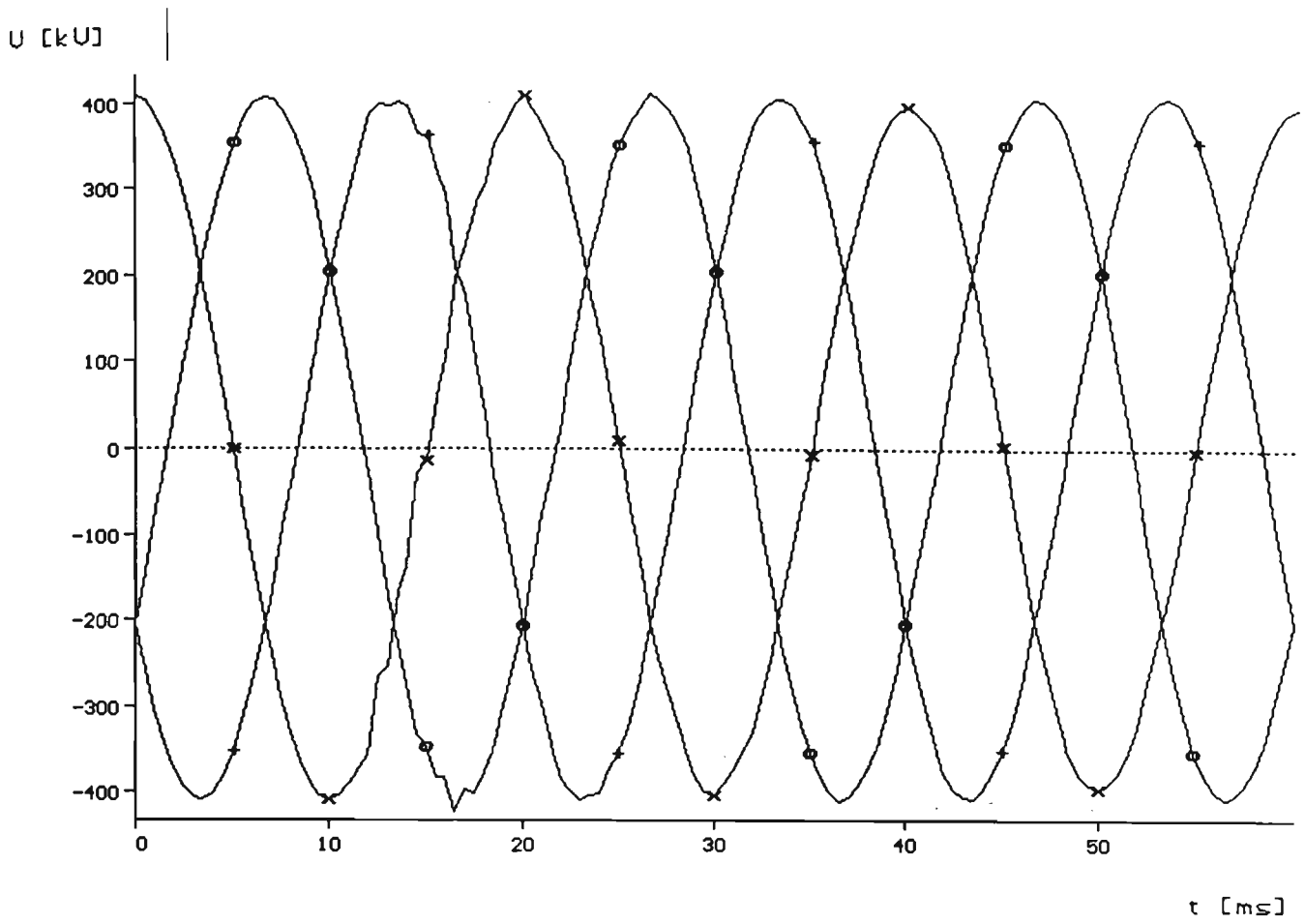


Fig. 8.59: Q End Three Phase Voltages, for A-G Fault at $l=0$ from the Sending

End P, Fault Cleared after 40 ms, (x): A, (o): B, (+): C

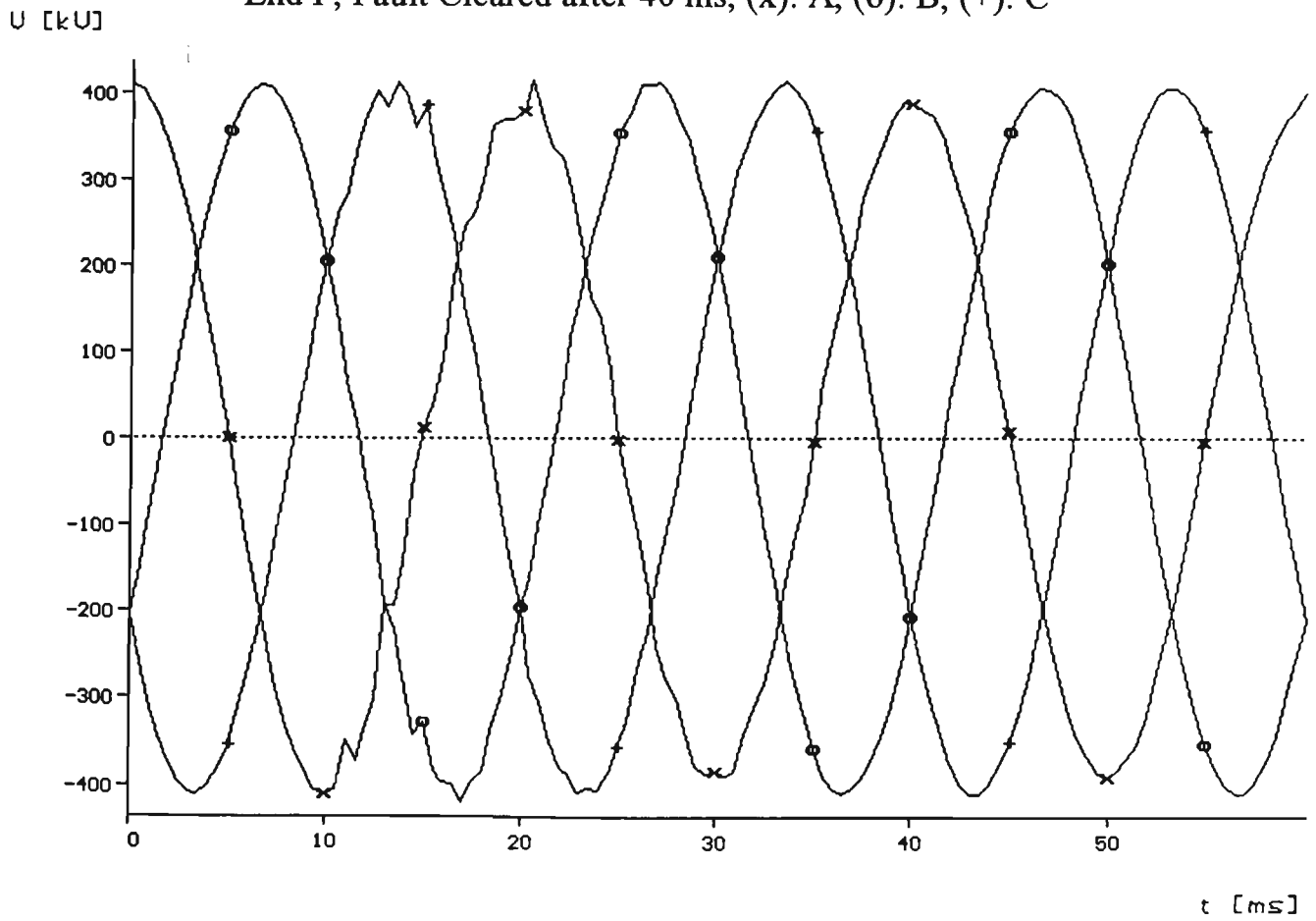


Fig. 8.60: Three Phase Sending End Voltages for A-G Fault at the Tee Point of
The Three Terminal System, (x): A, (o): B, (+): C

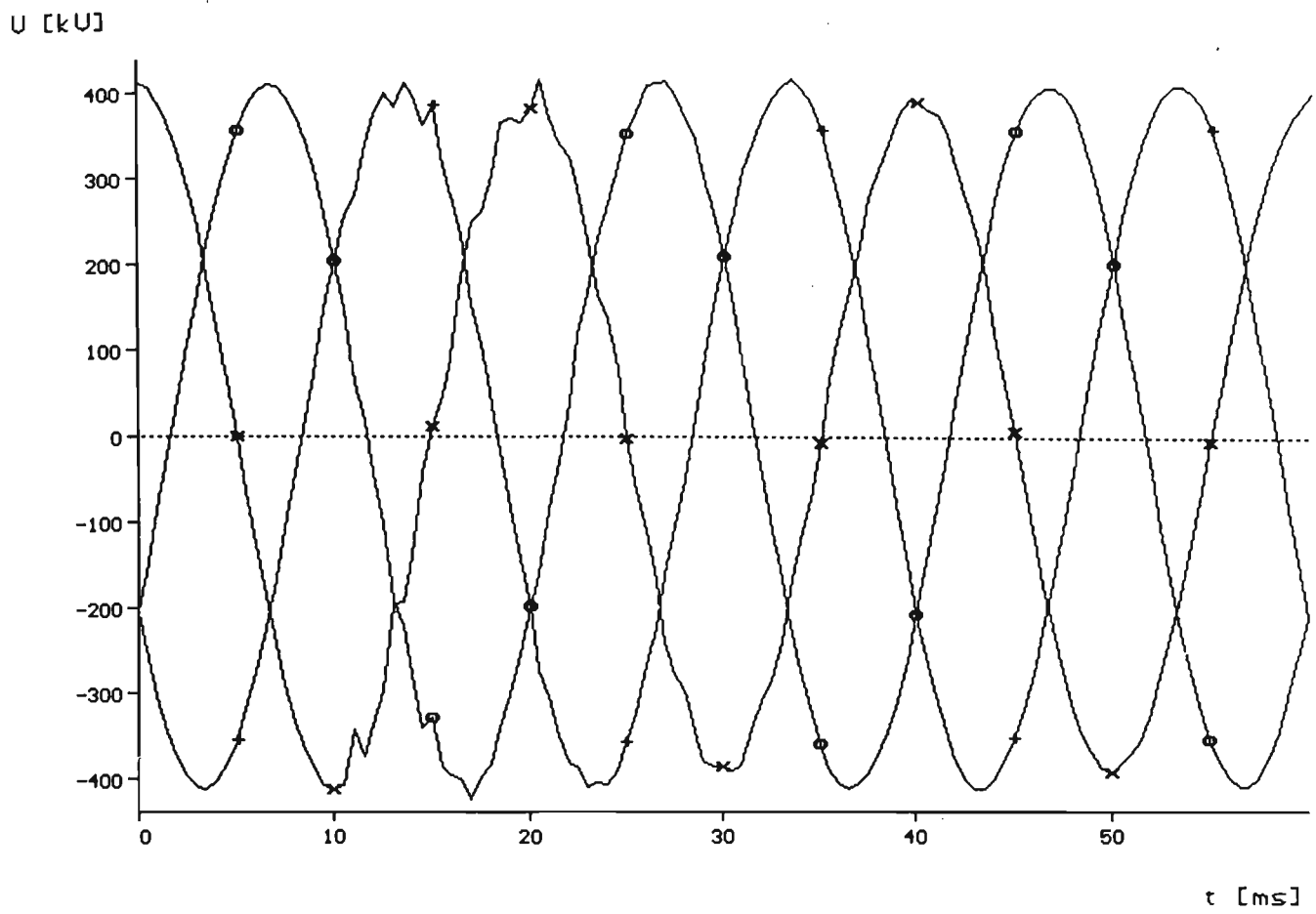


Fig. 8.61: Three Phase Receiving End Voltages for A-G Fault at $l=192$ km

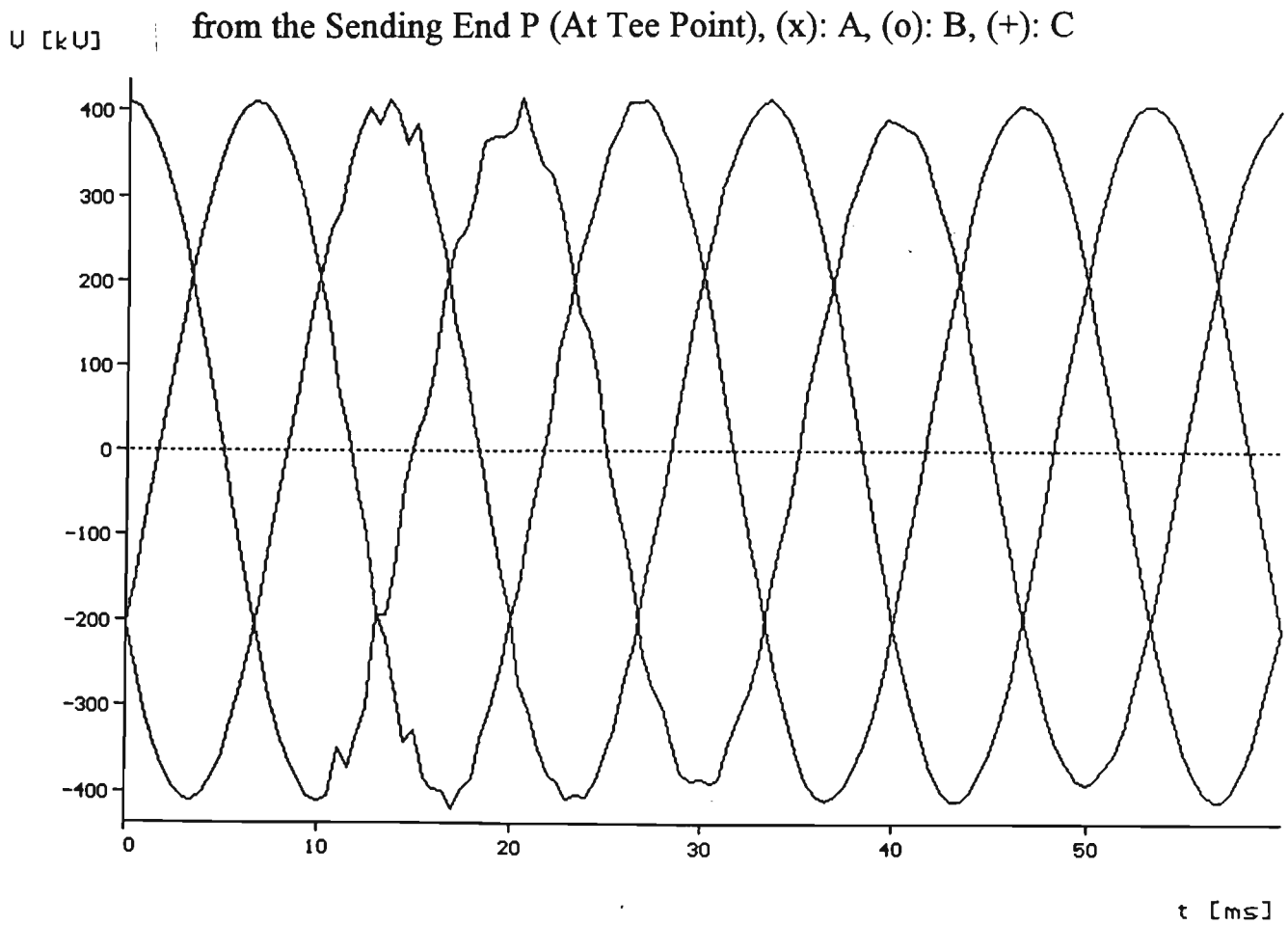


Fig. 8.62: Q End Three Phase Voltages for A-G Fault at the Tee Point, Fault
Cleared after 40 ms, (x): A, (o): B, (+): C

I [kA]

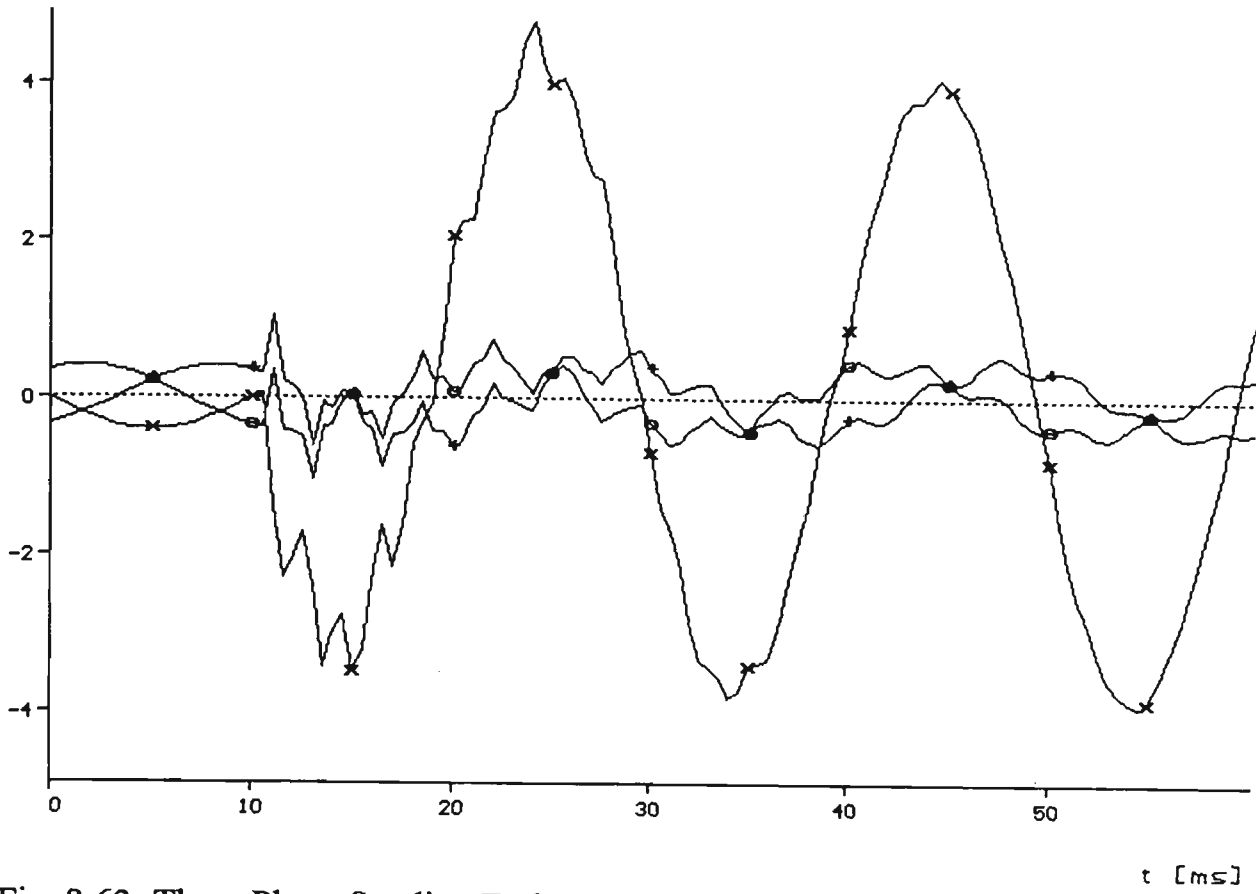


Fig. 8.63: Three Phase Sending End Currents for A-G Fault at the Tee Point
($l=192$ km), Fault Cleared after 40 ms, (x): A, (o): B, (+): C

I [kA]

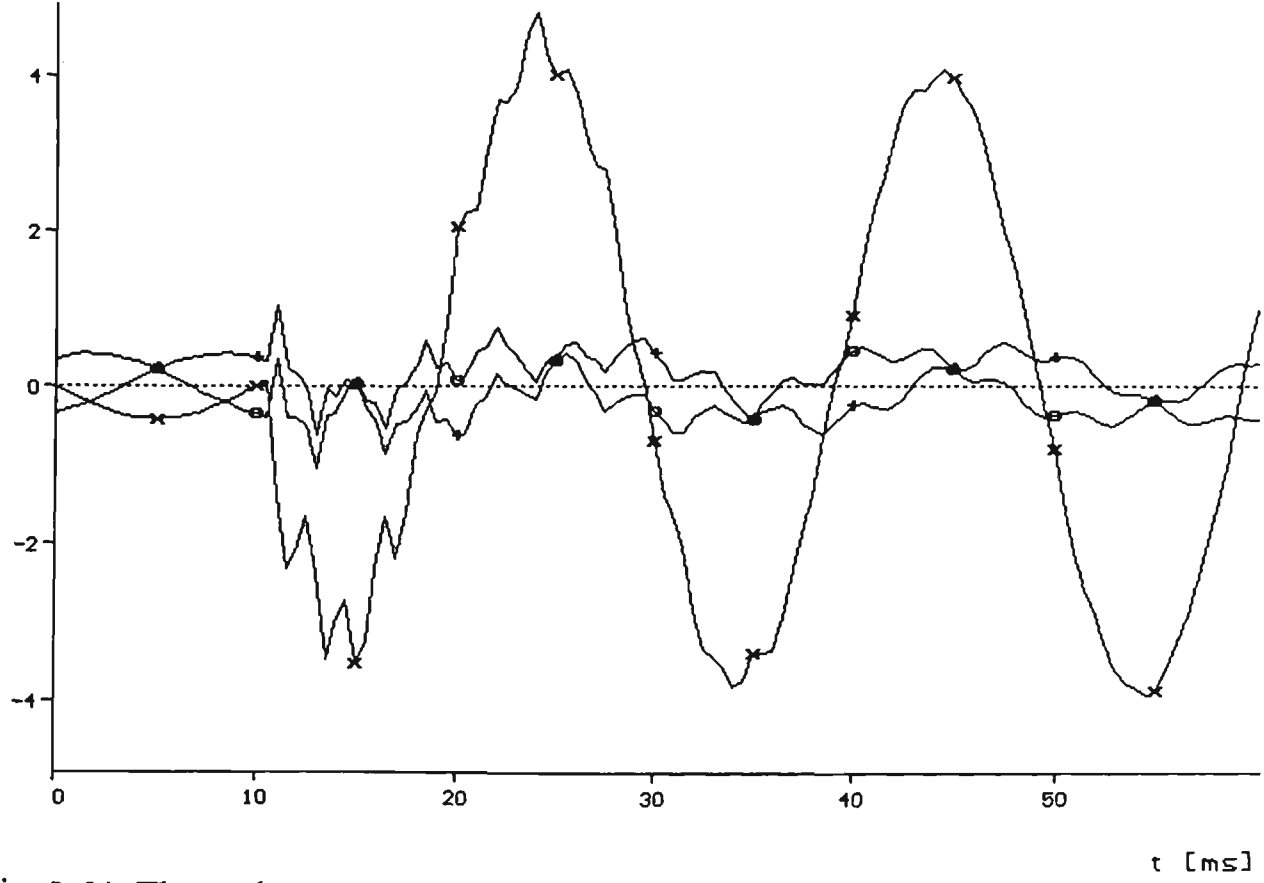


Fig. 8.64: Three Phase Receiving End Currents for A-G Fault at $l=192$ km (At
The Tee point), Fault Cleared after 40 ms, (x): A, (o): B, (+): C

I [kA]

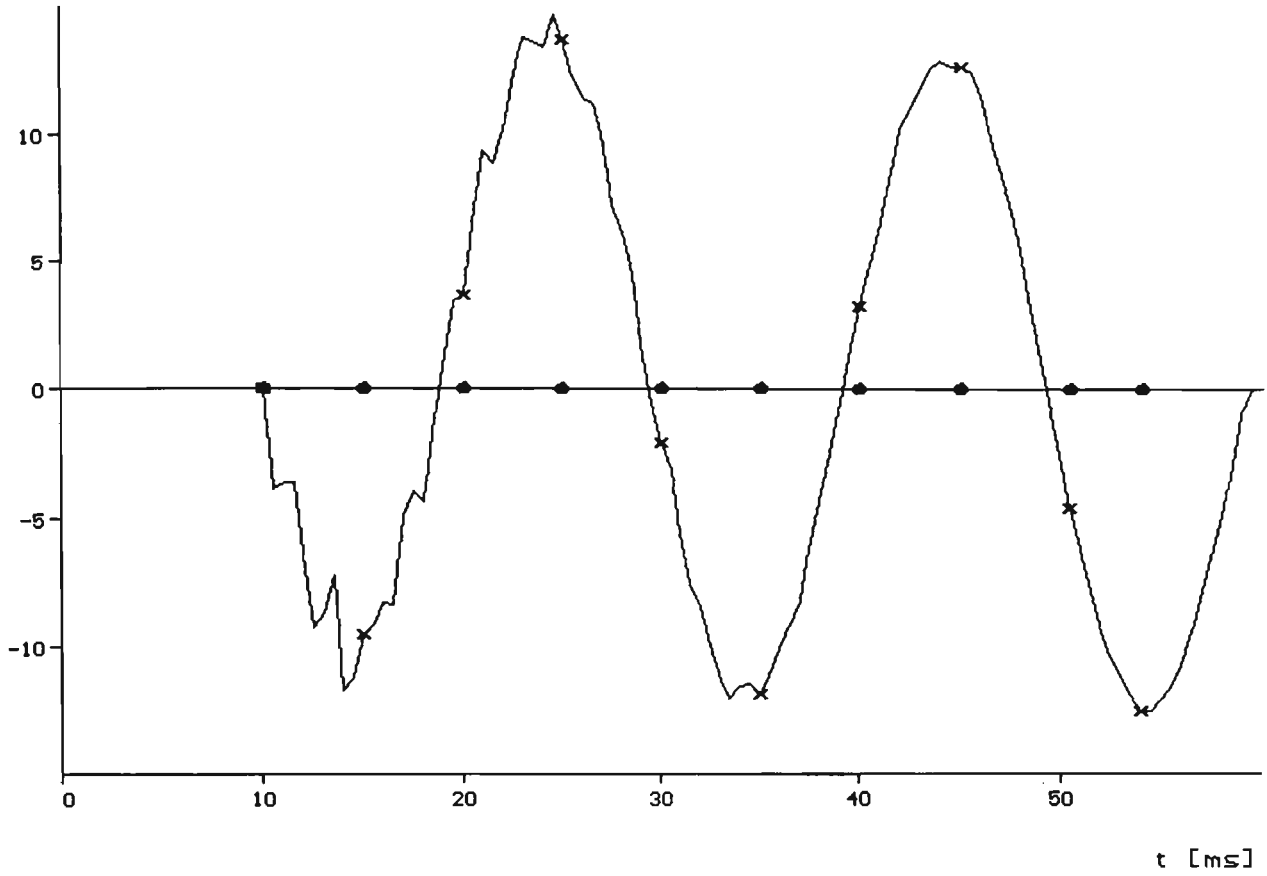


Fig. 8.65: Current Through the Faulty Path, for A-G Fault at $l=192$ km, Fault

Cleared after 40 ms.

I [kA]

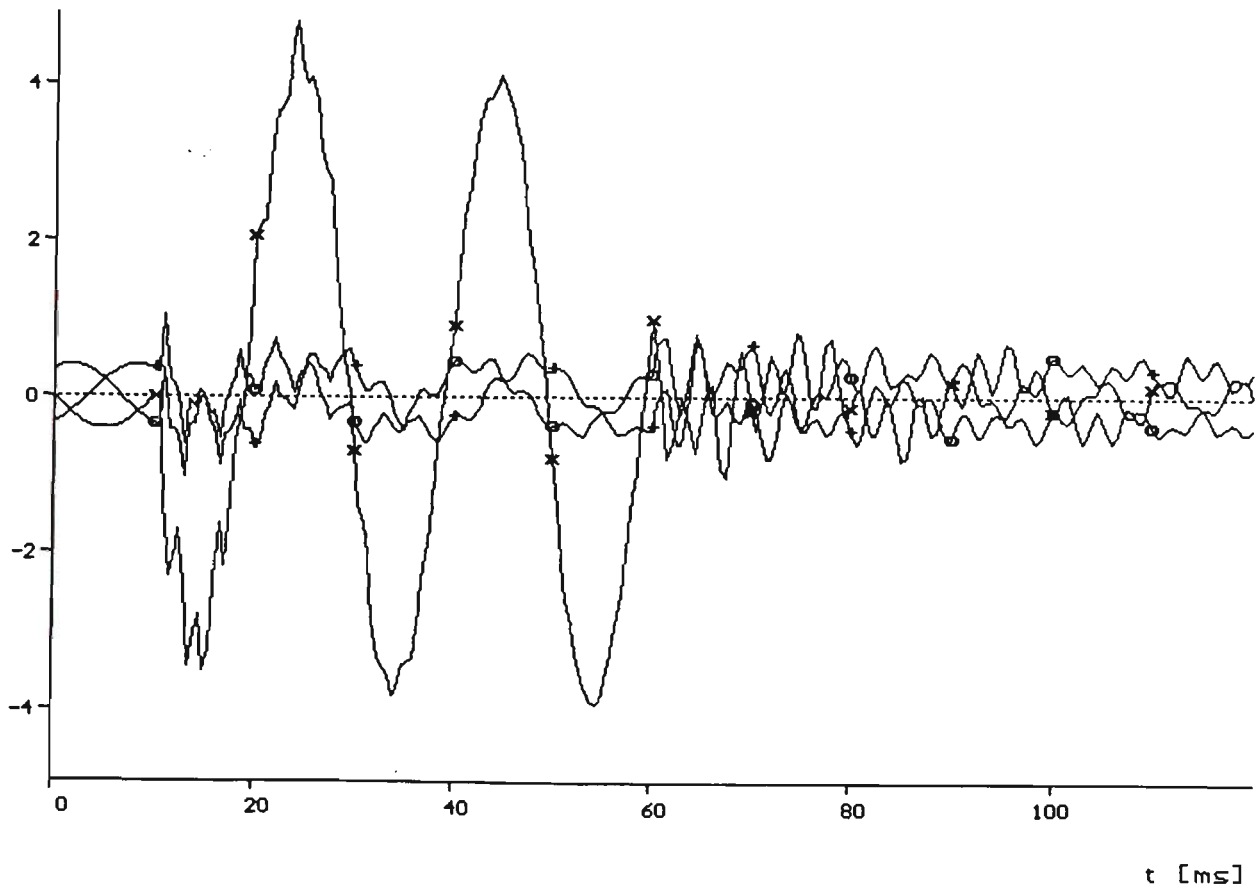


Fig. 8.66: Three Phase Sending End Currents for A-G Fault at $l=192$ km, Fault

Cleared after 40 ms, (x): A, (o): B, (+): C

the system under phase A to ground fault indicates that the noise on healthy phases and the faulty phase remain after clearing the fault for over 30 ms, which is shown in Fig.8.66.

8.3.3 Double Phase to Ground Faults

In case of a double phase to ground fault (AB-G), the voltages of the A and B phases was forced to collapse to zero, whereas, the third phase was continued as normally from the infinite source (end P), as it is shown in Fig. 8.67. The waveforms of the three phase voltages at the receiving end R and at the Q end of the tee feeder are given in Figs. 8.68 and 8.69 respectively.

The three phase waveforms of the currents at the sending end P, receiving end R, the Q end of the tee feeder and the currents through the fault path are given in Figs. 8.70, 8.71, 8.72 and 8.73 respectively.

8.3.4 Double Phase Free of Earth Faults

For double phase free of earth faults (AB) assumed at the sending end P of the three terminal system, the three phase voltages at the sending end P, receiving end R and the Q end of the tee feeder are shown in Figs. 8.74, 8.75 and 8.76 respectively. It is clearly shown that after clearing the fault, there are still some ripples superimposed on the sinusoidal waveforms.

The three phase waveforms of the currents are given at the receiving end R and the Q end of the tee feeder in Figs. 8.77 and 8.78 respectively. Since the length of each of the three feeders of the three terminal system is the same and is equal to 196 km, and since the fault at the sending end P, the contribution of

U [kV]

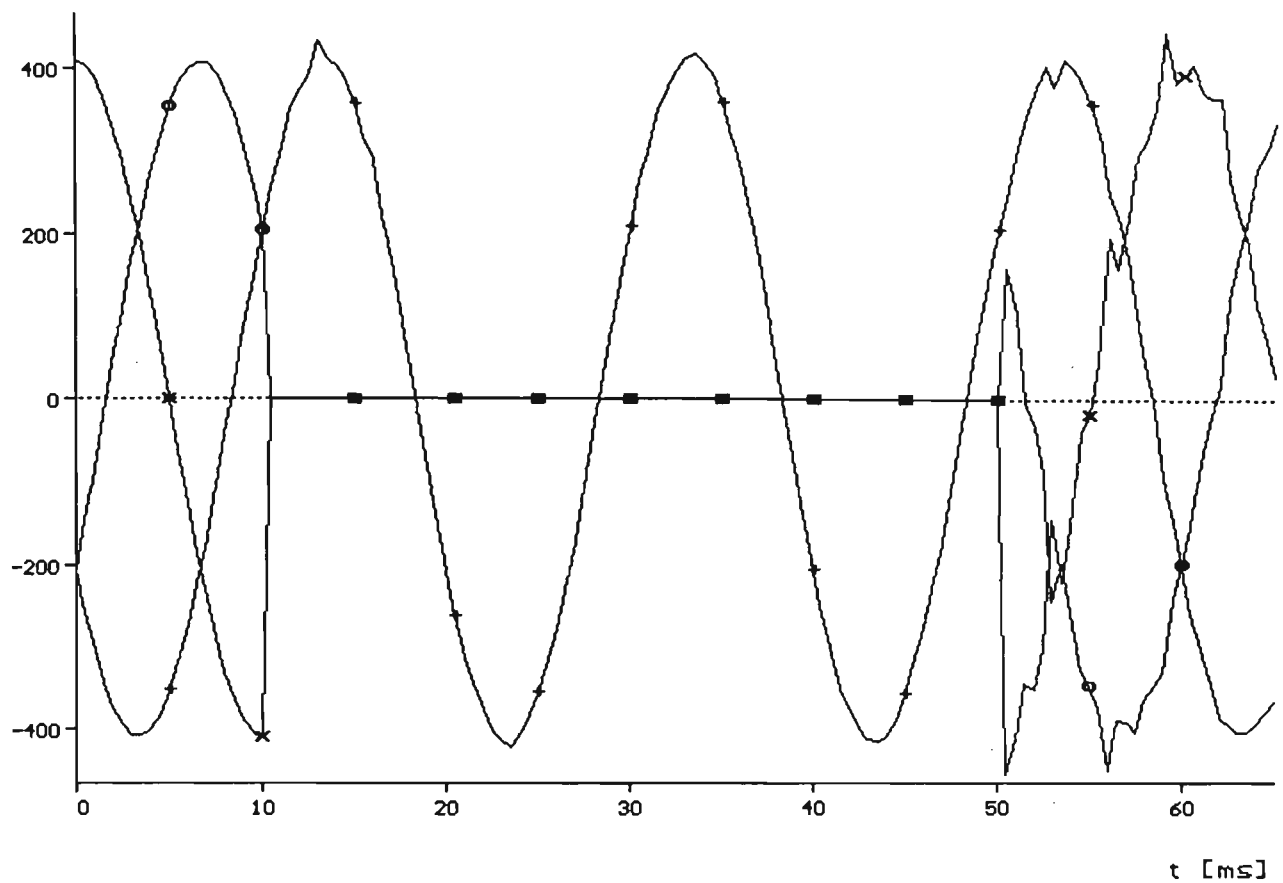


Fig. 8.67: AB-G Fault at $l=0$, Three Phase Sending End Voltages, Fault applied at $t=10$ ms and cleared at $t=50$ ms, (x): A, (o): B, (+): C

U [kV]

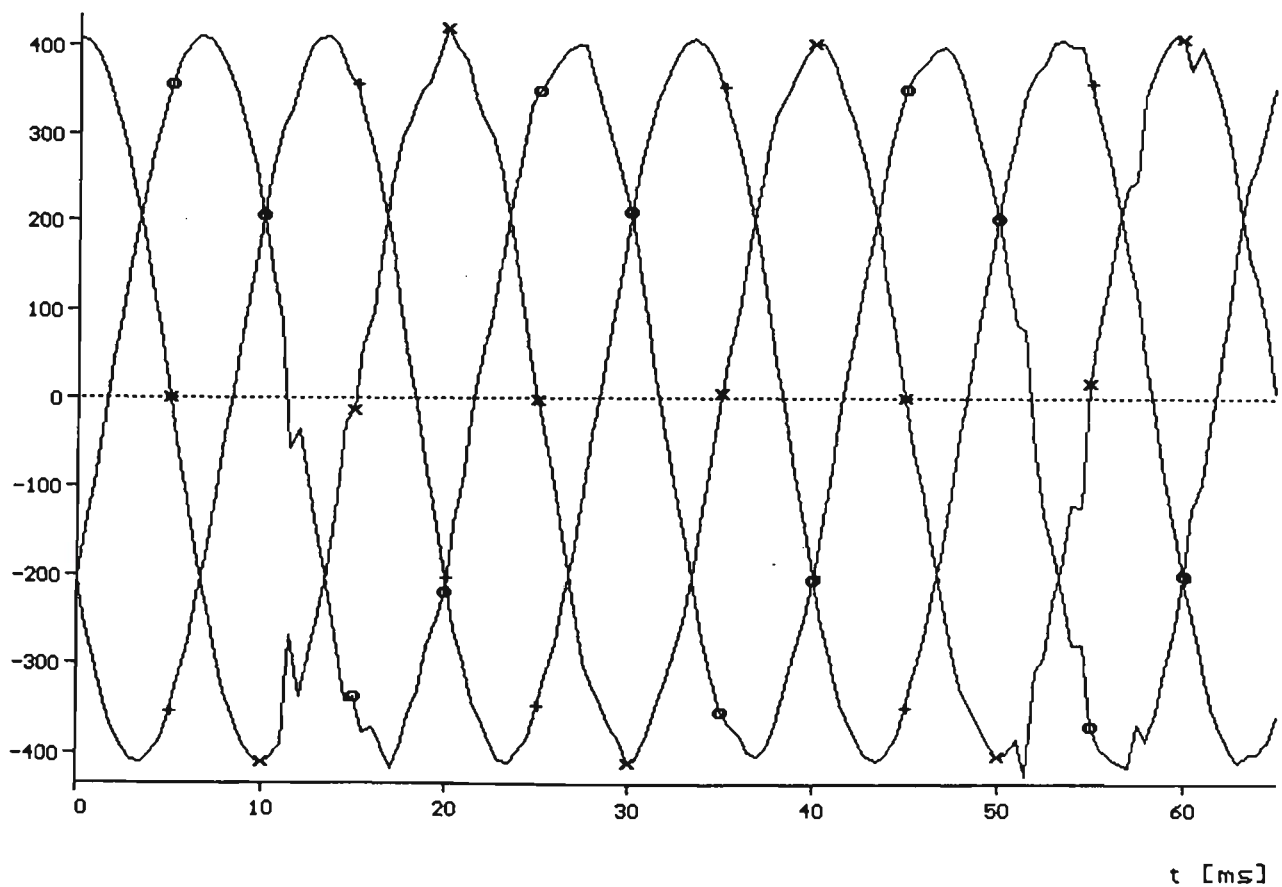


Fig. 8.68: Three Phase Receiving End Voltages for AB-G Fault at $l=0$ from P End, Fault Cleared after 40 ms, (x): A, (o): B, (+): C

U [kV]

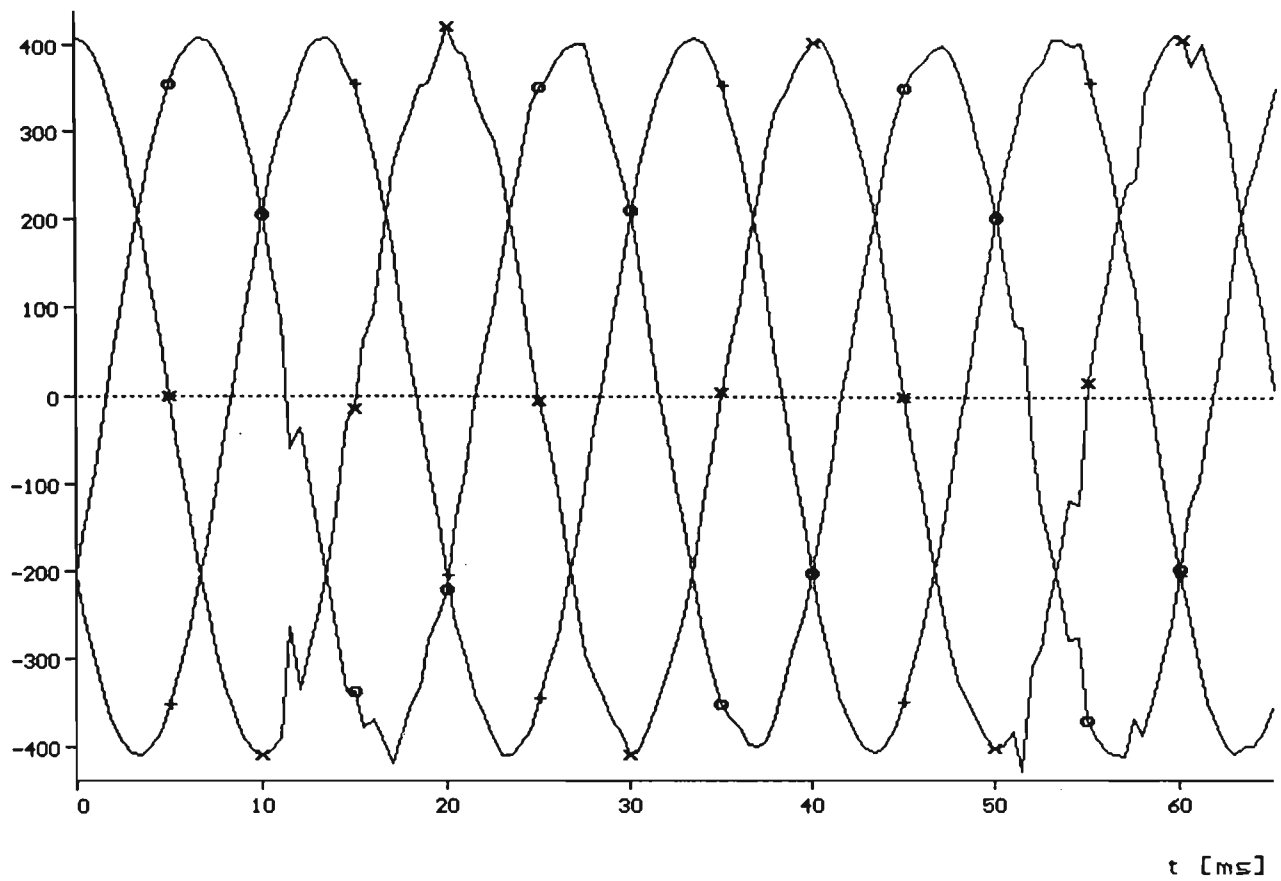


Fig. 8.69: Q End Three Phase Voltages for AB-G Fault at $l=0$ from End P,
Fault Cleared after 40 ms, (x): A, (o): B, (+): C

I [kA]

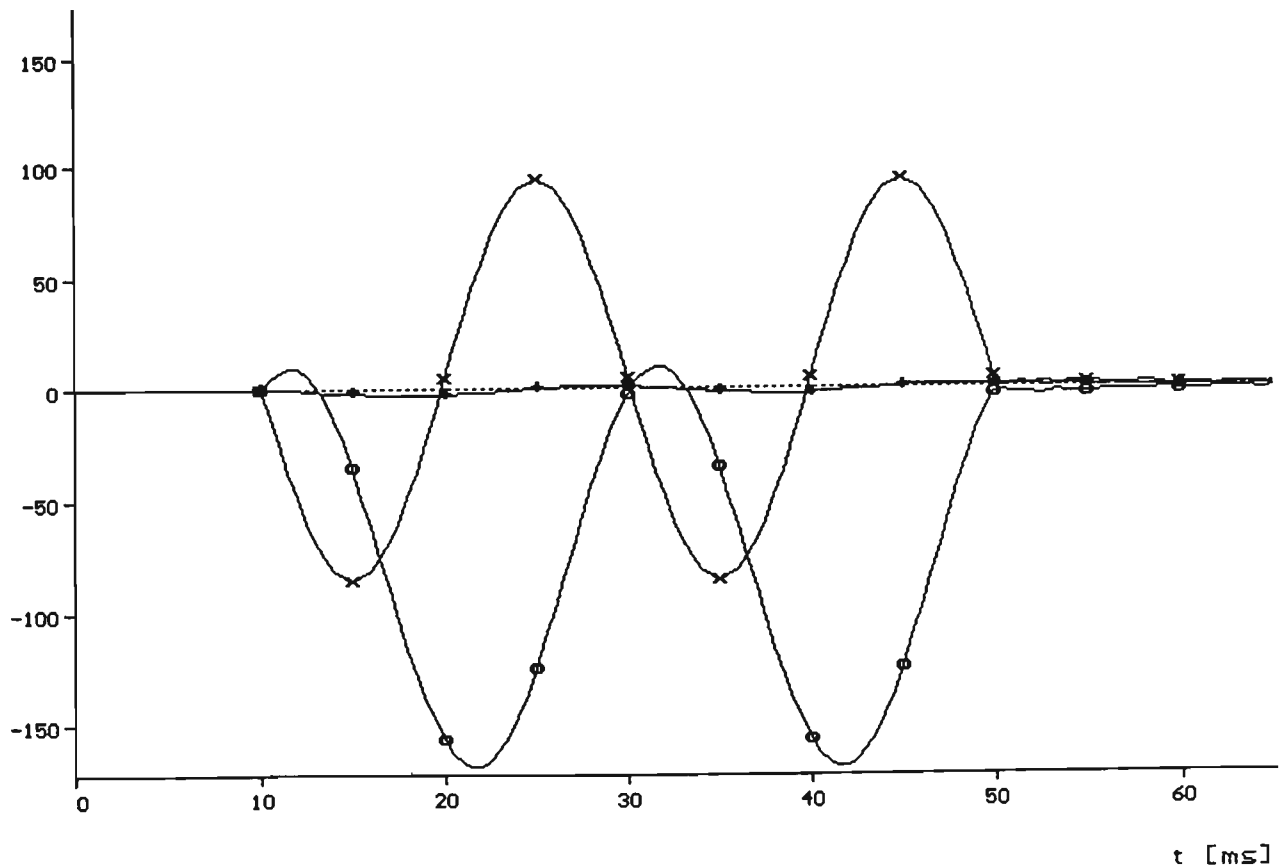


Fig. 8.70: Three Phase Currents at the Sending End for AB-G Fault at $l=0$ from
End P, Fault Cleared after 40 ms, (x): A, (o): B, (+): C

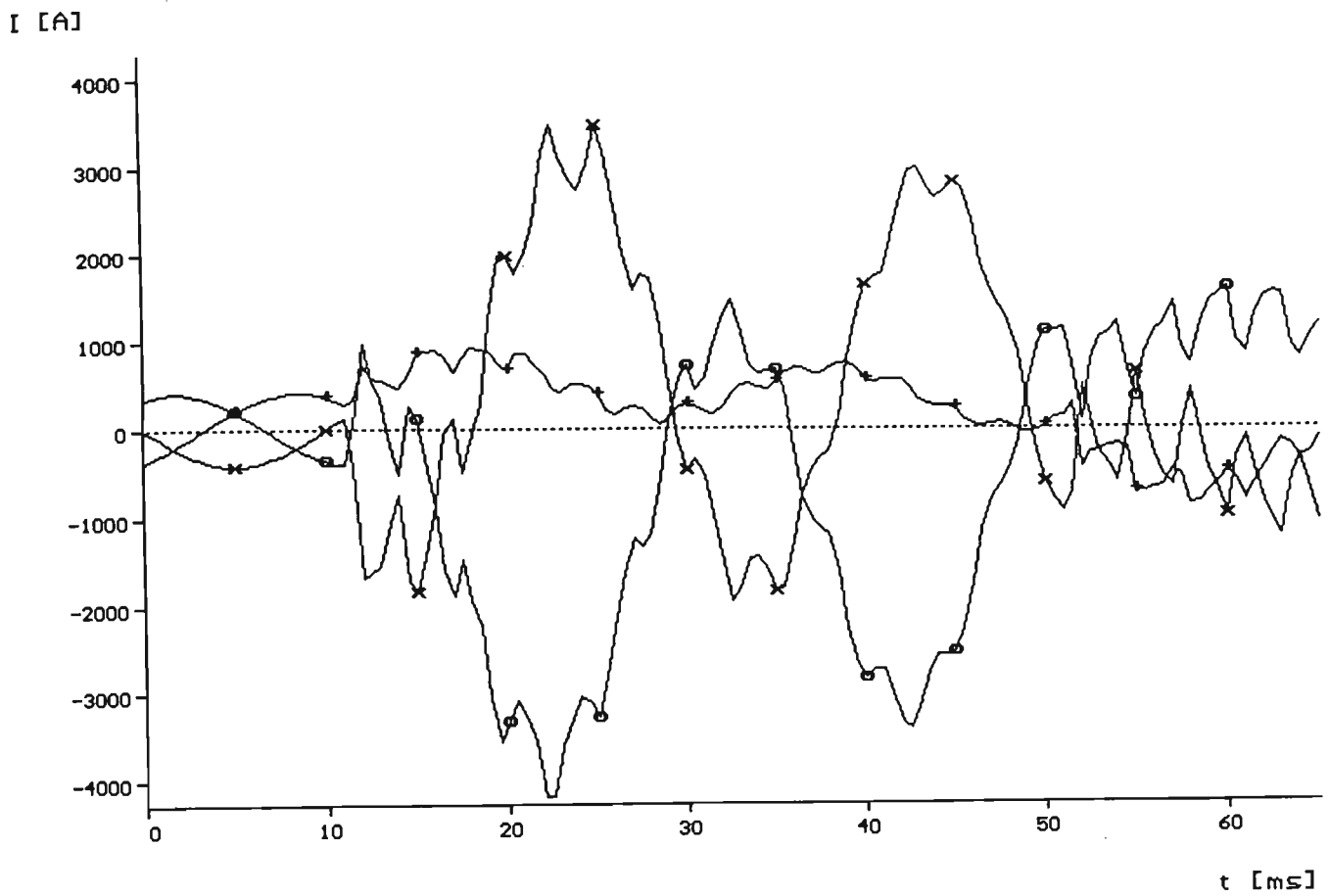


Fig. 8.71: Three Phase Receiving End Currents for AB-G Fault at $l=0$ for End

P, Fault Cleared after 40 ms, (x): A, (o): B, (+): C

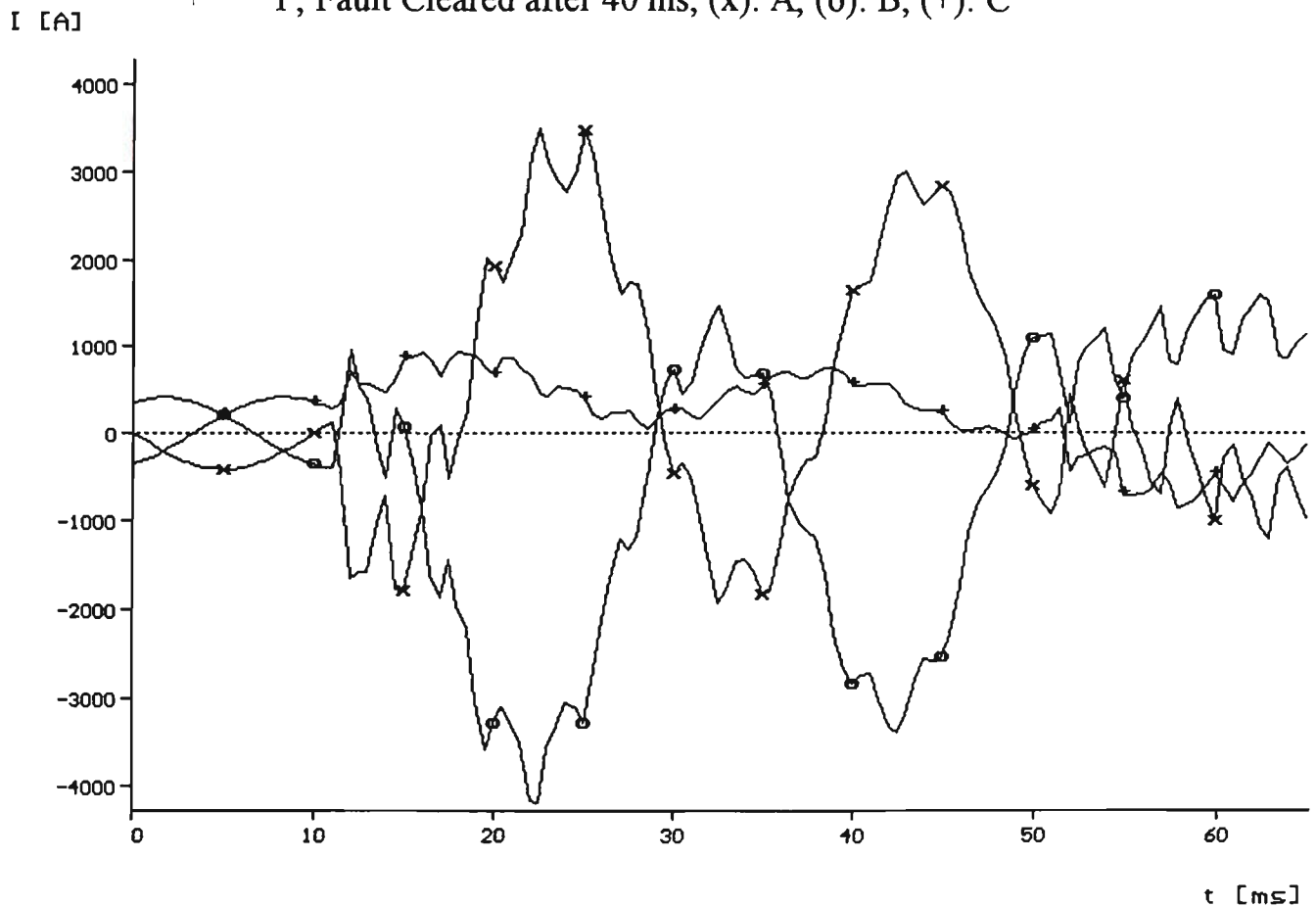


Fig. 8.72: Three Phase Currents at the Q End of the Three Terminal feeder, for AB-G Fault at $l=0$ from end P, (x): A, (o): B, (+): C

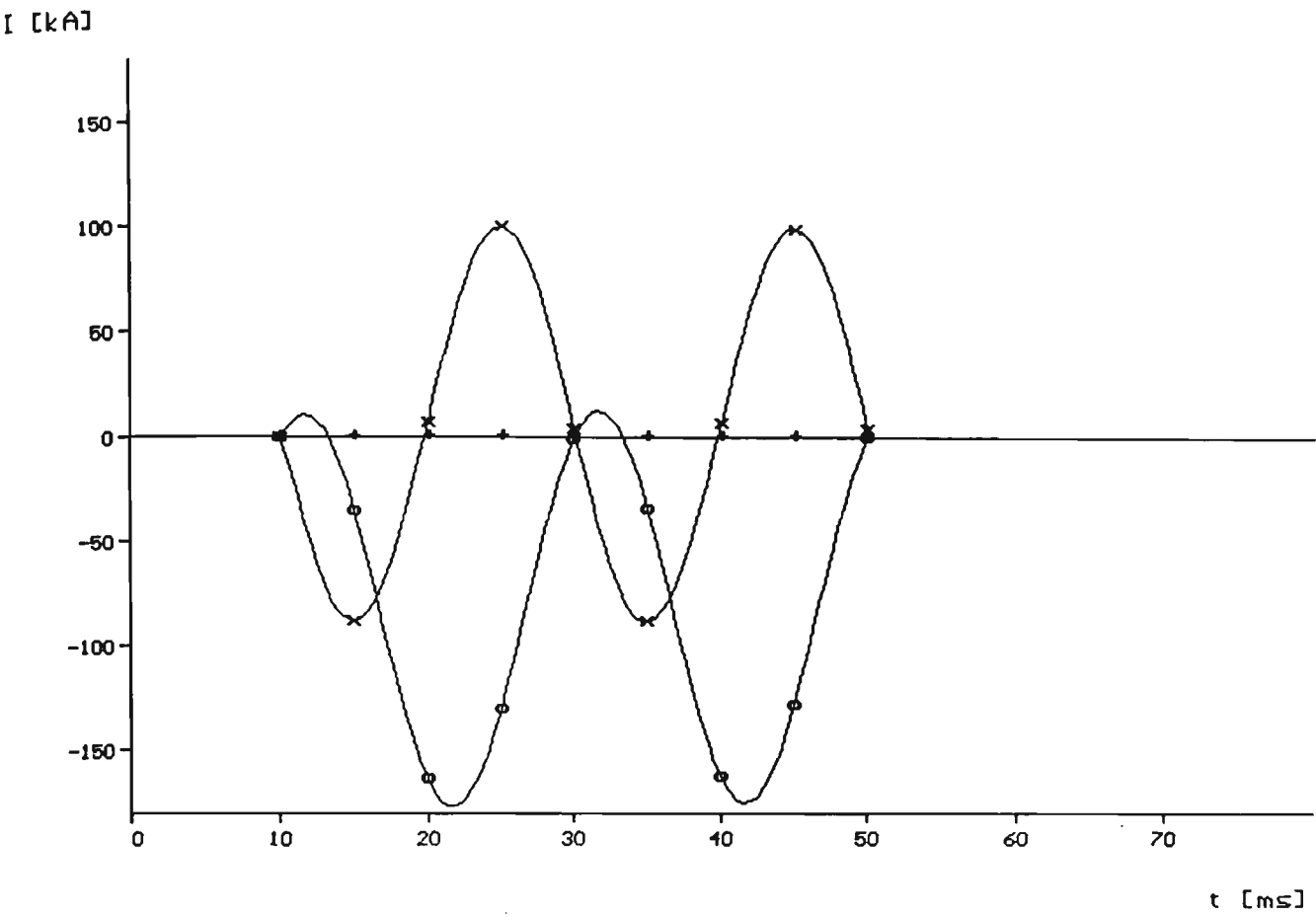


Fig. 8.73: Fault Currents Through the Fault at $l=0$ from End P, Fault Cleared after 40 ms, (x): A, (o): B, (+): C, AB-G Fault

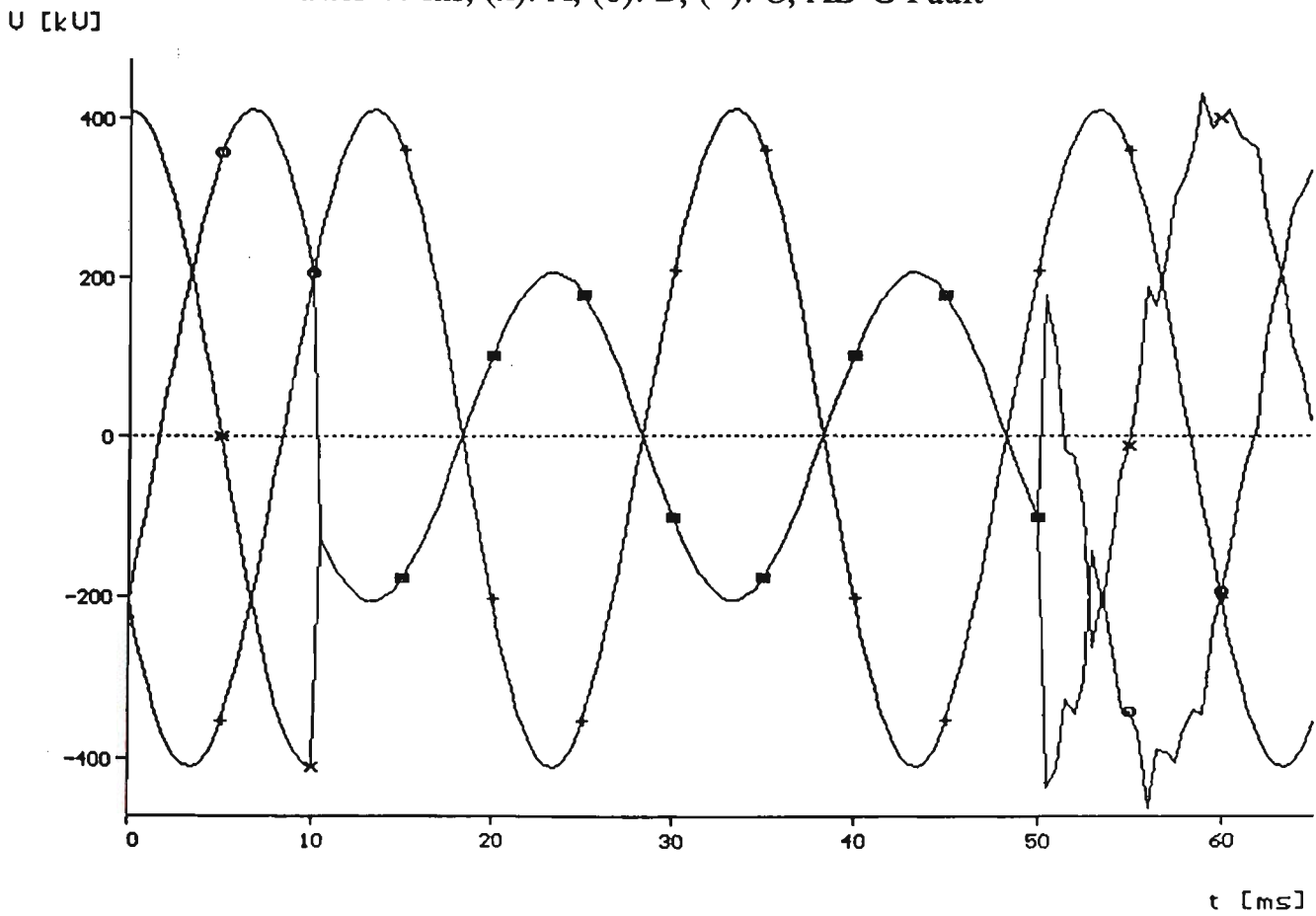


Fig. 8.74: Three Phase Sending End Voltages, AB Fault at $l=0$ from End P, Fault Cleared after 40 ms, (x): A, (o): B, (+): C

U [kU]

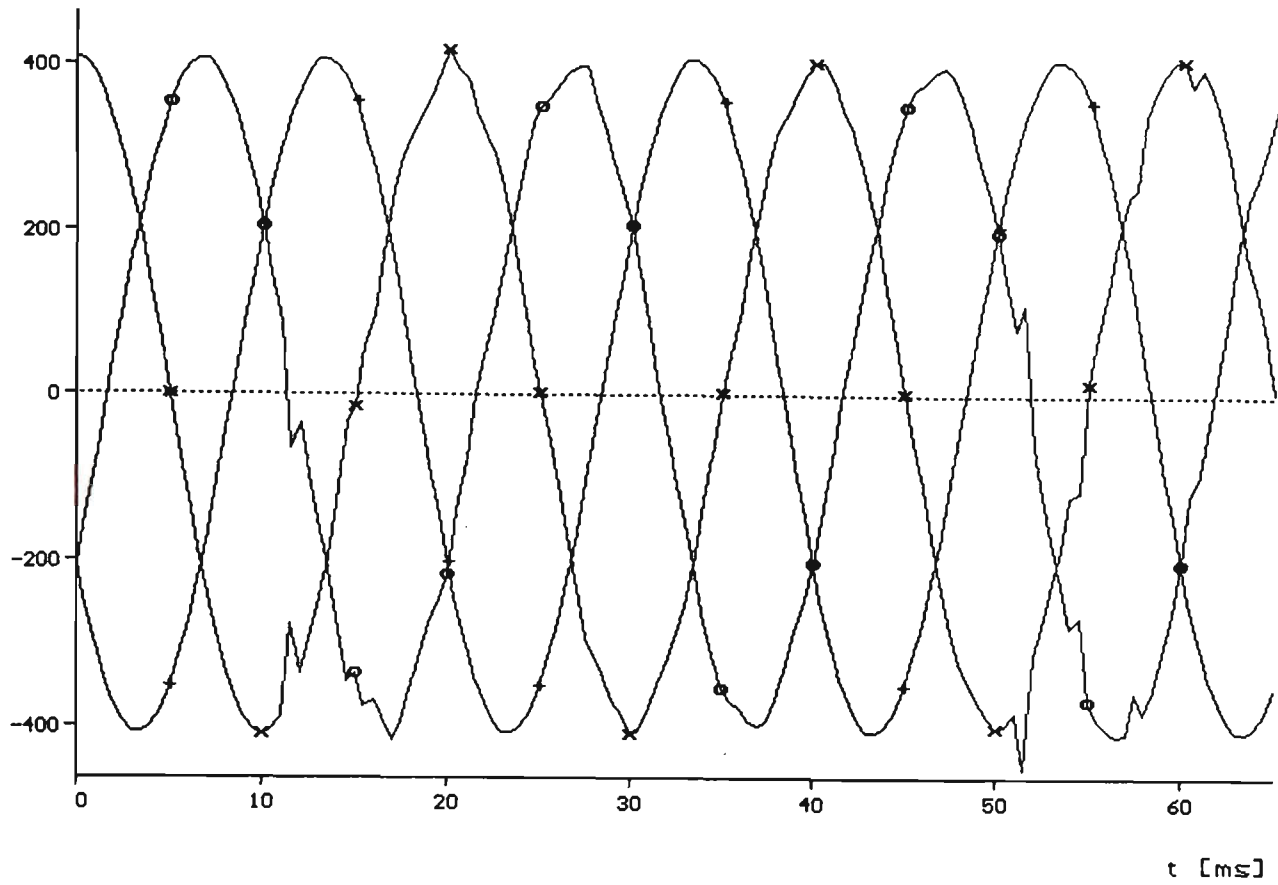


Fig. 8.75: Three Phase Receiving End Voltages for AB fault at $l=0$ from End P, Fault Cleared after 40 ms, (x): A, (o): B, (+): C

U [kU]

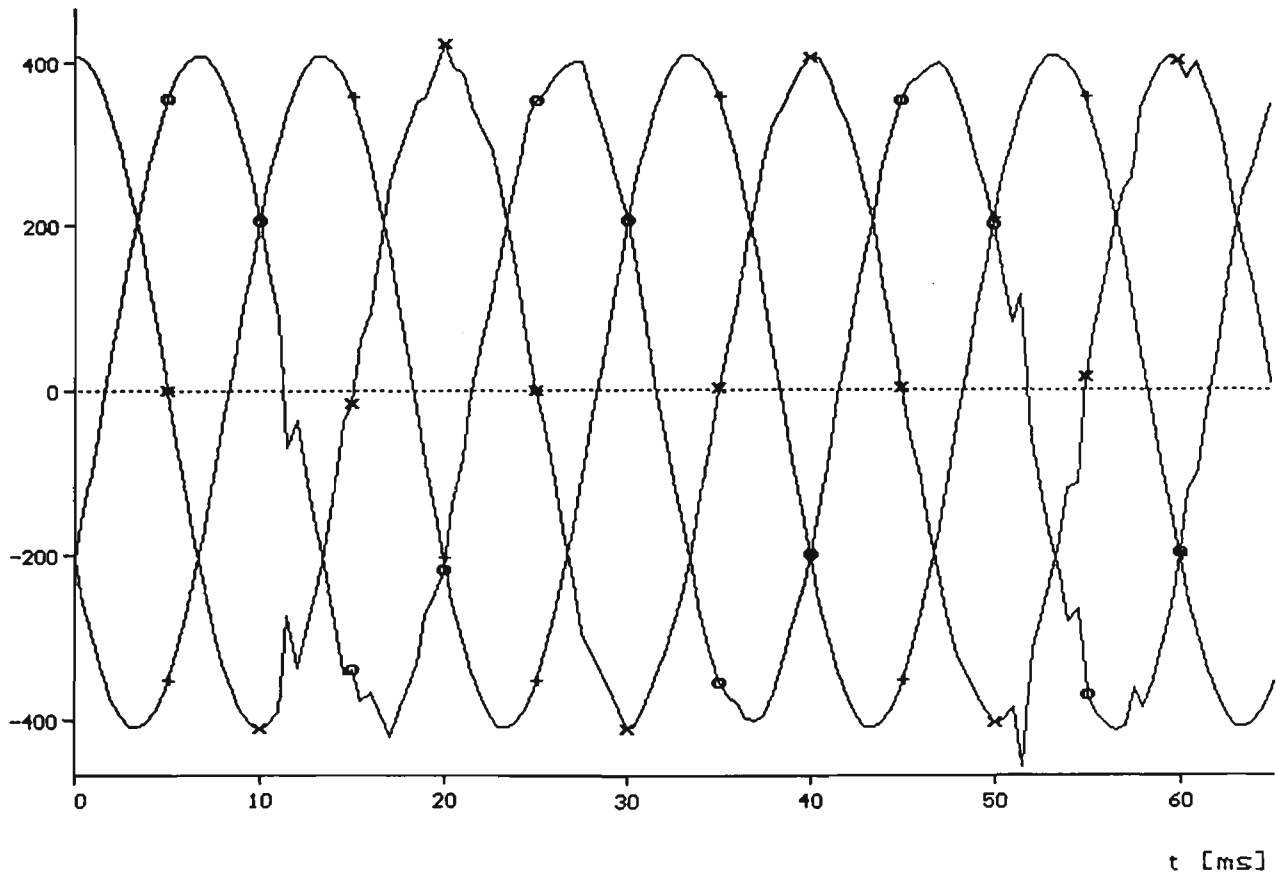


Fig. 8.76: Q End Three Phase Voltages for AB Fault At $l=0$ from End P, Fault Cleared after 40 ms, (x): A, (o): B, (+): C

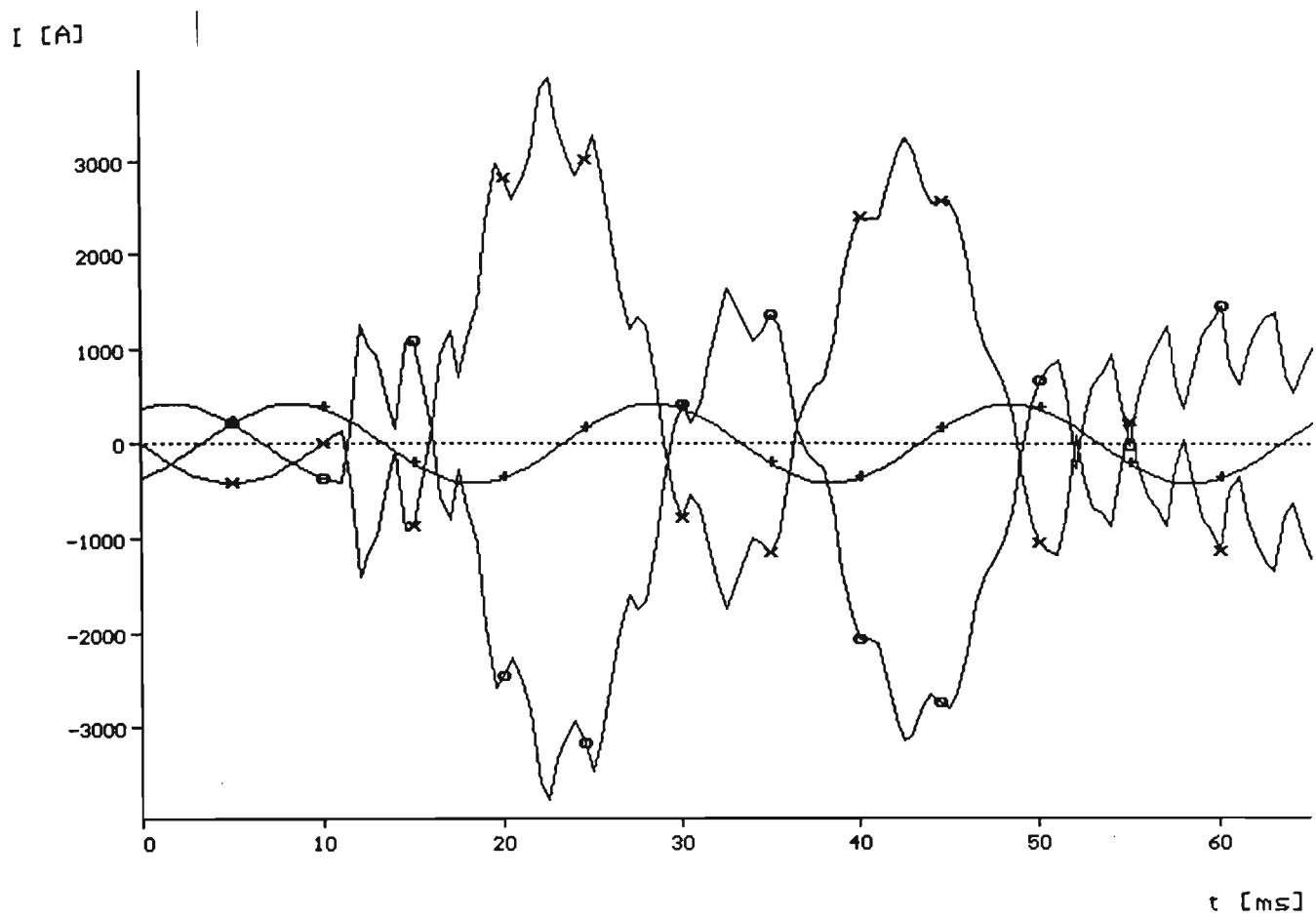


Fig. 77: Three Phase Receiving End Currents for AB fault at $l=0$ from End P,
 Fault Cleared after 40 ms, (x): A, (o): B, (+): C

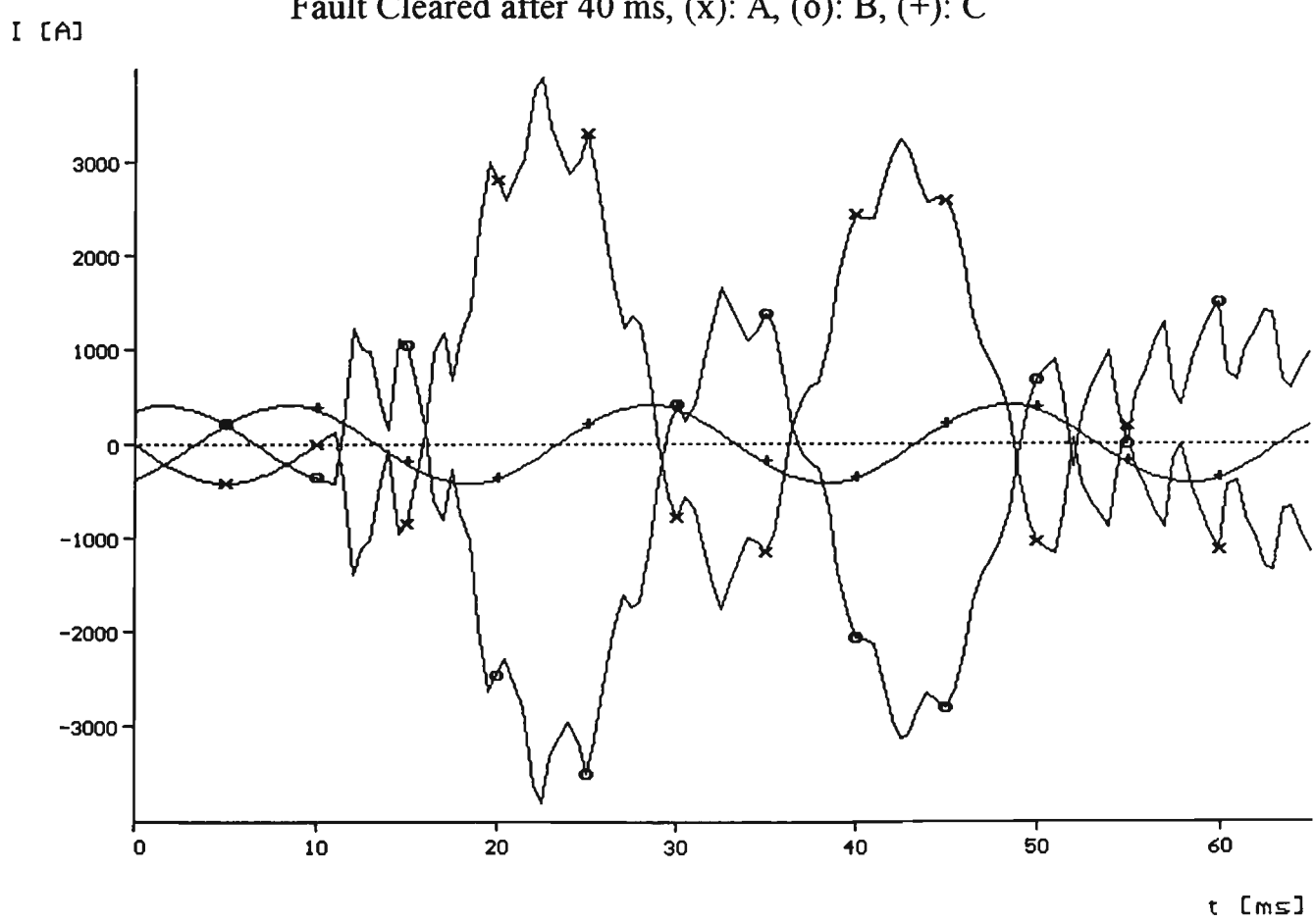


Fig. 8.78: Three Phase Q End Currents of the Three Terminal Feeder for AB
 Fault Cleared after 40 ms, (x): A, (o): B, (+): C

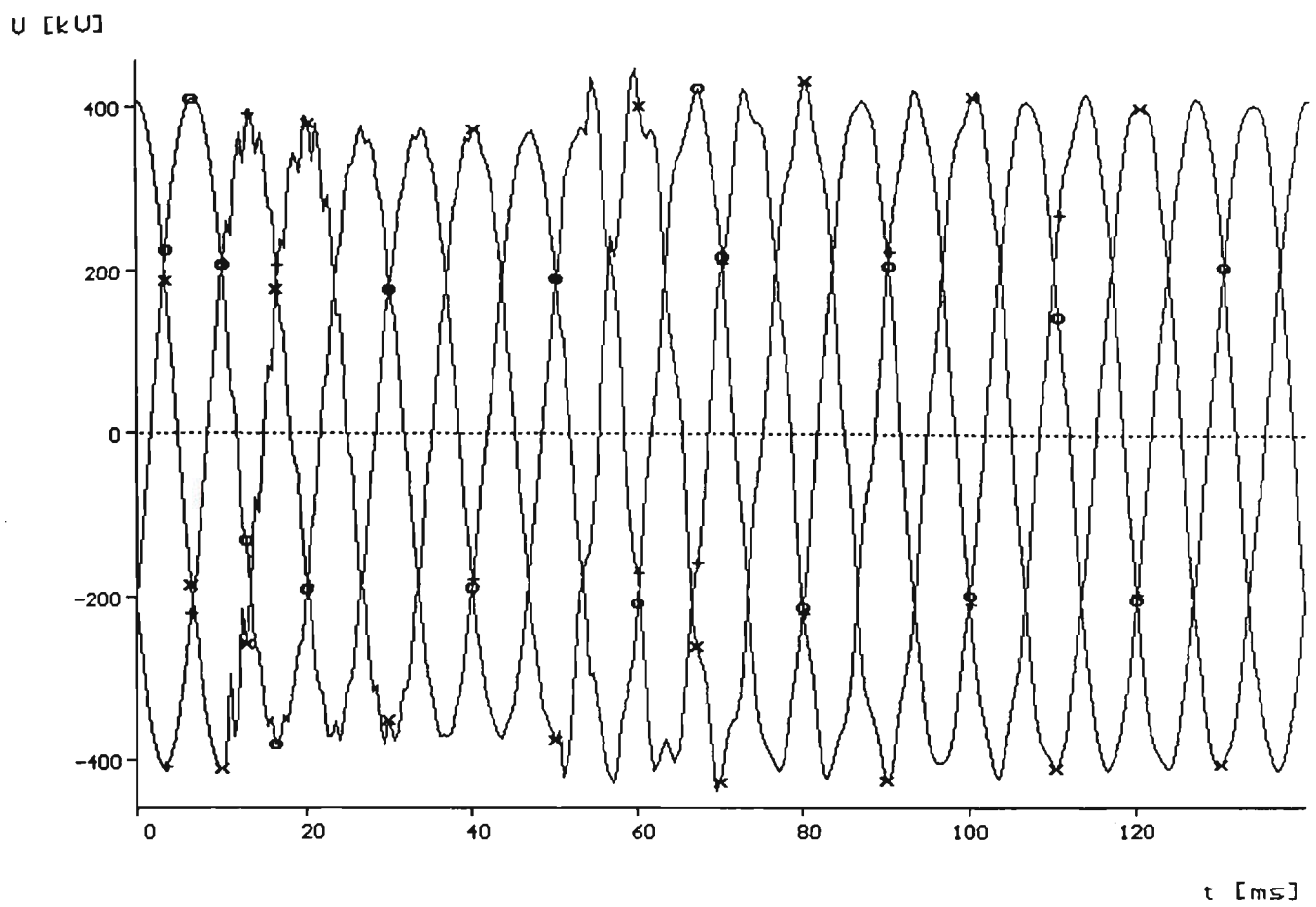


Fig. 8.79: Sending End Three Phase Voltage for a Three Phase -G Fault at $l=192$ km from End P (Tee Point) (x): A, (o): B, (+): C

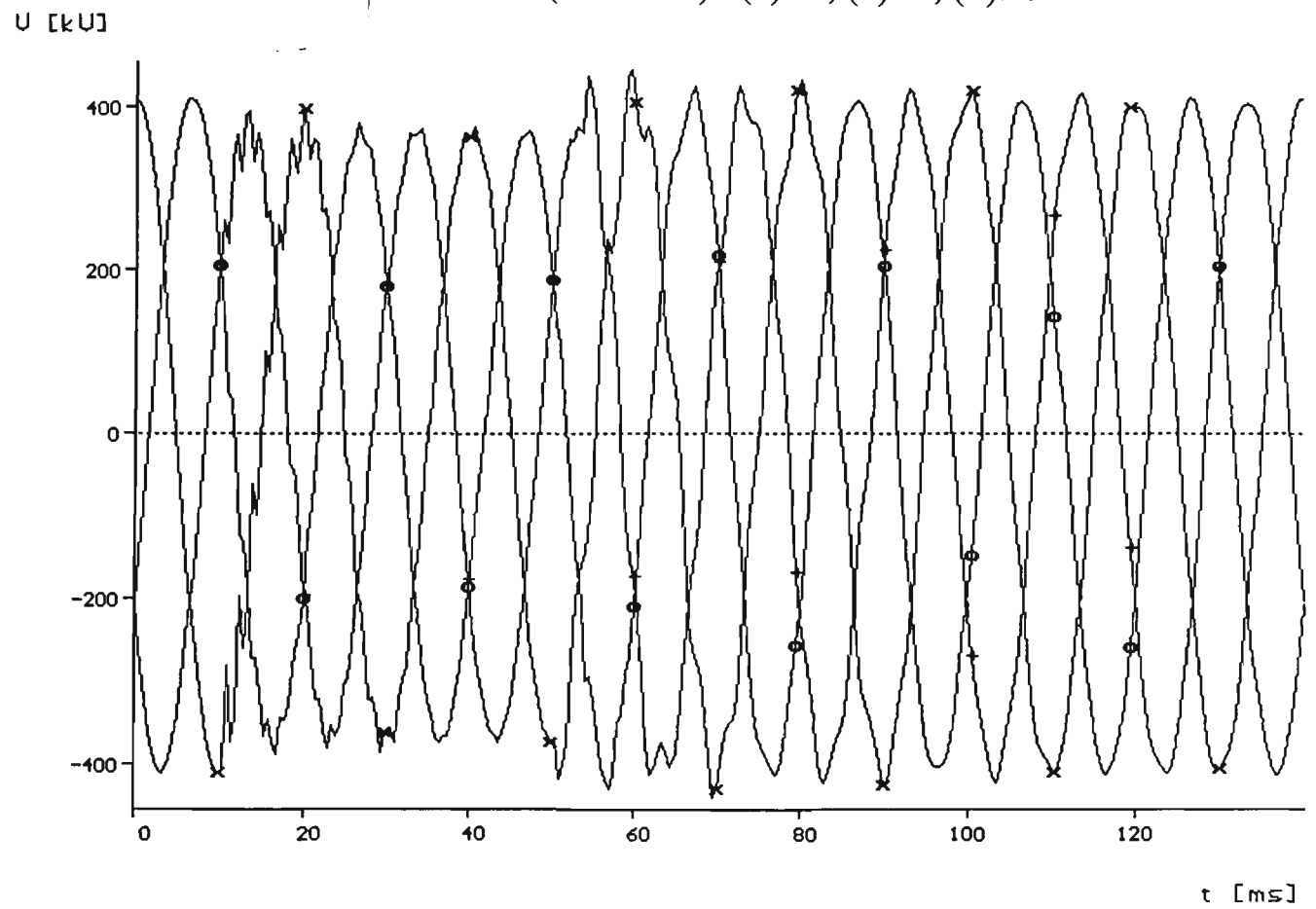


Fig. 8.80: Three Phase Receiving End Voltages for Three Phase -G Fault at the Tee Point of the Three Terminals, (x): A, (o): B, (+): C

the other sources (R and Q), which were all assumed equal in strength (35 GVA), the waveforms of both R and Q ends, as expected, are almost identical.

8.3.5 Three Phase faults

For a three phase to ground fault at the tee point T of the three terminal system, the contribution of each end is investigated. The waveforms of the three phase voltages at the sending end P, receiving end R and the Q end of the three terminal system are given in Figs. 8.79, 8.80 and 8.81 respectively. Since the strength of the three sources connected to the three ends of the transmission line have the same fault MVA (35 GVA each), as it was expected, the waveforms at the three ends look alike. During the fault inception, there is a similar reduction in the voltages at all three ends, as the short circuit was applied at the tee junction for a 40 ms duration. When the fault is cleared, there are some ripples on the voltage waveforms, which soon disappear after about 20 ms.

In order to study the response of the three terminals over a longer observation time, with the fault at the tee point of the system, the waveforms of the three phase currents were obtained for a 130 ms duration. During this period, the fault was applied at 10 ms, and was assumed to be cleared after 40 ms. These waveforms are shown for all three end of the transmission circuit, ie, the sending end P, the receiving end R and the Q end of the tee feeder in Figs. 8.82, 8.83 and 8.84 respectively. The three phase currents decay exponentially during the fault, and after removing the fault, a significant disturbance of phase currents continues for a considerable time. As for the voltage waveforms, the response for the three phase currents at all three ends of the tee feeder are similar for the same reasons stated earlier.

U [kV]

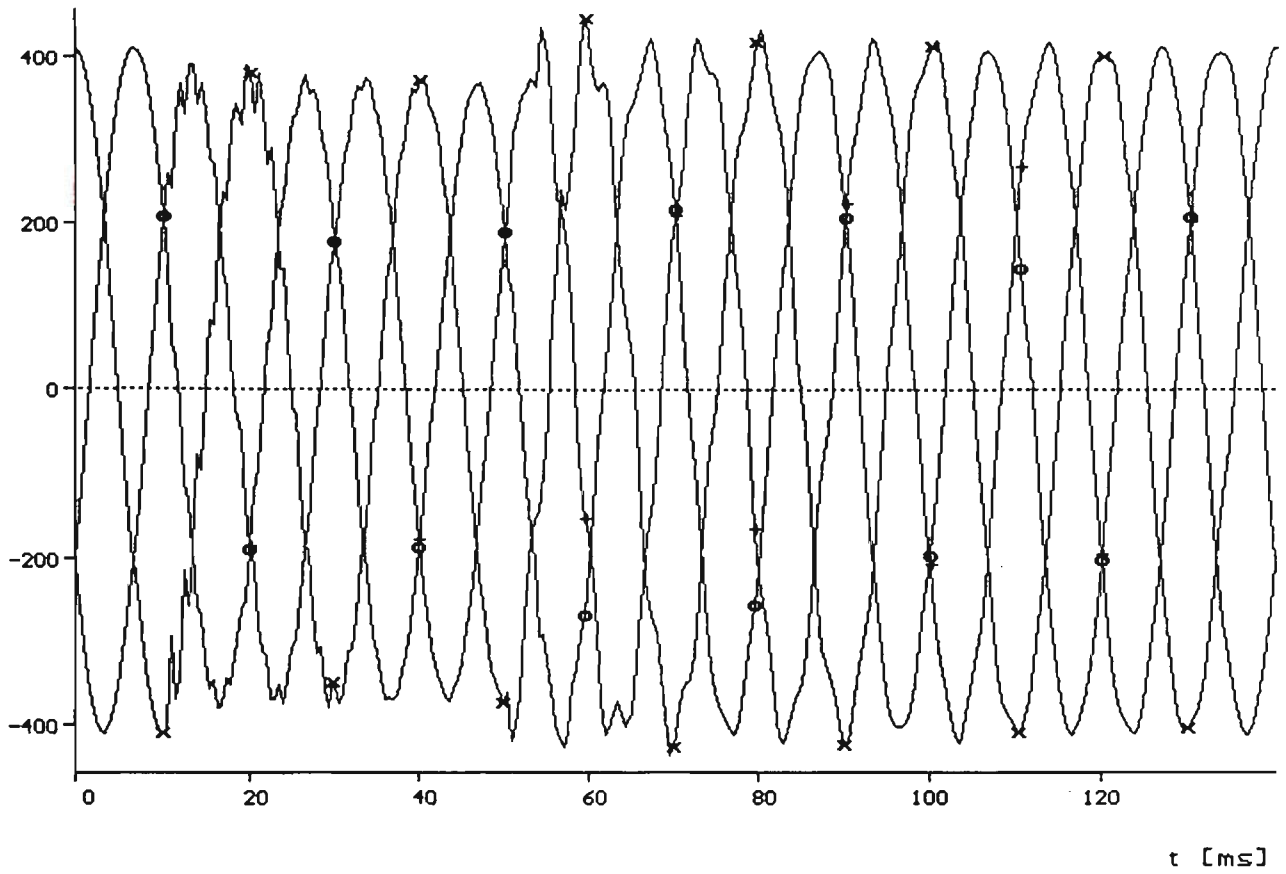


Fig. 8.81: Three Phase Voltages at the Q End of the Three Phase Feeder for Three Phase -G Fault at the Tee Point, (x): A, (o): B, (+): C

I [kA]

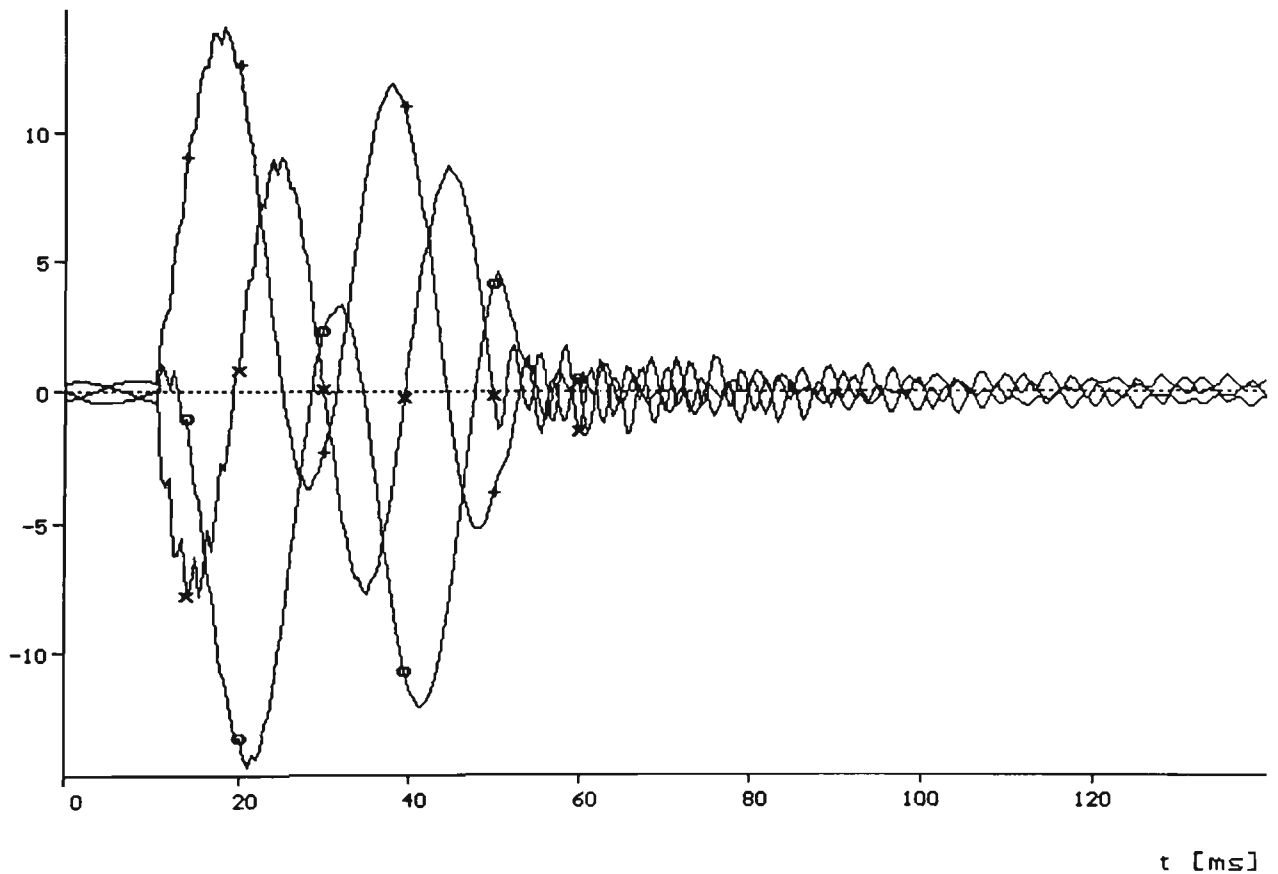


Fig. 8.82: Three Phase Currents at the Q end for Three Phase -G Fault at $l=192$ km from End P, Fault Cleared after 40 ms, (x): A, (o): B, (+): C

I [kA]

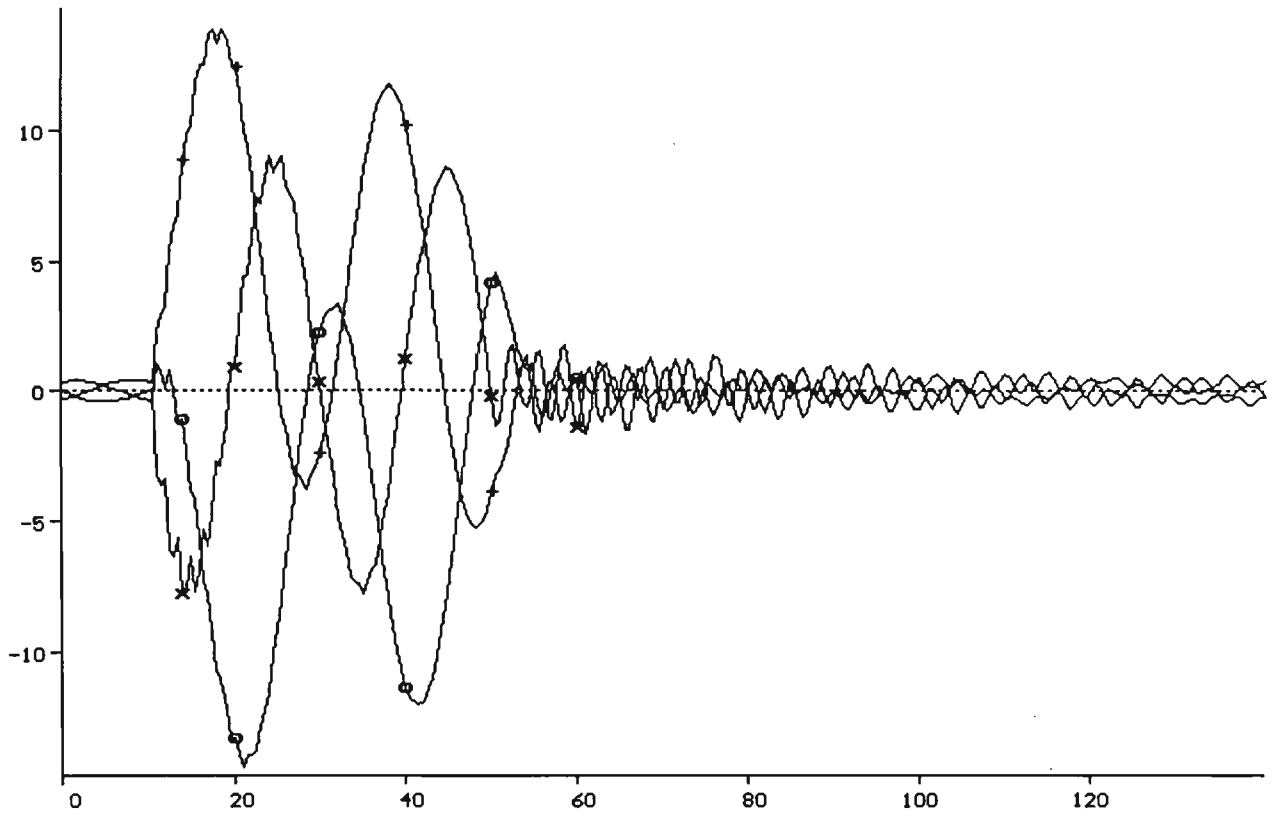


Fig. 8.83: Three Phase Currents at the Receiving End R for Three Phase -G^t [ms]
Fault at the Tee Point, fault Cleared after 40 ms, (x): A, (o): B, (+): C

I [kA]

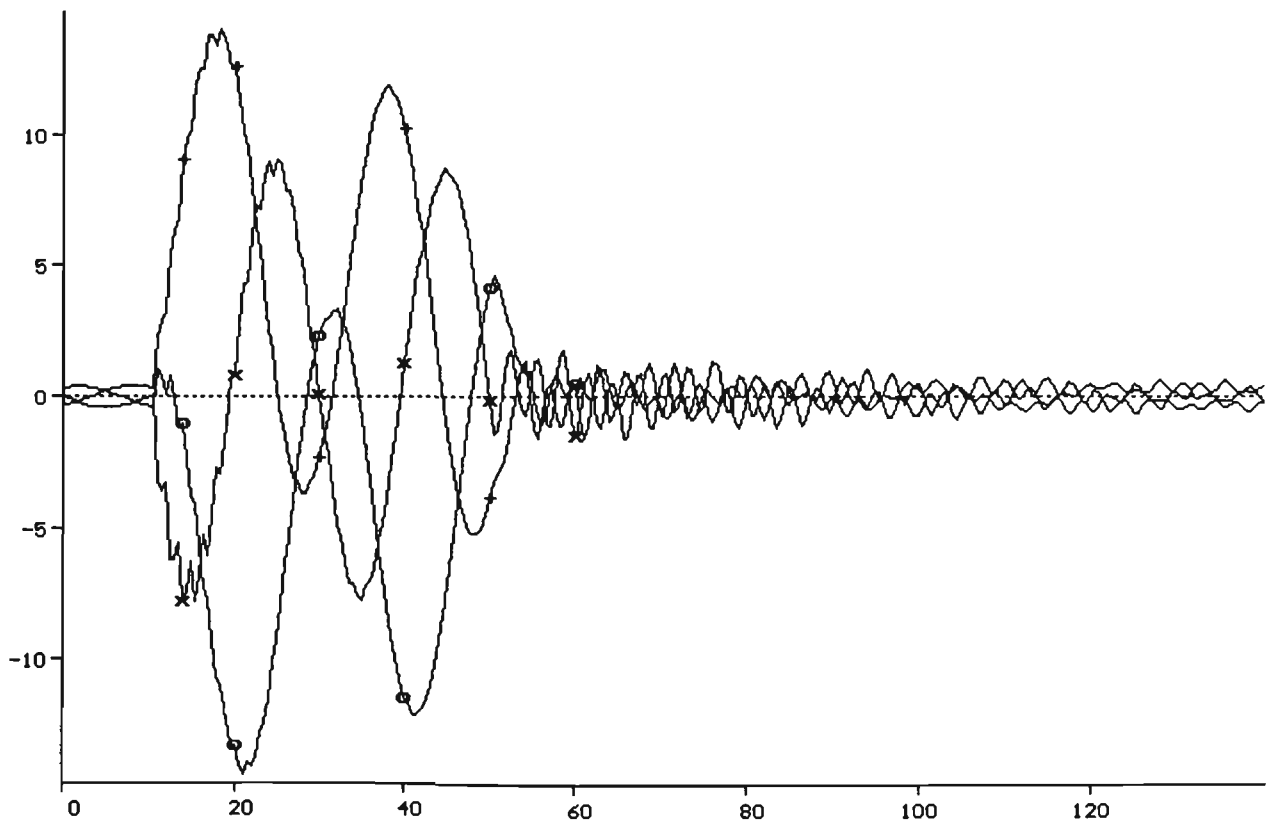


Fig. 8.84: Three Phase Sending End Currents for A Three Phase fault at the^t [ms]
Tee Point, fault Cleared after 40 ms, (x): A, (o): B, (+): C

In order to have a complete picture of system response under three phase fault short circuit conditions, the waveforms of the three phase fault currents through the faulty path are given in Fig. 8.85. The currents appear during the faulty period as expected, ie, they start at 10 ms until the fault was removed after 40 ms. The response is given for 130 ms of real system time.

8.3.6 Faults on Compensated Three Terminal System

For a compensated three terminal system with equal length for each of the three legs of the tee feeder system, a single phase to ground fault was applied at the sending end of the system given in Fig. 7.2. Each of the 500 kV transmission lines was assumed of 192 km length.

The waveforms of the sending end three phase voltages are given for a fault applied after 5 ms, and the fault is cleared after 40 ms, are given in Fig. 8.86, whereas, the receiving end R, and the Q end three phase voltage waveforms are given in Figs. 8.87 and 8,88 respectively.

The waveforms of phase A, B and C currents at the sending end are given separately as shown in Figs. 8.89, 8,90 and 8.91 respectively. The waveforms of the three phase currents at the receiving end R, and at the Q end of the tee feeder are shown in Figs. 8.92 and 8.93 respectively. Since a solid fault was assumed at the sending end P, the current through the faulty path flows during the fault inception time, ie, from 5 to 45 ms, which is shown in Fig. 8.94.

8.4 FAULTS THROUGH EARTH IMPEDANCE

For a single phase to ground fault at the sending end, through a linear resistor of 10 Ohms, the fault was assumed to occur after 5 ms of normal operation,

I [kA]

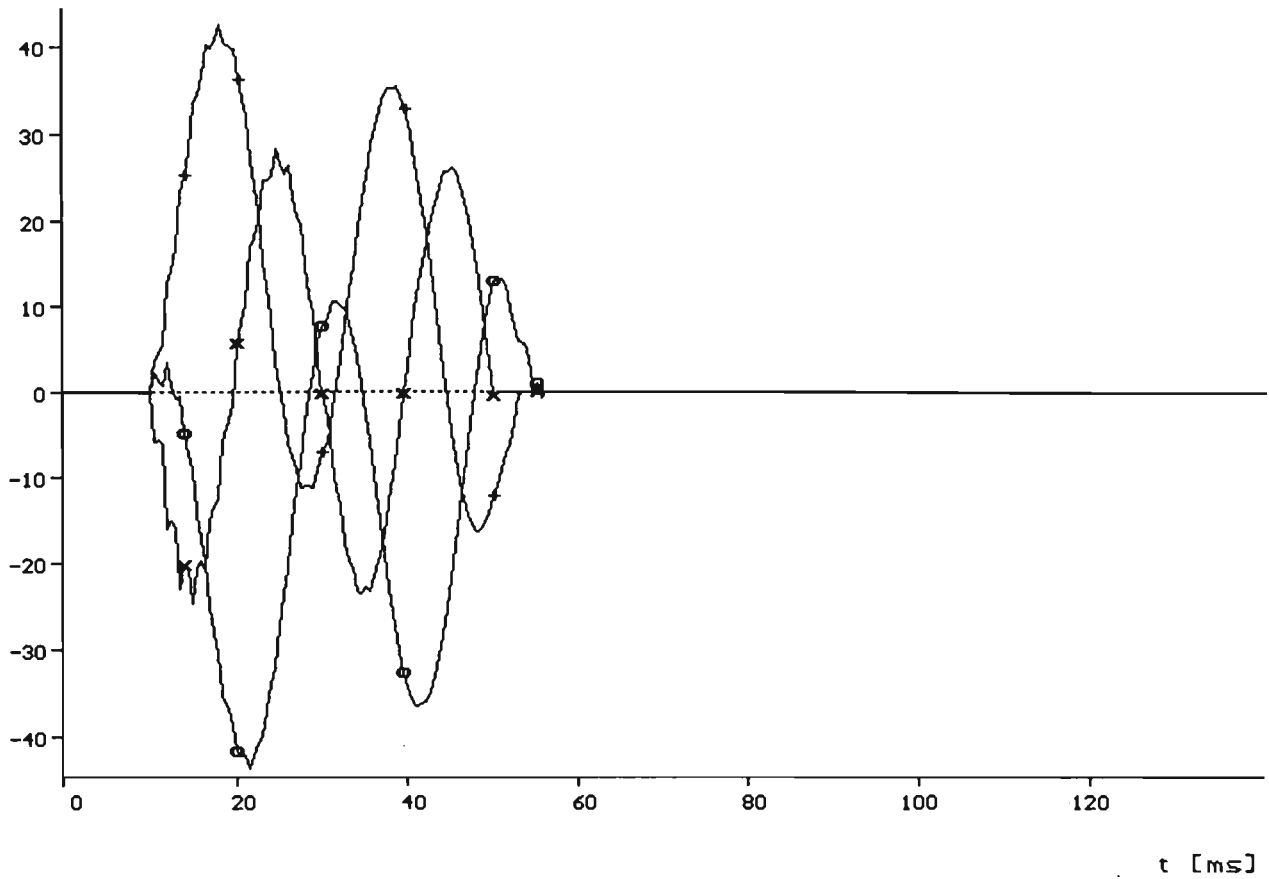


Fig. 8.85: Three Phase Currents Through the Faulty Path for Three Phase to G

Fault at the Tee Point, Fault Cleared after 40 ms, (x): A, (o): B, (+): C

U [kV]

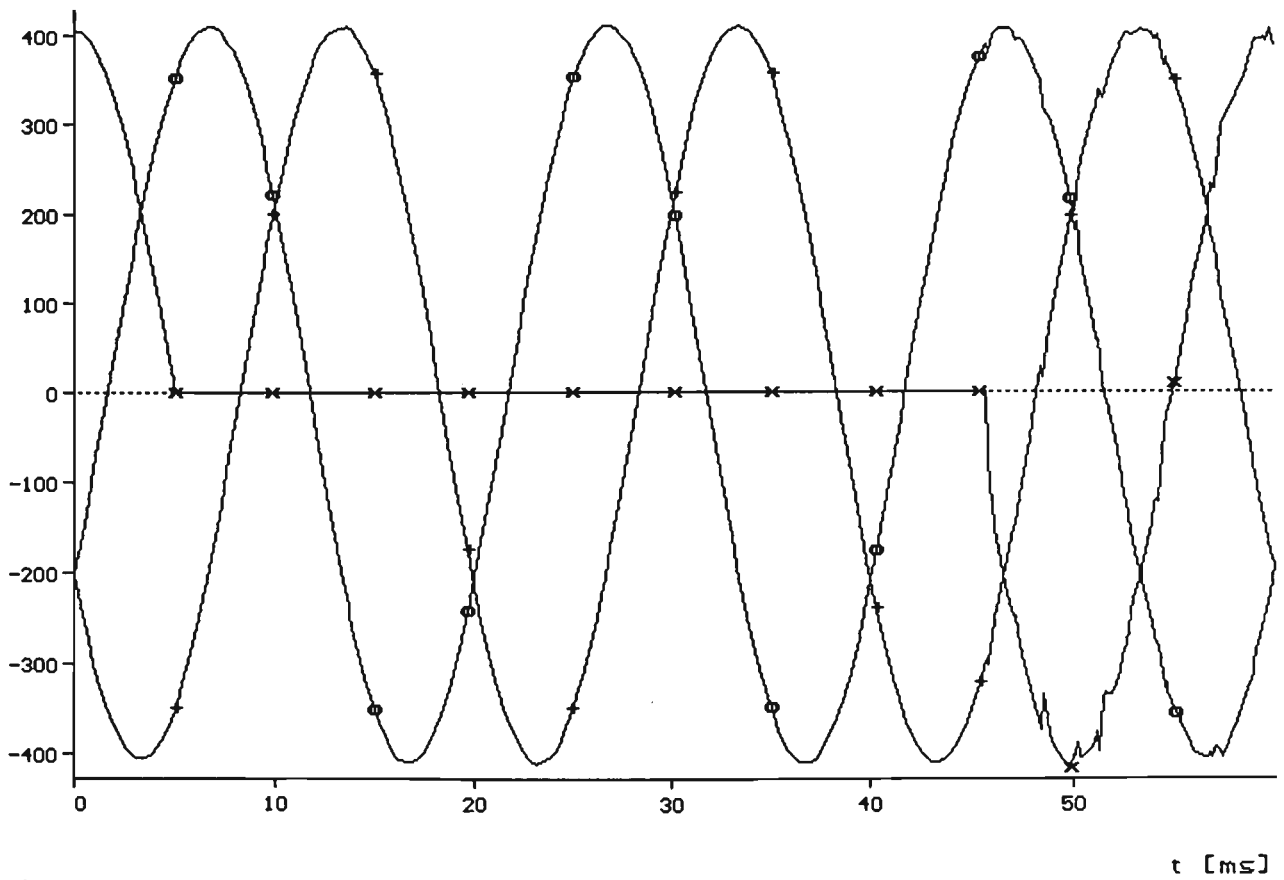


Fig. 8.86: A-G Fault at the Sending End, Three phase Voltages at the Sending

End of the Three Terminal Feeder, (x): A, (o): B, (+): C

U [kV]

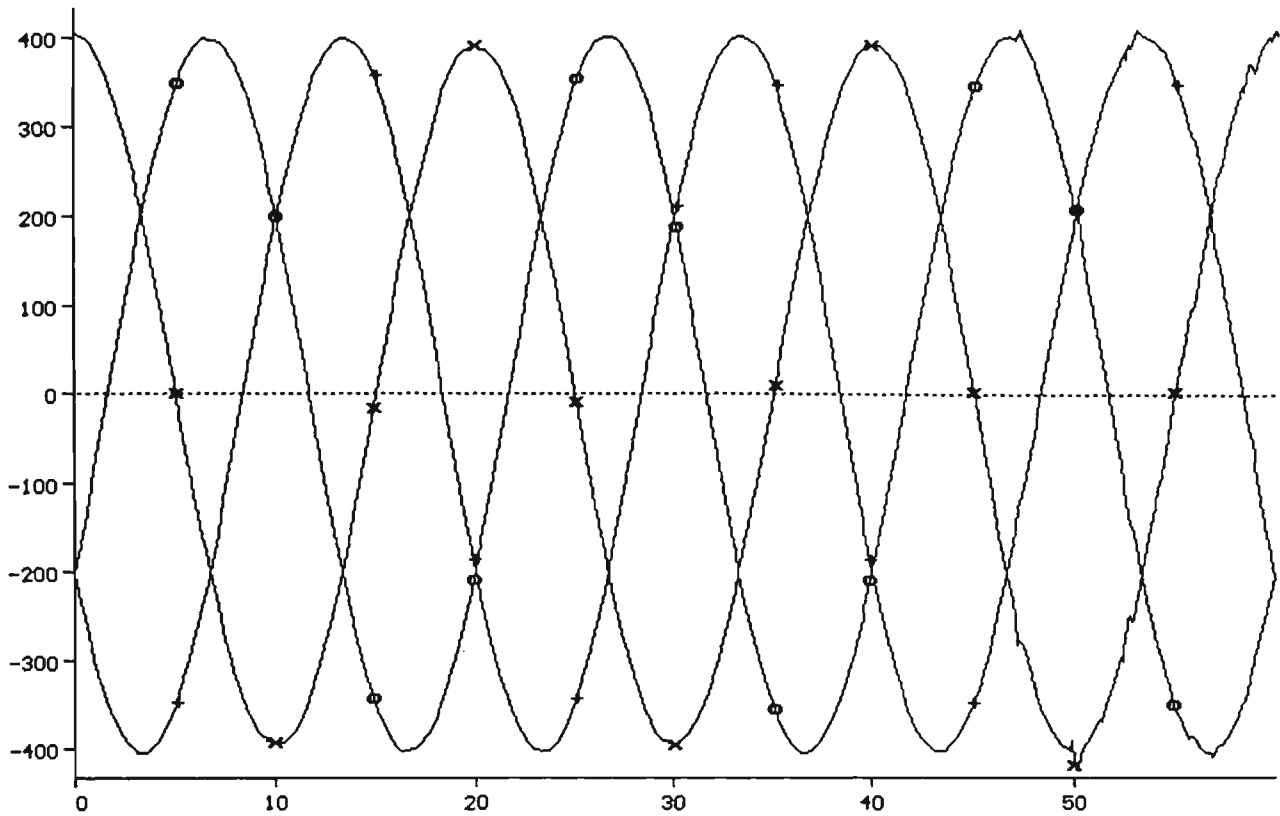
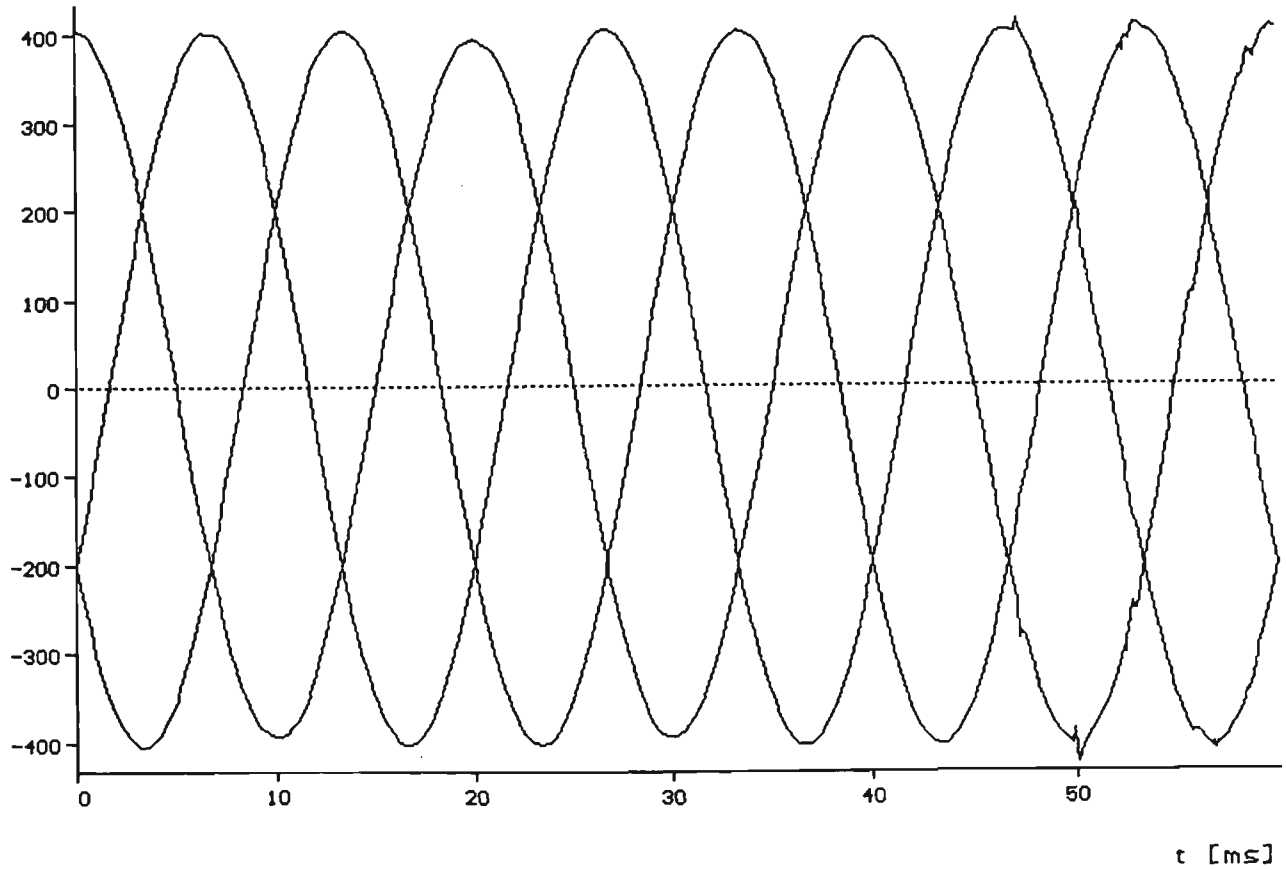


Fig. 8.87: Three Phase Receiving End Voltages for A-G fault at the P End of t [ms]
The Three Terminal Feeder, (x): A, (o): B, (+): C

U [kV]



t [ms]

Fi. 8.88: Three Phase Voltages at The Q End of the Tee Feeder, for A-G Fault
at $l=0$ from End P, (x): A, (o): B, (+): C

I [kA]

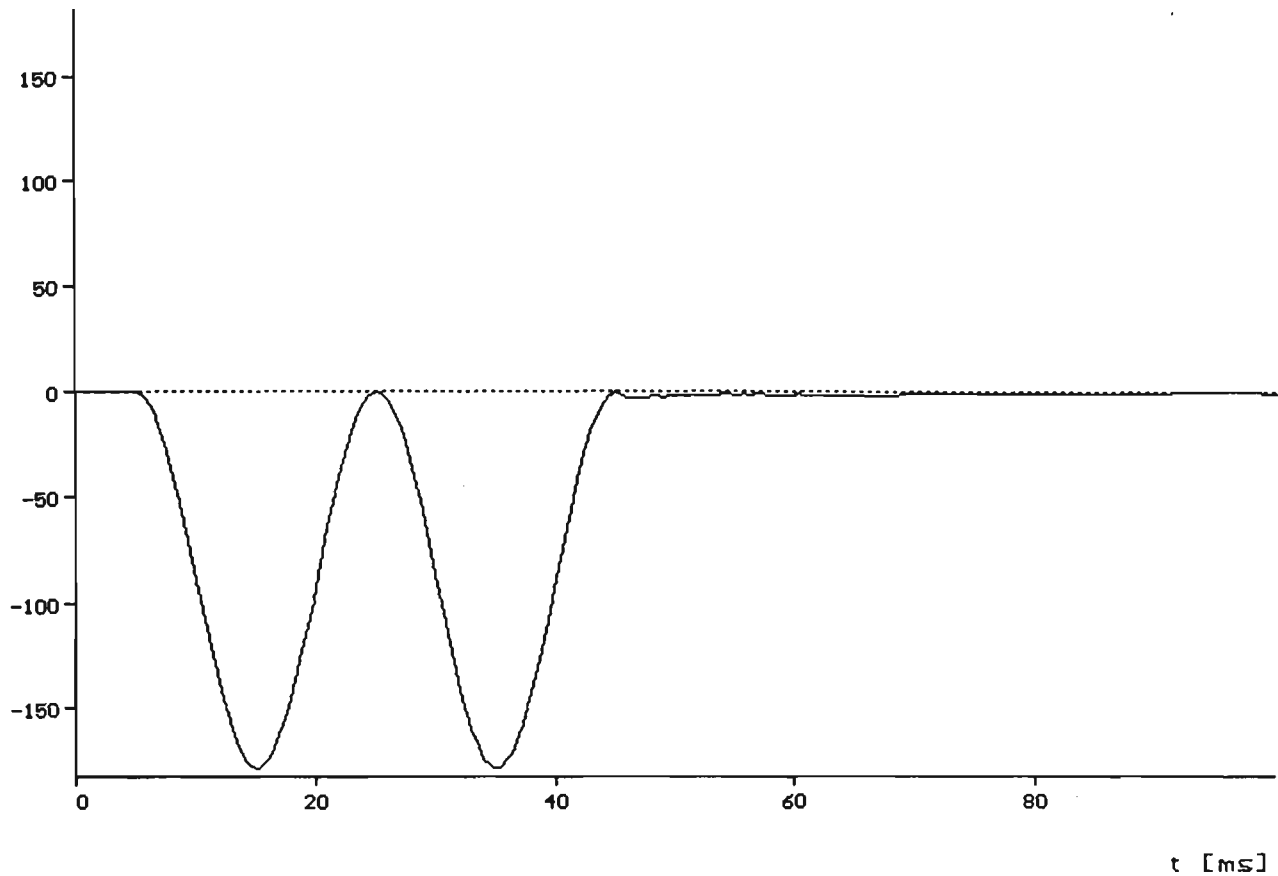


Fig. 8.89: A Phase Sending End Current for A-G fault at $l=0$ from End P, Fault Applied at 5 ms and Cleared after 40 ms.

I [A]

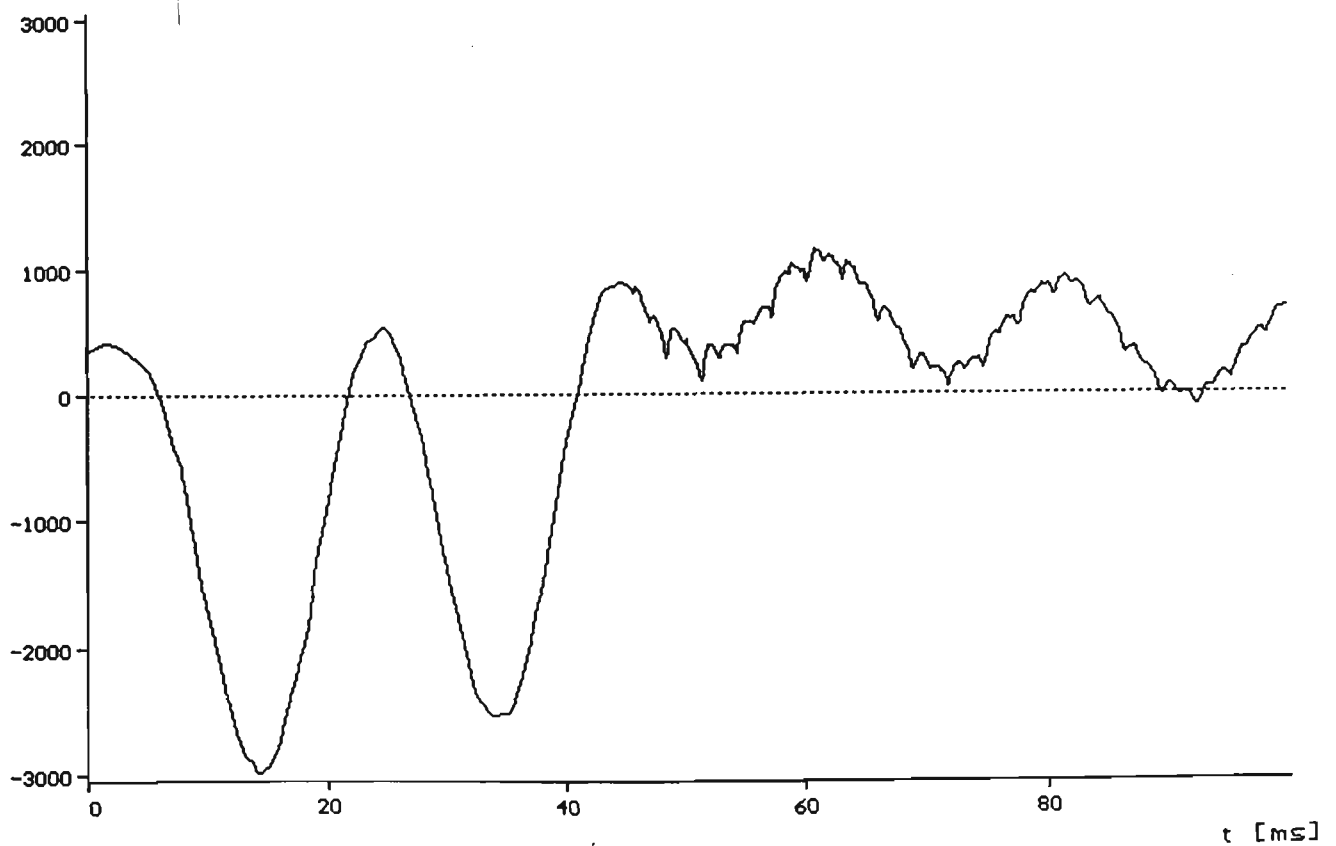


Fig. 8.90: Phase B Sending End Current for A-G fault at $l=0$ from End P, Fault Applied at $t=5$ ms and Cleared after 40 ms.

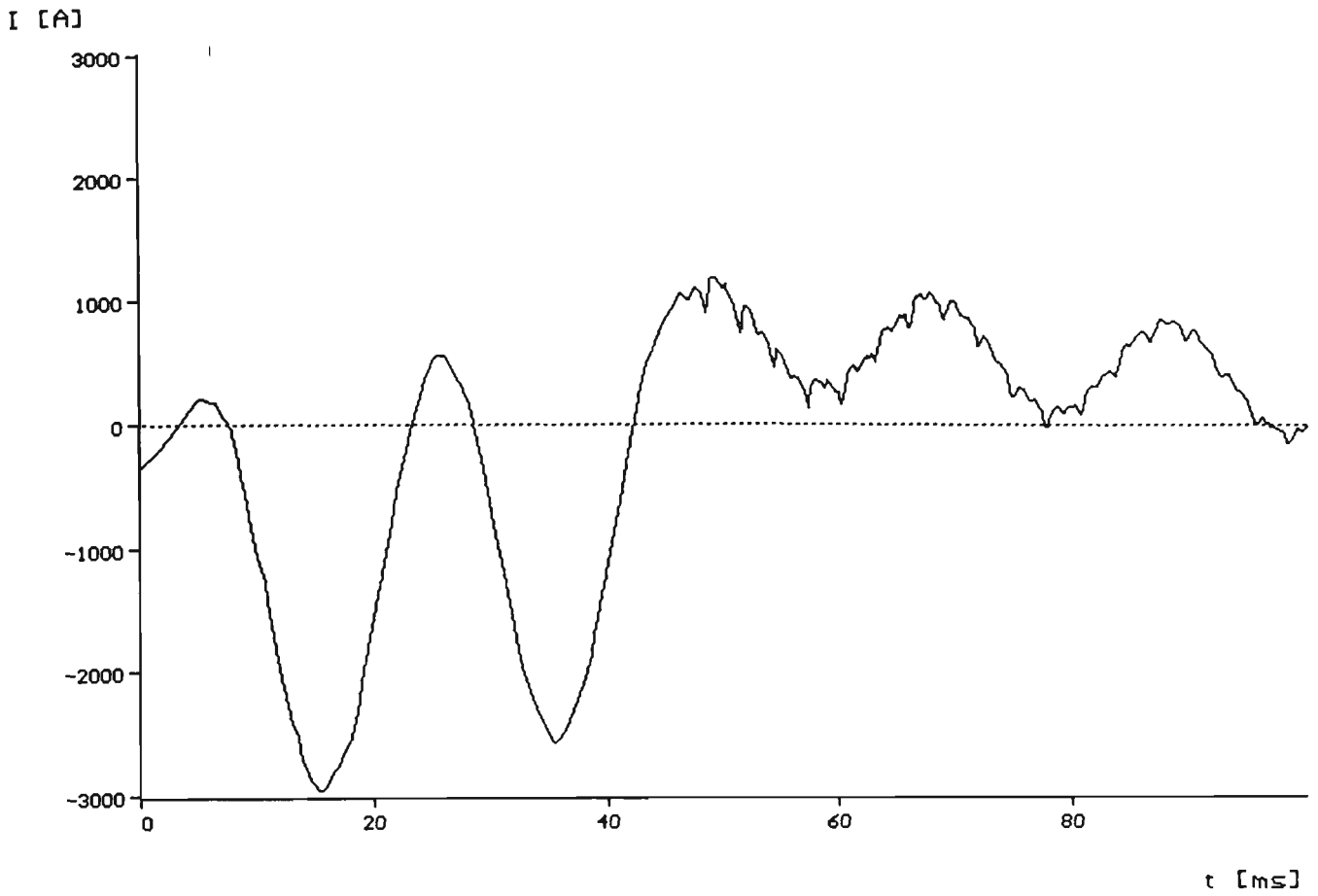


Fig. 8.91: Phase C Sending End Current for A-G Fault at $l=0$ from End P, Fault applied at $t=5$ ms and Cleared after 40 ms.

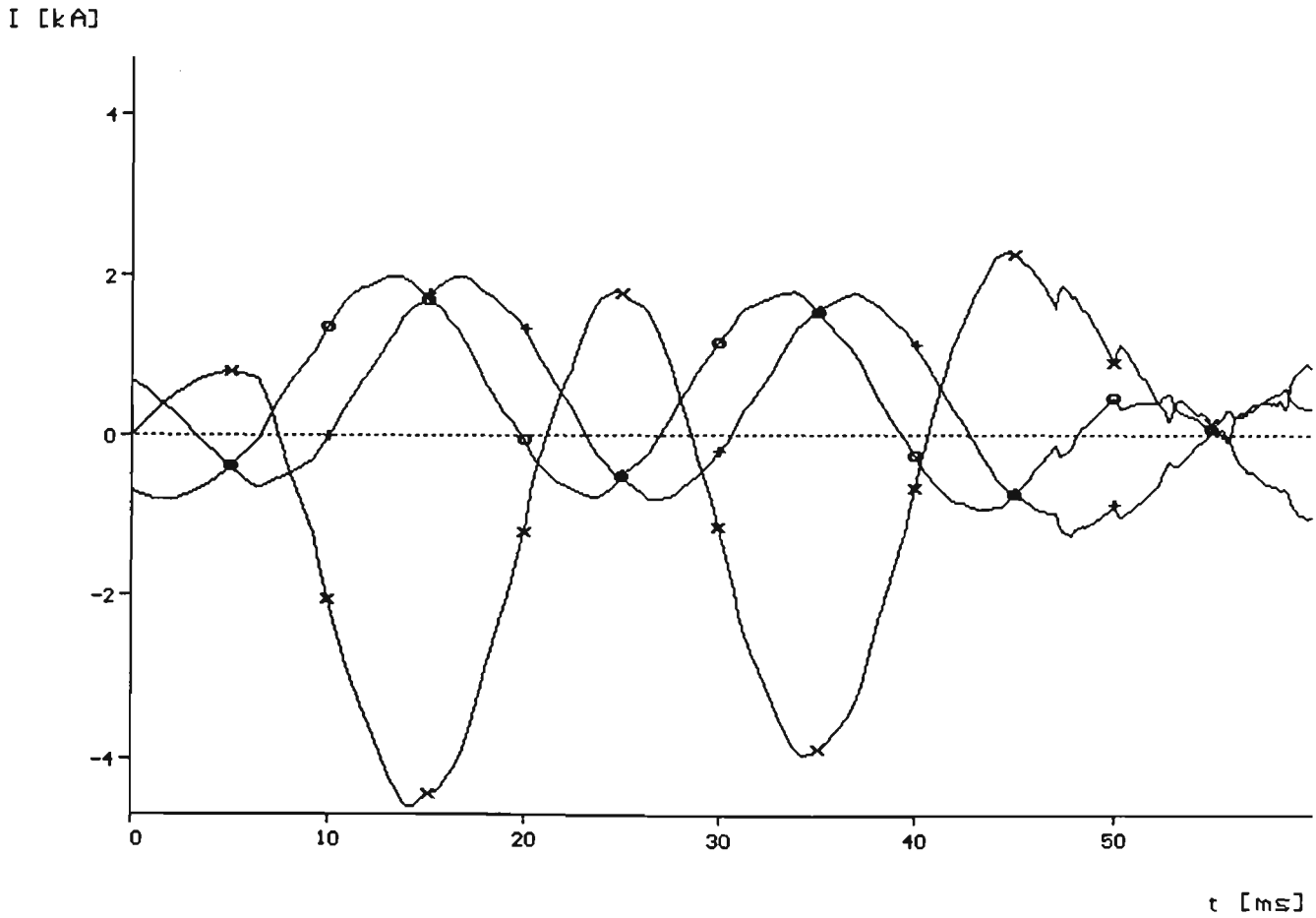


Fig. 8.92: Receiving End Three Phase Currents for A-G Fault at $l=0$ from End P of the Tee Feeder, Fault Cleared after 40 ms, (x): A, (o): B, (+): C

I [A]

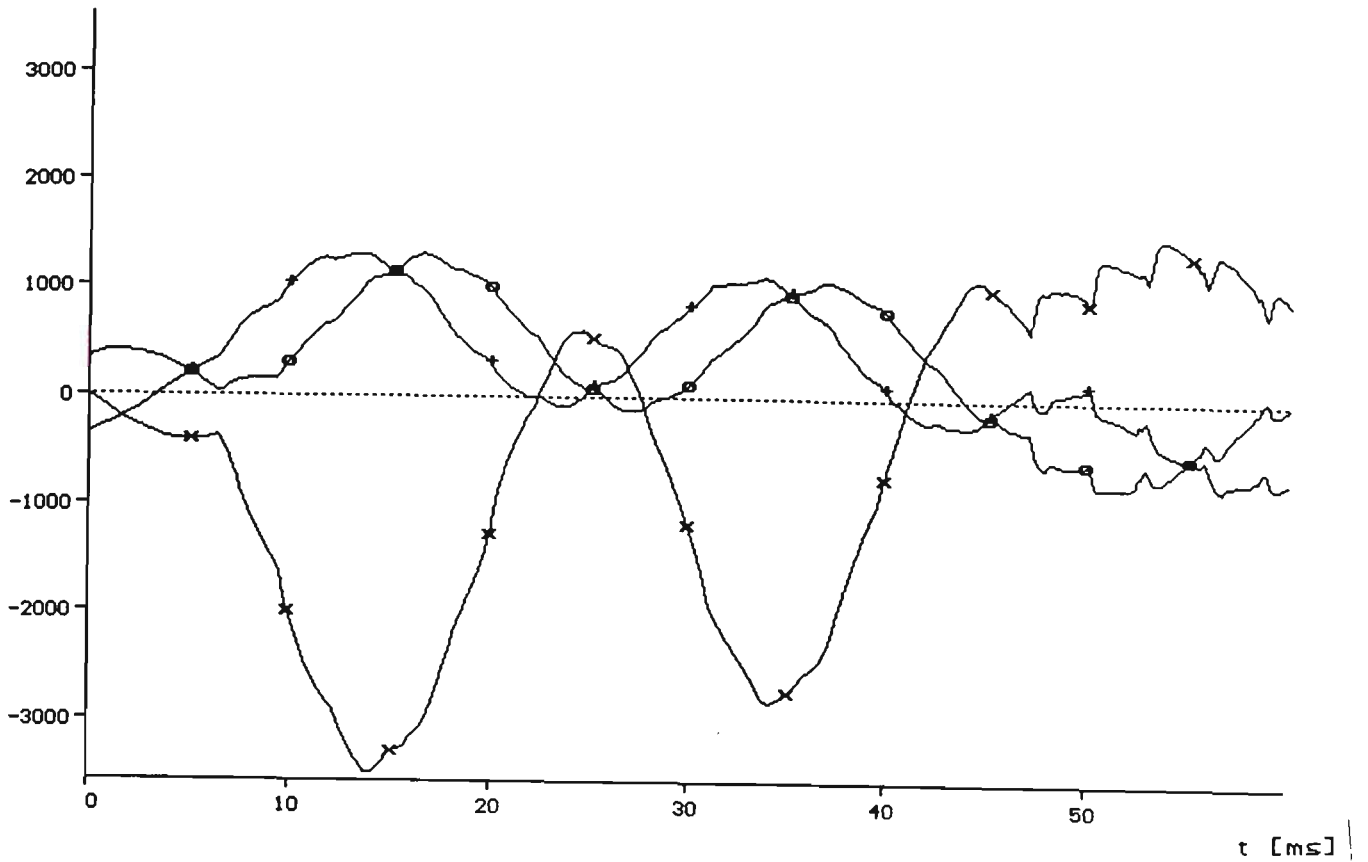


Fig. 8.93: Q End Three Phase Currents for A-G Fault at $l=0$ from End P of the Three Terminal Feeder, Fault Cleared after 40 ms, (x): A, (o): B, (+): C

I [kA]

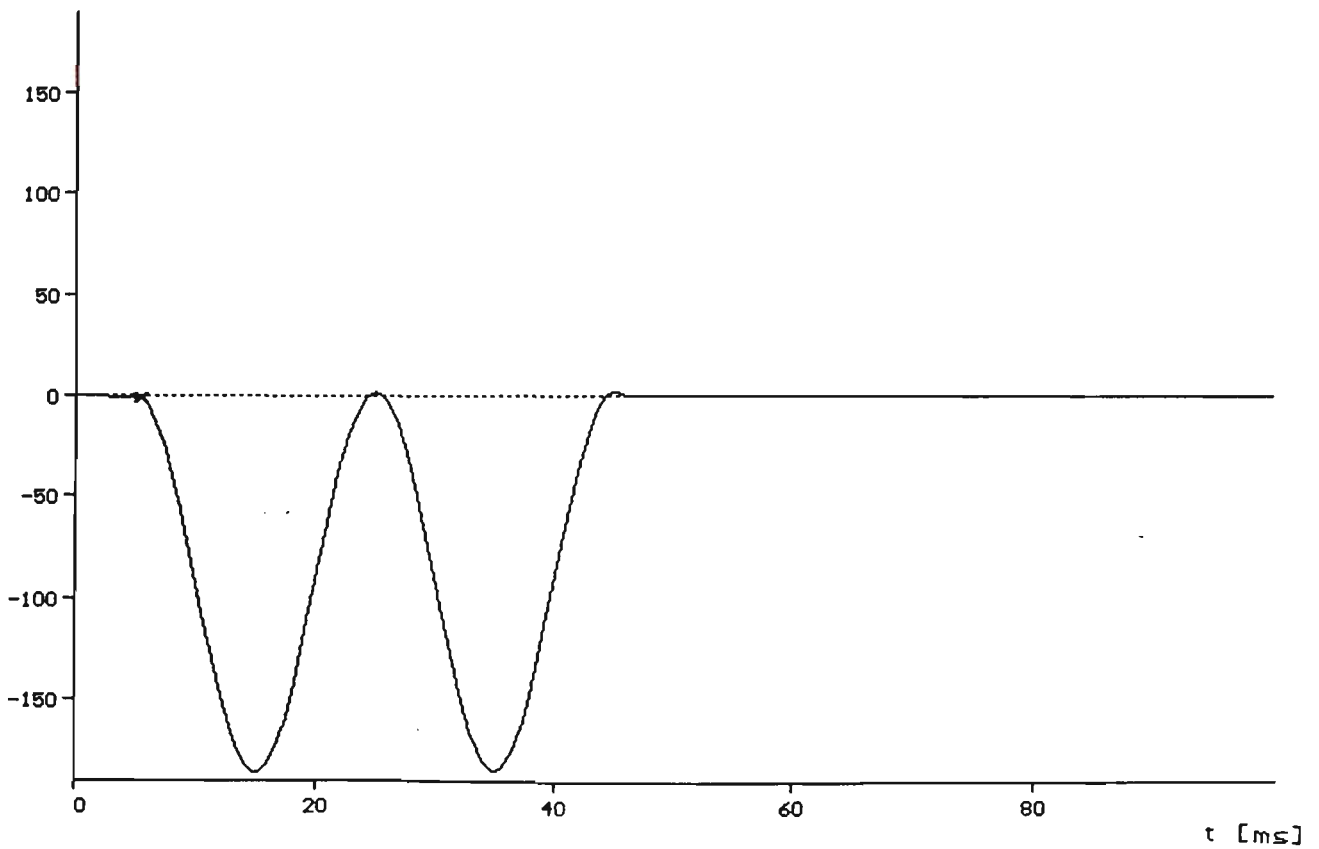
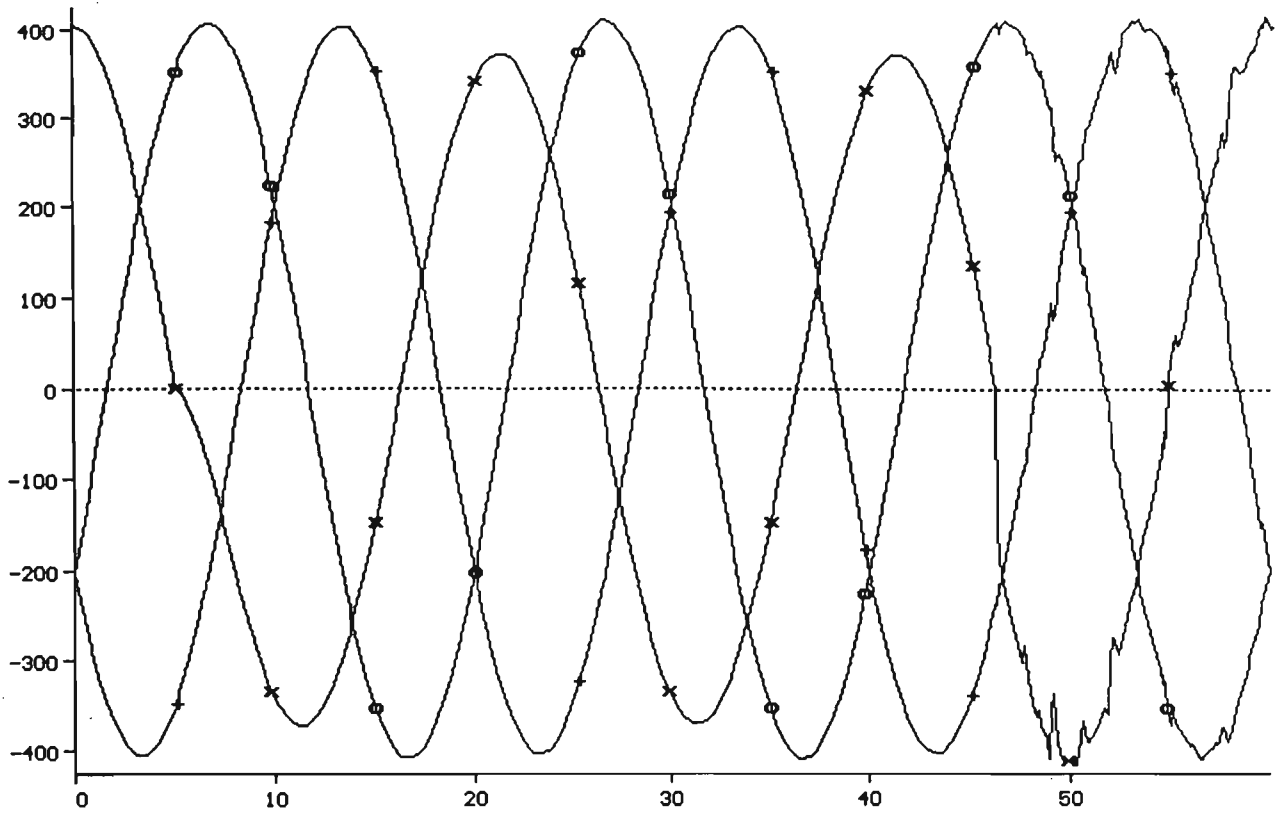


Fig. 8.94: A Current in the Faulty Path for A-G Fault at $l=0$ from End P of the Three Terminal Feeder, Fault Applied at $t=5$ ms and Cleared after 40 ms

and cleared after 40 ms. The three terminal compensated system was used for this test. Three phase fault voltages at the sending end P, receiving end R and Q end of the tee feeder are given in Figs. 8.95, 8.96 and 8.97 respectively. The phase A fault current is given in Fig. 8.98, and the other two sound phases B and C of the sending end current waveforms are given in Fig. 8.99. The receiving end R currents and the Q end of the feeder currents are shown in Figs. 8.100 and 8.101 respectively. The current through the 10 Ω resistor is given in Fig. 8.102.

U [kV]

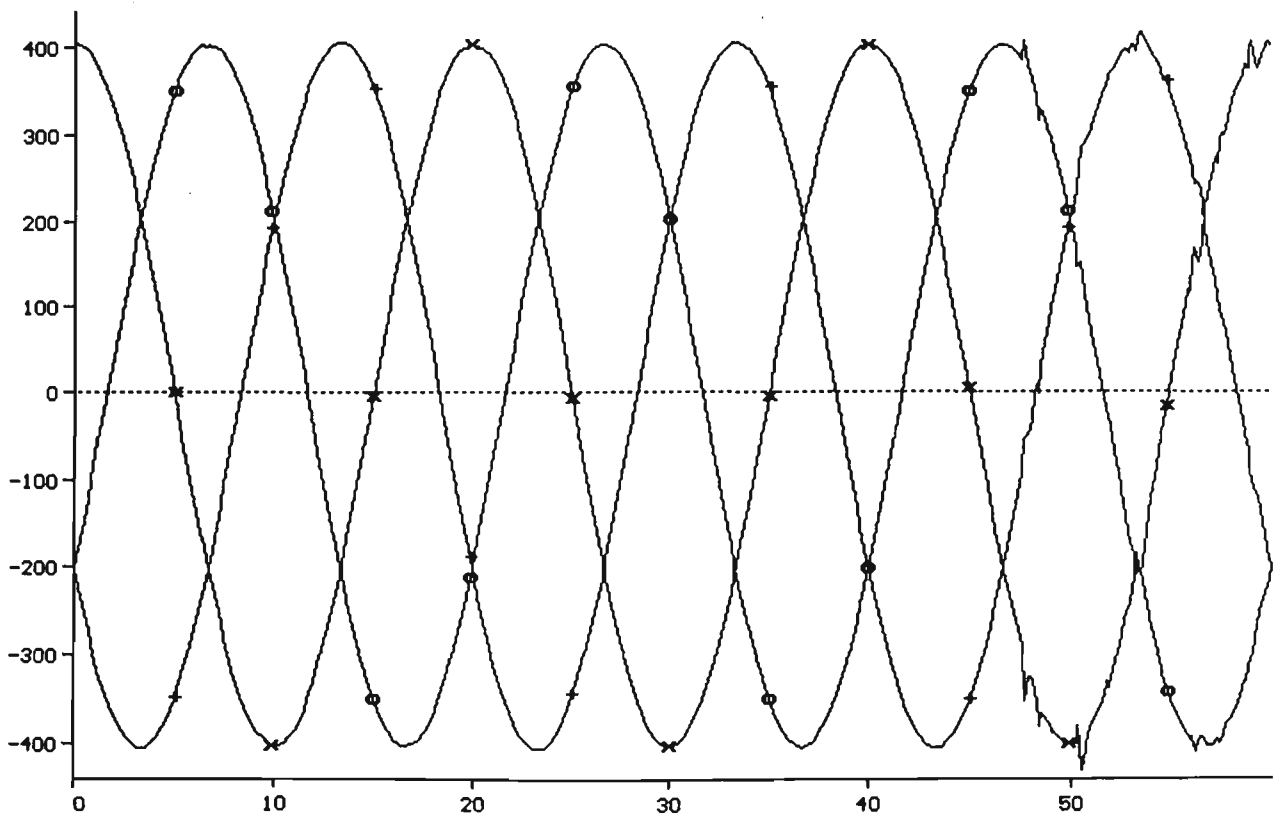


t [ms]

Fig. 8.95: Compensated Three Terminal Feeder, Three Phase Sending End

Voltage for A-G Fault at End P Through 10 Ohms Resistance

U [kV]



t [ms]

Fig. 8.96: Three Phase Receiving End Voltages for A-G Fault Through 10

Ohms Resistance at $l=0$ from end P of the Tee Feeder.

U [kV]

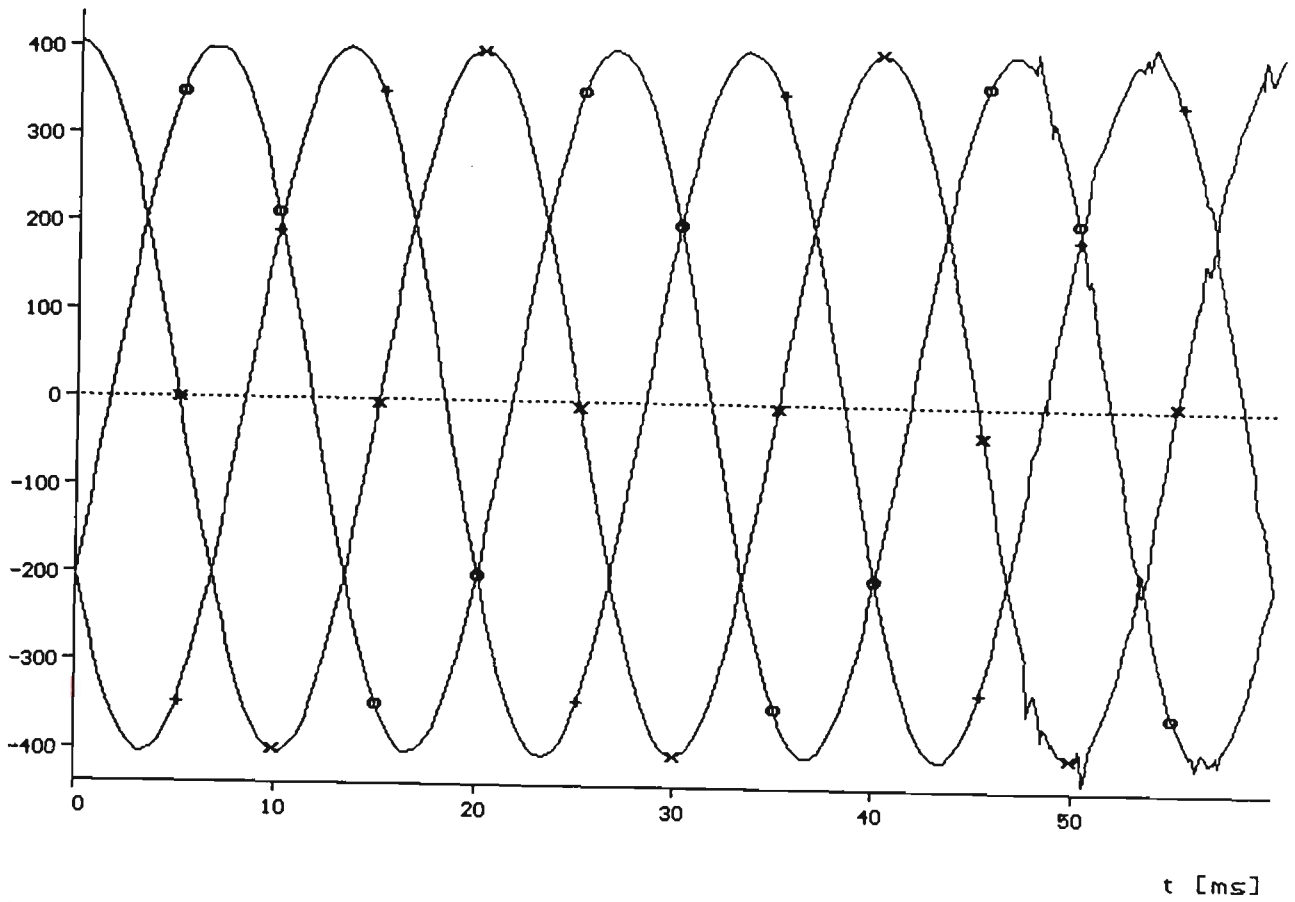


Fig. 8.97: Three Phase Q End Voltages for A-G Fault at $l=0$ From End P of the Three Terminal Feeder, Fault Cleared after 40 ms, (x): A, (o): B (+): C

I [kA]

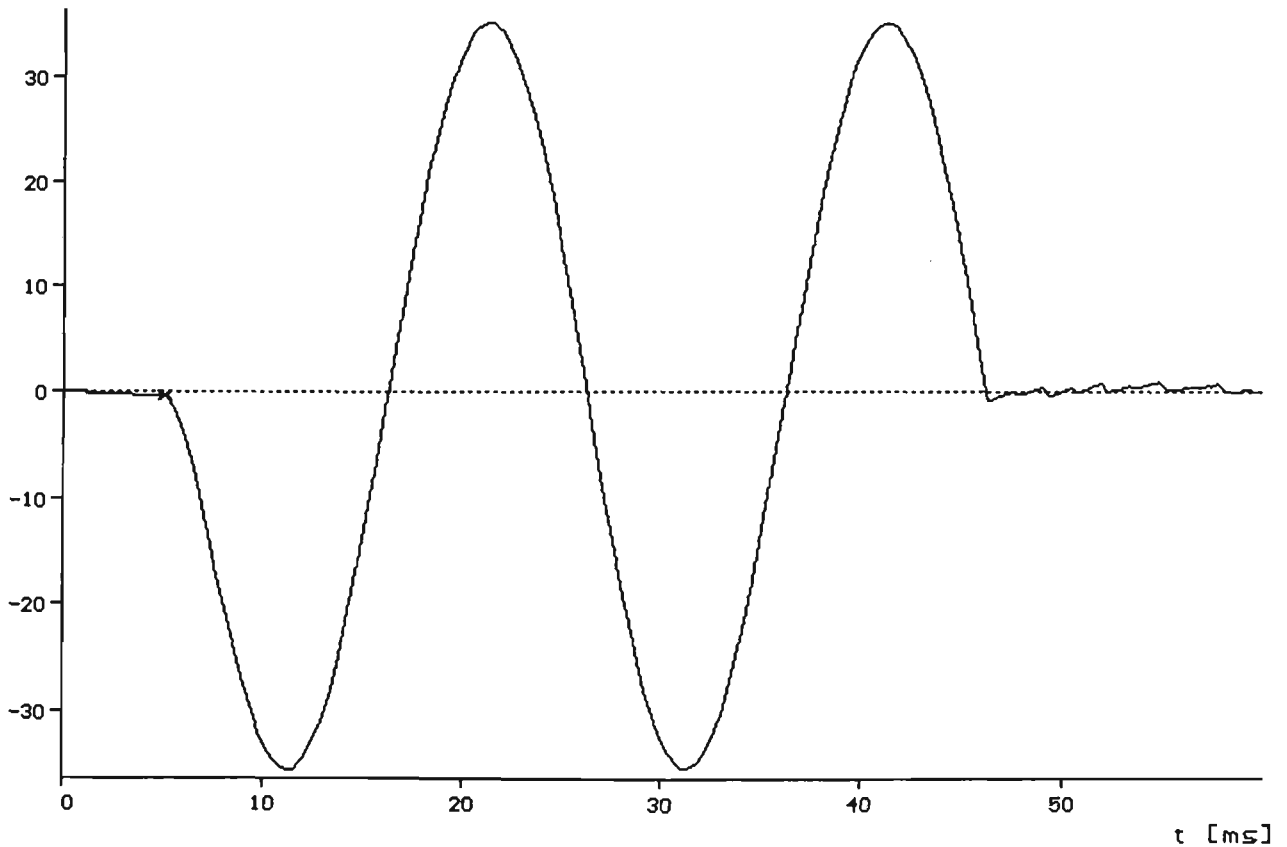


Fig. 8.98: Fault Current Through the Faulty Path for A-G Fault at $l=0$ from End P of the Three Terminal Feeder, (x): A, (o): B, (+): C

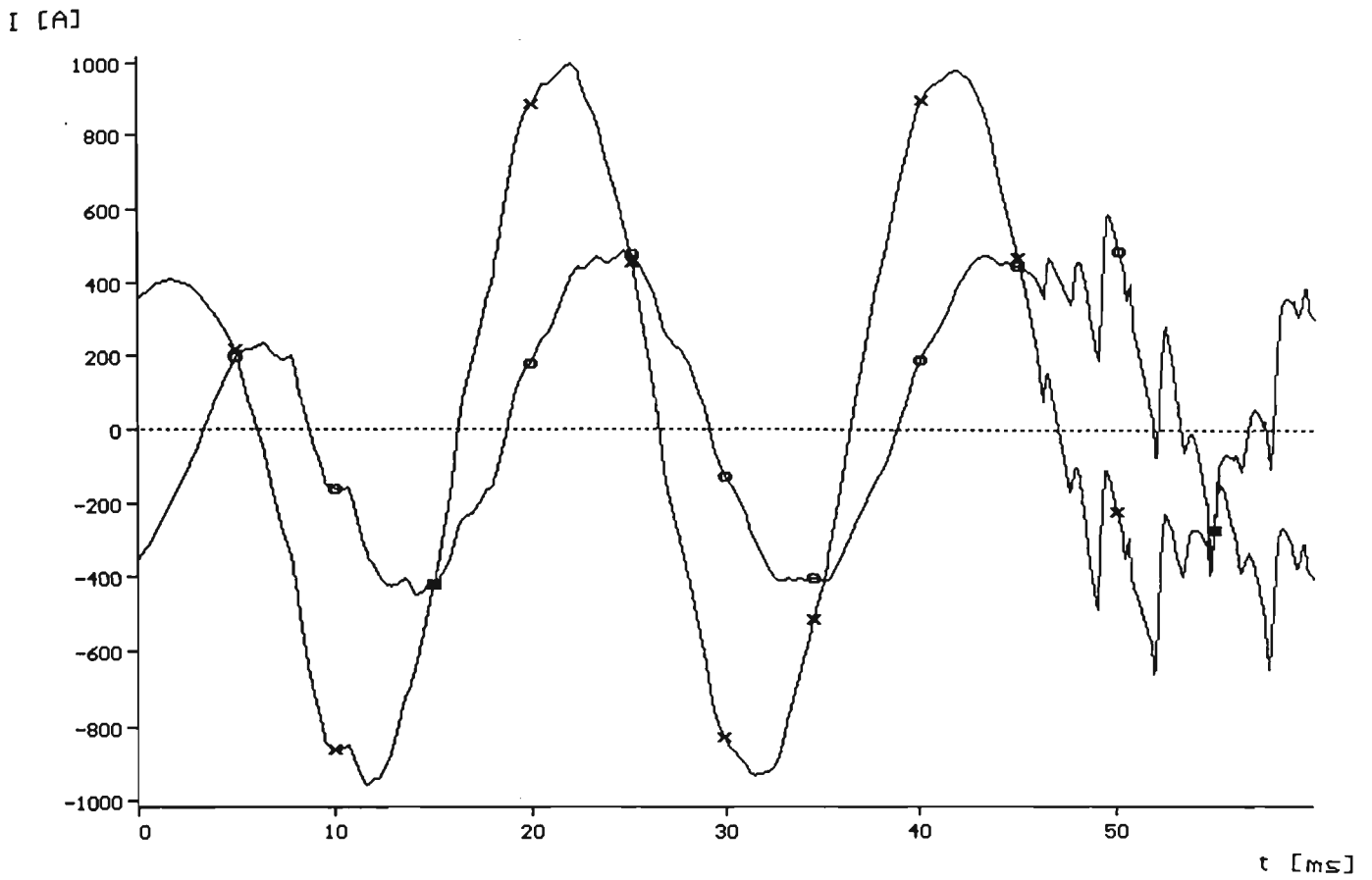


Fig. 8.99: Three Terminal Compensated Feeder, A-G Fault Through 10 Ohms Resistance at $l=0$ from End P, Phase B and C Sending End Currents.

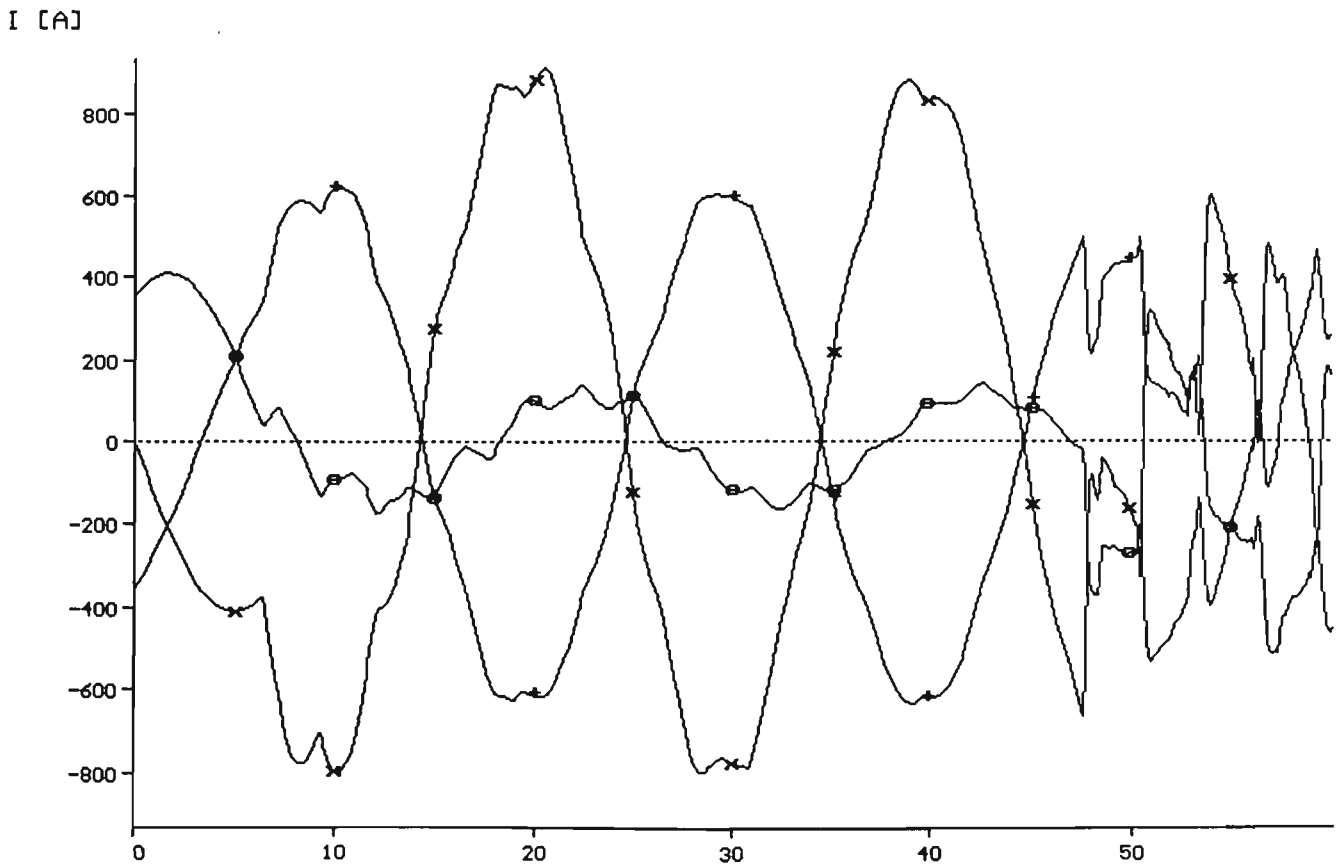


Fig. 8.100: Three Terminal Compensated Tee Feeder, A-G Fault at $l=0$ from End P, Phase B and C Receiving End Currents Through A Resistor = 10 Ohms.

I [A]

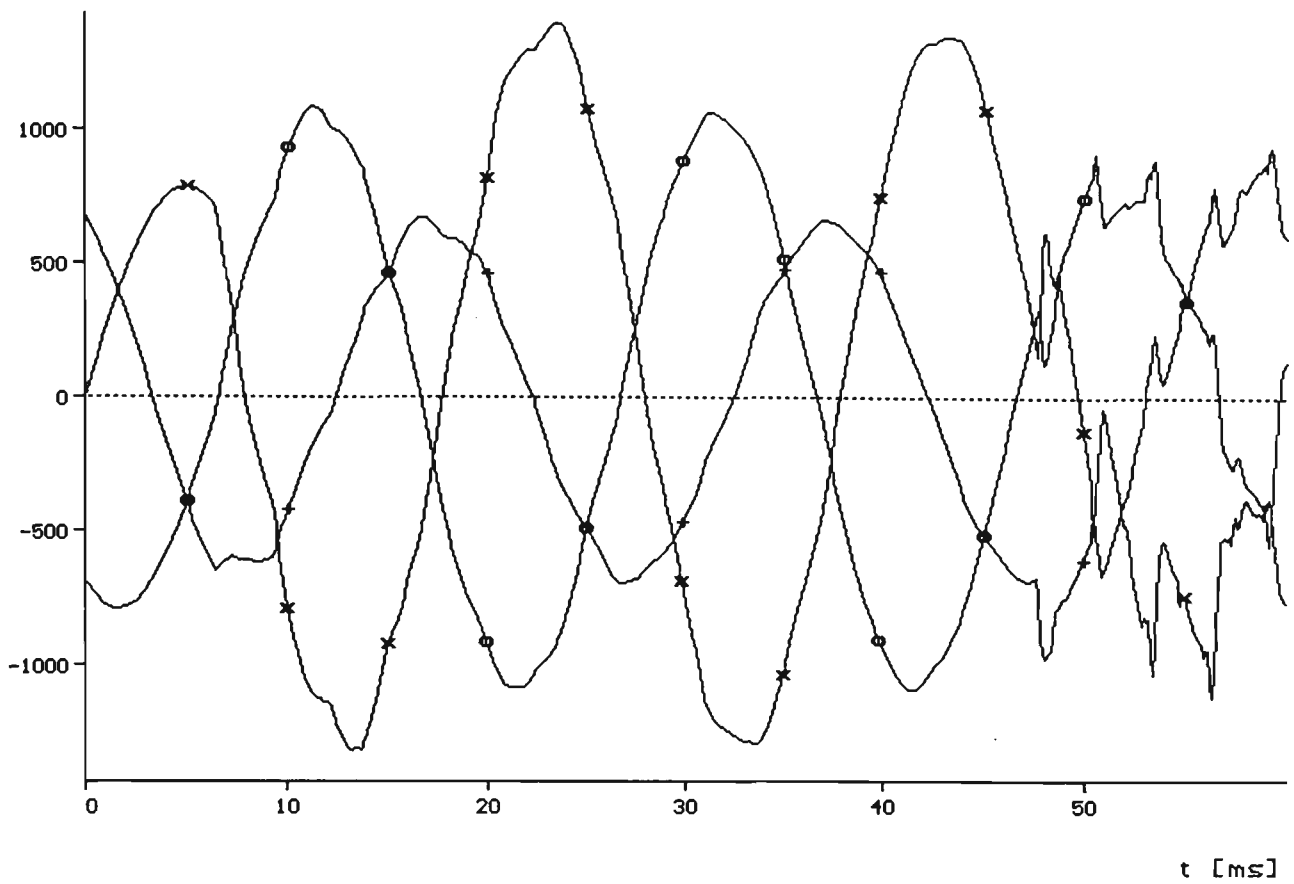


Fig. 8.101: Three Phase Currents at Q End of the Three Terminal Compensated

Feeder for A-G Fault at $l=0$ From End P, $R_f=10$ Ohms.

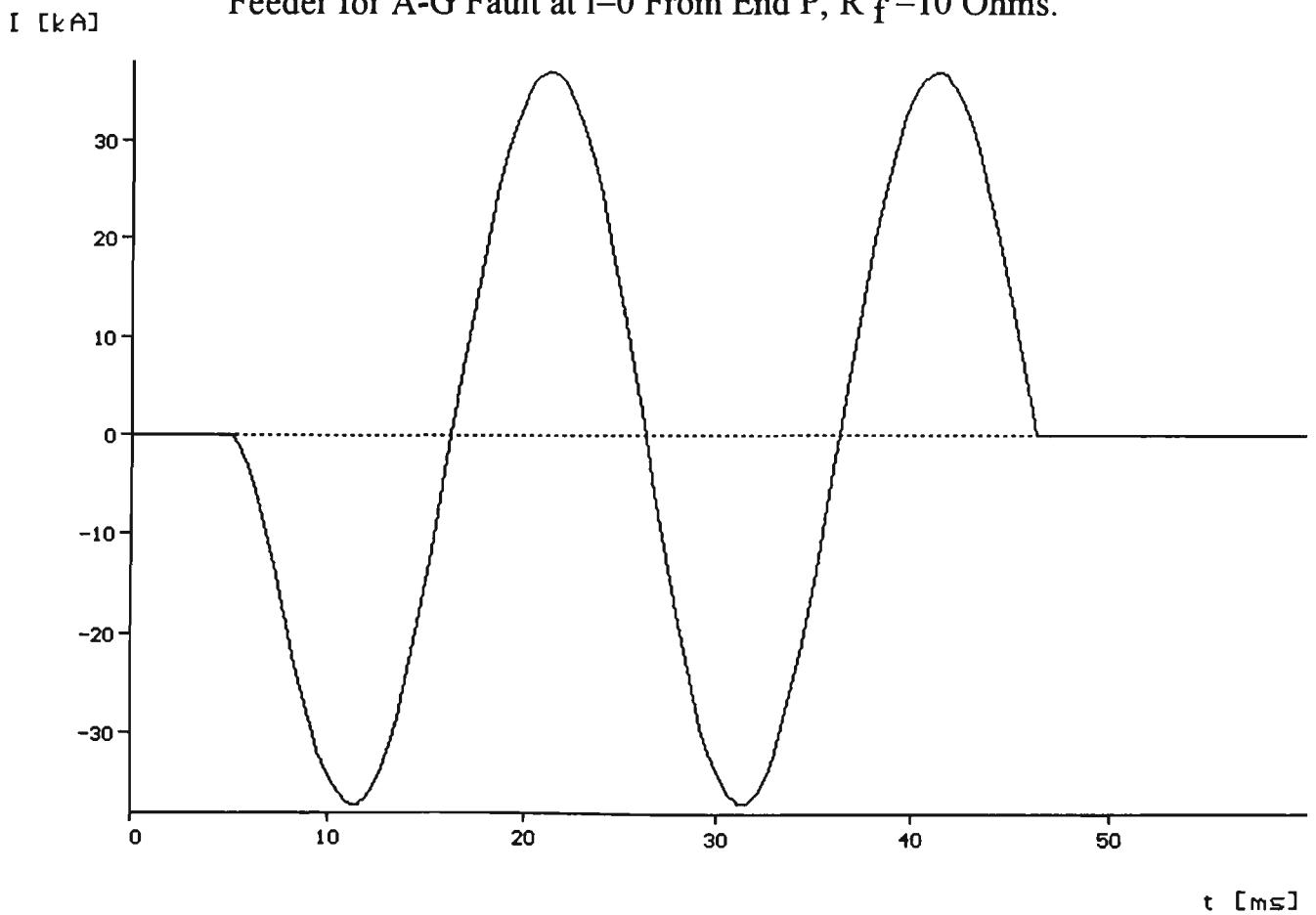


Fig. 8.102: Fault Current Through the Faulty Path for A-G Fault at $l=0$ From End P of The Compensated Three Terminal Feeder, $R_f=10$ Ohms.

Chapter 9

ANALYSIS AND TESTING OF THE FAULT LOCATION ALGORITHMS

9.1 INTRODUCTION

The need for accurate fault location algorithms for measuring the exact location of faults on EHV transmission line was explained in details in chapter 5. The development of the theory of accurate fault measurement for two and three terminal feeders was described in chapters 5 and 7 respectively. This chapter will consider the analysis and testing of the developed algorithms for faults on different location on EHV transmission lines under various fault conditions. Such assessment is carried out for both two and three terminal systems.

Factors which may influence the accuracy of measurement of fault location such as: line symmetry, shunt capacitance, fault resistance and remote source impedance, are considered in the studies conducted in this chapter. The results from studies on both two and three terminals are presented. The initial development was made on a single phase model. A separate computer programs were developed for single phase and three phase models for two and three terminal systems. The analysis of the tests on various systems are given in this chapter. Such results are presented for compensated and uncompensated systems. Shunt compensation of 75% for the transmission lines was considered for the positive phase sequence.

The voltages and currents measured at each end of the transmission line are usually filtered so as to produce a measure of the steady-state power frequency voltage and current phasors. The latter are obtained as data described by

means of post-fault processing applied to data captured during the fault clearance process.

9.2 SELECTION OF MODES

For testing the developed fault location algorithm, which is based on the use of the filtered power frequency current and voltage signals at both end of the transmission line, for the results obtained from studies under different faults conditions, the selection of modes for calculations is required. All types of faults will excite one aerial mode component, ie. modes 2 and/or 3 are always excited. It was found that although the earth-mode (mode 1) can also be utilised, it is unnecessary to do so except in the case of single circuit vertical conductor line configuration.

The presence of a significant level of residual currents is used to identify the presence of a fault involving earth and this in turn is used to display the fault location as determined by a mode 1 based evaluation of the developed fault location algorithm. When a fault does not involve earth, the fault location is determined by either mode 2 or mode 3 based evaluation of the fault location algorithm. The particular mode selected is that which is associated with the largest modal component. It was found that for most of the faults, mode three gives very accurate results.

9.3 TWO TERMINAL SYSTEMS

For a two terminal system, an EHV 500 kV transmission line interconnecting two sources, of horizontal configuration, the line first was considered to be fully transposed over the whole 384 km length. Untransposed transmission line

were considered in order to check the validity of the developed algorithms for the measurement of fault locations under different conditions.

A single phase model used in the initial work presented in this thesis has indicated that such model can be used for analysing balanced three phase faults under different conditions. This is due to the fact that three phase balanced faults can be solved using a single phase representation. Such analysis is based on the use of perfectly transposed transmission lines. In order to analyse more general systems, including untransposed transmission lines and unbalanced faults, a more accurate representation is achieved using modal analysis.

From the full three phase model, the filtered phase currents and voltages at the sending and receiving end of the line are used to derive the modal quantities. With the knowledge of the transmission line modal parameters, computed from line constants, the single phase model for fault location is extended to three phase systems with very high accuracy achieved in estimating the distance to fault. This chapter represents the results obtained from such models, and the assessment of these results revealed the validity of the developed methods for accurately estimating the location of faults on EHV transmission lines.

9.3.1 Three Phase Faults

For a three phase to ground fault at different locations on the transmission line, the results are given in Table 9.1, and shown in Fig. 9.1. It is evident, that the algorithm gives a very good estimates for fault locations which are not too close to both ends, and the most accurate results are found to be when the fault approaches the middle of the line.

Table 9.1: Three phase to ground fault.

Mode	L = 0 km	L = 96 km	L= 192 km	L=288 km	L=384 km
1	20.97658	174.3751	192.0000	379.5858	363.0234
2	16.44321	95.27717	192.0000	292.6791	367.5568
3	.4146221	95.97788	192.0000	288.0737	383.5854

The results of Table 9.1 are shown on Fig. 9.1.

Table 9.2: % Error in Fault Distance Estimation.

Actual Distance [km]	L = 0	L = 96	L = 192	L = 288	L = 384
Estimated Location [km]	.4146221	95.97788	192.0000	288.0737	383.5854
% Error	.1079745	-5.76 E-03	.00000000	1.920 E-02	-.1079798

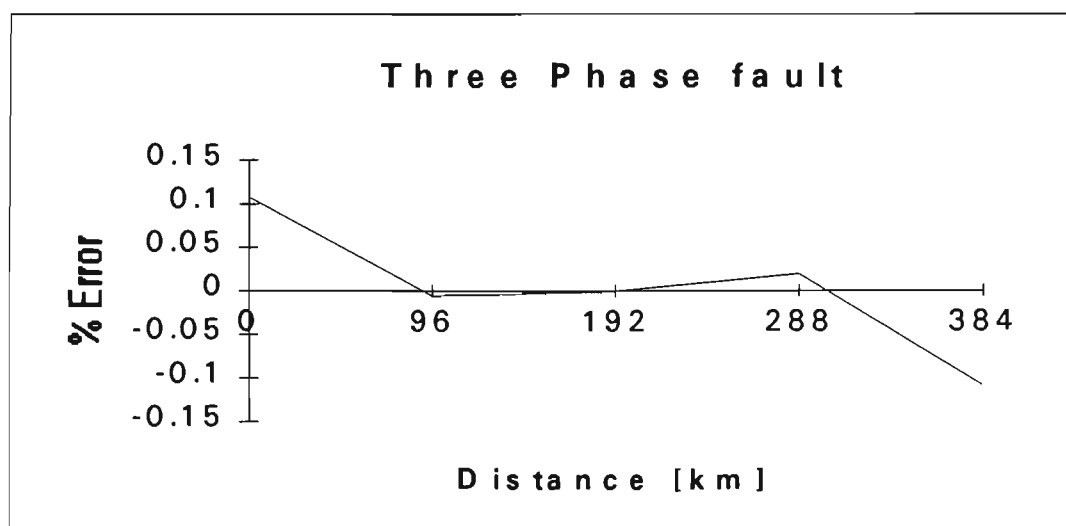


Fig. 9.1: Three phase to ground fault on 500 kV Transmission line

9.3.2 Single Phase to Ground Faults

For the two terminal two terminal power system, a single phase - to - ground fault on phase A has been applied at different locations of the EHV transmission line. The results obtained from the fault location algorithm for estimating the distance to fault are given in Table 9.3, which are shown in graphical form in Fig. 9.2. For this type of fault, higher accuracy is attained, particularly at the line termination (2.4%).

Table 9.3: Single Phase - to - Ground Fault.

mode	L = 0 km	L = 96 km	L=192 km	L=288 km	L=384 km
1	8.844460	100.0760	192.0000	283.9240	375.1555
2	16.44095	104.6801	192.0000	279.3199	367.5591
3	.4068660	95.78867	192.0000	288.2113	383.5931

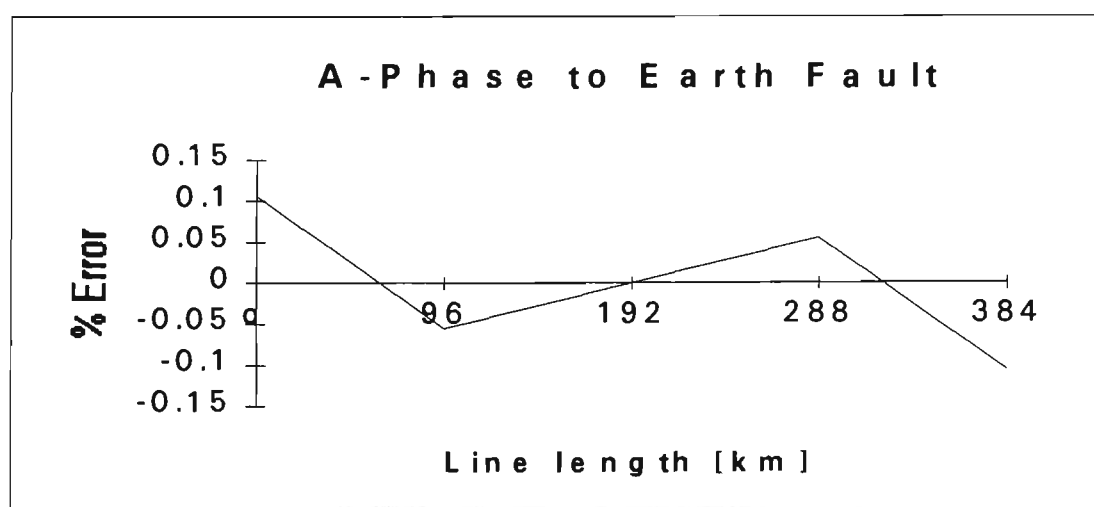


Fig. 9.2: Single Phase to ground fault on 500 kV Transmission Line

9.3.3 Phase to Phase to Ground faults

For double phase faults (AB-G Faults), the fault was applied at five different locations on the transmission line. The results of this test are given in Table 9.4, and in graphical form in Fig. 9.3.

Table 9.4: AB-G Faults on Two Terminal System

Mode	L = 0 km	L = 96 km	L=192 km	L=288 km	L=384 km
1	-1.736E-7	99.79424	192.0000	284.2057	375.1571
2	-1.269E-6	31.10125	192.0000	352.8987	370.7007
3	3.369E-8	95.97480	192.0000	288.0252	383.5866

% Error	8.773E-9	-6.562E-3	0.00000	6.564E-3	-1.07654

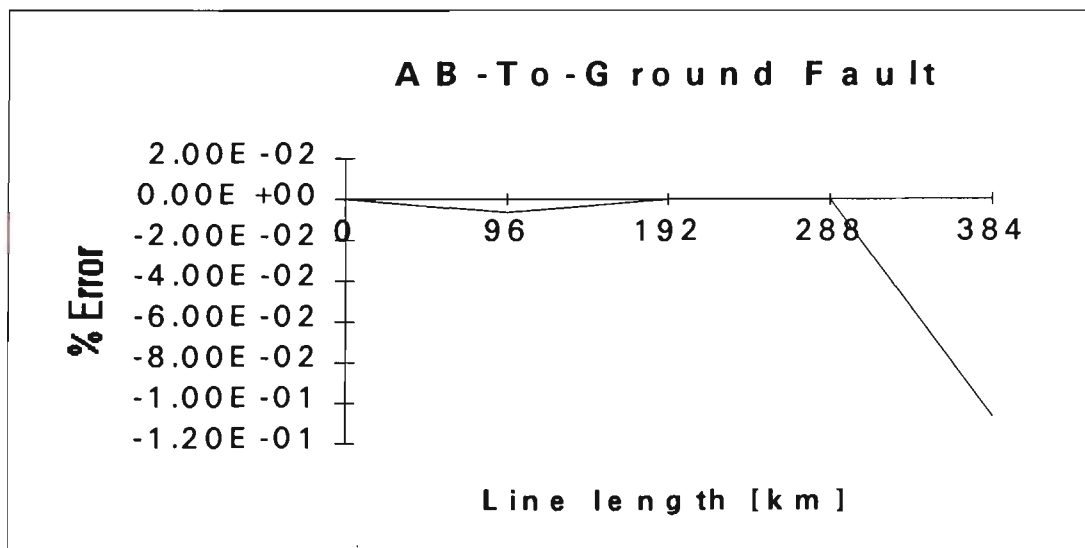


Fig. 9.3: Phase - to - Phase - to - Ground Faults

9.3.4 Phase-to-Phase Faults (AB Faults)

In case of double phase faults (AB faults), the fault had been applied on the transmission line at five locations as shown in Table 9.5, and given in Fig. 9.4

Table 9.5: Phase-To-Phase Faults (AB Faults).

Mode	L = 0 km	L=96 km	L=192 km	L=288 km	L=384 km
1	407.6157	-648.3021	192.0000	188.6240	114.2762
2	205.8558	572.5399	192.0000	190.5143	163.5875
3	.4127154	95.92381	192.0000	288.0254	383.5875

% Error	.1074780	-1.98E-02	.0000000	6.62E-03	-.1074155
---------	----------	-----------	----------	----------	-----------

As it is clearly shown in the results given in Table 9.5, since the fault involves phases A and B, the earth mode is irrelevant. These results are shown in Fig. 9.4.

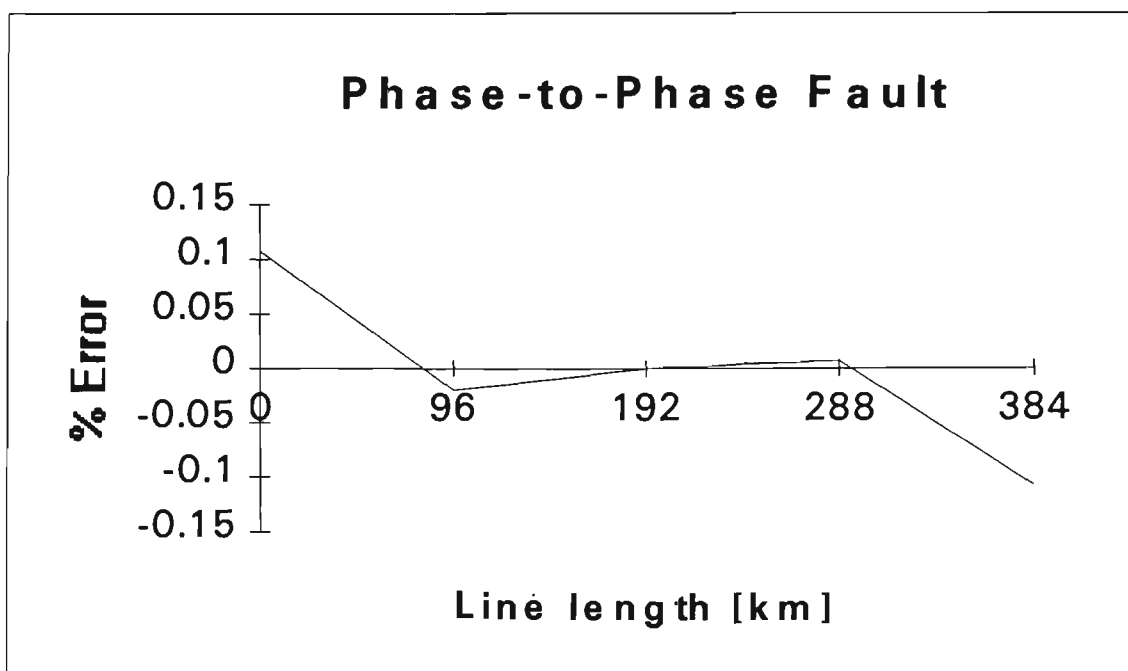


Fig. 9.4: Phase-To-Phase Faults (AB Faults) on Transmission Line

9.3.5 Compensated System

For a 75% shunt compensation of the 384 km transmission line used in the above studies, a three phase to ground fault was applied at the sending end of the line as an example which is shown in Table 9.6. It is clearly shown that the fault location algorithm gives accurate results even when the line is 75% compensated. The results of the compensated and uncompensated systems for other fault locations indicate that much less effect compensation has on the accuracy of fault location estimation, when the fault further away from line terminations.

In case of other types of faults, the impact of line compensation on the accuracy of fault location estimation is very little.

Table 9.6: Three Phase Faults on Compensated System .

Mode	Uncompensated System, Fault at L=0 km	Compensated System, Fault at L= 0 km
1	20.97658	105.7043
2	16.44321	15.06288
3	.4146221	1.757946
% Error (Mode 3)	.1079745	.4577985

9.3.6 Effect of Fault Impedance

Most of the faults on EHV transmission lines are accompanied with some sort of arcing before they develop into a proper short circuit. An approximate

representation of the arcing fault impedance would be in the form of a simple arcing resistance. This approach was undertaken in this work. However, for more accurate representation of arcing impedance, a non linear modelling could be used. From the graph given in Fig. 9.5, it is clear that there is a little effect on the accuracy of the fault location when the fault resistance was varied from 0 to 400 Ohms, under A - Phase to Ground Fault conditions.

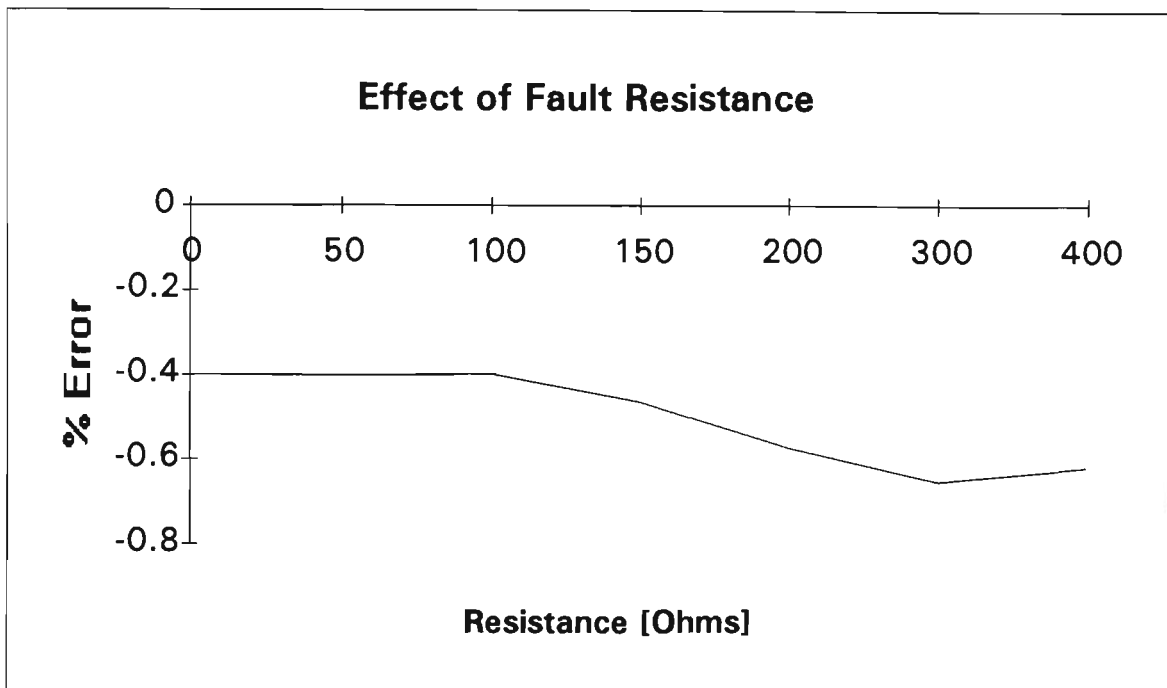


Fig. 9.5: Effect of Fault Resistance Variations on Accuracy

9.3.7 Prefault Loading of the Line

The control of active power and reactive power flow in the line depends on the relative phase shift and the magnitude of the voltages at the sending and receiving ends of the line. In order to simulate a power flow from system A to system B of Fig. 8.1, it was assumed that the three phase voltages of system A lead the corresponding three voltages of system B by 10 degrees. Under such conditions, the power will flow in the transmission line from A into B. A three

phase fault was applied at the sending end of the line (system A). The results of such study are given in Table 9.7.

Table 9.7: Prefault Line Loading Effect.

Mode	Without Prefault Loading	With Prefault Loading
1	20.97658	20.01752
2	16.44321	16.29909
3	.4146221	.4569117
% Error	.1079745	.1189874

9.3.8 Untransposed Lines

For untransposed EHV transmission line, a three phase to ground fault was applied at five locations, the results of which are given in Table 9.8, and shown in Fig. 9.6. The algorithm gives shows very good accuracy particularly as faults get further away from the transmission line terminations.

Table 9.8: Untransposed Transmission Line.

Mode	L = 0 km	L=96 km	L=192 km	L=288 km	L=384 km
1	-57.44538	102.8918	192.0000	281.1082	441.4454
2	30.60967	106.2928	192.0000	277.7072	353.3903
3	.3905597	95.63166	192.0000	288.3835	384.5440
% Error	-.101708	.095921	0.00000	-.099869	-.141666

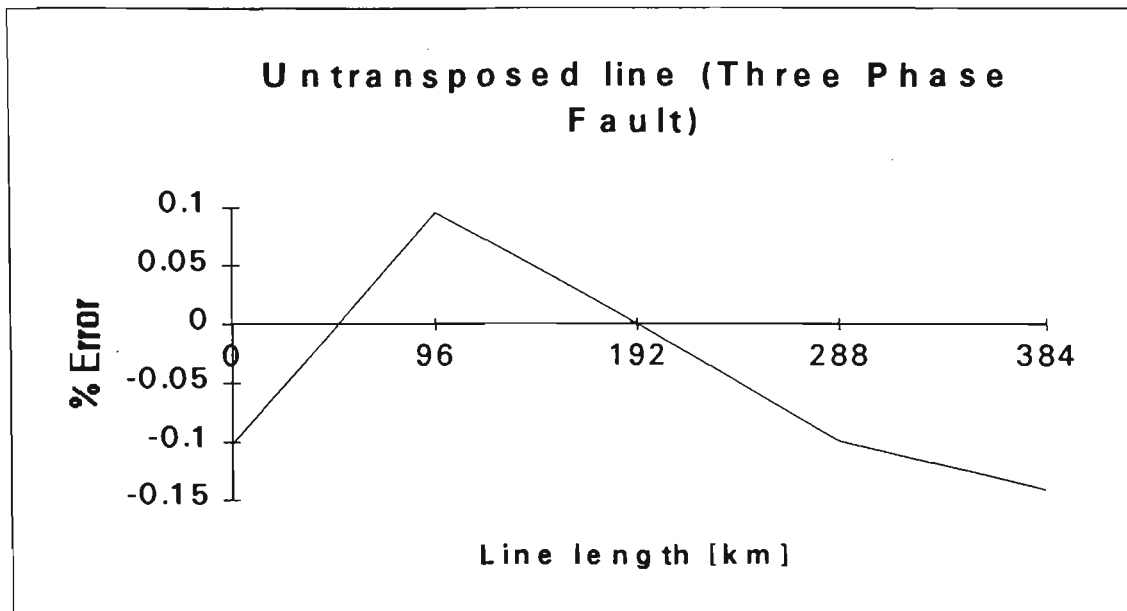


Fig. 9.6: Untransposed Transmission Line

9.3.9 Remote Source Impedance Variations

In practice, the remote source impedance variations could be a major source of error, as they may change due to different normal and abnormal switching of lines or generators. A distinct feature of these techniques is that the algorithms are free of any effect of such variations. A single phase to ground fault is applied at the end of the 96 km line for different levels of source B capacities, ranging from 0 to 35 GVA. The results of these tests are shown in Fig. 9.7.

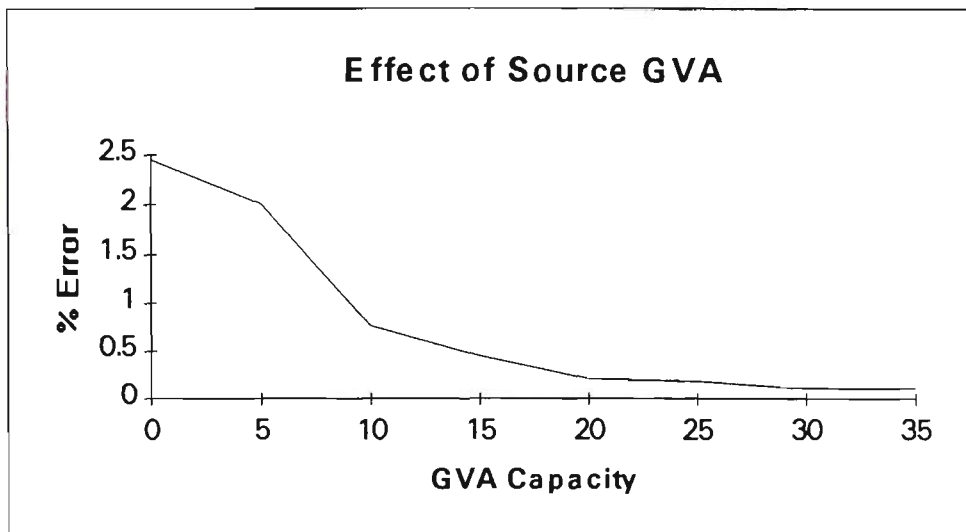


Fig. 9.7: Effect of Source Capacity Variations

9.4 THREE TERMINAL SYSTEM

The developed fault location algorithms described in chapter 7 is applied for a three terminal feeder as shown in Fig. 7.2, where the three tee feeder is comprised of three transmission lines, 192 km length each. The three ends are referred to as P, R and Q for the sending, receiving and tee feeder ends respectively. For the assessment of the accuracy of the algorithm, faults are applied at different location on the transmission line, and the estimated locations are compared with the actual locations. It was found that a very good accuracy is obtained, and exact location is obtained for fault at the tee junction of the system, and when the fault is further away from the three terminations of the system, the accuracy is improved. It is noticed that the error is negligible at the middle of each feeder.

As an example, a two-phase fault free of earth is shown in Table 9.9, where on each feeder of the teed system three locations were tested, at the sending end, at the middle and at the end of the section. Very accurate estimations were found for all tests, i.e. below .2% of the feeder length.

9.4.1 Phase to Phase faults

The transmission circuits were energised from three phase identical sources as follows (Fig. 9.8):

- *Sending End:*

$$E_{SA} = E_m \cos(\omega t) \quad (9.1)$$

$$E_{SB} = E_m \cos(\omega t + 240^\circ) \quad (9.2)$$

$$E_{SC} = E_m \cos(\omega t + 120^\circ) \quad (9.3)$$

- *Receiving End:*

$$E_{RA} = E_m \cos(\omega t) \quad (9.4)$$

$$E_{RB} = E_m \cos(\omega t + 240^\circ) \quad (9.5)$$

$$E_{RC} = E_m \cos(\omega t + 120^\circ) \quad (9.6)$$

- *Teed (Q) End:*

$$E_{QA} = E_m \cos(\omega t) \quad (9.7)$$

$$E_{QB} = E_m \cos(\omega t + 240^\circ) \quad (9.8)$$

$$E_{QC} = E_m \cos(\omega t + 120^\circ) \quad (9.9)$$

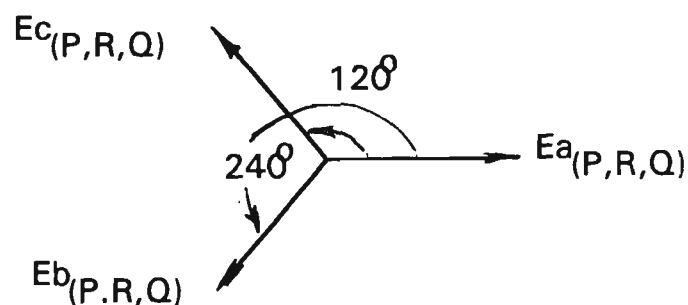


Fig. 9.8: Phasor Diagram of the Three - Phase Voltages at the Three Ends P, R and Q of the Three Terminals

The strength of each source was assumed = 35 GVA, from which the source impedance was calculated for each end. The results for these tests are given in

Table 9.10, for phase-to- phase (AB) faults applied on each feeder at three locations, ie, sending end, in the middle and at the receiving end for each particular feeder.

Results of three phase faults estimations at different locations indicate a very high accuracy, which in most cases was below 0.2%. It was noticed that when the fault occurs at the tee junction, the accuracy of the fault location algorithm is the best. In actual fact the exact distance was obtained when measured at any of the three feeder ends, ie, P, R and Q ends respectively.

The fault which gives higher error is the one which is close to any of the three ends, where the fault location algorithm estimate derived at the end which is closer to the fault is found with an error of about 0.2%.

Table 9.9: **Two Phase (AB) Faults.**

Mode	L = 0 km	L = 96 km	L = 192 km	Measured From
1	238.2782	194.5363	192.0000	S End
2	210.3203	193.1213	192.0000	S End
3	.3797687	95.88115	192.0000	S End
1	238.2782	194.5363	192.0000	R End
2	210.3203	193.1213	192.0000	R End
3	.3797687	95.88115	192.0000	R End
1	238.2782	194.5363	192.0000	Q End
2	210.3203	193.1213	192.0000	Q End
3	.379687	95.88115	192.0000	Q End

% Error	.1977962	-6.19014E-2	0.00000	S End
% Error	.1977962	-6.19014E-2	0.00000	R End
% Error	.1977962	-6.190314E-2	0.00000	Q End

As indicated in Table 9.9, in case of three terminal EHV transmission systems involving teed feeders, when a fault occurs on any section of a particular feeder, from the voltage indication, the appropriate end closer to the fault will give the correct estimation. Since there is hardly any signal through the earth, the earth mode can be neglected. It is noticed that the aerial mode 3 gives the most accurate results for the fault location estimation.

9.5 EFFECT OF POINT ON WAVE

In order to test the sensitivity of the estimation of distance to fault, a two phase fault was chosen (AB Fault), which is applied at different equal intervals on the EHV transmission line, ie, at 0, 96, 192, 288 and 384 kms. The two terminal system was chosen to have equal sources strength at both side of the transmission circuit, each defined by its fault MVA = 35 GVA. The transmission line is the same as above, ie horizontal configuration with two earth wires. The results of such a test are given in Table 9.10.

From the table, it is clear that the accuracy of the fault estimation along the entire feeder has not changed significantly, as compared with the data given in Table 9.5 above. In fact for some faults, the accuracy under such an angle (45°) is slightly reduced.

For proper comparison of the results for 0° and 45° , a graphical representation is given in Fig. 9.9, for faults at the same locations along the EHV transmission line.

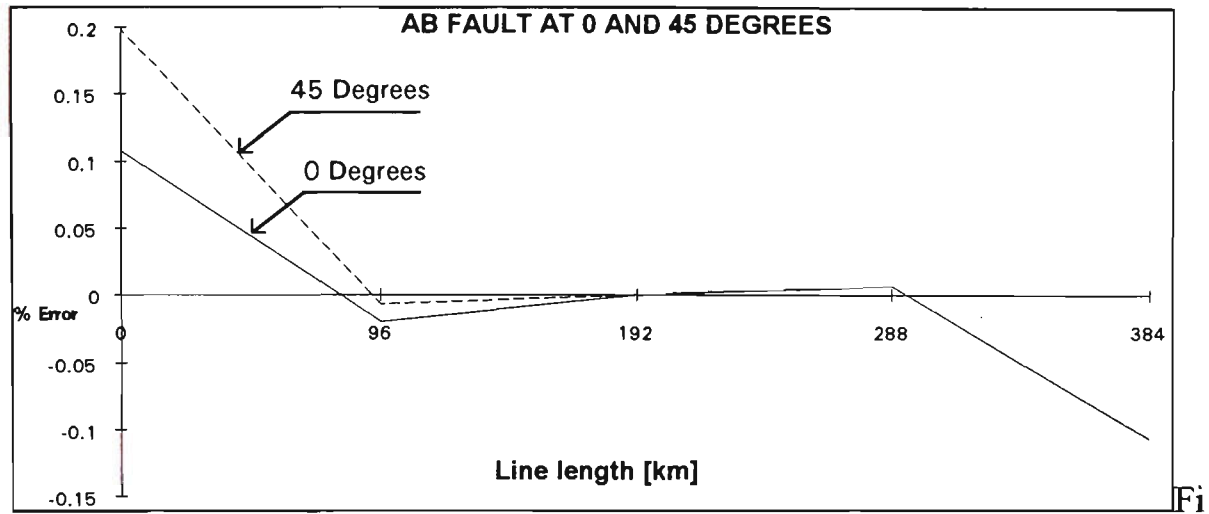


Fig. 9.9: Two Phase (AB) Fault at 0 and 45 Degrees

Table 9.10: AB Fault for 45° Advancement of Voltage Signals.

Mode	L = 0 km	L=96 km	L=192 km	L=288 km	L=384 km
1	238.2782	195.3738	192.0000	188.6261	14.16582
2	210.3202	193.4857	192.0000	190.5143	251.6388
3	.3797687	95.97459	192.0000	288.0254	383.5897

% Error, 0 Degrees	.1074780	-.0198424	0.00000	.00662009	-.1074155
% Error, 45 Degrees	.1977962	-.0066161	.000000	.00662009	-.1068513

The sources at both ends will have the following functions:

- *Sending End S:*

$$E_{SA} = E_m \cos(\omega t + 45) \quad (9.10)$$

$$E_{SB} = E_m \cos(\omega t + 285) \quad (9.11)$$

$$E_{SC} = E_m \cos(\omega t + 165) \quad (9.12)$$

- *Receiving End R:*

$$E_{RA} = E_m \cos(\omega t) \quad (9.13)$$

$$E_{RB} = E_m \cos(\omega t + 240) \quad (9.14)$$

$$E_{RC} = E_m \cos(\omega t + 120) \quad (9.15)$$

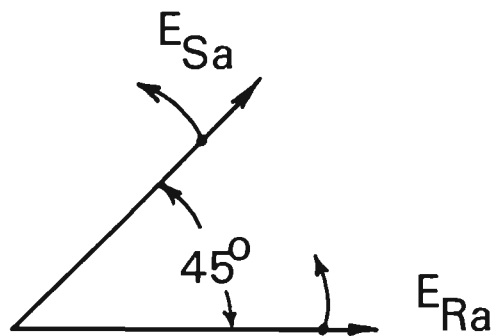


Fig. 9.10: Phase Shift between S and R Ends of 45°

The calculated estimations for faults at the termination of the transmission lines were found the least accurate. This is mainly due to the fact that when the fault is at these terminations, the voltage measured at the fault is nearly equal to zero. Since the algorithm computes the fault location using voltage and current phasors at all terminations, it is therefore expected to have difficulty in estimating these locations for voltage phasors near to zero values. This situation arises when the length of the line equal to zero kms or full length. This could be overcome using some memory action as it is known in distance relays. Such investigations were not studied in details and left for future work.

Chapter 10

CONCLUSIONS AND FUTURE WORK

10.1 INTRODUCTION

In order to be able to transport energy from the generation centres to the load location, modern power systems are interconnected using EHV transmission lines. The design of these lines depends on the power they carry, and they represent that part of the power system, which is exposed to public, and therefore could no longer be separated from their influence. The environmental impact of EHV transmission lines is regarded as one of the important aspects affecting the method and routing of transmission lines. The effect of the electric and magnetic fields radiated from EHV transmission lines is being studied extensively, because of the extra awareness of the public to such issues. There is no concrete scientific evidence so far about the effect of such fields on human and animals. These issues are not investigated in this work, since they are outside the scope of this research.

This thesis has extensively analysed the performance of the EHV transmission lines under steady state and transient conditions, using the modern theory of transmission lines for different objectives. These studies were conducted in order to study and investigate the behaviour of the power transmission lines, before, during and after the faults, with one clear focus in mind, ie, the development, testing and assessing a highly accurate methods for estimating the exact location of these faults on these lines. In conducting such analysis, the objective has been to use mathematical models, to develop algorithms for accurately locating the distance to fault on power lines, so that the energy could

be restored as soon as possible after fault clearance, which improves services to customers by the utilities, and could have significant economic benefits.

10.2 GENERAL CONCLUSIONS

1. From the comprehensive analysis of the literature, it was evident, that there is a need for the development of accurate methods for estimating the distance to fault on EHV transmission lines. This was mainly due to the fact, that existing fault location methods are based on some assumptions which reduce the accuracy of estimating the exact location of the fault on transmission lines. Loss of accuracy in the existing schemes is mainly due to non linearity of fault impedance, effect of the remote infeeds, non-transposition of conductors, neglect of shunt capacitance, the dependence on the change in power system source configuration, and the fact that there is a need for measuring current and voltage signals from conventional transducers.
2. In the early stages of this research, it was established that in order to develop a fault location algorithm free from the effects of the above mentioned factors, the new scheme has to use travelling wave techniques using modal analysis based on the frequency variance of the system parameters, where digital signal processing can be used. The non-transposition of the transmission line conductors should be taken into consideration, including the effect of shunt elements. The non linearity of fault impedance should not affect the measurement, and the source impedance variations should not affect the accuracy of estimation. The new scheme should be free from the effect of the remote source infeed.
3. The thesis has thoroughly investigated the theory and analysed in details

the behaviour of the transmission line under different conditions. By investigating the performance of the polyphase multi conductor transmission lines, accurate methods for calculating transmission line parameters, based on the early work by Galloway et. al.(12), these include the basic per unit length series and shunt impedance matrices, the positive, negative and zero sequence impedances, the propagation parameters (the characteristic impedance, natural modes of propagation and their attenuation and velocity), and the exact π - network of line sections.

4. In developing the computer program for calculating the transmission line parameters, the following practical considerations were taken into account: conductor stranding and the skin effects in them; variable current penetration return path with finite conductivity and its contribution parameters as given by Carson (1); proximity of aerial earth wires; mutual coupling of second circuit on the tower or nearby circuits and unsymmetrical conductor placing at different hight on the same tower with and without transposition
5. The behaviour of transmission lines under steady state conditions was carried out for a simple configuration first, based on the theory of travelling wave, and the solution of the wave equation for a single conductor system, which is developed to analyse a complicated multi - phase multi conductor system. All analysis are developed in general form based on matrix algebra.
6. When Fourier Transform is used, the final product becomes one of solving the steady - wave equation at a range of frequencies. Due to the

multiplicity of conductors in a power transmission system, the solution of the resultant simultaneous differential equations, which are independent, becomes very complex. Consequently, the steady-state properties of transmission lines are obtained using the method of modal analysis (Appendix A1).

7. The solution of the wave equation at the power frequency provides all system parameters in the steady-state condition. Therefore, the faulty transmission line is represented in a series of cascaded sections before and after the fault. The digital simulation was based on expressing the relationships between the two sides of the first two port networks to the fault through the transfer matrix of the section constants. The output of the first section was related to the receiving end parameters through the transfer matrix of constants representing the second section.
8. For long transmission lines, discrete transposition of conductors is performed at the termination of each section or at intermediate points there in. These discrete transpositions must be modelled because they represent points of abrupt electrical discontinuity. Due to conductor swapping, transmission lines are joined to a section with different characteristic impedance. Therefore, partial reflection of the incident travelling wave components can occur at these points. For untransposed lines, this requires a simple matrix multiplications, and for transposed lines, it is important to consider the reorientation of conductors, which can be achieved by using a transposition matrix as explained in chapter 3

9. Because of the emphasis on the transmission lines in this research, the source representation used in all studies was a simple infinite busbar represented in form of a constant 500 kV voltage behind a constant source impedance. This representation included the mutual coupling between conductors of different phases. Such representation was used for both two and three terminal systems. To facilitate different loading conditions for the transmission line, the phase angle of each source can be controlled to change the power flow in the line.

10. In designing the shunt reactors for the transmission line, for a 75% compensation for the positive phase sequence; $h_1 = 0.75$, the zero sequence compensation factor h_0 is calculated to be = 0.6185, for the 4 legged reactor used in all studies involving shunt compensation.

Shunt compensated transmission lines behaviour was investigated extensively, including the effect of such compensation on the fault location algorithm. It was found from the studies conducted, that the accuracy of estimation of fault location on shunt compensated lines is only slightly affected. However, from the studies conducted on shunt compensated systems using digital simulation methods, high accuracy was obtained. This finding was confirmed by the results presented in chapter 9.

11. The fault location algorithm developed for a single phase transmission line is extended to three-phase multi conductor, polyphase transmission lines using the theory of modal analysis, which involves basically finding the matrix eigenvectors of the $[Z].[Y]$ product ($[Q]$), and the $[Y].[Z]$ product ($[S]$). By using this technique, the voltages and currents derived

from each phase A, B, and C at each end of the line, are transformed to corresponding modal voltage and current quantities 1, 2 and 3 by means of the corresponding [Q] and [S] eigenvectors matrices, as explained in details in chapter 5.

12. Shunt reactors, which are used to control the amount of reactive power generated by the transmission line, when the line is lightly loaded or open from one end, have little effect on the accuracy of the fault location technique developed in chapter 5. The consequence of the shunt reactors connected at both the ends of the transmission line, for the two terminal EHV system, was found to have some effect on the equivalent impedance of the sources at both sides. From all tests carried out on the fault location algorithms for two and three terminal systems, it was found that variation of source impedance has very little effect on the accuracy of estimation of the distance to fault. The results of tests carried out in chapter 9, and the theory derived in chapter 6 for the two terminal system confirmed this finding. It must be stated that there is a scope for further investigations of this problem, which will be discussed in the section for future work. Analyses were carried out for the 4 legged reactor scheme, which was investigated for 75% compensation for the positive phase sequence resulting in the zero phase sequence compensation of 61.85%, as explained in chapter 4.
13. The algorithm developed for three terminal system was found to be very accurate, particularly for faults near the tee point of the system. In order to evaluate the fault location on any part of the three terminal system, information about the voltage and current phasors at the three ends are processed. For this purpose, in actual schemes, some type of

synchronisation is required. Any mismatch in the measured data at the three ends would be seen in the phase angle of the sampled data, which can be corrected by shifting the data at the unsynchronised ends few samples until the errors due to sampling are minimised.

The faulty leg is defined by using a comparison procedure of the three voltages at the three ends of the three terminal system. From the measured voltages, it is possible to establish the faulty section by comparing each time and evaluating the relationship between the sampled data. For a fault, say near the sending end, the voltage at other two ends will be very similar, whereas, the voltage at the sending end will be different. When there no significant difference between the voltages of the three ends, it can be assumed that the fault is practically at the tee point itself.

14. To design a proper protection criteria for a high speed protection system based on digital and microprocessor principles, and to construct a modern fault locator for estimating the distance to faults on transmission lines, a detailed knowledge of the behaviour of transmission lines under transient conditions is required. In order to have a comprehensive picture about all possible faults on transmission lines, a number of studies were conducted on the 500 kV transmission line of 384 km length. Such studies involved applications of balanced and unbalanced faults on the line, where the whole system was represented in three phase form.

Dynamic response of the power system showing the transient waveforms at different locations was obtained and presented fully in chapter 8. Such valuable information would assist design engineers to construct highly accurate relays and fault locators, which will employ modern digital

technology and microprocessors in their design. Understanding the behaviour of the primary system, including the high frequency components superimposed on the power frequency signals, will lead to more realistic precision equipment, which are capable to react and operate on signals other than the conventional power frequency signals used in the current technology.

The analysis of voltage and current waveforms under different fault conditions are given in chapter 8. These analysis clearly indicate the presence of very distorted waveforms, which are the main source of causing delays and sometimes wrong operation and inaccurate measurement, due to these signals. The existing technology is based on operation criteria based on purely sinusoidal and power frequency signals. The studies shown in chapter 8 indicate that the disturbance caused by the faulty conductors propagates to the sound conductors, due to the mutual coupling of the three phases. Such a situation, where the faulty and sound phases possess highly distorted signals, must be taken seriously in designing the future protection, measurement, instrumentation and control equipment. The studies given in chapter 8 would be valuable for such designs.

10.3 TESTING AND ASSESSMENT

The developed fault location algorithms were subjected to a very comprehensive testing procedure, in order to reveal and assess the accuracy of the methods proposed in this work. The results of such tests are given in chapter 10, where each proposed scheme was tested under the following fault conditions:

- Single Phase to Ground Faults (A - G)

- Double Phase to Ground Faults (AB - G)
- Double Phase Free of Earth Faults (AB)
- Three Phase to Ground Faults (ABC - G)

For all the above faults, the location of the fault on the EHV transmission line was assumed at $L = 0, 96, 192, 288$ and 384 kms respectively. From the results shown in chapter 9, it was found that the fault location algorithms developed in chapters 5 and 7 for two and three terminal systems respectively, are very accurate. It was revealed that the greatest inaccuracy of approximately 0.2% of the total line lengths (few hundreds of meters) occurs under close up faults (close to line terminations). As the faults occur further away from line terminations, the accuracy becomes extremely high. At a fault 96 km from the sending end, the third mode measurement indicated a very highly accurate estimate of the fault location (in most cases few tens of meters from the exact actual location).

The detailed analysis of the results from the tests conducted in chapter 9 were carried out to assess the behaviour of the developed algorithms for the following conditions:

- The effect of line transposition
- The effect of fault impedance
- The effect of prefault loading of the line
- The effect of point on wave of fault inception
- The effect of remote source infeed
- The effect of variations in the source impedance
- The effect of line shunt compensation
- The effect of different types of faults
- The effect of the fault location along the line

The above conditions are analysed in detail in chapter 9. The results were carried out in details for the two terminal systems, and for some conditions, the studies were conducted on the three terminal teed feeder systems. The results shown in chapter 9 indicate that the algorithms for both two and three terminal EHV systems, give very accurate results. It must be emphasised that the most accurate results were obtained in all cases from the measurements based on the mode 3 results. It is clear, that even earth faults, which excite all three modes, mode 3 gave the best and the most accurate results.

In all studies conducted on two and three terminal systems, the faults near the middle of the transmission line gave extremely accurate estimations (few meters different from the actual fault location). In fact for a fault exactly at the middle of the line for two terminal systems, and at the tee point of three equal teed feeders, gave in all studies under all fault conditions mentioned above, a distance equal exactly to the actual fault location (ie a zero error). This result was consistent in all studies, which one may expect, since faults in the middle of the line will have equal and opposite effect caused by currents and voltages of the two ends of the line.

In observing the signals required for the fault location algorithm, ie, voltage and current phasors for both the sending and receiving ends of the line, the values were found exactly equal for the two terminal systems. In case of three terminal systems, when all three teed feeders are equal in length, the fault at the tee point caused exactly equal values for the sending end S, receiving end R and the Q end of the teed feeder. This in turn caused a similar effect caused by the flow of currents in the line, which assist the estimation procedure, because of the way signals are processed. In fact, for all cases tested for the three terminal systems, the accuracy of estimation was below 0.3%, and as the fault

approaches the tee point, this error diminished gradually, and completely disappeared for faults at the tee point (for equal teed feeders). The error at this point (tee point) was found to be 0.0% in all studies.

10.4 FUTURE WORK

The investigations carried out in this thesis on the development of accurate algorithms for the estimation of fault location on EHV transmission have involved detailed analysis of the theory of transmission lines, steady-state and transient response of the systems under consideration, analysis of the natural modes in transmission lines, and their use to calculate the fault location on the lines studied, development and application of matrix algebra in all formulations of system parameters, and the development of a several computer programs.

These include: a program for calculating transmission line parameters, a program for modal analysis, and a program for the two terminal EHV transmission line simulation, and a program for the three terminal system. This required the development of a large number of special subroutines for calculating eigenvalues and eigenvectors and matrix manipulations. In addition to all this the use of the EMTP program (the ATP, which is the PC version) has been very useful for the transient studies presented in chapter 9.

Apart from the studies described above, there are some interesting problems which could well complement this research. Hence, it is proposed that the future research should continue in this field in the following areas:

- The effect of series compensation on the accuracy of distance to fault estimation
- The effect of parallel lines on the fault location algorithm

- The study of teed feeders of different lengths
- The effect of different line configurations and constructions on the accuracy of estimation of fault locations
- The effect of open conductor faults on the accuracy of fault location estimation
- Analysis of fault location algorithms with various prefault loading of the transmission line
- Investigate the behaviour of the developed algorithms under non linear fault impedance conditions
- Investigate why the developed algorithms are less accurate at the terminations of the lines. Suggest a solution for improving the accuracy under such conditions

One of the important features which will be based on the work presented in this thesis, would be naturally the actual design and construction of the fault locators for the two and three terminal systems. The development of a digital scheme for a modern fault locator will be an ultimate aim of the research program, for which this thesis has laid a solid foundation. The work will require detailed signal processing based on the modern digital technology and the use of microprocessors. There is a strong link between the work presented in this thesis, and the work proposed for future research and good customer services. There is nothing more efficient and satisfying for the utility engineers than to be able to restore power supply to customers as soon as possible.

There are other implications of such quick power restoration related to maintaining system stability, when the system is able to operate according to the designed schedule, particularly maintaining the transmission links for normal and emergency power flow between interconnected power systems. The quicker the restoration of transmission lines is, the higher the probability

of gaining system stability. This could be achieved only when fault locators are capable of estimating the distance to fault as accurately as possible. With the schemes developed and tested in this thesis, it seems that this task is a quite feasible one.

Appendix A1

MODAL ANALYSIS AND WAVE PROPAGATION

A1-1 INTRODUCTION

In order to study the wave propagation phenomena on HV and EHV transmission lines, modal analysis theory has been used, particularly for surges and power line carrier (PLC) evaluations. One of the difficulties in the analysis is evaluation of series earth-return impedance of the line. Traditionally, Carson⁽¹⁾, series have been employed for the computation of these parameter⁽¹²⁾. The evaluation of eigenvectors of the ZY matrix in three-phase lines with centre-phase symmetry was given by Wedepohl⁽¹⁰⁾, together with the development of the theory of natural modes as applied to the polyphase transmission lines.

In this chapter, matrix analysis is described for voltage and current propagation along a conductor system above an imperfectly conducting ground. The theory used here is based on basic matrix algebra, when square matrices and their functions are considered as operators in a vector space. The transmission lines conductor voltages and currents are presented as vectors which are resolved into modes or eigenvectors of the propagation matrix. It will be shown that in spite of the fact that modal transformation is not power invariant, the modes are independent but not orthogonal⁽¹⁰⁾.

It is possible to describe modal signals on a multi conductor system as constant frequency signals which propagate without distortion. These signals propagate usually with a single attenuation (α) and phase shift (β). Over the last fifty years, the theory of modal analysis and natural modes has been successfully

applied to fault analysis⁽³⁷⁾, carrier current propagation (110,111), radio noise performance of transmission lines (113), power line carrier communication (4), fault location⁽⁶⁰⁾, switching of unloaded lines (22), and recovery voltages on circuit breakers⁽²⁰⁾, and many other applications in communication theory and power system.

The behaviour of a multi conductor system may be described by resolving the phase voltage and currents into incident and reflected component waves. These are the so-called natural modes of the transmission system and are functions only of its basic parameters (11). The proportions in which they occur are determined by applying the appropriate boundary conditions (10). Current and voltage signals on a three-phase power line may be considered to propagate simultaneously in three natural modes, in a manner similar to symmetrical components. Each mode is characterised by its own specific impedance, attenuation, and constant ratios of phase voltages and currents. The actual voltage and current on each phase at any point on the line are the sums of the three mode voltages and mode currents at that point respectively. These modes, numbered in sequence of increasing impedance (114), are:

- Mode 1:** Currents flow in the same direction in all three phases, returning through the ground. Mode 1 has the highest attenuation due to ground return.
- Mode 2:** Currents flow in opposite directions in the two outer phases, the centre phase taking no part in the propagation. Attenuation is higher than for mode 3.

Mode 3: The current in the centre phase has approximately twice the magnitude of that in the two outer phases, and flows in the opposite direction. Mode 3 has the lowest attenuation.

Only the mode 3 component will arrive at the end of a long transmission line section, the mode 1 and mode 2 components being almost completely attenuated along the way. The illustration of these three modes is given in Fig A1.1, where the flow and direction of all three modes of the current in all three conductors and the ground return are shown.

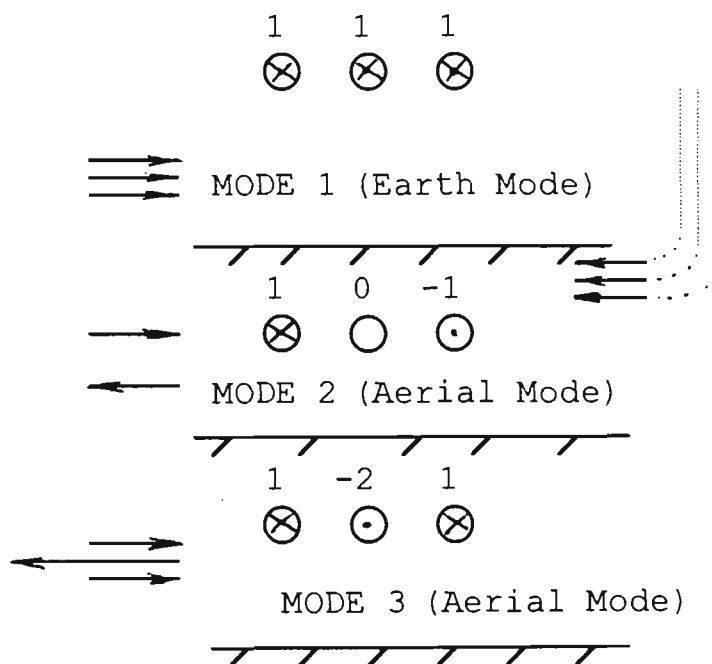


Fig. A1.1: Modal Current Illustrations

In general terms, the objectives of modal analysis (114, 115) are to find

- modal propagation constants;
- voltage and current modal matrices;
- characteristic impedance matrix $[Z]$;
- reflection free termination network;
- modal uncoupled reflection free termination network.

From the modal analysis, properties of modal transformations are deduced⁽¹¹⁰⁾. Such analysis shows that when earth correction terms are used in the description of the transmission line, the propagation constant matrix can be used to determine the modal transformations. Also in reference 110, it is shown that to evaluate the phase quantity results numerically, it is necessary to perform a modal (eigenvalue) transformation.

Modal signals on multi conductor lines are most simply defined as constant frequency signals which propagate without distortion. This concept is very useful in analysing travelling wave and carrier current propagation, as well as radio-noise performance of transmission lines ⁽¹¹³⁾.

A1-2 MODAL ANALYSIS PROPERTIES

The initial work with modal analysis in radio-noise design calculations of transmission lines was performed by Adams⁽¹⁰⁹⁾, using transmission line constants calculated for a perfect earth, which simulated an earth with infinite conductivity. It has been described by Hedman⁽¹¹⁰⁾, that the following properties apply to modal analysis:

- (1) Modal transformation matrices can be developed from the propagation constant matrix when earth connection terms are incorporated in the description of transmission line constants.
- (2) When a lossless earth is assumed, the propagation constant matrix is diagonal and cannot be used to determine modal transformation.

- (3) The voltage and current propagation constant matrices in phase quantities are transposed and the voltage and the current modal propagation constants are equal.
- (4) The current and voltage modal transformation obtained from the complex propagation constant matrix are related by the equation $[L_i] = [L_e]$ where L_i and L_e are the modal propagation constants of current and voltage respectively.
- (5) Modal transformations obtained from the complex propagation matrix are orthogonal.
- (6) Analysis of multi - phase propagation in phase quantities requires a modal analysis to numerically evaluate the results.

It is known that when analysing the propagation problem, a system is specified in terms of self and mutual impedances and capacitances. These constants are then used in transmission line equations, which are solved to produce the desired results as explained in reference 10.

Carson (112) points out that, while this technique is rigorously valid only if perfect conductors are embedded in a perfect dielectric, it nevertheless specifies a system which is accurate to a high degree of approximation imperfect conductors and dielectric in a system which could be employed for efficient transmission of electric energy.

A1-3 INFINITE TRANSMISSION LINES ANALYSIS

In order to understand the physical phenomena relevant to the theory of natural modes, one must first analyse the problem completely in terms of phase quantities, from which modal transformation is developed.

A1-3.1 Phase Quantities Analysis

Generally, when analysing coupled systems, the tendency is to proceed at the earliest possible point to a transformation which will simplify the final numerical solution. Such attitude may lead to loss of physical insight into certain aspects of the problem.

The analysis given in reference 10 are general in that the R, L, G, and C matrices can include all system parameters as well as earth connection terms. A Fourier Transform converts partial-differential equations into ordinary differential equations valid at a constant frequency. An exponential form of solution is assumed, but it is shown to be an actual one when the assumed form is substituted into differential equations and the propagation constants of the assumed form are equated to parameters of the differential equations. The differential equations are completely solved by satisfying boundary conditions in the standard manner, i.e.,

$$[\lambda_e] = \sqrt{Z(w)Y(w)} \quad \text{A1.1}$$

$$[\lambda_i] = \sqrt{Y(w)Z(w)} \quad \text{A1.2}$$

It is clear that in the propagation constants for current $[\lambda_i]$ and voltage $[\lambda_e]$, the difference is determined by the order of multiplication of Z and Y matrices.

For the case when the Z and Y matrices are symmetrical, $[\lambda_e]$ is equal to $[\lambda_i]$, which means that the current and the voltage propagation constants are its transpose. This fact leads to the conclusion that the eigenvalues of the voltage and current propagation constant matrices are equal.

From reference 10, an interesting results evolves from the numerical evaluation of the solution to the initial differential equation is:

$$V = e^{-[\lambda_e]x} [V_0] \quad \text{A1.3}$$

In equation A1.3, expansion of (e) to a matrix exponent in numerical terms can be effected in different ways. When $[\lambda_e]$ is 3x3 matrix, the results are:

$$\begin{aligned} e^{-[\lambda_e]x} = & \frac{e^{-\lambda_1 x}}{(\lambda_1 - \lambda_2)(\lambda_1 - \lambda_3)} \{[\lambda_e] - \lambda_2[1]\} \cdot \{[\lambda_e] - \lambda_3[1]\} + \\ & \frac{e^{-\lambda_2 x}}{(\lambda_2 - \lambda_1)(\lambda_2 - \lambda_3)} \{[\lambda_e] - \lambda_1[1]\} \{[\lambda_e] - \lambda_3[1]\} + \\ & \frac{e^{-\lambda_3 x}}{(\lambda_3 - \lambda_1)(\lambda_3 - \lambda_2)} \{[\lambda_e] - \lambda_1[1]\} \cdot \{[\lambda_e] - \lambda_2[1]\} \end{aligned} \quad \text{A1.4}$$

In equation A1.4, λ_1, λ_2 and λ_3 are eigenvectors of the $[\lambda_e]$ matrix, and they are the values which satisfy the characteristic equation derived from the voltage propagation constant matrix. Therefore, analysis of propagation on overhead transmission lines, conducted completely in phase quantities, requires an eigenvalue analysis when actually producing general numerical results.

When substituting equation A1.4 in A1.3, the result still appears rather formidable. In order to clarify this, one concept of matrix algebra will suffice:

the concept of an eigenvector. If $[e_1]$ is an eigenvector of the $[\lambda_e]$ matrix, the following equation is valid:

$$[\lambda_e] \cdot [e_1] = \lambda_1 \cdot [e_1] \quad \text{A1.5}$$

When λ_1 is the eigenvalue associated with the eigenvector $[e_1]$. By assuming that $[V_0]$ in equation A1.3 is equal to $[e_1]$, for a specific example, it is evident that each term in A.4 will be multiplied by $[e_1]$.

For example, the following equation is a portion of the required operation, using equation A1.5:

$$\{[\lambda_e] - \lambda_2[1]\}[e_1] = [\lambda_e][e_1] - \lambda_3[e_1] = \lambda_1[e_1] - \lambda_3[e_1] = (\lambda_1 - \lambda_3)[e_1] \quad \text{A1.6}$$

where the term $(\lambda_1 - \lambda_3)$ is just a number, not a matrix. Therefore, it may be used in equations without regard to the order of multiplication as is required in matrix operations. Repeated use of equation A1.6 produces:

$$e^{-[\lambda_e]x} [e_1] = e^{-\lambda_1 x} [e_1] \quad \text{A1.7}$$

If a voltage proportional to the eigenvector of the $[\lambda_e]$ matrix is applied to the system, this voltage will propagate with only attenuation and phase shift as described in equation A1.7. The propagation constant for this signal will be equal to the eigenvalue of $[\lambda_e]$ associated with the eigenvector $[e_1]$ described in equation A1.5. Furthermore, any voltage applied to the system can be broken into the sum of three components proportional to the eigenvector of $[\lambda_e]$ as seen in the following equation:

$$[V_0] = [e_1] + [e_2] + [e_3] \quad \text{A1.8}$$

If this voltage is applied to equation A1.3, using equations A1.4 and A1.5, will result in the following:

$$[V] = e^{-[\lambda_1]x} [e_1] + e^{-[\lambda_2]x} [e_2] + e^{-[\lambda_3]x} [e_3] = e^{-\lambda_1 x} [e_1] + e^{-\lambda_2 x} [e_2] + e^{-\lambda_3 x} [e_3] \quad \text{A1.9}$$

Equation A1.9 shows that any arbitrary signal applied to the system will propagate as three distinct natural signals or in three natural modes of propagation, and the three signals will be proportional to the eigenvectors of the propagation constant matrices.

A1-3.2 Modal Quantities Analysis

The detailed analysis of transmission line propagation for an infinite line, using modal transformations in the original differential equations, is shown in reference 110. In the analysis it is assumed that $[L_e]$ and $[L_i]$ exist and are square matrices, respectively transforming modal voltages to phase voltages and modal currents to phase currents. Using the assumed solution technique incorporated in Appendix 6.1 of reference 110, the modal propagation constant for current and voltage become:

$$[\lambda_e'] = [L_e]^{-1} \left\{ \sqrt{[Z(w)][Y(w)]} \right\} [L_e] \quad \text{A1.10}$$

$$[\lambda_i'] = [L_i]^{-1} \left\{ \sqrt{[Y(w)][Z(w)]} \right\} [L_i] \quad \text{A1.11}$$

As described in reference 110, the modal characteristic impedance becomes:

$$[Z_e'] = [L_e]^{-1} \left\{ \sqrt{[Y(w)][Z(W)]} \right\} [L_i] \quad \text{A1.12}$$

Equation A1.12 shows that the current and voltage transformation matrices are used to convert the phase characteristic impedance matrix. In equation A1.7, it was seen that when a voltage proportional to the eigenvector of $[\lambda_e]$ is applied to a line, the signal will propagate undistorted, that is, the same ratio of voltage on the phases will appear on the receiving end as was applied on the sending end of the line. Interpreting the modal transformation of the propagation constant matrix equations A1.10 and A1.11, as the transformation obtained from the eigenvalue analysis of the phase propagation constant matrix, two points become clear:

1. The modal propagation constant for current $[\lambda_i']$ and voltage $[\lambda_e']$ will be equal to diagonal matrix made up of complex terms.
2. The modal transformation $[L_e]$ will define the eigenvectors or modal voltages which will propagate undistorted on the transmission line, and $[L_e]$ is a square matrix, the first column of which is a modal voltage. Any voltage applied to the line in this ratio will propagate as a modal voltage. Correspondingly, the second and third columns of $[L_e]$ will be the second and third eigenvectors or modal voltages.

A1-4 PROPERTIES OF MODAL TRANSFORMATION MATRIX

From the previous analysis in section 3 of this chapter, it is obvious that relationships exist between current and voltage transformation. It is also

known that the two matrix $[\lambda_i]$ is the transpose of $[\lambda_e]$, hence equations A1.10 and A1.11 can be rewritten as :

$$[L_e]^{-1}[\lambda_e][L_e] = [\lambda_d] \quad \text{A1.13}$$

and

$$[L_i]^{-1}[\lambda_i][L_i] = [\lambda_d] \quad \text{A1.14}$$

where $[\lambda_d]$ is a diagonal matrix of the modal propagation constants, that is, the eigenvalues of the $[\lambda_e]$ and $[\lambda_i]$ matrices. Transposing equations A1.13 and A1.14 produces:

$$[\lambda_d] = \left\{ [L_e]^{-1}[\lambda_e][\lambda_e] \right\}_t = [L_e]_t [L_e]_t [L_e]_t^{-1} \quad \text{A1.15}$$

$$\text{and } [\lambda_d] = \left\{ [L_i]^{-1}[\lambda_i][\lambda_i] \right\}_t = [\lambda_i]_t [\lambda_i]_t [\lambda_i]_t^{-1} \quad \text{A1.16}$$

Equating equations A1.15 & A1.16 with A1.13 and A1.14 respectively, and if $[L_e]^{-1}$ and $[L_e]_t^{-1}$ are eigenvectors, then:

$$[L_i]^{-1} = [L_e]_t \quad \text{A1.17}$$

$$[L_i] = [L_e]_t^{-1} \quad \text{A1.18}$$

An additional property of modal transformation to be evaluated is the power invariance. In order to determine if modal transformation matrices are power invariant, the power flow in the network is evaluated from the phase quantities in the standard manner.

$$P = [I]_t^* [V] \quad \text{A1.19}$$

where $[I]_t^*$ equals the transpose conjugate of the phase current column matrix.

Using the transformation:

$$[V] = [L_e][V'] \quad \text{A1.20}$$

and

$$[I] = [L_i][I'] \quad \text{A1.21}$$

Equation A1.19 produces:

$$P = [I']_t^* [L_i]_t^* [L_e][V'] \quad \text{A1.22}$$

Using equations A1.17 and A1.18 in A1.22

$$P = [I']_t^* [L_e]^{-1*} [L_e][V'] \quad \text{A1.23}$$

The property of power invariance is maintained if:

$[L_e]^{-1*} [L_e] = 1$, but since $[L_e]^{-1} [L_e] = 1$ requires $[L_e]^{-1*} \neq [L_e]^{-1}$, so that the modal transformation matrices are not power invariant in the general case.

The difference between the total power calculated in modal and phase quantities is quite small as indicated in reference 110. The lack of the power invariance property of modal transformation matrices does not severely restrict use of this method in analysing power system problems. Primary difficulty occur only if modal currents and voltages are available and the total power is desired, requiring transformation back to phase quantities for this calculation.

A1-5 MODAL ANALYSIS

The application of the theory of natural modes and modal analysis^(14,15) has resulted in considerable advances in the analysis of multi conductor EHV transmission lines. A theoretical formulation of a method of multi conductor transient analysis, which combines the use of the modified Fourier transform and the theory of natural modes was developed by Wedepohl and Mohamed⁽¹⁴⁾. The virtues of this particular formulation are that the frequency dependence of parameters can be taken into account irrespective of the complexity of the expression defining their steady-state values. Because of the multiplicity of conductors in a power transmission system, the solution of the resultant simultaneous differential equation which are independent becomes very complex.

Wedepohl⁽¹⁰⁾ described the steady-state propagation properties of transmission lines are readily obtained using the method of modal analysis. This involves constant frequency signals which propagate without distortion. They propagate with a single attenuation and phase shift.

$$\gamma = \alpha + j\beta \quad \text{A1.24}$$

where α = attenuation constant

β = phase shift

The modes of propagation for a multi-conductor system are calculated from the system parameters using the solution to the wave equation in the steady-state:

$$\frac{d^2V}{dx^2} = PV \quad \text{A1.25}$$

$$\frac{d^2 I}{dx^2} = P_t I \quad \text{A1.26}$$

where:

$$P = ZY \quad \text{A1.27}$$

$$P_t = YZ \quad \text{A1.28}$$

As it was described earlier in by selecting a suitable linear transformation, the system of coupled differential equation can be resolved into three decoupled independent differential equations. That the linear transformation must diagonalise the P matrix.

$$[V] = [S][V_c] \quad \text{A1.29}$$

$$[I] = [Q][I_c] \quad \text{A1.30}$$

where $[V_c]$ and $[I_c]$ are the column vector matrices of the voltage and current respectively, and $[S]$ and $[Q]$ are matrices of eigenvalues $[P]$ and $[P]^t$ respectively.

The linear transformations result in the following decoupled differential equations⁽³⁾ allowing a component for component solution:

$$\frac{d^2 V_c}{dX^2} = S^{-1} P S V_c = \gamma^2 V_c \quad \text{A1.31}$$

$$\frac{d^2 I}{dX^2} = Q^{-1} P^t Q I_c = \gamma_1^2 I_c \quad \text{A1.32}$$

Since mutual coupling has been eliminated, equations A1.31 and A1.32 can be solved as a series of simple wave equations, the solution being:

$$V_e = V_i e^{-\psi x} + V_r e^{+\psi x} \quad \text{A1.33}$$

where

$$\psi = Q\gamma Q^{-1} \quad \text{A1.34}$$

From the detailed analysis described in chapter 4, a system of two port ABCD parameters can be calculated from the basic wave equations. The system transfer matrices are:

$$\begin{bmatrix} v_s \\ I_s \end{bmatrix} = \begin{bmatrix} A & B \\ C & D \end{bmatrix} \begin{bmatrix} V_r \\ I_r \end{bmatrix} \quad \text{A1.35}$$

where

$$\begin{aligned} A &= \cosh(\psi x) \\ B &= \sinh(\psi x) Z_0 \\ C &= Y_0 \sinh(\psi x) \\ D &= Y_0 \cosh(\psi x) Z_0 \end{aligned} \quad \text{A1.36}$$

Z_0 and Y_0 are the polyphase surge impedance and admittance respectively. The matrix function theory permits the easy evaluation of Z_0 , Y_0 and the hyperbolic functions. For example:

$$Z_0 = Q\lambda^{-1}QZ \quad \text{A1.37}$$

$$Y_0 = YQ\lambda_1^{-1}Q^{-1} \quad \text{A1.38}$$

and

$$\cosh(\psi x) = Q\cosh(\gamma x)Q^{-1} \quad \text{A1.39}$$

A1-6 PHYSICAL INTERPRETATIONS

Any set of phase conductor currents or voltages existing at any point of lossy and reflection free 3-phase line can be resolved into three sets of natural mode components.

A set of phase quantities corresponding to one mode only cannot be resolved into other modes. This means that the modes are independent and there is no intermode coupling on a uniform line.

At any point of a line the mode components must add up to the actual phase quantities and the total power derived from phase currents and voltages must be equal to the sum of mode powers. Furthermore, the ratio of mode voltage to mode current is constant on each phase conductor and it is called "mode characteristic impedance".

The ratio of phase components of each mode is also constant. Each mode propagates with a specific attenuation per unit length.

The eigenvalues and eigenvectors completely describe the mode of propagation of the voltage and current modal signals. If a voltage proportional to eigenvector is injected into the system then it will propagate with one attenuation and phase shift described by the associated eigenvalue. Any voltage applied to the system can be expressed as the sum of three components proportional to the eigenvectors, ie:

$$[V_0] = [e_1] + [e_2] + [e_3] \quad \text{A1.40}$$

Equation A.38 means that any arbitrary signal applied to the system will propagate three distinct natural modes, or in three natural modes of propagation, and the three signals will be proportional to the eigenvectors of the propagation constant matrix $[P]$. The three modes of propagation can also be expressed as one ground mode and two aerial modes of propagation.

A1-7 CONCLUSION

The theory of natural-modes can be applied to the solution of the steady-state and transient analysis of multi conductor HV and EHV transmission lines. From the steady-state equations, the analytical formulation can be extended for multi conductor line transients through the modal analysis and the application of the modified Fourier transform technique. An inherent advantage of the modal analysis approach is that the network's steady-state formulation is applicable to transient calculation, when the system is analysed on the frequency spectrum, which results in efficiencies during computation.

When lossless earth is assumed, the propagation constant matrix is diagonal and cannot be used to determine modal transformation. The voltage and current propagation constant matrices in phase quantities are transposed, and the voltage and current modal transformations obtained from the complex propagation constant matrix are orthogonal.

The eigenvalue analysis when used in conjunction with digital computers for modal analysis on multi conductor transmission lines, is particularly attractive and requires special mathematical skills in matrix algebra. With the aid of the theory of natural modes, it was shown that any set of phase conductor currents or voltages existing at any point of a lossy and reflection 3-phase line can be resolved into three natural mode components. A set of phase quantities

corresponding to one mode only, cannot be resolved into other modes. Therefore, the modes are independent and there is no intermode coupling on a uniform line.

The use of the theory of natural modes has made the unbalanced analysis of three-phase power systems possible by using two port equivalent networks, to derive the solution for the network independently from each mode energisation. To evaluate the total response of the network, the superposition method is then used. Such a technique is employed in all calculations performed in this work in the frequency domain.

Appendix A2

SOFTWARE IMPLEMENTATION

A2-1 COMPUTATION METHODOLOGIES

The computed voltage and currents phasors from the faulted power system at both ends of the transmission line, and at the three ends in case of three terminal systems, are converted to modal quantities using the theory described above. In particular, as it is explained in details in chapter 5, the computation of the fault location on EHV transmission lines, requires the modal characteristic impedance, modal propagation constants and the modal quantities for voltage and current phasors.

In addition to this the transmission line constants, i.e., Z and Y which are usually known for any transmission line, the line parameter program calculates the series impedance matrix, the shunt admittance or susceptance matrix and all the necessary eigenvalues and eigenvectors necessary for accurately computing the distance to fault.

The simple flow chart given in Fig. A2.1, demonstrates the necessary steps for computing the distance to fault, through the software.

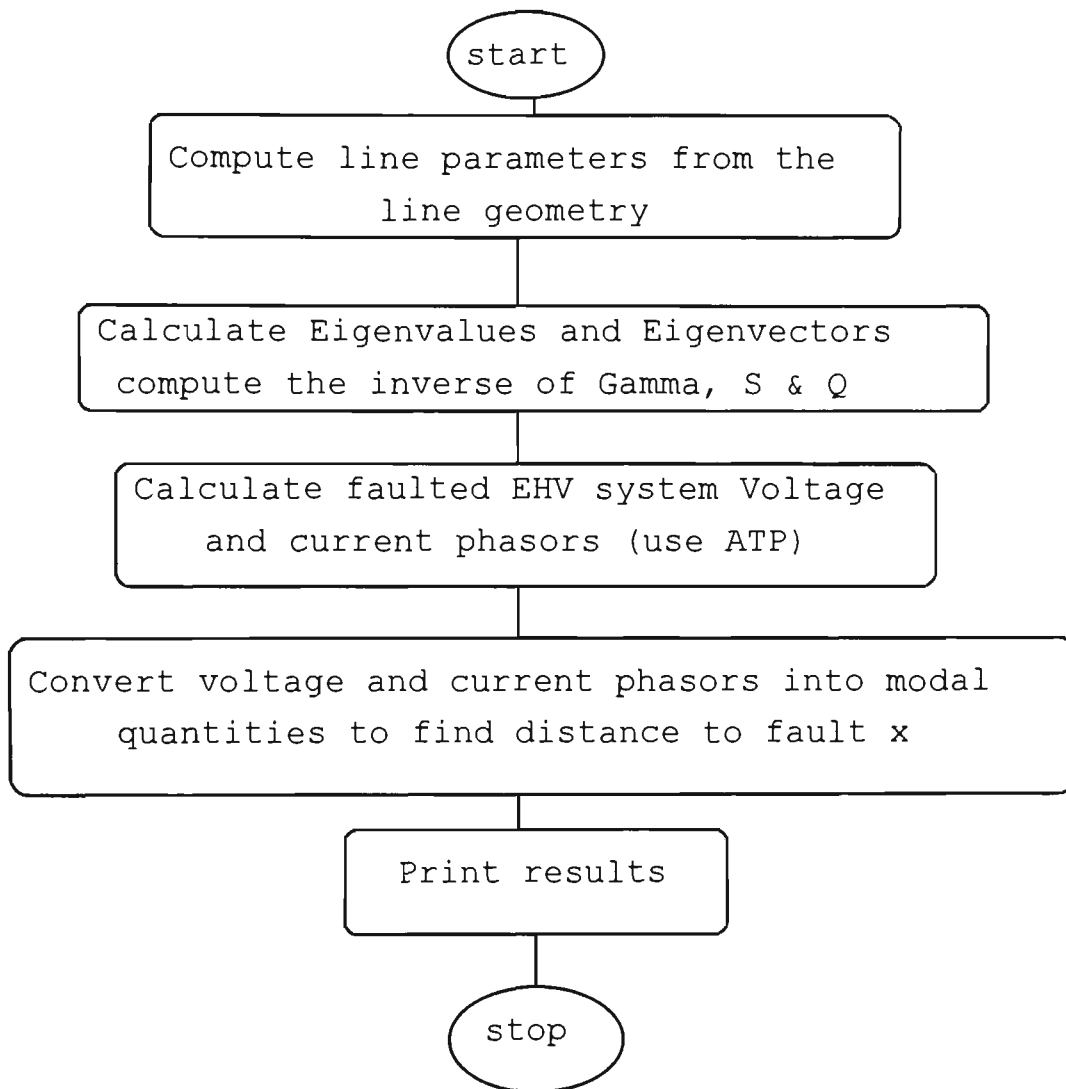


Fig. A2.1: Simplified Flow Chart Showing Computation Steps

A2-2 MODAL TRANSFORMATION

Considering a three phase, two terminal EHV transmission line, the calculation of modal currents and voltages is carried out as follows:

$$[I_{Modal}]_{3 \times 1} = [S]_{3 \times 3}^{-1} [I_{a,b,c}]_{3 \times 1} \quad \text{A2.1}$$

and

$$[V_{Modal}]_{3 \times 1} = [Q]_{3 \times 3}^{-1} [V_{a,b,c}]_{3 \times 1} \quad \text{A2.2}$$

Consequently, the distance to fault is calculated as follows:

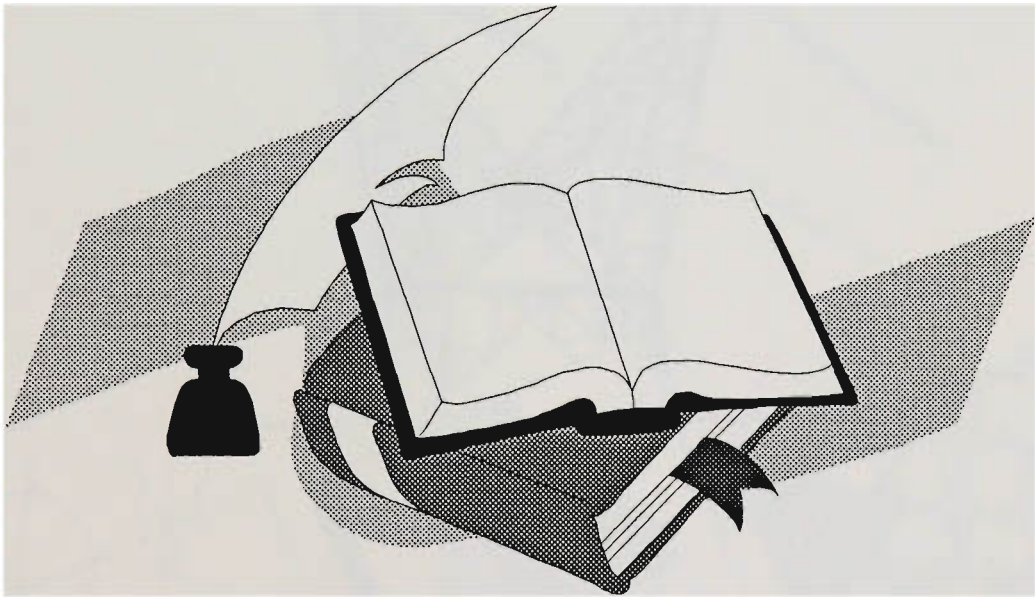
$$\begin{bmatrix} x_1 \\ x_2 \\ x_3 \end{bmatrix} = \begin{bmatrix} \frac{1}{\gamma_1} \tanh^{-1} \left(-\frac{B_1}{A_1} \right) \\ \frac{1}{\gamma_2} \tanh^{-1} \left(-\frac{B_2}{A_2} \right) \\ \frac{1}{\gamma_3} \tanh^{-1} \left(-\frac{B_3}{A_3} \right) \end{bmatrix} \quad \text{A2.3}$$

All matrices are given in the above equations are described in details in chapter four.

Equation A2.3 gives thee distances related to one earth mode and two aerial modes. Generally, x_1, x_2 and x_3 are complex numbers, the imaginary parts are neglected. It was explained in Appendix A1, that mode 3 has minimum attenuation, which is confirmed in the results given in chapter nine, where, in most cases, particularly when the ground is not involved, mode 3 has given the best accuracy for estimating the distance to fault, calculated using equation A2.3.

Appendix A3

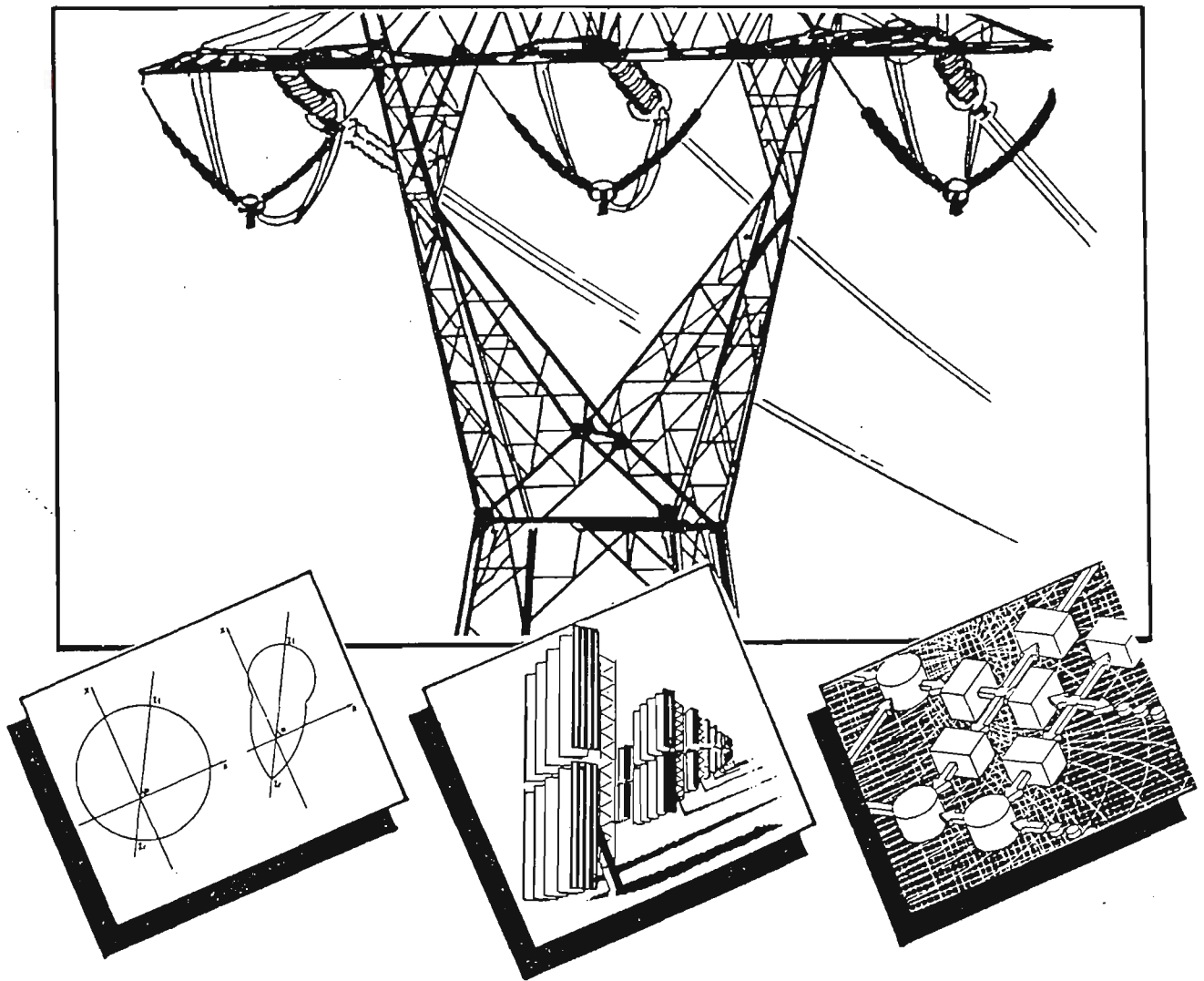
PUBLISHED WORK





AUPCEC' 91

Australasia Universities
Power and Control
Engineering Conference



CONFERENCE PROCEEDINGS

3-4 October 1991

Monash University Victoria Australia

Editors: M. Aldeen
M. Al-Dabbagh

ACCURATE FAULT LOCATION FOR EHV TRANSMISSION LINES

L. AL-DABBAGH, A. KALAM,
Department of Electrical and Electronic Engineering,
Victoria University of Technology, Footscray Campus,
P.O. Box 64, Vic.3011.

A. PALAMARCZUK,
Power Grid Development Department,
SECV, Monash House, 15 William Str., Melbourne 3001

ABSTRACT

Accurate fault locators contribute to availability and security of High Voltage Energy Systems, which consequently results in an increased economy of these systems. This paper describes an accurate fault location algorithm for EHV transmission lines. The post-fault processing of data captured during the fault clearance is used to produce steady-state power frequency voltage and current phasors at each end of the line.

1. INTRODUCTION

The transmission of bulk power from remote generation to load centres and the interconnection of power systems is materialized using Extra-High voltage (EHV) transmission lines. The protection systems for such transmission circuits is based on modern high speed schemes. Such protection systems isolate the faulty transmission line very quickly and hence eliminate any severe consequences of faults on transmission lines and other parts of the system. Therefore, it becomes more and more difficult to locate faults on lines based on visual information. In order to reduce circuit outage times, and restore electric energy to consumer, accurate fault location techniques are required.

Conventional methods based on the measurement of impedance to fault, do not provide accurate information about fault location, neither do post-fault clearance tests give conclusive results. Small errors in measurements may require detailed local examination over several kilometers of a typical transmission line, which means unnecessary delay in energy restoration.

Takagi et. al. [1], Wiszniewski [2], Eriksson et. al. [3] and Cook [4] proposed methods which use fault current distribution factors, pre-fault and post-fault currents and post-fault voltages from one line terminal. Impedances of equivalent sources connected to the line terminals are

required. In practice, system configuration changes under different operating conditions modifying distribution factors. Sachdev and Agarwal [5] proposed an approach in which use is made of local digital impedance and relay current data as well as corresponding data from remote end. This method in general is reported to be accurate, but appreciable errors are acknowledged for certain fault resistance is inaccurate for location near the mid point of the line, where the fault current contribution from both ends are equal [6].

In this paper, an accurate fault location algorithm is presented. This work is based on the early research proposed by Johns and Jamali [7].

2. FAULT LOCATION ALGORITHM.

The main factors affecting the accuracy of fault location methods used above are: 1) Non-linearity of the fault impedance in the fault path; 2) The variation in the source impedance in the actual system and the values assumed in setting fault location equipment; 3) Non-transposition of line conductors and the effect of shunt capacitance; 4) The effect of remote source infeed; and 5) The need to utilize voltage signals derived from conventional capacitor voltage transformers.

It is evident from the published literature, that there is no single fault location method at present which takes all previous factors into consideration. The proposed method is based on accurate monitoring and filtering the voltage and current measured at each end of the transmission line, so as to produce a measure of the steady-state power frequency voltage and current phasors. The latter are obtained as data, described by means of post-fault processing, applied to data captured during the fault clearance process.

In considering single phase model of a simple power system given in Fig.1, the post fault steady-state voltage V_F for a fault at a distance X from the end S can be obtained in terms of the voltages

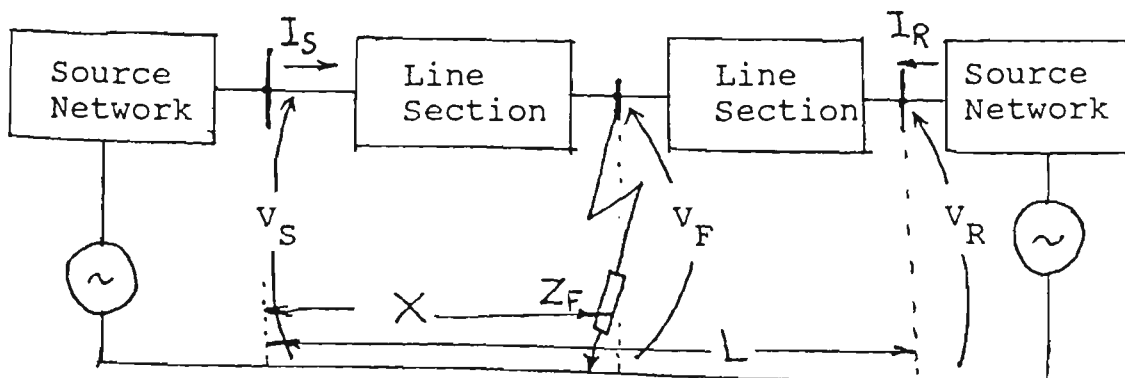


Fig.1: Sample faulty power system.

and currents measured at the ends:

$$V_F = \cosh (\gamma x) V_S - Z_0 \sinh (\gamma x) I_S \quad (1)$$

$$V_F = \cosh (\gamma(L-x)) V_R - Z_0 \sinh (\gamma(L-x)) I_R \quad (2)$$

where: Z_0 = surge or characteristic impedance = $(Z/Y)^{1/2}$ (3)

$$\gamma = \text{line propagation constant} = (ZY)^{1/2} \quad (4)$$

Z and Y are line series impedance and shunt admittance per unit length respectively.

Rearranging equations 1 and 2, an accurate evaluation of the distance to the fault X is given as:

$$X = [\tan^{-1}(-B/A)]/\gamma \quad (5)$$

$$\text{where: } A = Z_0 \cosh(\gamma L) I_R - \sinh(\gamma L) V_R + Z_0 I_S \quad (6)$$

$$\text{and } B = \cosh(\gamma L) V_R - Z_0 \sinh(\gamma L) I_R - V_S \quad (7)$$

For a given transmission line, usually line parameters are known and can be calculated, whereas voltage and current phasors can be measured at both ends of the transmission line.

3. THREE PHASE MODEL.

In case of a three phase line, the vector of voltages and currents ($[V_{Fa,b,c}]$, $[I_{Sa,b,c}]$) etc. at various points of interest are related using the 2-port matrices $[A_S]$, $[B_S]$, $[A_R]$, $[B_R]$, which in turn are 3X3 matrices defined using the line series impedance matrix $[Z]$ and the line shunt admittance matrix $[Y]$.

It is possible to derive an expression for fault location in form of three pairs of 1 and 2 equations corresponding to modes 1,2 and 3 (7). For example a mode-2 based evaluation is given by:

$$X = [\tan^{-1}(-B_2/A_2)]/\gamma_2 \quad (8)$$

4. PERFORMANCE EVALUATION.

In order to evaluate the algorithm performance, single-phase model was first developed. Preliminary results show that the use of a three-phase representation is necessary. With the single phase model, only three-phase faults can be

evaluated. For unbalanced faults, it is important to represent all three phases in a comprehensive model.

5. CONCLUSION.

An accurate fault location algorithm for EHV transmission lines is represented. A single phase model for testing the algorithm is developed. From the preliminary results using the model, it is concluded that a three phase model is required, particularly for evaluating fault locations under unbalanced faults. However, the single phase model can be used for three phase balanced faults. It is hoped that a comprehensive three phase fault location model will be developed for accurate measurement.

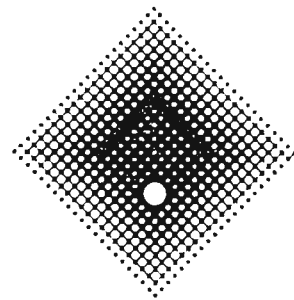
6. REFERENCES.

- [1] Takagi, T, et. al., "Development of a New Type Fault Locator Using One Terminal Voltage and Current Data", Trans. IEEE, Vol. PAS-101, No.8, August 1982, pp.2892-2898.
- [2] Wiszniewski, A, "Accurate Fault Impedance Locating Algorithm", Proc. IEE, Vol.130, Part C, No. 6, November 1983, pp.311-314.
- [3] Eriksson, L, et. al., " An Accurate Fault Locator With Compensation for Apparent Reactance in the Fault Resistance Resulting from Remote-end Infeed", Trans. IEEE, Vol.PAS-104, No. 2, Feb. 1985, pp. 424-436.
- [4] Cook, V., "Fundamental Aspects of Fault Location Algorithm Used in Distance Protection", Proc. IEE, Vol.133, Part C, No. 6, Sep. 1986, pp.359-368.
- [5] Schadev, M.S., and Agarwal, R., "Accurate Fault Location Estimates From Digital Impedance Relay Measurement", IEE Conference Publication No. 249, April 1985, pp.180-184.
- [6] Jeyasurya, B., and Rahman, M.A., "Accurate Fault Location of Transmission Lines Using Microprocessors", Proc.of the 4th IEE International Conference on Developments in Power System Protection, April 1989, 13-17.
- [7] Johns, A.T., and Jamali, "New Accurate Transmission Line Fault Location Equipment", *ibid*, pp. 1-4.
- [8] Wedephol, L.M., "Application of Matrix Methods to the Solution of Travelling-wave Phenomena in Polyphase Systems", Proc.IEE, 110, (2), 1963, pp.2200-2212.
- [9] Johns, A.T., and Aggarwal, R.K., "Digital Simulation of Faulted Transmission Lines with Particular Reference to Very-high speed Protection", Proc.IEE, 123, (4), pp.353-359.

**SECOND INTERNATIONAL CONFERENCE
ON
MODELLING AND SIMULATION**



MS'93



**Melbourne, Australia
12-14 July, 1993**

**"Modelling and Simulation:
Keys to Technological Advances"**

**Proceedings
Volume 1**

Victoria University of Technology
P. O. Box 14428 MMC, Melbourne, Victoria, Australia, 3000.

ACCURATE ALGORITHMS FOR MODELLING TRANSMISSION LINE PARAMETERS

Larissa Al-Dabbagh and Akhtar Kalam
Save Energy Research Group
Department of Electrical and Electronic Engineering
Victoria University of Technology
P.O.Box 14428 MMC, Melbourne
Victoria 3000, Australia

ABSTRACT

The computation of the steady state and transient phenomena in power systems requires accurate simulations for all elements of the power systems such as generators, transformers, transmission lines, etc. This paper is concerned about the modelling of the transmission line, which can be used in any simulation for power system studies. The paper describes the advantages of having accurate modelling of the transmission line using modern transmission line theory based on the solution of the travelling wave equations.

1. INTRODUCTION

For any configuration of a transmission line, before any type of calculation is carried out, it is required to calculate the parameters of the line accurately. In this paper, the calculation of circuit parameters is derived for a single or double circuits transmission lines. The effect of the earth and earth wires is included in the derived algorithms. The method followed is based on an early work as described by Galloway et al (1).

2. BASIC CONSIDERATIONS

In power systems, the calculation of line parameters are necessary for many studies ; some are listed below:

- a) Short circuit calculations; load flow analysis; steady-state and transient stability studies; protection settings; harmonic analysis and quality of power supply. Such studies require the calculation of line parameters at the power frequency and some other harmonics.
- b) Interference with communication lines; power line carrier transmission; Switching and lightning effects; behaviour of protection systems and relays under transient conditions. These require the evaluation of the parameters at frequencies ranging from few hertz to a few hundred MHz.

Calculating line parameters in power systems for the above purposes is very important, particularly this is essential in modern power systems, to secure reliable system design, planning and operation. The parameters which are required for the accurate studies in power systems are:

- i) the basic per unit length series and shunt impedance matrices;
- ii) the positive, negative and zero sequence impedances of single and/or double circuit lines and associated inter-phase and intercircuit mutual couplings;

- (iii) the propagation parameters such as the characteristic impedance, natural modes of propagation and their attenuation and velocity;
- (iv) the exact equivalent π - network of line sections of different lengths.

With the availability of high speed digital computers, there is no longer a need to compromise accuracy of calculations for easy and approximate formulae. The use of the commonly applied technique based on Geometric Mean Distance and Geometric Mean Radius (GMD and GMR) respectively, which neglect some important factors for the sake of achieving simplicity in calculation, is not required any more. This is mainly due to the fact that such technique makes some other parameters meaningless and therefore impossible to derive.

In the derivation of the algorithms for accurately calculating the line parameters, the following basic and practical considerations will be taken into account:

- (i) conductor stranding and the skin effects;
- (ii) variable current penetration return path with finite conductivity and its contribution parameters as given by Carson's infinite series (2) which is found to contribute as much as 40% of the values under ideal conditions even at power frequency;
- (iii) proximity of aerial earth wires;
- (iv) mutual couplings of a second circuit on the same tower or nearby circuits;
- (v) unsymmetrical conductor placing at different heights on the same tower with or without transposition.

3. TRANSMISSION LINE SERIES IMPEDANCE MATRIX

In the derivation, it will be assumed that the lines lengths are very much greater than the spacings between the conductors and the ground surface. The series impedance are defined in terms of quantities per unit length (ohm/km)

Considering a 3 conductor line shown in Fig.1, the voltage drops

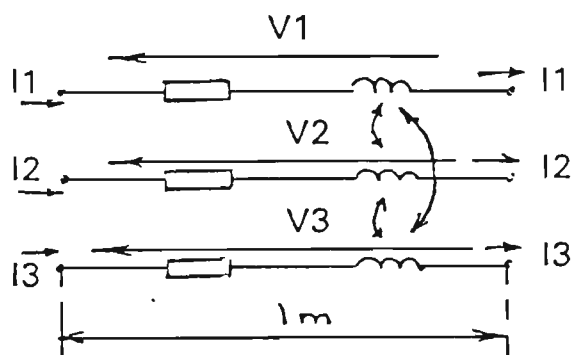


Fig. 1: Transmission line section

V_1 , V_2 and V_3 along one km length of the line are related to the currents I_1 , I_2 and I_3 that the flow in the series circuit of the line in condensed matrix form:

$$[\mathbf{v}] = [\mathbf{z}] [\mathbf{I}]$$

(1)

where, $[\mathbf{z}]$ is defined as the series impedance matrix of the line per unit length, $[\mathbf{v}]$ is the vector of series voltage drops, and $[\mathbf{I}]$ is the vector of series conductor currents. Equation (1) is valid irrespective of whether the voltages V_1 , V_2 , V_3 and the currents I_1 , I_2 , I_3 are balanced or unbalanced. For an n number of conductor line $[\mathbf{z}]$ is a $n \times n$ symmetric matrix.

In equation (1), the $[z]$ matrix can be resolved into three components, i.e., $[z_g]$, $[z_e]$ and $[z_c]$, so that:

$$[z] = [z_g] + [z_e] + [z_c] \quad (2)$$

where $[z_g]$ is purely reactive matrix and is due to the flux external to the conductors, assuming a ground of infinite conductivity.

The (i,j) th element of $[z_g]$ (Fig.2), is given by:

$$z_g(i,j) = (j\omega\mu_0 / 2\pi) * \ln(D_{ij} / d_{ij}) \quad \Omega/m$$

where d_{ij} = distance between the i th conductor and the j th conductor for $i \neq j$;

d_{ii} = external radius of the i th conductor for $i = j$, and in the case of bundled conductors, the geometric mean radius (GMR) of the bundle.

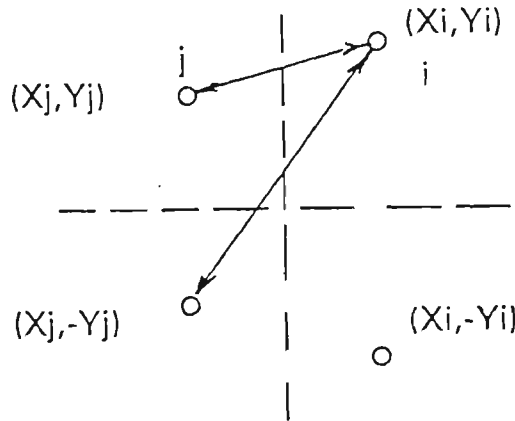


Fig. 2: Schematic diagram of conductors.

D_{ij} = distance between the i th conductor and the image of the j th conductor on the ground surface. In the above arrangement, it is assumed that conductor coordinates with respect to ground surface as x - axis, and centre line of the tower as y - axis.

The $[z_e]$ component is a full matrix with resistive and reactive elements. This is due to finite conductivity of the ground, and is known as the impedance of the earth return path. The (i,j) element of the $[z_e]$ matrix is given by the infinite integral equation (2):

$$z_e(i,j) = (j\omega\mu_0 / \pi) \int_{\beta=0}^{\infty} \frac{\cos((x_i - x_j)\beta) \cdot \exp(-\beta(y_i - y_j))}{(\beta + \sqrt{\beta^2 + j\omega\mu \nabla})} d\beta \quad (3)$$

where (x_i, y_i) and (x_j, y_j) are the coordinates of conductor i and conductor j ; ∇ = conductivity of soil in Ω -m; β = integration parameter varying from 0 to ∞ . Analytical solution of this integral gives Bessel function (3).

The last component in equation (2), i.e. $[z_c]$ is a diagonal matrix with both resistive and reactive components, and is due to the impedance of the conductor itself.

It is common to use the manufacturers' values at power frequency. The resistance r_c of a conductor is usually given in ohm/km; but the internal reactance of the conductors is given indirectly by means of the geometric mean radius (GMR) of the conductors.

The conductor internal impedance is calculated from the formula:

$$x_c = (j\omega\mu_0 / 2\pi) \dots \ln(r / GMR) \quad \Omega/m \quad (4)$$

where r = external radius of the conductor

and GMR = geometric mean radius of the conductor

For bundled conductors the conductor internal resistance and reactance are derived by the number of conductors in a bundle (4) (Fig.3):

D_s is the GMR of conductors of the poly-phase line, and d is the distance between conductors within the bundle (Fig.3)

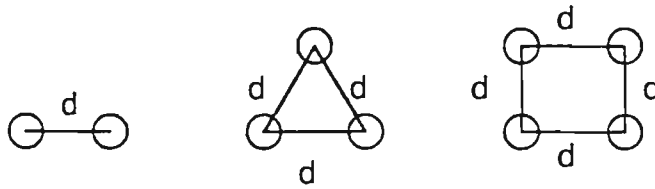


Fig.3: Bundle arrangement of conductors

4. TRANSMISSION LINE SHUNT ADMITTANCE MATRIX

Capacitance of EHV transmission line is the result of the potential difference between conductors; it causes them to be charged in the same manner as the plates of a capacitor when there is a potential difference between them. The capacitance between conductors is the charge per unit of potential difference. Capacitance between parallel conductors is a constant depending on the size and spacing of the conductors.

In case of three conductor transmission line shown in Fig.4, when the conductors 1, 2 and 3 are at potentials V_1 , V_2 and V_3 with respect to the ground, there are shunt currents i_1 , i_2 and i_3 . These currents are different from the series load currents which were considered in the previous section. These currents and voltages are related by the matrix equation:

$$[i] = [Y] [V] \quad (5)$$

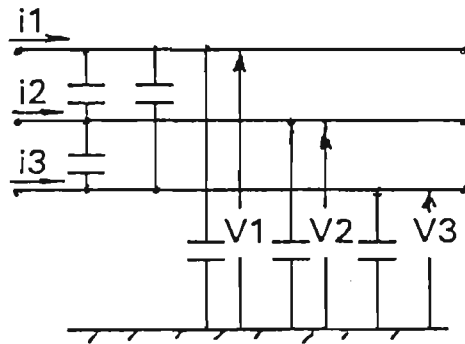


Fig.4: One section representation

In equation (5), $[Y]$ is a symmetric matrix and is defined as the shunt admittance matrix of the line per unit length. This equation is valid for both balanced and unbalanced conditions. The $[Y]$ matrix can be expressed as follows:

$$[Y] = j\omega 2\pi\epsilon_0 [B]^{-1} \quad (6)$$

The (i,j) element of $[B]$ is given by:

$$B[i,j] = \ln (D_{ij}/d_{ij}) \quad (7)$$

The error due to finite conductivity of soil is so small that the $[Y]$ matrix is not usually corrected for the effect of non-ideal ground.

5. EFFECT OF AERIAL GROUND WIRES

In case of the presence of aerial ground wires, they are first considered as additional phase conductors and the entire Z and Y matrices are formed. Consider the configuration of a three phase transmission line with two aerial earth wires as shown in Fig.4, the matrix equation relating voltages of the five conductors to their corresponding voltage drops are as follows:

$$V_c = Z_{cc} I_c + Z_{ce} I_c \quad (8)$$

$$\begin{matrix} V_e & & Z_{ec} & Z_{ee} & I_e \\ & & & & \end{matrix}$$

Because of the fact that conductors 4 and 5 are earthed, $V_4 = 0$; and $V_5 = 0$, which means that the $[V_e] = 0$. Solving equation (8) for V_c , when substituting for $V_e = 0$, the following is derived:

$$[I_e] = -[Z_{ee}]^{-1} [Z_{ec}] [I_c] \quad (9)$$

In the same way, $[V_c]$ can be described as follows:

$$\begin{aligned} [V_c] &= [Z_{cc}] [I_c] + [Z_{ce}] [I_e]; \text{ and considering equation (9) will result in:} \\ [V_c] &= ([Z_{cc}] - [Z_{ce}] [Z_{ee}]^{-1} [Z_{ec}]) [I_c] \end{aligned} \quad (10)$$

Equation (10) indicates that earth wire effects are taken into consideration by modifying the full $[Z]$ matrix to give a new equivalent impedance of a 3x3 dimension as follows:

$$[Z_{eq}] = [Z_{cc}] - [Z_{ce}] [Z_{ee}]^{-1} [Z_{ec}] \quad (11)$$

$$\begin{matrix} i_c & & Y_{cc} & & & & V_c \\ & & & & & & \\ & & & & & & \\ & & & & & & \\ & & & & & & \\ & & & & & & \end{matrix} = \quad (12)$$

$$\begin{matrix} i_e & & Y_{ec} & Y_{ee} & & & V_e \\ & & & & & & \end{matrix}$$

The potential of the earth is zero, i.e., $[V_e] = 0$, hence:

$$i_c = [Y_{cc}] [V_c], \text{ where in this case } [Y_{eq}] = [Y_{cc}]$$

Because of the fact that $[v_e] = [0]$;

$$i_c = [Y_{cc}] [V_c]; \text{ i.e. } [Y_{eq}] = [Y_{cc}] \quad (13)$$

which means that the effect of aerial wires is accounted for by forming the full Y matrix as is explained in section 4. By eliminating the rows and columns corresponding to the earth wires, i.e. 4 and 5 in the above example to give a 3 x 3 equivalent shunt admittance. In spite of the fact that a line with three phase wires and two earth wires is considered in the above described case, the same procedure can be applied to any line with any number of phase conductors and earth wires to formulate the equivalent impedance and admittance matrices.

6. ELECTRICALLY SHORT TRANSMISSION LINES

In this section a method for calculating the derived parameters for electrically short lines is given.

The method is based on symmetrical components, assuming conductor symmetry. To simplify analysis for some problems, the phase voltages V_a, V_b, V_c , and the currents I_a, I_b, I_c are transformed into another set of quantities known as symmetrical components, using linear transformation. The new quantities $[V_{012}]$ are obtained by transforming the phase quantities $[V_{abc}]$, i.e.;

$$[V_{012}] = [T]^{-1} [V_{abc}] \quad (14)$$

and for the currents:

$$[I_{012}] = [T]^{-1} [I_{abc}] \quad (15)$$

and using the transformation matrix we can write:

$$[V_{abc}] = [T] [V_{012}] \quad (16)$$

and:

$$[I_{abc}] = [T] [I_{012}] \quad (17)$$

It is now clear that we can express equation (1) above, can be transformed from phase quantities into symmetrical components using similar technique, i.e. :

$$[V_{abc}] = [Z_{abc}] [I_{abc}] \quad (18)$$

and:

$$[i_{abc}] = [Y_{abc}] [V_{abc}] \quad (19)$$

are transformed into symmetrical component quantities as follows:

$$[V_{012}] = [Z_{012}] [I_{012}] \quad (20)$$

and

$$[i_{012}] = [Y_{012}] [I_{012}] \quad (21)$$

where:

$$[Z_{012}] = [T]^{-1} [Z_{abc}] [T] \quad (22)$$

$$\text{and } [Y_{012}] = [T]^{-1} [Y_{abc}] [T] \quad (23)$$

It is important to note that when the sequence impedance and admittance matrices $[Z_{012}]$ and $[Y_{012}]$ are diagonal matrices, the symmetrical components become mutually independent, and therefore mutually dependent phase voltages and currents can be resolved into mutually independent symmetrical component voltages and currents. Furthermore, $[Z_{012}]$ and $[Y_{012}]$ become diagonal only and only when $[Z_{abc}]$ and $[Y_{abc}]$ are balanced.

$$[Z_{abc}] = \begin{bmatrix} z_s & z_m & z_m \\ z_m & z_s & z_m \\ z_m & z_m & z_s \end{bmatrix} \quad (24)$$

for which:

$$[Z_{012}] = \begin{bmatrix} z_s + 2z_m & 0 & 0 \\ 0 & z_s - z_m & 0 \\ 0 & 0 & z_s - z_m \end{bmatrix} \quad (25)$$

From equation (25), we can write: $Z_0 = Z_s + 2Z_m$, $Z_1 = Z_s - Z_m$, and $Z_2 = Z_s - Z_m$, which are defined zero, positive and negative sequence impedances respectively. Similar definitions can be derived for zero, positive and negative sequence admittances.

In spite of the fact that symmetrical component method is widely used, it is important to note that such method becomes powerful only when the three phase network is balanced but the terminal conditions may or may not be balanced. There is no advantage in symmetrical component method if the network itself is unbalanced, in which case direct solution in term of phase quantities becomes simpler. Therefore, it is necessary to stress that whenever a sequence quantity of a line or a component of a network is referred to, *it is implicitly assumed that the line or the component is balanced*. This applies even if the lines are regularly transposed, when their sequence impedances and admittances are referred to, they are assumed to be regularly transposed.

7. PROPAGATION PARAMETERS

For long transmission lines, the representation of the line can be defined in a different way. As it is described by Wedepohl (2), let

$[P] = [Z][Y]$ and let $\lambda_1, \lambda_2, \dots, \lambda_n$ be the n eigenvalues of the $n \times n$ matrix P . Let Q_1, Q_2, Q_n be the n number of linearly independent $n \times 1$ eigenvectors of the matrix P corresponding to the eigenvalues.

The eigenvalues λ_i are assembled diagonally to form $(n \times n)$ diagonal matrix $[\lambda]$. The n eigenvectors are also assembled in the same order as the corresponding eigenvalues to form $(n \times n)$ matrix $[Q]$. This means, for 3 conductor transmission line:

$$[\lambda] = \begin{bmatrix} \lambda_1 & 0 & 0 \\ 0 & \lambda_2 & 0 \\ 0 & 0 & \lambda_3 \end{bmatrix} \quad (26)$$

It can be shown⁽³⁾ that:

$$[Q] \cdot [P] \cdot [Q]^{-1} = [\lambda] \quad (27)$$

The columns of Q (i.e. the eigenvectors) are called the natural modes distributions of voltages on the line conductors and the corresponding eigenvalues give the *natural mode propagation constants* $\gamma_1, \gamma_2, \gamma_3$ by the relationships:

$$\gamma_1 = \sqrt{\lambda_1}, \gamma_2 = \sqrt{\lambda_2}, \gamma_3 = \sqrt{\lambda_3} \quad (28)$$

In general, the propagation constants are complex quantities which can be expressed as follows:

$$\gamma_1 = \alpha_1 + j\beta_1; \gamma_2 = \alpha_2 + j\beta_2; \gamma_3 = \alpha_3 + j\beta_3 \quad (29)$$

where α_1, α_2 , and α_3 are called the attenuation constants (nepers/m) and β_1, β_2 and β_3 are called the phase shift constants (radian/m) of the natural modes 1, 2 and 3 respectively. The natural mode velocities are, of course, given by:

$$C1 = w / \beta_1; C2 = w / \beta_2; \text{ and } C3 = w / \beta_3 \quad (30)$$

For currents, similar natural distribution matrix S exists such that:

$$S = Q_1^{-1} \quad (31)$$

The propagation constants of current modes are the same as those of voltage modes. The characteristic impedance of transmission lines is defined as:

The propagation constants of current modes are the same as those of voltage modes. The characteristic impedance of transmission lines is defined as:

$$[Z_0] = [Q] [\gamma^{-1}] [Q]^{-1} [Z] \text{ ohm} \quad (32)$$

The natural mode characteristic impedance matrix $[Z_0]$ is a diagonal matrix given by:

$$[Z_0] = [\gamma^{-1}] [Q]^{-1} [Z] [Q]^{-1} \quad (33)$$

8. REPRESENTATION OF LONG TRANSMISSION LINES

In the previous sections, the parameters $[Z]$ and $[Y]$ are distributed and expressed in per unit length. For lines of length ℓ , the line can be represented by a π -network as shown in Fig.5.

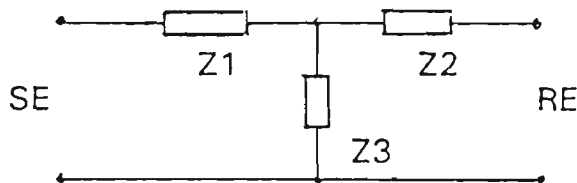


Fig.5 : Equivalent π representation of the line

The above representation gives accurate results for 50 Hz lines of up to about 100 km. In case of longer lines, the lumping of parameters leads to errors. However, an equivalent π network can be derived between the sending end (SE) and the receiving end (RE) as shown in Fig.10., the following definitions are applied:

$$Z_{SR} = Z_0 \sinh(\gamma \ell) \quad (34)$$

and

$$Y_{SS} = Y_0 \tanh(\gamma \ell / 2) \quad (35)$$

The same equivalent circuit can be derived for positive, negative and zero-sequence components independently.

In case of unbalanced transmission line analysis (phase co-ordinates), equations (36) and (37) are valid, but Z_{SR} , Z_{SS} , Z_0 , Y_0 and $\gamma \ell$ are all matrices involving evaluation of matrix functions.

9. RESULTS AND CONCLUSIONS

In order to test the accuracy of the algorithm, a typical 132 kV transmission line is given (Fig.6). The calculations of transmission line parameters are given including propagation constant and characteristic impedance. The sequence impedance are also given for balanced three-phase transmission line.

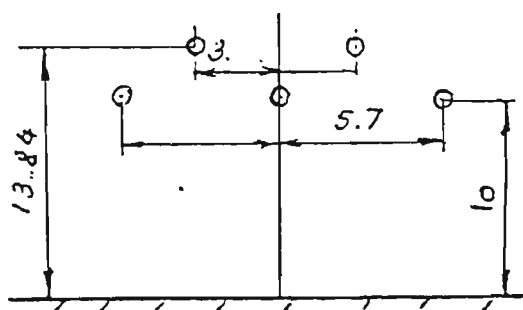


Fig.6: Transmission line configuration.

shown that for most of the realistic cases, the transmission line is not symmetrical, due to the geometry of the line, and the fact that the line may not be perfectly transposed. The results for the given transmission line are given in table.

The data for the line are: a) phase conductors are 7/30 - .346/ .346 cm steel/Al, outer diameter = 2.421 cm; b) earth wire: 7/1 - .477 cm, outer diameter = 1,430 cm, mean sag = 6 m., soil resistivity = 100 Ω m, horizontal construction.

Table 1: Results of 132 kV line, horizontal construction.

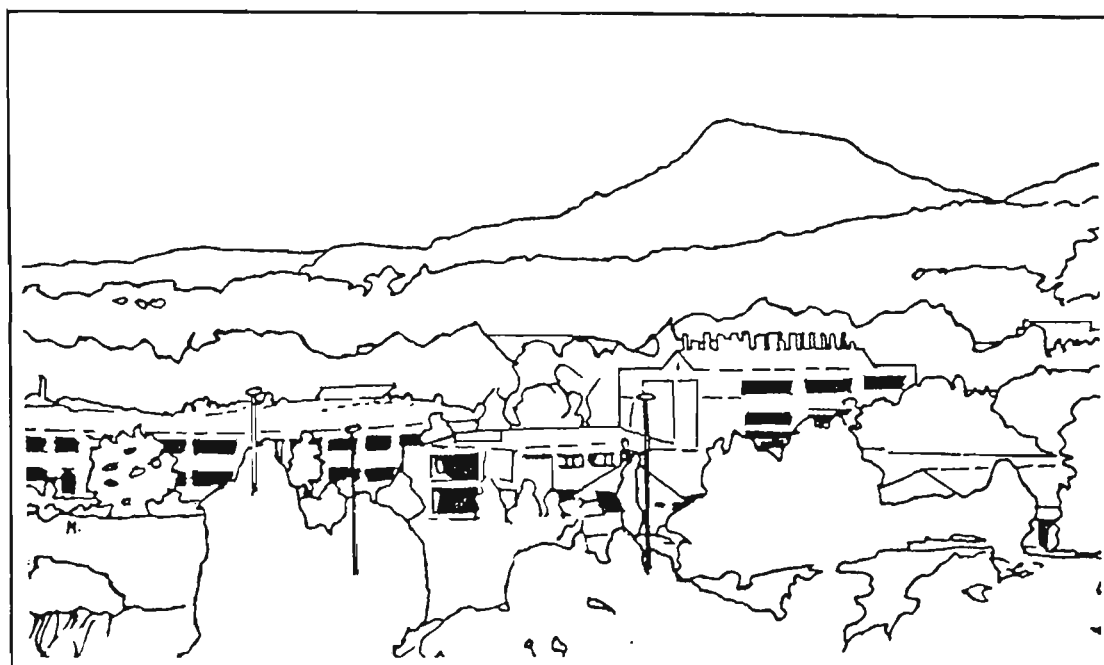
Series resistance (Ohm/km)			Series reactance (Ohm/km)			Shunt admittance (Ohm/km)		
.239859	.133720	.139438	.751310	.221300	.268581	.003039	-.000120	-.000368
.133720	.239859	.139438	.221300	.751310	.268581	-.000120	.003039	-.000368
.139438	.139438	.248353	.268581	.268581	.742193	-.000368	-.000368	.003118
Sequence Parameters								
Z_1 Ohm/km			Z_2 Ohm/km			Z_0 Ohm/km		
0.10516E+00+j0.49545E+00			0.10516E+00+j0.49545E+00			0.51775E+00+j0.12539E+00		
Z_s - Interphase mutual Impedance Ohm/km						Z_m - Phase self Impedance Ohm/km		
0.24269 E+00 + j 0.74827						0.1375E+00 + j 0.25282E+00		
Propagation parameters of the line								
Z_c Ohm/km					Y_c mS			
506.943	< -8.39	95.811	< -20.25	128.027	< -15.79	2.138	< 7.01	0.284 < 175.48
95.811	< -20.25	506.943	< -8.39	128.027	< -15.79	0.284	< 175	.5 2.138 < 7.01
128.027	< -15.79	128.027	< -15.79	501.277	< -8.83	.48	< -178	.48 < 178 2.231 < 7.32

10. REFERENCES

- (1) GALLOWAY, R., H., SHOROCKS, W., B., and WEDEPOHL, L., M.: "Calculation of electrical parameters for short and long polyphase transmission lines", Proc.IEE, 1964, 111, (12), pp.2051-2059
- (2) WEDEPOHL, L, M.: "Application of matrix methods to the solution of travelling-wave phenomena in poly-phase systems", ibid, 1963, 110, (12), pp.2200-2212
- (3) MATTISSON, M., J., SYLVIA, J., DAY, MULLINEUX, N., PARTON, K., C., and REED, J., R. : " Some effects of the frequency dependence of transmission-line parameters", ibid, 1969, 116, (7), pp.1209-1216

AUPEC'93

Proceedings of the
Australasian Universities
Power Engineering Conference
Volume 2



University of Wollongong, Australia
29th September to 1st October 1993

Edited by V J Gosbell



ANALYSIS OF FAULT LOCATION ALGORITHM FOR EHV TWO AND THREE TERMINALS TRANSMISSION LINES

Larissa Al-Dabbagh and Akhtar Kalam

Save Energy Group
Department of Electrical and Electronic Engineering
Victoria University of Technology
PO Box 14428, MMC, Melbourne, Vic 3000

ABSTRACT

In this paper a method for accurate fault location of two terminal transmission lines, which is extended to cater for three terminals. The paper presents the effect of both 2 and three terminal EHV transmission lines on the accuracy of fault location algorithm. Different methods of feeder configuration have various consequences on the accuracy of fault location. The paper provides analysis of the two and three terminal EHV transmission lines and discusses the effect of mutual coupling, line transposition and type of fault on the accuracy of measurements. The method of calculation is based on modal analysis and the use of current and voltage phasors extracted from the two and three terminals of the considered system.

1 Introduction

It is important to accurately measure the exact location of faults occurring on EHV transmission lines. This is due to the fact that there is little visual evident of the location of the fault, hence a delay in the repair of the line means longer undue outage of the line. Furthermore, post clearance tests performed on the line at reduced voltage can be misleading and inconclusive. The use of conventional methods for the measurement of the fault location using simple impedance measurement is not reliable and inaccurate.

An online digital fault locator for overhead transmission lines was suggested by Sunt et. al. (1). This locator takes input signals from existing c.t.s and p.t.s and works on a reactance-ratio-measurement principles. The device is dependent on Z_S/Z_L , although it provides a 2% accuracy within $Z_S/Z_L = 20$, the error for larger values is high. A fault location estimator was proposed by Gill et. al. (2), which is based on dynamic system parameters estimation for double-end fed transmission line using 1/4 to 1 cycle window of data at one local end only, based on lumped parameter simulation of the line. Takagi et. al. (3), have proposed a new type of fault locator which calculates the reactance of a faulty line, with a microprocessor, using one-terminal voltage and current data of the transmission line. A provision is made for correcting the error due to the load flow, fault resistance and unsymmetrical arrangement of the line.

Saha et. al. (4) have proposed a scheme for a fault locator based on a microprocessor which uses compensation techniques to improve accuracy. Pre-fault and fault data extracted from the ac currents and potentials are used to compute the distance to fault. Remote indication on local print-out of the fault information are provided. Cook (5) described the fundamental aspects of fault location algorithms used in distance protection. Two algorithms used were considered precise, containing no simplifying assumptions and their overall accuracy is limited only by the accuracy of the digital impedance relays at both ends of the protected circuit.

Srinivasan et. al. (6) described a new fault location algorithm for radial transmission lines with loads. The fault distance is obtained by solving an implicit equation where the load models can represent constant impedance, constant power, constant current or any combination of these. The scheme uses the pre-fault and faulted-state measurements and requires the solution of an implicit equation.

The above methods used for the determination of fault location are based on some assumptions and simplifications such as considering perfectly balanced transmission line, which has a considerable effect for untransposed transmission lines. By neglecting the shunt capacitance of the line, additional error is introduced to accuracy encountered in the measurement. The mutual coupling between phases of one line adds other factors to the errors in locating the fault (7).

In case of fault location algorithm for two terminal transmission lines, the derivation of the algorithm is based on the measurement of current and voltage signals at both ends of the transmission line (8). Takahashi et. al. (9) proposed a substation fault location system using optical current transducers. The data measured by the optical current transducers provides reliable and fast determination of fault location for the purpose of prompt and effective recovery from power failures. This method defines on which feeder is the fault, rather than the exact location on a particular feeder. Under busbar fault conditions, it is capable to determine on which busbar the fault has occurred.

The development of fault location algorithm for two terminal networks is not directly applicable for three or multi-terminal transmission lines. This applies particularly to algorithms used for conventional fault location methods using one-terminal ac voltage and current. Nagasawa (10) et. al. describes a new fault location algorithm for multi-terminal two parallel transmission lines. The method uses the magnitude of the differential current at each terminal and also uses an algorithm based on a three-terminal fault location algorithm and an equivalent conversion from n-terminal to a three-terminal system. The EMTP (Electromagnetic transient program) is used for simulating the results.

This paper presents a new method for calculation of the exact fault location in two and three terminal EHV transmission lines. Basically, the new technique is based on digital computation of the power frequency component of the three-phase current and voltage phasors at the line terminals. As for the two terminal transmission line (8), the algorithm developed for the three-terminal transmission line is virtually independent of fault resistance and largely insensitive to variations in source impedance, line configuration including line transposition (11). The paper briefly describes the basic theory used in developing the algorithm for two and three terminal EHV transmission lines.

2 Two terminal system

In order to determine the precise fault location on EHV transmission lines interconnecting two sources as shown in Fig.1, the faulty power system is represented by its equivalent circuit for source network and the two sections of the transmission line sections, before and after the fault location. In case of a single phase representation it is possible to derive the following (7,8) relationships for steady state voltage V_f across the fault at a distance x from the sending end, expressed in terms of measured voltages and currents at both ends of the faulty line:

$$V_f = \cosh(Gx)V_s - Z_0 \sinh(G(L-x))I_s \quad (1)$$

$$V_f = \cosh(G(L-x))V_r - Z_0 \sinh(G(L-x))I_r \quad (2)$$

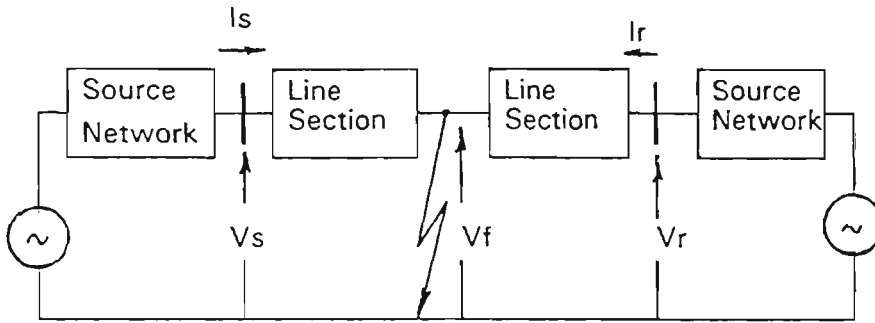


Fig.1: Two-terminal transmission line

In equations (1) and (2), the propagation constant G and surge impedance Z_0 are defined as $G = \sqrt{ZY}$, $Z_0 = \sqrt{Z/Y}$ respectively. In this context, Z is the line series impedance and Y is the line shunt admittance per unit length. Equation (1) and (2) are equated to eliminate V_f , and by rearrangement, the distance to fault x can be calculated as follows:

$$x = \tanh^{-1}(-B/A)/G \quad (3)$$

$$\text{where: } A = Z_0 \cosh(GL)I_r - \sinh(GL)V_r + Z_0 I_s \quad (4)$$

$$B = \cosh(GL)V_r - Z_0 \sinh(GL)I_r - V_s \quad (5)$$

In calculating x from equation (3), there is a small imaginary part which can be neglected. Usually, for any transmission line, the line parameters are known, and from the measured phasors of voltages and currents at the sending and receiving ends of the line, equation (3) gives accurate calculation of the fault location on the faulty line.

For the analysis of three phase transmission lines, equations (1) and (2) can be extended by expressing the sending end and the receiving end vectors of voltages and currents as $[I_s, abc]$, $[I_r, abc]$, $[V_s, abc]$, $[V_r, abc]$. Using the two port network representation, and considering Fig.2, the following matrix equation can be expressed:

$$[V_f, abc] = [A_s][V_s, abc] - [B_s][I_s, abc] \quad (6)$$

$$[V_f, abc] = [B_r][V_r, abc] - [A_r][I_r, abc] \quad (7)$$

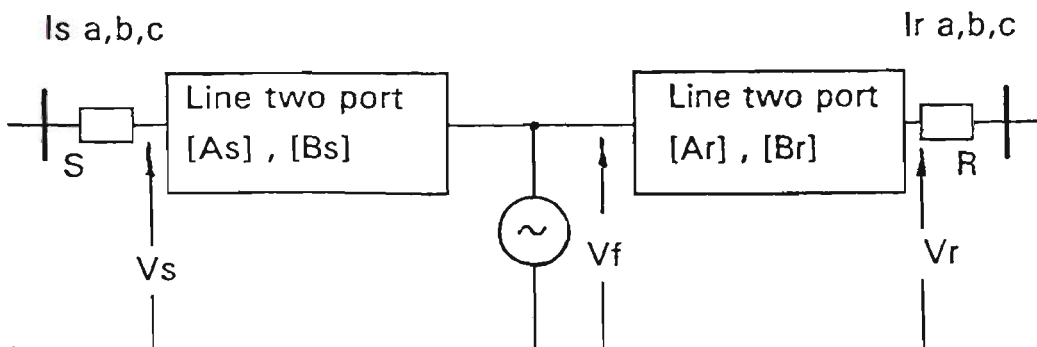


Fig.2: Equivalent three phase two-port system

For most applications, line sections are treated as homogeneous, and if required, these sections can be formed to include any discrete line transposition.

3 Theory of natural modes

The theory of natural modes (12) is used in developing the single phase circuit representation from three-phase by de-coupling equations (6) and (7) into uncoupled or independent equations which actually describe equivalent single phase networks similar to Fig.1. Modal analysis involves finding the matrix of Eigenvectors of the $[Z][Y]$ product ($[Q]$), and the $[Y][Z]$ product ($[S]$). By applying this theory, the voltages and currents derived from each phase a,b,c at each end would be transformed to corresponding modal voltage and current quantities 1,2 and 3 by means of the corresponding $[Q]$ and $[S]$ Eigenvector matrices:

$$[V_{sn}] = \begin{bmatrix} V_{s1} \\ V_{s2} \\ V_{s3} \end{bmatrix} = [V_{s1} V_{s2} V_{s3}]^T = [Q]^{-1} [V_{sa} V_{sb} V_{sc}]^T \quad (8)$$

and

$$[I_{sn}] = \begin{bmatrix} I_{s1} \\ I_{s2} \\ I_{s3} \end{bmatrix} = [I_{s1} I_{s2} I_{s3}]^T = [S^{-1}] [I_{sa} I_{sb} I_{sc}]^T \quad (9)$$

Therefore, for each single circuit, there are three pairs of such equations corresponding to the modes 1,2 and 3. If we want, for example node 1, the equation would be:

$$V_{f1} = A_{s1} V_{s1} - B_{s1} I_{s1} \quad (10)$$

$$V_{f1} = A_{r1} V_{r1} - B_{r1} I_{r1} \quad (11)$$

For double circuit transmission lines, there will be six modes, which result in six pairs of equations similar to the form of equation (10) and (11). For each mode, these equations can be equated to define the relevant distance to fault x , e.g., for mode 1:

$$x = \tanh^{-1} (B_1 / A_1) / G_1 \quad (12)$$

where:

$$A_1 = Z_{o1} \cosh(G_1 L) I_{r1} - \sinh(G_1 L) V_{r1} + Z_{o1} I_{s1}$$

$$B_1 = \cosh(G_1 L) V_{r1} - Z_{o1} \sinh(G_1 L) I_{r1} - V_{s1}$$

For calculating modal surge impedance, the matrix product is calculated, i.e.,

$$[Z_{on}] = [G]^{-1} [Q]^{-1} [Z][S]$$

in which $[G]$ is a diagonal matrix of modal propagation constants comprising the square root of Eigenvectors of matrix product $[Z][Y]$. In fact $[Zon]$ takes the form $[Zo1 Zo2 Zo3]$, the individual values being modal surge impedances.

4 Three terminal system

A typical three-terminal transmission line is given in Fig. 3a for the steady state conditions and Fig. 3b for the same system under fault conditions.

The algorithm for accurate fault location for two terminal transmission lines described in section 3 is extended in this section to include three terminal lines.

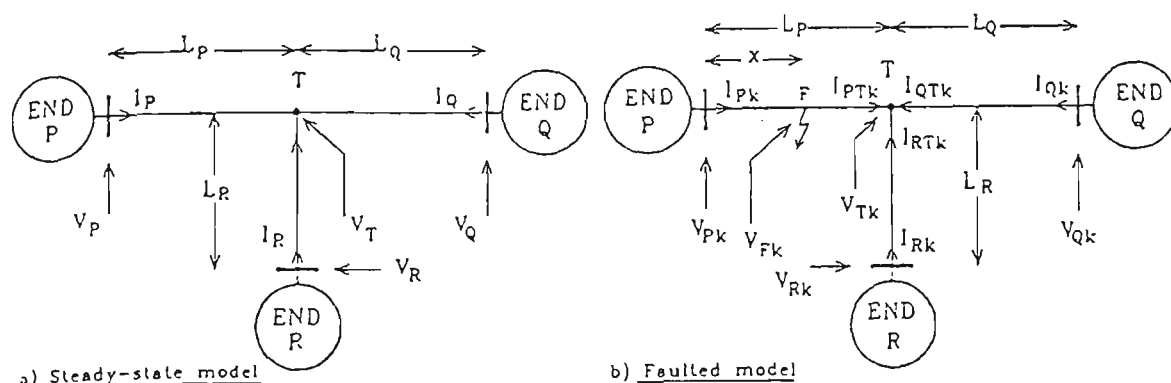


Fig. 3a: Three terminal system:
steady state condition

Fi. 3b: Three terminal system:
fault condition

To evaluate the fault location on any part of the three terminal transmission line, information about the voltage and current phasors at the three ends has to be obtained. To satisfy this requirement, some type of data synchronisation is required. This means that the data must have a common reference point(13). It should be stated that in practice, if one end is designated as reference, then the mismatch in recorded data at any of the other two ends rarely ever exceeds two samples when compared to the reference-end data (14). However, in the fault location algorithm, it is emphasised that means for synchronising data within the computation procedure to maintain a high degree of accuracy, particularly when there is any possible mismatch of data in case when the three fault recorders at the three ends were triggered at different time.

It is required to evaluate the voltage at the tee point from the knowledge of the pre-fault power frequency voltage and current phasors which are obtained using Discrete Fourier Technique(DFT) (14). The voltage relationship obtained at the T point as function of voltages and currents at the three ends are given as follows:

$$V_{PT} = \cosh(GL_P)V_P - Z_o \sinh(GL_P)I_P \quad (13)$$

$$V_{QT} = \cosh(GL_Q)V_Q - Z_o \sinh(GL_Q)I_Q \quad (14)$$

$$V_{RT} = \cosh(GL_R)V_R - Z_o \sinh(GL_R)I_R \quad (15)$$

When the data is synchronised, and taking end P say as a reference, $V_{PT}=V_{QT}=V_{RT}=V_T$. Any mismatch would be seen in the phase angles of the sampled data, which can be corrected by shifting the data at the unsynchronised ends few samples until the errors due to sampling are minimised.

5 Faulty section identification

Considering Fig. 3a, it is possible to define the faulty leg of the three terminal transmission line using a comparison procedure for the three voltages V_P , V_Q and V_R phasor measurements. From the measured voltages, it is possible to establish the faulty section by comparing each time and evaluating the relationship between the sampled values. If a fault say near the R end occurs, the voltage at the other two ends P and Q will be very similar but the voltage for R will be different. If there is no significant difference in the voltages obtained from the data received from all three ends, it can be assumed that the fault is at the tee point itself.

6 Fault location algorithm

The technique followed in locating the fault from the nearest end is similar to that of the two terminal transmission line. Consider a fault at point F of the three terminal system given in Fig. 3b on the PT leg. Using the two-port matrix relationship, both the fault point and the tee point phasors as a function of the phasors at the three ends are given as:

$$V_{Fk} = \cosh(G_k x)V_{Pk} - Z_{ok} \sinh(G_k x)I_{Pk} \quad (16)$$

and:

$$V_{Fk} = \cosh(G_k L_{Pk} - G_k x)V_{Tk} + Z_{ok} \sinh(G_k L_{Pk} - G_k x)I_{PTk} \quad (17)$$

also:

$$V_{Tk} = \cosh(G_k L_{Rk})V_{Rk} - Z_o \sinh(G_k L_{Rk})I_{Rk} \quad (18)$$

$$I_{PTk} = Y_{ok} \sinh(G_k L_{Qk}) - \cosh(G_k L_{Qk})I_{Qk} + Y_{ok} \sinh(G_k L_{Rk})V_{Rk} - \cosh(G_k L_{Rk})I_{Rk} \quad (19)$$

where:

$$D_k = -V_{Pk} + A_k \cosh(G_k L_{Pk})Z_{ok} \sinh(G_k L_{Pk})$$

$$C_k = -Z_{ok}I_{Pk} + A_k \sinh(G_k L_{Pk}) - Z_{ok}B_k \cosh(G_k L_{Pk})$$

$$B_k = -\cosh(G_k L_{Qk})I_{Qk} + Y_{ok} \sinh(G_k L_{Rk})V_{Rk} - \cosh(G_k L_{Rk})I_{Rk} + Y_{ok} \sinh(G_k L_{Qk})V_{Qk}$$

$$A_k = \cosh(G_k L_{Qk})V_{Qk} - Z_{ok} \sinh(G_k L_{Qk})I_{Qk}$$

where k=1 for Earth mode, 2 and 3 for Aerial modes, x is the distance to fault. A simple manipulation of equations (16-20) yields:

$$X = \tanh^{-1}(D_k / C_k) / G_k \quad (20)$$

where:

$$D_k = -V_{Pk} + A_k \cosh(G_k L_{Pk}) + Z_{ok} \sinh(G_k L_{Pk})$$

$$C_k = -Z_{ok}I_{Pk} + A_k \sinh(G_k L_{Pk}) - Z_{ok}B_k \cosh(G_k L_{Pk})$$

$$B_k = -\cosh(G_k L_{Qk})I_{Qk} + Y_{ok} \sinh(G_k L_{Rk})V_{Rk} - \cosh(G_k L_{Rk}) + Y_{ok} \sinh(G_k L_{Qk})V_{Qk}$$

$$A_k = \cosh(G_k L_{Qk})V_{Qk} - Z_{ok} \sinh(G_k L_{Qk})I_{Qk}$$

7 Algorithm assessment

The modelling used for assessing the algorithm is based on an early work (14), which includes both the distributive nature of the line, and its frequency dependent parameters. This modelling provides a realistic instantaneous values of voltages and currents at the terminating busbars, for any type of fault and source conditions. Results are presented for 400 kV transmission line given in reference (11), and the following relevant parameters:

i) earth resistivity (assumed homogeneous) = 100 $\Omega.m$

ii) source X/R ratio = 30, $Z_{so}/Z_{s1}=0.5$.

The error expected is expressed as a percentage of the length of a particular leg of the tee and given as:

$$\%error = \frac{X_{estimated} - X_{actual}}{L_{tee}} \times 100 \quad (21)$$

The analysis of the accuracy of the fault location algorithm for symmetrical tee configuration given in Fig. 3b is carried out (14). The results are given in Fig. 4a and Fig. 4b, for single phase to ground and double phase to ground faults respectively. It is clear from these results that in selecting modes, a higher degree of accuracy is attained when using Earth-mode (mode

1) based signals rather than the two Aerial modes (mode 2 and 3). It is generally found that the asymmetry associated with single-circuit vertical construction lines manifests itself into causing larger error when utilising Aerial-modes rather than the Earth mode based signals.

The effect of line transposition is presented for a single-phase to ground and two-phase to ground faults also shown in Fig. 4a and 4b respectively. In comparing the results, it is apparent that there is some improvement in the measurement accuracy for the transposed line. However, it is important to emphasise that the percentage error for both transposed and untransposed lines is between (0.25-0.6) on the symmetrical tee arrangement.

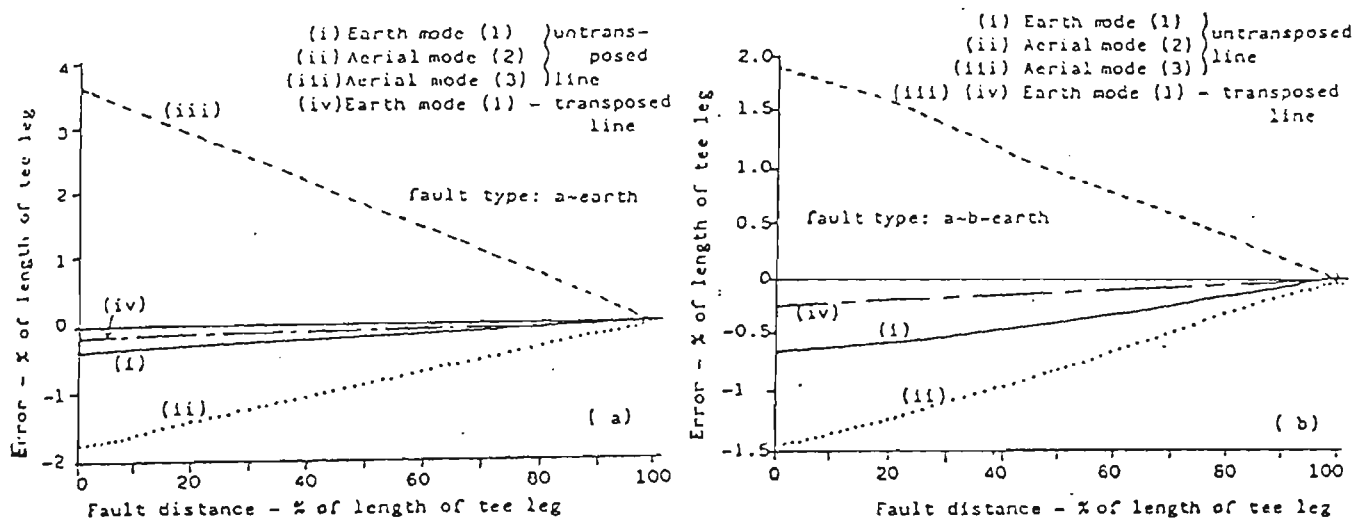


Fig. 4 a,b: Percentage error

8 Conclusions

The paper has described accurate algorithms for the measurement of fault location on the two and three terminal EHV transmission lines. The presented algorithms are based on the superimposed modal signals by extracting the fundamental phasors from voltage and current signals. The synchronised data from all three terminals are compared in order to determine the faulty leg of the tee configuration. From the results of the studies performed on EHV transmission lines, the algorithms presented are highly accurate even for untransposed lines. However, it is important to note, that for faults to ground, the Earth component reflected much less percentage error in the measurement as compared to the Aerial modes. This situation is particularly evident for single circuit vertical construction lines which is particularly due to the relatively high degree of asymmetry associated with them.

For faults not involving the ground and symmetrical three-phase faults, fault location has to be based on Aerial modes, due to the absence of the Earth mode for such faults. This means that the fault location algorithms would be applied to all three modes, and for significant level of the residual current being used to identify the presence of a fault involving the earth.

9 References

- (1) Sunt, M.T., and Paithankar, Y.G., "Online fault locator for overhead transmission lines", Proc. IEE, Vol. 126, No. 11, November 1979, pp.1181-84

- (2) Richards, G.G., Tan, Owen T., "An accurate fault location estimator for transmission lines", IEEE Transactions on Power Apparatus and Systems, Vol. PAS-101, No. 4, April 1982, pp. 945-950
- (3) Takagi, T., Yamakoshi, Y., Yamaura, M., Kondow, R., Matsushima, T., "Development of a new type fault locator using the one-terminal voltage and current data", *ibid*, vol. PAS-101, No. 4, August 1982, pp. 2892-98
- (4) Saha, M.M., and Eriksson, L., "Microprocessor based accurate fault locator with remote-end infeed compensation", IEE Proc., Publication No. 249, 3rd International Conference on Development in Power System Protection, April 1989, pp. 193-198
- (5) Cook, V., "Fundamental aspects of fault location algorithm used in distance protection", IEE Proc., Vol. 133, Pt. C, No. 6, September 1986, pp. 359-368
- (6) Srinivason, K, St-Jacques, A., "A new fault location algorithm for radial transmission lines with loads", IEEE Transactions on Power Delivery, Vol. 4, No. 3, July 1989, pp.1979-87
- (7) Johns, A.T., Jamali, S., "New accurate transmission line fault location equipment", IEE Proc. on 3rd International Conference on Developments in Power System Protection", UK, 1989, pp.1-4
- (8) Al-Dabbagh, L., Kalam, A., "Accurate fault location for EHV transmission lines", Proc. AUPCEC'91-Australasia Universities Power and Control Engineering Conference, Monash University, October 1991, pp.226-29
- (9) Takahashi, E, Nakahito, K, Katsukawa, H, Kato, S, " Development of Substation Fault Location System Using Optical Current Transducers", CIGRE Symposium, Berlin, April, 1993, 110-01, pp. 1-6
- (10) Nagasawa, T., Abe, M., Otsuzuki, N., Emura, T., Jikihara, Y., and Takenchi, M., "Development of a new fault location algorithm for multi-terminal two parallel transmission lines", 0-7803-0219-2/19110009-6348/1991 IEEE, pp. 348-361
- (11) Johns, A.T., and Aggarwal, R.K., "Digital simulation of faulted EHV transmission lines with particular reference to very-high-speed protection", Proc. IEE, 1976, 123, (4), pp.353-359
- (12) Wedepohl, L.,M., " Application of matrix methods to the Solution of Travelling-Wave Phenomena in Polyphase Systems", Proc. IEE, 110, (12), pp.2200-2212.
- (13) Bornard, P., Tesseron, J.M., Bastide, J.C., and Nourris, M., "Field experience of digital fault recorders and distance relay in EHV substation", IEEE trans on power apparatus and systems, Vol. PAS-103, No. 1, January 1984
- (14) Aggarwal, R.K., Coury, D.V., Johns, A.T., and Kalam, A., "A practical approach to accurate fault location on Extra High Voltage teed feeders", A paper presented at the IEEE/PES 1992 Summer Meeting, Seattle, WA, July 12-16 1992, pp. 1-8



IEE

Jordan Centre



PROCEEDINGS

OF

JIPSC - 93

JORDAN INTERNATIONAL
POWER SYSTEM CONFERENCE

OCTOBER 4-6, 1993

VENUE :

FACULTY OF ENGINEERING AND TECHNOLOGY
UNIVERSITY OF JORDAN
AMMAN, JORDAN

SPONSORS :

UNIVERSITY OF JORDAN
IEE JORDAN INTERNATIONAL CENTRE

ACCURATE FAULT LOCATION ALGORITHM FOR EHV TRANSMISSION LINES OF MODERN POWER SYSTEMS

L. Al-Dabbagh, A. Kalam,

Victoria University of Technology

ABSTRACT

This paper describes the development of accurate algorithm for measuring fault location on EHV transmission lines. The method is based on using matrix algebra for multi phase transmission lines using the theory of natural modes. Phase quantities are captured after the fault, are transformed into modal quantities to allow the use of real conductor currents and voltages for any type of balanced or unbalanced transmission system. The analysis of the developed algorithms are given in order to show the benefits from using such techniques for accurate fault location detection on multi conductor transmission lines.

1. INTRODUCTION.

Power systems are considered one of the most complex engineering systems. This due to the vast number of generators, transmission line, and sub transmission systems. In order to transfer the bulk power from the location it is generated to the place where it is used, hv and ehv transmission lines are used.

The reliability and high quality of power supply depends on the accuracy of protection and control systems used. In order to maintain system stability, high and ultra high speed protection systems are used. For, the restoration of power will depend on accurate methods for isolating the faulty part of the power system as soon as possible, and the ability to locate the precise distance to fault along the faulty line. The required accuracy will depend on the method used for detection, and will be directly related to the accuracy of measuring the signals used in the fault location algorithm employed. Different fault location methods have been developed (1-5), for measuring the distance to fault. In modern fault location devices (6) although some improvement has been made, it is reported that the high accuracy of locating the fault remains a problem, in spite of the efforts to improve their performance.

The major draw back of most of the fault location devices, is due to the assumptions made and which are incorporated in the fault location algorithm. Assumptions like perfect balanced transmission line could have significant affect in case of untransposed lines. The fact that shunt capacitance is not considered can have additional contribution to the error experienced in the measurement of fault location. Mutual

coupling between phases of one line, and between different circuits of transmission lines adds other factors to the inaccuracy in locating the faults (7).

In order to improve the accuracy of fault location techniques for ehv and uhv transmission lines, the fault location algorithm proposed in this paper is based on an early work by Johns et. al.(7). The derivation of the main current and voltage signals is made from an accurate measurements of fault signals in the frequency domain, which considers the affect of travelling waves and the solution of the wave equation for the faulty transmission circuits (8). A basic power system consisting of a ehv transmission circuit interconnecting two power sources of different strengths. The sending end and receiving end of the line are separated by the fault location, which is assumed along the line. Both sources have contribution to the fault, and the accuracy of measuring the sending end and receiving end voltages and currents, will affect the accuracy of measuring the fault location.

The accurate measurement of fault is particularly important when unmanned sub stations are subjected to faults. Such faults result in the dispatch of maintenance personnel to the site. Power is usually restored after determining the location of the fault and evaluating the situation. Such situation arises particularly when there is limitation on the remote monitoring information about the fault. A recent work by Takahashi et al (9) indicates the development of a substation fault location system using optical current transducers(OCT's). The data measured by the OCT's provides reliable and fast determination of fault location for the purpose of prompt and effective recovery from power failures. The effectiveness of this method is demonstrated in defining on which feeder is the fault, rather than the exact fault location on a particular feeder. It determines on what section of a busbar is the fault location under busbar fault conditions.

This paper describes the fault location algorithm for measuring the location of the fault along the ehv transmission lines accurately (10). The basis of the approach followed in this paper addresses the foregoing problems and takes into account the practical limitations, hence extending the capabilities for variety of practically encountered system and fault conditions. The method is based on utilising voltage and current signals at both ends of the EHV transmission line. The capture of signals from data during faults. By using

modal analysis, and based on the superposition technique, superimposed modal quantities used instead of the total phase values. This reduces the error which may be caused by line loading or source impedances.

2. SYSTEM CONFIGURATION

The single line diagram for the system considered is given in Fig.1. The fault can be applied at any location of the transmission line. Source impedance can be changed to reflect the short circuit level at each end. The system is represented by equivalent networks for the each source, the line section to the fault location, and the line section after the fault location. The distance to fault x and the total line length L are also shown.

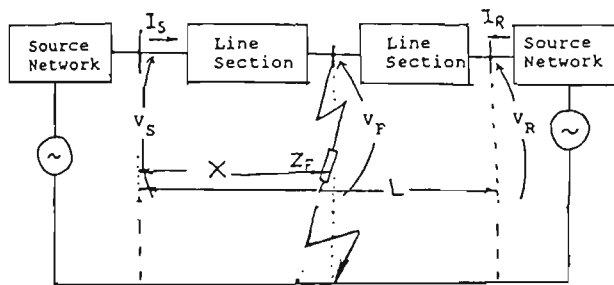


Fig. 1: Single line representation

In the following section, it will be shown, that there is no need to define precisely the fault impedance and the characteristics of the fault path, since the algorithm used will eliminate these factors from the computation of the fault location.

3. SINGLE PHASE LINE

For a single phase line shown in Fig.1 above, the following relationships are applicable for steady state voltage V_f across the fault at a distance x from the sending end, expressed in terms of measured voltages at the sending and receiving ends:

$$V_f = \cosh(Gx) V_S - Z_0 \sinh(G(L-x)) I_S \quad (1)$$

$$V_f = \cosh(G(L-x)) V_R - Z_0 \sinh(G(L-x)) I_R \quad (2)$$

In the above equations, both the propagation constant G and the surge impedance Z_0 are defined as $G = \sqrt{ZY}$, $Z_0 = \sqrt{Z/Y}$ respectively, where Z is the line series impedance and Y is the line shunt admittance per unit length. In order to avoid any difficulty in defining the precise value and characteristics of the fault path, equations (1) and (2) are equated to eliminate the V_f , and by some rearrangement, an accurate evaluation of the distance to fault as measured from the sending end is derived as:

$$x = [\tanh^{-1}(-B/A)] / G \quad (3)$$

where:

$$A = Z_0 \cosh(GL) I_R - \sinh(GL) V_R + Z_0 I_S \quad (4)$$

$$B = \cosh(GL) V_R - Z_0 \sinh(GL) I_R - V_S \quad (5)$$

In defining all the parameters in equation (3), the distance to fault can be computed accurately. In calculating x , there will be a small imaginary which is neglected, and only the real part is considered. The parameters of the line (Z and Y) are known usually, and from the measured phasers of voltages and currents at both ends, the precise distance to fault can be computed.

4. THREE PHASE LINE

The computation of distance to fault described above can not be implemented directly for poly-phase transmission lines, since a number of phases is involved. Basically the method can be extended to cater for multiphase circuits. In order to derive the expression for three phase transmission line as shown in Fig.2 which is given as a single line diagram.

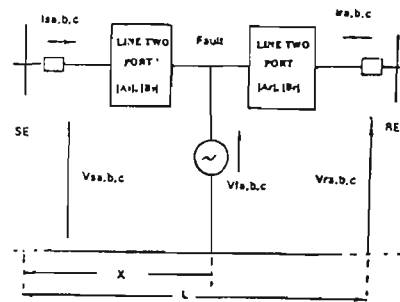


Fig. 2: Single line diagram of three phase line

In case of three phase voltages and currents, we will use vectors and arrays for describing different parameters, e.g., the sending end and receiving end currents and voltages are described as: $[I_{s,a,b,c}]$, $[I_{r,a,b,c}]$, $[V_{s,a,b,c}]$, and $[V_{r,a,b,c}]$, etc, and based on the two port network representation, the two port matrices $[A_S]$, $[B_S]$, $[A_R]$, $[B_R]$ are all 3×3 matrices. These are usually defined from line parameters, i.e. line series impedance and shunt admittance matrices (Z and Y). Considering Fig.2, the multi phase equivalent of equations (1) and (2) can be expressed as follows:

$$[V_{fa,b,c}] = [A_S] [V_{sa,b,c}] - [B_S] [I_{sa,b,c}] \quad (6)$$

$$[V_{fa,b,c}] = [B_R] [V_{ra,b,c}] - [A_R] [I_{ra,b,c}] \quad (7)$$

In most cases the line sections are treated as homogeneous. If it is necessary, these section can be formed to include any discrete line transposition.

5. MODAL ANALYSIS

The important aspect in applying the fault location algorithm developed for single phase circuit into multi phase circuits lies in de-coupling equations (6) and (7) into uncoupled or independent equations which in effect describe equivalent single-phase networks similar to Fig.1. In order to do this, the

theory of natural modes is used. The method is well described in reference (11), and used in many power systems analysis papers (8), for analysing the power system under fault conditions.

The method of modal analysis is basically involves finding the matrix of Eigenvectors of the $[Z][Y]$ product ($[Q]$), and the $[Y][Z]$ product ($[S]$). Using this technique, the voltages and currents derived from each phase a,b,c at each end would be transformed to corresponding modal voltage and current quantities 1, 2, 3 by means of the corresponding $[Q]$ and $[S]$ Eigenvector matrices:

$$[V_{sn}] = \begin{bmatrix} V_{s1} \\ V_{s2} \\ V_{s3} \end{bmatrix} = [V_{s1} V_{s2} V_{s3}]^T = [Q]^{-1} [V_{sa} V_{sb} V_{sc}]^T \quad (8)$$

$$[I_{sn}] = \begin{bmatrix} I_{s1} \\ I_{s2} \\ I_{s3} \end{bmatrix} = [I_{s1} I_{s2} I_{s3}]^T = [S]^{-1} [I_{sa} I_{sb} I_{sc}]^T \quad (9)$$

In using the theory of natural modes, even the multi conductor transmission line can be represented in a form similar to the one given in Fig.1, ie, the multi phase transmission line can be represented as a single phase uncoupled models. Therefore, for each single circuit, there are three pairs of such equation corresponding to the modes 1, 2, 3. For mode 2 for example, the equations would be:

$$V_{f2} = A_{s2} V_{s2} - B_{s2} I_{s2} \quad (10)$$

$$V_{f2} = A_{r2} V_{r2} - B_{r2} I_{r2} \quad (11)$$

In case of double circuit transmission line, there will be six modes, which in turn result in six pairs of equations similar to the form of equations (10) and (11). For each mode these equations can be equated to define the relevant distance x, e.g for mode two:

$$x = [\tanh^{-1} (-B_2/A_2)] / G_2 \quad (12)$$

where:

$$A_2 = Z_{o2} \cosh(G_2 L) I_{r2} - \sinh(G_2 L) V_{r2} - V_{s2} \quad (13)$$

$$B_2 = \cosh(G_2 L) V_{r2} - Z_{o2} \sinh(G_2 L) I_{r2} - V_{s2} \quad (14)$$

In order to calculate each modal surge impedance, the matrix product is calculated: $[Z_{on}] = [G]^{-1}[Q]^{-1}[Z][S]$, in which $[G]$ is a diagonal matrix of modal propagation constants comprising the square root of Eigenvectors of the matrix product $[Z][Y]$ (W). Therefore, $[Z_{on}]$ takes the form of $[Z_{o1} Z_{o2} Z_{o3}]$, the individual values being modal surge impedances. If perfect line transposition is assumed, the calculation of modal surge impedances and propagation constants is simplified since it is readily shown, for example the mode 2 surge impedance for a single circuit line can be expressed directly in terms of the positive phase sequence line impedance Z_1 and shunt admittance Y_1 per unit length of line as $Z_{o2} = \sqrt{Z_1/Y_1}$, similarly $G_2 = \sqrt{Z_1 Y_1}$. The assumption of

perfect transposition leads to Eigenvector matrices which are equal, ie, $[S] = [Q]$, and which are independent of the line geometry. In this case there is no need to calculate the voltage and current Eigenvectors, and they will take the following form:

$$[S] = [Q] = \begin{bmatrix} 1 & 1 & 1 \\ 1 & 0 & -2 \\ 1 & -1 & 1 \end{bmatrix} \quad (15)$$

The algorithm has been found accurate even when perfect line transposition is assumed.

6. FAULT LOCATION MEASUREMENTS

In order to test the accuracy of the algorithm, faults were injected on a transmission line in a digital simulation, and from the voltage and current phasers at both ends of the line, the modal transformation is carried out, so that the values are entered into the algorithm to compute the distance to fault x. For a single phase representation, the algorithms was found extremely accurate, ie, for any location of the fault, along the line, the assumed and measured location have been found to be identical.

For testing the algorithm further, a three phase model has been developed for computing fault location from the voltage and current phasers. Modal analysis is used to calculate the earth and aerial modes, from which a separate distance to fault is computed for each mode, which in turns define the fault location.

7. CONCLUSIONS

From the analysis carried out in this paper, an accurate fault location algorithm is presented. The algorithm uses the basic transmission line parameters, ie, the characteristic impedance and propagation constant, together with the measured post fault phase voltages and currents at both terminals of the transmission line. The use of the modal analysis has simplified the computation, by using the natural modes of propagation, instead of phase quantities, which in turn allowed the use of models developed for a single phase representation to calculate the fault location for any type of fault, ie, balanced and unbalanced, for a balanced or unbalanced polyphase transmission lines.

8. REFERENCES

- [1] Richards, G.G., Tan, O.T., "An Accurate Fault Location Estimator for Transmission Lines", IEEE Transactions on Power Apparatus and Systems, Vol. PAS-101, No. 4, April 1982, pp. 945-950.
- [2] Takagi, T, Yamakoshi, Y., Yamaure, M., Kondow, R., Matsushima, T., "Development of a New

Type Fault Locator Using The One-Terminal Voltage and Current Data", *ibid*, Vol. PAS-101, No. 8, August 1982, pp. 2892-2898.

- [3] Murari, M.S, Erikson, L., "Microprocessor-Based Accurate Locator With Remote-End Infeed Compensation", *IEE Proc. on 3rd International Conference on Development in power System protection*", Publication No. 249, April, 1985, pp. 193-198.
- [4] Ando, M, Schwenitzer, E.O., Baker, R.A., "Development and Field-Data Evaluation of Single-End Fault Locator for Two-Terminal HVDC Transmission Lines", Part I: Data Collection System and Field Data, *IEEE Transaction on Power Apparatus and Systems*, Vol. PAS-104, No. 12, December 1985, pp. 3524-3530.
- [5] Cook, V., "Fundamental Aspects of Fault Location Algorithms Used in Distance Protection", *IEE Proc*, Vol. 133, Pt. C, No. 6, September 1986, pp. 359-368.
- [6] Kondow, R., Sugiyama, Y., Yamada, M., "Microprocessor-Based Fault Locator", *IEE Proc. on 3rd International Conference on Developments in power Systems Protection*", UK, 1989, pp. 188-192.
- [7] Johns, A.T., Jamali, S., "New Accurate Transmission Line Fault Location Equipment", *ibid*, pp. 1-4.
- [8] Johns, A.T., Aggarwal, R.K., "Digital Simulation of Faulted ehv Transmission Lines With Particular Reference to Very- High-Speed Protection", *Proc. IEE*, 123, (4), pp. 353-359.
- [9] Takahashi, E, Nakahito, K, Katsukawa, H, Kato, S, "Development of Substation Fault Location System Using Optical Current Transducers", *CIGRE Symposium, Berlin, April, 1993, 110-01*, pp. 1-6
- [10] Al-Dabbagh, L., Kalam, A., "Accurate Fault Location for ehv Transmission lines", *Proc. AUPCEC'91, Australasia Universities Power and Control Engineering Conference, Monash University, Melbourne, Australia, October 1991*, pp.
- [11] Wedepohl, L., M., "Application of matrix methods to the Solution of Travelling-Wave Phenomena in Polyphase Systems", *Proc. IEE*, 110, (12), pp. 2200-2212.

BIBLIOGRAPHY

1. Carson, J.R., "Wave Propagation in Overhead Wires with Ground Return", Bell System Technical Journal, 1926, 5 pp. 538-54.
2. Carson, J. R., " The Present Status of Wire Transmission Theory and Some of its Outstanding Problems ", Bell Systems Technical Journal, Vol. 5, 1928, pp. 268 - 280.
3. Wedepohl, L. M., Wasley, R. G., " Propagation of Carrier Signals in Homogeneous, Non homogeneous and Mixed Multi conductor Systems ", Proc. IEE, Vol. 115, No. 1, January 1968, pp. 179-185.
4. Cristina, S., D ' More, M., " Prediction of the Optimum Coupling for PLC Propagation on Double Circuit and High Phase Order Transmission Lines ", IEEE Transactions on Power Apparatus and Systems, Vol. PAS - 103, No. 2, February, 1984.
5. Pullen, F. D., " The Calculated Electromagnetic Fields surrounding Carrier - Bearing Power Conductors ", Ibid, Vol. PAS - 94, No. 2, March/April 1975.
6. Cristina, S., D ' More, M., " Effect of Reflection waves on Polyphase Non - Uniform Power Line Carrier Channels: A New Propagation Matrix Model ", ibid, Vol. PAS - 100, No. 4, April 1981.
7. Cristina, S., D ' More, M., " Performance Sensitivity of A Power Line Carrier Channel ", ibid, Vol. PAS - 98, No. 4, July/August 1979.
8. Cristina, S., D ' More, M., " Electromagnetic Interference from Digital Signal Transmission on Power Line Carrier Channels ", IEEE Transaction on Power Delivery, Vol. 4, No. 2, April 1989.
9. " Power Line Harmonic Effects on Communication Line Interference ", IEEE Working Group on Power System Harmonics, IEEE Transaction on Power Apparatus and Systems, Vol. PAS - 104, No. 9, September 1985.
10. Wedepohl, L. M., "Application of Matrix Methods to the Solution of Travelling-wave Phenomena in Polyphase Systems", Proc. IEE, 1963, 110, (12), pp. 2200-2212.
11. Wedepohl, L. M., Wasley, R. G., " Wave Propagation in Polyphase transmission Systems, Resonance effects due to discretely bonded earth wires ", Proc. IEE, Vol. 112, No. 11, November 1965.

12. Galloway, R. H., Shorrocks, W. B., Wedepohl, L. M., "Calculation of Electrical Parameters for Short and Long Polyphase Transmission Lines", Proc. IEE, Vol. 111, No. 12, Dec. 1964, pp. 2051-59.
13. Wedepohl, L. M., "Electrical Characteristics of Polyphase Transmission Systems With Special Reference to Boundary - Value Calculations at Power - Line Carrier Frequencies ", Proc. IEE, Vol. 112, No. 11, November 1965.
14. Wedepohl, L. M., Mohamed, S. E. T., "Multi conductor Transmission Lines - Theory of Natural Modes and Fourier Integral Applied to Transient Analysis", *ibid*, Vol. 116, No. 9, Sept. 1969, pp. 1553-63.
15. Wedepohl, L. M., Mohamed, S. E. T., "Transient Analysis of Multi conductor Transmission Lines with Special Reference to Non-linear Problems", *ibid*, Vol. 117, No. 5, May 1970, pp. 979-988.
16. Wedepohl, L. M., Indulkar, C. S., "Wave Propagation in Non homogeneous Systems, properties of the chain matrix ", Proc. IEE, Vol. 121, No. 9, September 1974.
17. Meyer, W. S., Dommel, H. W., "Numerical Modelling of Frequency-dependent Transmission Line Parameters in an Electromagnetic Transient Program", IEEE Transaction, PAS, No. 1973, pp. 1401-1409.
18. Battisson, M. J., Day, S. J., Mullineux, N, Parton, K. C., "Some Effect of the Frequency Dependence of Transmission - Line Parameters ", Proc. IEE, Vol. 116, No. 7, July 1969.
19. Carroll, D. P., Nozari, F., "An Efficient Computer Method for Simulating Transients on Transmission Lines with Frequency Dependent Parameters ", IEEE Transactions on Power Apparatus and Systems, Vol. PAS - 94, July / August 1975.
20. Bickford, J. P., Doepel, P. S., "Calculation of Switching Transients with Particular Reference and Like Energisation", Proc. IEE., Vol. 114, No. 4, April 1967, pp. 465-77.
21. Johns, A. T. and Al-Rawi, A. M., "Development in the Simulation of Long-Distance Single-Pole-Switched EHV Systems", *ibid*, 1984, 131, (2), pp. 67- 77.
22. Battison, M. J., Sylvia, S. Day, Mullineux, N., Parton, K. C., Reed, J.R., "Calculation of Switching Phenomena in Power Systems", *ibid*, Vol. 114, No. 4, April 1967, pp. 478-86.

23. Emetine, A., "Modified Travelling Techniques to Solve Electrical Transients on Lumped and Distributed Constant Circuits", *ibid*, Vol. 120, No. 4, April 1973, pp. 479-503.
24. Wasley, R. G., Selvavinayagamoorthy, "Forward and Backward Response Functions for Transmission Line Transient Analysis", *IEEE Transactions, PAS*, May 1973, pp. 685-92.
25. Cochran, W. T., Cooley, J. W., and et al, "What is Fast Fourier Transform", *Proc. of the IEEE*, Vol. 55, No. 10, October 1967, pp. 1664- 76.
26. Day, Sylvia J., Mullineux, N., Reed, J.R., "Developments in Obtaining Transient Response using Fourier Transforms, Part I: Gibbs Phenomena and Fourier Integrals", *Int. J. Engg. Educ.* Vol. 3, 1965, pp. 501-506.
27. Day, Sylvia J., Mullineux, N., Reed, J.R., "Developments in Obtaining Transient Response using Fourier Transforms, Part II: Use of the Modified Fourier Transform", *ibid*, Vol. 4, 1966, pp. 31-40.
28. Day, Sylvia, J., Mullineux, N., Reed, J.R., "Developments in Obtaining Transient Response Using Fourier Transforms, Part III: Global Response", *ibid*, Vol. 6, 1968, pp. 259-265.
29. Mullineux, N, Reed, J. R., Development in obtaining Transient Response using Fourier Transforms: Part IV - Survey of the Theory ", *ibid*, 1972, pp. 256 - 267.
30. Ametani, A., "Development of Exponential Fourier Transform and its Application to Electrical Transients", *Proc. IEE*, Vol. 126, No. 1, Jan. 1979, pp. 51-56.
31. Jackson, L., Patrickson, J. B. and Wedepohl, L. M., "Distance Protection: Optimum Dynamic Design of Static Relay Comparators", *Proc. IEE*, 1968, 115, (2), pp. 280-287.
32. Johns, A. T., "Generalised Phase Comparator Techniques for Distance Protection. Theory and Operation of Multi-input Devices", *ibid*, 1972, 119, (11), pp. 1595-1603.
33. Johns, A. T., "Discussion on Generalised Phase Comparator Techniques for Distance Protection", *ibid*, 1975, 122, (7), pp. 747-749.
34. Johns, A. T., Martin, M. A., Barker, A., Walker, E. P., Crossley, P. A., " A New Approach to EHV Directional Comparison Protection Using Digital Signal Processing Techniques ", *IEEE Transaction on Power Systems*, Vol. PWRD - 1, No. 2, April 1986.

35. Johns, A. T., El - Din Mahmoud, M. M., " New Approach to Ultra - High - Speed Phase Selection in Single - Pole Autoreclosure Schemes ", IEE Proceedings, Vol. 133, Pt. C, No. 4, May 1986
36. Hamilton, F. L. and Ellis, N. S., "Developments in Bench Testing Facilities for Protective Gear", Reyrolle Rev., 1956, 166, pp. 21-29.
37. Johns, A. T. and Aggarwal, R. K., "Digital Simulation of Faulted e.h.v. Transmission Lines with Particular Reference to Very High Speed Protection", Proc. IEE, 1976, 123, (4), pp. 353-359.
38. Johns, A. T., Agrawal, P., " New Approach to Power Line Protection Based upon the Detection of Fault Induced High Frequency Signals ", IEE Proc., Vol. 137, Pt. C, No. 4, July 1990, pp. 307 - 313
39. Johns, A. T., " Generalised - Phase - Comparator Technique for Distance Protection ", IEE Proc., Vol. 119, No. 11, November 1972, pp. 1595 - 1603
40. Humpage, W. D., Wong, K. P., Al-Dabbagh, M. H. and Mukhtar, E. S., "Dynamic Simulation of High Speed Protection", *ibid*, 1974, 121, (6), pp. 474-480.
41. Kothari, G. C., Parthasarathy, K., Ashok Kumar, B. S. and Khincha, M. E., "Computer Aided Analysis of High Speed Protective Relays", *ibid*, 1974, 121, (7), pp. 687-694.
42. Humpage, W. D., Kit - Po Wong, " Electromagnetic Transient Analysis in EHV Power Networks ", Proceedings of the IEEE, Vol. 70, No. 4, April 1982, pp. 379 - 391
43. Dommel, H. W., " Digital Computer Solution of Electromagnetic Transients in Single - and - Multiphase Networks ", IEE Trans. Power Apparatus and Systems, Vol. PAS - 88, April 1969, pp. 388 - 399
44. Uram, R., Miller, R. W., " Mathematical Analysis and Solution of Transmission - Line Transients , I - Theory, IEEE Transactions on PAS, November 1964, pp. 1116 - 1123
45. Uram, R., Miller, R. W., " Mathematical Analysis and Solution of Transmission - Line Transients, II - Applications, *ibid*, pp. 1123 - 1137
46. Kalam, A, " A Computer Method for Solving Fault - Transient Phenomena in EHV Transmission System ", Proc. on International Conference on Modelling and Simulation, Melbourne, 1987, pp. 195 - 203

47. Kalam, A., McLean, C., " Transient Fault Analysis of Faulted Overhead Transmission Lines and Their Associated Protection ", CEPST '84, November 1984, pp. 1 - 12.
48. Aggarwal, R. K., Johns, A. T. and Kalam, A., "Computer Modelling of Series Compensated EHV Transmission Systems", *ibid*, 1984, 131, (5), pp. 188-196.
49. Perz, M. C., " Natural Modes of Power Line Carrier on Horizontal Three Phase Lines ", IEEE PS Communications Committee, Nuclear Radiation Effects Conference, Toronto, Ont., Canada, April 1967, pp. 679 - 691
50. Kalam, A., "Simulation of Series Compensated Lines and Their Associated Protection", Ph. D. Thesis, University of Bath, 1981.
51. Johns, A. T., Martin, M. A., Barker, A., Walker, E. P. and Crossley, P. A., "A New Approach to EHV Direction Comparison Protection Using Digital Signal Processing Techniques", IEEE Transactions on Power Systems, Vol. PWRD-1, No. 2, 1986, pp. 24-34.
52. Clayton, R. P., " Solution of Transmission - Line Equations for Lossy Conductors and Imperfect Earth ", IEE Proc., Vol. 122, No. 2, February 1975, pp. 177-182
53. Souillard, M., Sarquiz, Ph., Mouton, L., " Development of Measurement Principles and of the Technology of Protection Systems and Fault Location Systems for Three-Phase Transmission Lines ", International Conference on Large Electric Systems, GIGRE, Part 34 - 02, August 1974, pp. 1-13.
54. Richards, G. G. and Tan, Owen T., "An Accurate Fault Location Estimator for Transmission Lines", *ibid*, 1982, Vol. PAS-101, No. 4, pp. 945-950.
55. Takagi, T., Yamakoshi, Y., Yamaura, M., Kondow, R. and Matsushima, T., "Development of a New Type Fault Locator using the One Terminal Voltage and Current Data", *ibid*, 1982, Vol. Pas-101, No. 8, pp. 2892-2898.
56. Sant, M. T. and Paithankar, Y. G., "On line Digital Fault Locator for Overhead Transmission Line", Proc. IEE, 1979, 126, (11), pp. 1181-1185.
57. Saha, M. M. and Eriksson, L., "Microprocessor-based Accurate Fault Locator with Remote end Infeed Compensation", Proc. of 3rd International Conference on Development in Power System Protection", April 1985.
58. Eriksson, L., Saha, M. M. and Rockefeller, G. D., "An Accurate Fault Locator with Compensation for Apparent Reactance in the Fault Resistance

- Resulting from Remote-end Infeed", *ibid*, 1985, Vol. PAS-104, No. 2, pp. 424-436.
59. Ando, M., Scheitzer, E. O. and Baker, R. A., "Development and field-data Evaluation of Single-end Fault Locator for Two-terminal HVDC Transmission lines, Part I: Data Collection System and Field Data", *IEEE Transaction*, 1985, Vol. PAS-104, No. 12, pp. 3531-33.
60. Cook, V., "Fundamental Aspects of Fault Location Algorithms Used in Distance Protection", *Proc. IEE*, 1986, Vol. 133, Pt. C., No. 6, pp. 359- 368.
61. Ibe, A. O. and Cory, B. J., "Fault Location Algorithm for Multiphase Power Lines", *ibid*, Vol. 134, Pt. C., No. 1, January 1987, pp. 43 - 50.
62. Crossley, P. A. and McLaren, P. G., "Distance Protection Based on Travelling Waves", *IEEE Trans.*, PAS-102, 1983, pp. 2971-2983.
63. Sachdev, M. S. and Aggarwal, R., "Accurate Fault Location Estimates from Digital Impedance Relay Measurements", *Proc. of 4th International Conference on Development - Power System Protection*, Edinburgh, 1989, pp. 180-184.
64. Srinivasan, K. and St. Jacques, A., "A New Fault Location Algorithm for Radio Transmission Lines with Loads", *IEEE Trans. on Power Delivery*, 1989, Vol. 4, No. 3, pp. 1676-1682.
65. Kondow, R., Sugiyama, Y. and Yamada, M., "Microprocessor-based Fault Locator", *Proc. 4th International Conference on Development Power System Protection*, 1989, Edinburgh, pp. 188-192.
66. Wiszniewski, A., "Fault Location Correction of Errors due to Current Transformers", *ibid*, 1989, pp. 185-187.
67. Johns, A. and Jamali, S., "New Accurate Transmission Line Fault Location Equipment", *ibid*, 1989, pp. 1-5.
68. Jeyasurya, B., Rahman, M. A., " Accurate Fault Location of Transmission Lines Using Microprocessors ", *ibid*, 1989, pp. 13- 17.
69. Nagasawa, T., Abe, M, Otsuzuki, N., Emura, T., Jikihara, Y., Takeuchi, M., "Development of a new Fault Location Algorithm for Multi - Terminal Two Parallel Transmission Lines ", *IEEE International Conference on HV Transmission Lines*, Texas, USA, 1991, pp. 348 - 361.
70. Ranjbar, A. M., Shirani, A. R., Fathi, A. F., " A New Approach for Fault Location Problem on Power Lines ", *IEEE Transaction on Power Delivery*, Vol. 7, No. 1, January 1992, pp. 146 - 151.

71. Yoshida, Y., Kawazoe, S., Ibuki, K., Yamada, K., Ochi, N., "New fault locating system for air-insulated substations using optical current detector", IEEE Winter Meeting, 92 W. M 194-1 PWRD, 1992, pp. 1-7.
72. Youssef, Omar, A. S., "A new technique for location of transmission line faults using single-terminal voltage and current data", Proc. Electric Power System Research, 23 (1992), pp. 123-128.
73. El-Hami, M, Lai, Druvala, D. J., Johns, A. T.," A new travelling-wave based scheme for fault detection on overhead power distribution feeders", IEEE Winter Meeting, 92 W. M 211-3 PWRD, 1992, pp. 1-8.
74. Gale, P. F., Crossley, P. A., Bingyin, Xu, "Fault location based on travelling waves", Proc. IEE on International conference on Development in Power System protection, UK, 1992, pp. 54-59.
75. Takahashi, E., Nakahito, K., Katsukawa, H., Kato, S., "Development of a substation fault location system using optical current transducers", Proc. GIGRE Symposium on Diagnostic and maintenance Techniques, Berlin, 19-21 April, 1993, pp. 110-01-6.
76. Lai, L. L, Ndeh-Che, F., "A new approach to protecting transmission systems with fault generated noise", Proc. IEE 2nd International Conference on Advances in Power System Control, Operation and management, Hong Kong, December 1993, pp. 170-175.
77. Dutta, P. .K., and Duttagupta, P. B., "Novel signal processing technique for fault detection and location in HV transmission lines", *ibid*, pp. 673-678.
78. Jihong, He., Jiali, He., Yaming, Sun, Li, K. K., "Accurate fault location method for extra high voltage transmission lines", *ibid*, pp. 189-193.
79. Al-Dabbagh, L., and Kalam, A., " Accurate fault location algorithm for EHV transmission lines", Proc. AUPEC'91-Australasia Power and Control Conference, Monash University, October 1991, pp. 226 - 229.
80. Al-Dabbagh, L., and Kalam, A., "Analysis of fault location algorithm for EHV two and three terminals Transmission lines, Proc. of Australasia Universities Power Engineering Conference, University of Wollongong, September, 1993, pp. 347-354.
81. Al-Dabbagh, L, and Kalam, A., "Accurate Algorithms for Modelling Transmission Line Parameters ", International conference on modelling and simulation, Victoria University of Technology, Melbourne, July, 1993, pp. 210 - 215.

82. Stagg, G. W., El-Abiad, A. H., " Computer Methods in Power System Analysis", McGraw - Hill Kogakusha, Ltd., Tokyo, Japan, 1968
83. Brown, H. E., " Solution of Large Networks By Matrix Methods ", John Wiley & Sons, Inc., 1974
84. Elgerd, O. I., " Electric Energy Systems Theory, An Introduction, McGraw - Hill International Book Company, Tokyo, Japan, 1983
85. Nagrath, I. J., Kothari, D. P., " Modern Power System Analysis ", Tata McGraw - Hill Publishing Company Ltd, New Delhi, 1980.
86. Steavenson, D. W., " Elements of Power System Analysis ", McGraw Hill International Book Company, Singapore, 1982.
87. Demidovich, B. P., Maron, I. A., " Computational Mathematics ", Mir Publisher, Moscow, 1981
88. " Alternative Transient Program Rule Book ", Vol. 1 and Vol. 2, Leuven EMTP Centre (L. E. C), Belgium, 1987.
89. Johns, A. T., El-Nour, M., " Performance of Distance Protection of EHV Feeders Utilising Shunt - Reactor Arrangement for Arc Suppression and Voltage Control ", IEE Proc., Vol. 127, No. 5, September 1980, pp. 304 - 316.
90. Johns, A. T., M., El-Nour, M, and Aggarwal, R. K., "Performance of distance protection of e.h.v. feeders utilising shunt reactor arrangements for arc suppression and voltage control", IEE Proc., Vol. 127, Pt. C, No 5, September 1980, pp. 304 - 316.
91. Aggarwal, R. K., Coury, D. V., Johns, A. T., and Kalam, A., " A practical approach to accurate fault location on Extra High Voltage teed feeders", A paper presented at the IEEE / PES 1992 Summer Meeting, Seattle, WA, July 12-16 1992, pp. 1- 8.
92. Selvavinyagamoorthy, S., " Computation of Electrical Parameters of Power Transmission Lines ", University of West India, April 1983.
93. Kimbark, E. W., " Selective-pole switching of long double circuit EHV line ", IEEE Trans. Vol Pas-95, No 1, January/February 1976
94. Knudsen, N., "Single Phase switching of transmission lines using reactors for extinction of the secondary arc", CIGRE report No 310, 1962

95. Kimbark, E. W., " Suppression of ground fault arcs on single pole switched EHV lines by shunt reactors", IEEE Trans. on power apparatus and systems, March 1964.
96. Bickford, J. P and El-Dewieny, R., M., K., " Energisation of transmission lines from inductive source, Effect if non simultaneous closure also investigated ", Proc. IEE, Vol. 120, No. 8, August 1973.
97. Edlinger, A., et. al., " The use of high voltage reactors for the compensation of extra high voltage transmission lines ", CIGRE report No. 402, 1964.
98. Barthold, L. O., et. al., " Static shunt devices for reactive power ", CIGRE report 31-08, 1974.
99. Parton, J. E., et. al., " Three phase iron cored harmonic free reactor ", 10th Universities Power Engineering Conference, January 1975, Aston University, Birmingham, UK.
100. Pacheco, E. J. P., " System voltage control using saturated iron cored reactors ", Ph. D. Thesis, UMIST, UK, 1977.
101. Engberg, K., et. al., " Reactors and capacitors controlled by transistors for optimum power system VAR control ", Technical seminar on reactive power compensation in power systems at the University of Birmingham, 11-12 September, 1979.
102. Friedlander, E., " Static network stabilisation - recent progress in reactive power control ", GEC Journal, Vol. 33, No. 2, 1966.
103. Ainsworth, J. D., et. al., " Application of saturated reactors to ac voltage stabilisations for HVDC transmission and other large convertors ", A paper recommended by IEEE PES summer meeting and EHV/UHV conference, Vancouver, Canada, July 15 - 20 1973.
104. Peterson, H. A, and Dravid, N. V., " A method for reducing dead time for single - phase reclosing in EHV transmission ", IEEE Trans. Vol. PAS - 88, No. 4, April 1969.
105. Balsler, S. J., et. al., " Single pole switching. A comparison of computer studies with field test results ", Paper T73 406 - 6, presented at the IEEE PES summer meeting and EHV/UHV conference, Vancouver, B.C., Canada, July 16 - 20 1973.
106. Kimbark, E., W., " Charts of three quantities associated with single - pole switching ', IEEE Trans., Vol. PAS 94, No. 2, March/April 1976.

107. Abu Elnour, M. A. H., " The Simulation of Shunt Compensated Power Transmission Systems and their Associated Distance Protection Equipment ", Ph. D. Thesis, The University of Bath, 1980
108. Bornard, P., Tesseron, J. M., Bastide, J. C., and Nourris, M., " Field experience of digital fault recorders and distance relay in EHV substation", IEEE trans on power apparatus and systems, Vol. PAS-103, No. 1, January 1984.
109. Adams, G. E., " Wave Propagation Along Unbalanced High Voltage Transmission Lines ", Transaction AIEE PAS, Vol. 78, August 1959, pp. 639 - 647
110. Hedman, D. E., " Propagation of Overhead Transmission Lines : I - Theory of Modal Analysis ", IEEE Transactions on Power System Communications, 1965, pp. 200 - 2004.
111. Hedman, D. E., " Propagation on Overhead Transmission Lines : II - Earth Conductance and Practical Results ", *ibid*, 1965, pp. 205 - 211.
112. Carson, J. R., " Regorous and Approximate Theorems of Electrical Transmission Along Wires ", Bell Sys. Tech. J., Vol. 7, January 1928, pp. 11 - 25
113. Barthold, L. O., " Radio - Frequency Propagation on Polyphase Lines ", AIEE Transactions on Communications, July, 1964, pp. 665 - 671
114. Jones, D. E., Bozoki, B., " Exponential Evaluation of Power Line Carrier Propagation on 500 - kV Line ", IEEE Trans. on Power System communications, January, 1964, pp. 16 - 23
115. Perz, H. C., " Propagation Analysis of HF Currents and Voltages on Lossy Power Lines ", *ibid.*, 1973, pp. 2032 - 2042

